



The
University
Of
Sheffield.

Exploitation of the UDP-glucose hydrolase NUDT22 as novel target in cancer therapy

Melanie Walter

A thesis submitted in fulfilment of the requirements for the degree of
Doctor of Philosophy

June 2022

The University of Sheffield

Faculty of Medicine, Dentistry and Health
Department of Oncology and Metabolism

Supervisor: Dr Patrick Herr

I. Declaration

This thesis includes one manuscript (Chapter 3), which was part of a collaborative effort with me as main contributor and which is partly published as a preprint. My detailed contribution is outlined at the beginning of the chapter.

Thesis chapter 1.2 includes a published review in unaltered form written by myself, with the title “Re-discovery of pyrimidine salvage as target in cancer therapy”.

The described NUDT22 inhibitors in Chapter 5 of this thesis are currently under consideration with industrial partners. Based on intellectual properties (IP) requirements, I was not allowed to include the previously prepared manuscript including the detailed development steps as well as chemical structures. Consequently, I could only include the enzymatic and cellular evaluation of the compound series.

No part of this thesis has been submitted in support of an application of any degree or qualification at the University of Sheffield or any other University or Institute of learning.

A handwritten signature in black ink that reads "Melanie Walter". The signature is written in a cursive, flowing style.

Melanie Walter

Sheffield, June 2022

II. Acknowledgements

Firstly, I would like to thank my supervisor, Patrick, for giving me this amazing opportunity and for being the best mentor I could have wished for. Thank you so much for all your support and guidance, for always believing in me and for everything you have taught me during the last three years. Without you, I would not feel half as ready for the next steps ahead of me. I will definitely miss working with you. Thank you (and Bettina) for being a friend and for making me miss Germany a lot less.

I would like to thank everyone in FU03 and the former Helleday group for all their help with research and experiments, but also for the time spent outside of the lab, coffee breaks, lunch at Notty House and trips to the pub. I will never forget our trip to visit the other part of the Helleday group in Stockholm at the beginning of my PhD. A special thanks to Vicky, for all your help, for being so welcoming, for our endless chats and for always listening. Thank you to my second supervisor, Thomas, and to Evert, for enabling me to come to Stockholm to introduce me to computer-aided drug design.

Thank you to the INTEGRATA consortium and all the fellows, for the endless training and development opportunities and for the great time spent together. Thank you to Alberto for hosting me in Bologna and for all your insights into molecular modelling and drug development.

A special thanks to my oldest friends, for always being there even if we are miles apart. Thank you for being a constant in my life, when everything else is changing.

To Ike, who constantly encouraged me in moments of self-doubt and never got bored listening to me talking about science. Without you, this would not have been possible and I am immensely grateful to have you by my side, now and forever.

Lastly, my biggest gratitude goes to my parents and Daniel without whom I would not be where I am today. Thank you for always believing in me and for simply being there in good and bad times.

III. Table of contents

I. Declaration	I
II. Acknowledgements.....	II
IV. Table of Non-Manuscript Figures.....	VI
V. List of Non-Manuscript Tables	VII
VI. Non-Manuscript Abbreviations.....	VIII
Abstract	XII
1. Introduction	1
1.1 NUDT22 is a NUDIX protein family member	1
1.1.1 The Nudix protein family and its role in cancer	1
1.1.2 NUDT22 is a UDP-glucose hydrolase	9
1.2 Pyrimidine synthesis and cancer.....	15
1.3 DNA replication stress and genome instability in cancer.....	35
1.3.1 DNA replication and DNA replication stress response.....	35
1.3.2 Differences in DNA replication stress response in cancer	42
1.3.3 DNA replication stress as target in cancer therapy.....	44
1.4 Objectives	49
2. Materials and Methods	50
2.1 Antibodies	50
2.2 Cell lines and culturing conditions	52
2.3 CRISPR/Cas9 gene editing.....	52
2.4 Growth curve.....	53
2.5 Glutamine starvation	53
2.6 Drug exposure for cell viability assessment	53
2.7 Western blotting	54

2.8	DNA fibre.....	55
2.9	EdU incorporation	56
2.10	Immunofluorescence and microscopy.....	57
2.11	Mouse xenograft study.....	57
2.12	Computational drug design and compound evaluation	58
2.12.1	Ligand source and compound database	58
2.12.2	Computational protein preparation	58
2.12.3	<i>In silico</i> screen of NCI/DTP compound database	59
2.12.4	Chemical optimisation of Compound A	60
2.12.5	Enzyme activity assay	61
2.12.6	Differential Scanning Fluorimetry	61
2.12.7	Cellular Thermal Shift Assay	62
2.12.8	Immunofluorescence and microscopy	63
2.13	Statistical analysis.....	64
3.	NUDT22 promotes cancer growth through pyrimidine salvage.....	65
3.1	Context of research and contributions.....	65
3.1.1	Context or research	65
3.1.2	Contributions	66
3.2	Manuscript.....	67
3.3	Supplementary material	101
4.	Development of NUDT22 small molecule inhibitors with computer-aided drug design.....	107
4.1	Introduction	107
4.1.1	Aims.....	109
4.2	Results	110
4.2.1	<i>In silico</i> screening of NCI/DTP to identify starting point for NUDT22 inhibitors	110
4.2.2	Biochemical evaluation of top compounds identified in <i>in silico</i> screen	114

4.2.3	<i>In silico</i> Hit optimisation	116
4.2.4	Binding interactions of TH012008 and its amide derivatives with NUDT22.....	119
4.2.5	Enzymatic activity of TH012008 amide derivatives.....	124
4.2.6	Target engagement of TH012008 amide derivatives.....	127
4.3	Discussion.....	129
5.	Evaluation of first-in-class NUDT22 inhibitors.....	136
5.1	Introduction	136
5.1.1	Aims.....	139
5.2	Results	140
5.2.1	Effect of inhibitors A1, A2 and A3 exposure on enzymatic activity and cell viability	140
5.2.2	Target engagement of NUDT22 inhibitors A1, A2 and A3	141
5.2.3	Dose-response evaluation of Inhibitor 4, 5 and 6	142
5.2.4	Target engagement of NUDT22 inhibitors A3, A4, A5 and A6.....	144
5.2.5	Inhibitor A3, A4, A5 and A6 and DNA damage	146
5.3	Discussion.....	148
6.	General discussion	151
6.1	Transcriptional regulation of NUDT22 by p53 in cancer.....	151
6.2	Biological function of NUDT22 in cancer versus non-cancer cell lines.....	153
6.3	NUDT22 as target in breast cancer.....	157
6.4	Identification of first-in-class NUDT22 inhibitors to be used as chemical probes.....	160
7.	Conclusion and future perspectives.....	164
8.	References	167
9.	Appendix – Research contributins	181
9.1	Publications.....	181
9.2	Conferences and presentations	181

IV. Table of Non-Manuscript Figures

Figure 1. The human NUDIX protein family.....	3
Figure 2. Overview of genetic alterations of NUDIX family members in cancer..	5
Figure 3. MTH1, NUDT2 and NUDT5 expression alterations in cancer.....	8
Figure 4. NUDT22 is a UDP-glucose hydrolase.	10
Figure 5. NUDT22 expression alterations in cancer.....	14
Figure 6. DNA replication.	36
Figure 7. DNA replication stress.....	39
Figure 8. Drug discovery pipeline.....	107
Figure 9. Co-crystal structure of NUDT22 with its substrate UDP-glucose (5LOR.pdb).....	110
Figure 10. Virtual screen workflow leading to the identification of the two hit compounds TH012002 and TH012008.	112
Figure 11. Chemical optimisation of TH012008 by amide coupling and second virtual screen to identify TH012008 analogues with improved activity towards NUDT22.	117
Figure 12. Binding model of NUDT22 with UDP-glucose and TH012008.....	119
Figure 13. NUDT22 stabilisation upon NUDT22 inhibitor binding.....	128
Figure 14. Four pillars of survival for target validation with a chemical probe.	136
Figure 15. . Exposure with inhibitors A1, A2 and A3 reduced cell viability only at top concentrations.....	140
Figure 16. Inhibitor A3 stabilises NUDT22 in U2OS cell lysate.	141
Figure 17. Inhibitors A3, A4, A5 and A6 are potent NUDT22 inhibitors.....	142
Figure 18. Effects of A3, A4, A5 and A6 on cell viability.....	143
Figure 19. Inhibitor A3, A4, A5, and A6 directly engage NUDT22..	145
Figure 20. All four NUDT22 inhibitors induce DNA damage.....	147
Figure 21. NUDT22 mediates a novel pyrimidine salvage pathway.	154

V. List of Non-Manuscript Tables

Table 1. Overview of a selection of Phase I and II clinical trials of inhibitors targeting key players in the DNA replication stress response alone or in combination with other DNA damage inducing agents.....	46
Table 2. Overview of antibodies used in western blot (WB), immunofluorescence (IF), DNA fibre and EdU incorporation experiments.....	50
Table 3. sgRNA used for CRISPR/Cas9 gene editing in U2OS, hTERT-RPE1 and MCF7 cells.....	52
Table 4. Overview of 5-Fluorouracil and the two identified hit compounds TH012002 and TH012008.....	115
Table 5. . Binding affinity, ligand efficiency and ligand interactions of TH012008 and its amide analogues identified in the virtual docking screen.....	121
Table 6. IC50 and chemical structures of TH012008 amide analogues.....	124

VI. Non-Manuscript Abbreviations

2-oxo-(d)ATP	2-oxo-(deoxy)adenosine triphosphate
5-FU	5-fluorouracil
8-oxo-(d)ATP	8-oxo-(deoxy)adenosine triphosphate
8-oxo-(d)GTP	8-oxo-(deoxy)guanine triphosphate
8-oxo-(d)GTPase	8-oxo-(deoxy)guanine triphosphatase
9-1-1 complex	Rad9-Hus1-Rad1 DNA clamp complex
Acetyl-CoA	Acetyl Coenzyme A
ADMET	Absorption, distribution, metabolism, excretion, toxicity
ADPR	Adenosine 5'diphosphoribose
ALK	Anaplastic lymphoma kinase
AMP	Adenosine monophosphate
AMW	Molecular weight (Da)
AP ₄ A	Diadenosine tetraphosphate
ATCC	American Type Culture Collection
ATM	Ataxia telangiectasia mutated
ATP	Adenosine triphosphate
ATR	Ataxia telangiectasia and Rad3 related
ATRIP	ATR-interacting protein
BER	Base-excision repair
BSA	Bovine serum albumin
CADD	Computer-aided drug design
CDKs	Cyclin-dependent kinases
CETSA	Cellular thermal shift assay
CHK1/2	Checkpoint kinase 1/2
CldU	5-chloro-2'-deoxyuridine
DIPP	Diphosphoinositol polyphosphate Phosphohydrolase
dCK	Deoxycytidine kinase
dCTP	Deoxycytidine triphosphate
DDR	DNA damage response
DDKs	DBF4-dependent kinases

DHODH	Dihydroorotate dehydrogenase
DMEM	Dulbecco's Modified Eagle Medium
DNA-PKcs	DNA-proteinkinase dependent catalytic subunit
DSBs	DNA double strand breaks
DScore	Docking score/binding affinity
dsDNA	double-stranded DNA
DSF	Differential scanning fluorimetry
dNTP	Deoxynucleoside triphosphate
dTTP	Deoxythymidine triphosphate
EdU	5-ethynyl-2'-deoxyuridine
ER	Estrogen receptor
EMT	Epithelial-mesenchymal transition factor
ETAA1	Ewing tumour associated antigen 1
FANCD2	Fanconi anaemia group D2
FBS	Fetal bovine serum
G1P	Glucose 1-phosphate
G6P	Glucose 6-phosphate
GDP-D-mannose	Guanosine diphosphate-D-mannose
GTE _x	Genomic Tissue Expression
HBA	Hydrogen bond acceptor
HBD	Hydrogen bond donor
H-bond	Hydrogen bond
HER2	Human epidermal growth factor receptor 2
HIF1 α	Hypoxia-inducible factor 1- α
HPA	Human Protein Atlas
HR	Homologous recombination
HTS	High throughput screening
HU	Hydroxyurea
IdU	5-iodo-2'-deoxyuridine
K _i	Inhibitory constant
K _m	Michaelis-Menten constant
KO	Knockout
LC-MS	Liquid chromatography - mass spectrometry
LE	Ligand efficiency

MMR	Mismatch repair
MTH1	MutT homologue 1
mtp53	Mutant p53
NCI/DTP	National Cancer Institute/Developmental Therapeutics Program
NMP	Nucleoside monophosphate
NDP	Nucleoside diphosphate
NER	Nucleotide-excision repair
NHEJ	Non-homologous end joining
NUDIX	Nucleoside diphosphate linked to another moiety X
NUDT22i	NUDT22 inhibitors
OIS	Oncogene-induced senescence
OXPHOS	Oxidative phosphorylation
PAINS	Pan Assay Interference compounds
PARP	Polyadenosine 5'diphosphoribose polymerase
PBS	Phosphate buffered saline
PCNA	Proliferating cell nuclear antigen
PDAC	Pancreatic ductal adenocarcinoma
PDB	Protein data bank
PFA	Paraformaldehyde
PGM	Phosphoglucomutase
PIKK family	Phosphatidylinositol-3 kinase-related kinase family
PR	Progesterone receptor
PPP	Pentose phosphate pathway
PTMs	Posttranslational modifications
P-X	Phosphorylated moiety X
Rb	Retinoblastoma protein
REOS	Rapid elimination of swill
RMSD	Root-mean-square deviation
RNR	Ribonucleotide reductase
ROS	Reactive oxygen species
RFA	Replication factor A
RFC	Replication factor C
RPA	Replication protein A

SAR	Structure activity relationship
SDF	Structure-data file
sgRNA	Single guided RNA
SSBs	Single stranded DNA breaks
ssDNA	Single stranded DNA
STR	Short-tandem repeat
TBST	Tris buffered saline + 0.05% Tween 20
TCA	Tricarboxylic acid
TCGA	The Cancer Genome Atlas
T _m	Melting temperature
TOPBP1	Topoisomerase II binding protein
TPSA	Topological polar surface area
TPP	Trans-proteomic profiling
TS	Thymidine synthase
UDP-glucose	Uridine diphosphate-glucose
UDP-galactose	Uridine diphosphate-galactose
UGDH	UDP-glucose 6-dehydrogenase
UGP2	UDP-glucose pyrophosphorylase
UMP	Uridine monophosphate
UMPS	Uridine monophosphate synthetase

Abstract

NUDT22 is a hitherto unstudied family member of the NUDIX protein superfamily. Our group previously identified a specific substrate activity for NUDT22 towards uridine diphosphate (UDP)-glucose resulting in the generation of glucose 1-phosphate (G1P) and the pyrimidine precursor uridine monophosphate (UMP). Fast proliferating cells such as cancer cells can adapt the more energy-efficient nucleoside salvage pathways to maintain sufficient nucleotide pool levels for cell proliferation and to prevent DNA replication stress. Together with the observed *NUDT22* expression alterations in cancer, we hypothesised a specific role of NUDT22 in nucleotide synthesis and the potential exploitation of NUDT22 as novel target in cancer therapy.

Here, we assessed the effects of *NUDT22* knockout in osteosarcoma U2OS, non-cancer retinal pigment epithelial hTERT-RPE1, and in breast cancer MCF7 cells on cell proliferation, nucleotide levels, DNA replication stress, DNA damage induction, DNA replication fork speed and cell cycle progression. We determined synergistic changes in cell survival, DNA damage induction and cell cycle progression upon targeting pyrimidine *de novo* synthesis with nucleoside analogues and other anti-cancer agents in *NUDT22* KO cells and their respective controls. We performed gene expression database analysis of the cancer genome atlas (TCGA) as well as genotype-tissue expression (GTEx) program to assess changes in *NUDT22* levels in cancer versus healthy tissue and determined the role of NUDT22 as potential cancer target *in vitro* and in a MCF7 breast cancer xenograft model. Furthermore, we exploited our group's previously solved co-crystal structure of NUDT22 in complex with UDP-glucose in virtual screens for the development of NUDT22 inhibitors. The identified and chemically optimised compounds were further evaluated based on enzymatic and cellular activity as well as their target engagement with recombinant protein and in cell lysate.

In conclusion, we propose the discovery of a novel pyrimidine salvage pathway through NUDT22 controlling pyrimidine levels for DNA replication stress prevention and cancer growth maintenance. Our *in vitro* and *in vivo* findings suggest that NUDT22 is an emerging target for cancer therapy. In addition, we identified potential first-in-class NUDT22 inhibitors that engage their target in both recombinant protein and cell lysate.

1. Introduction

1.1 NUDT22 is a NUDIX protein family member

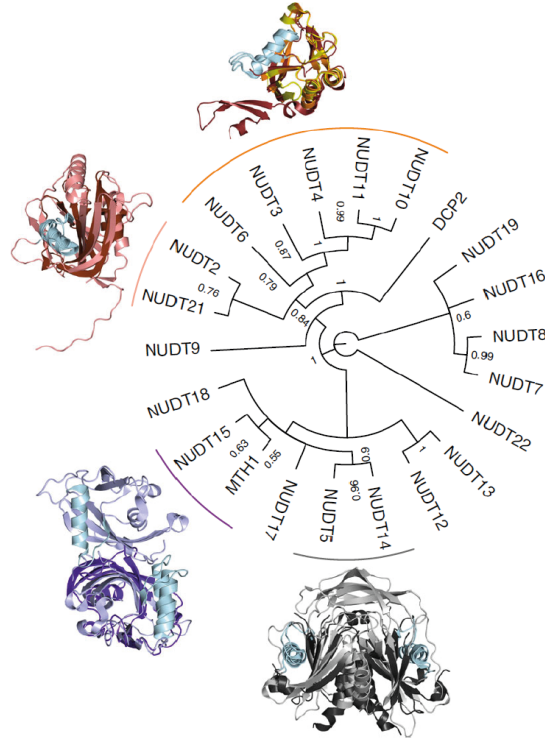
1.1.1 The Nudix protein family and its role in cancer

The NUDIX protein superfamily is a species-wide conserved protein family of pyrophosphohydrolases that convert nucleoside diphosphate linked to another moiety **X** (NDP-X) resulting in the synthesis of the corresponding nucleoside monophosphate (NMP) and phosphorylated moiety X (P-X) [1].

Responsible for catalytic activity is the coordination and activation of divalent cations by the family-conserved NUDIX box motif located in the loop-helix-loop structural fold of the proteins, with Mg^{2+} as most prominent cation among the protein family members. The NUDIX box typically consists of a 23-amino acids sequence $Gx_5Ex_5[UA]xREx_2EEExGU$, where U represents an aliphatic, hydrophobic residue such as isoleucine, leucine or valine, and x can be any amino acid. The glutamine (E) residues REx_2EE in the core of the motif direct the binding of the individual cation. However, other amino acid side chains and structural motifs located in different parts of the NUDIX protein structure coordinate substrate specificity and binding. One structural motif responsible for substrate coordination is the family-specific NUDIX fold domain, an $\alpha/\beta/\alpha$ sandwich structural motif in the N-terminal region of the proteins (*Fig. 1B*).

With the discovery of the antimutagenic 8-oxo-(deoxy)guanine triphosphatase (8-oxo-(d)GTPase) MutT in *Escherichia coli* in 1954, the family was first known as MutT family and family members were considered to act as sanitising enzymes to prevent the accumulation and incorporation of toxic nucleotides and their corresponding metabolites [2,3]. Decades of research have, however uncovered a more versatile biological role of NUDIX hydrolases in metabolism and homeostasis as well as mRNA processing [1,4,5]. In addition, due to the high variability of substrates between family members as well as shared specificities to the same substrate of several NUDIX hydrolases, the exact biological functions of some family members have yet to be determined [4,6].

A



B

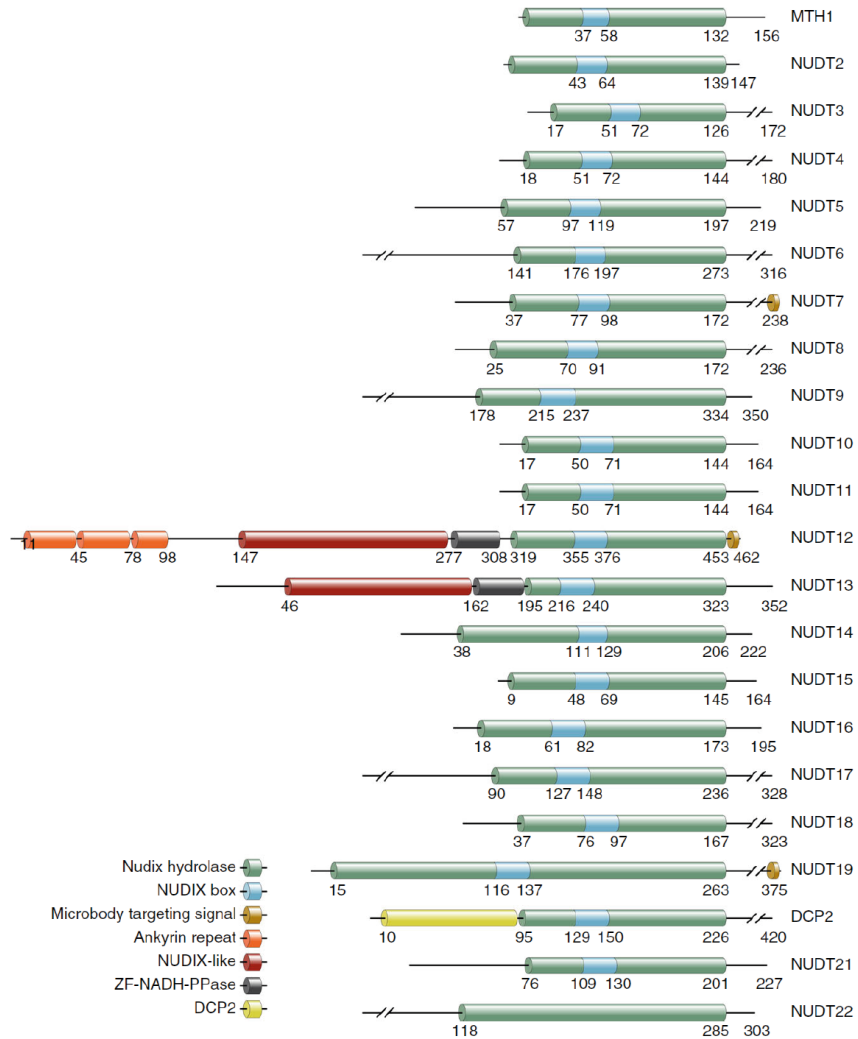


Figure 1. The human NUDIX protein family. **A** Phylogenetic analysis of protein structures of all 22 human NUDT22 family members revealed three groups in between the NUDIX protein family with NUDT22 as most distant outlier. **B** Comparison of the structural domains shows the family-preserved NUDIX box motif (light blue) inside the NUDIX hydrolase domain (green) as well as additional domains responsible for substrate specificity and biological function. However, the length of the NUDIX hydrolase domain as well as the localisation of the NUDIX box varies among the different family members. This figure is adapted from Carreras-Puigvert et al., 2017 [4].

The human NUDIX hydrolase family consists of 22 family members encoded by 24 genes and 5 pseudogenes with the human equivalent to MutT, MutT homologue 1 (MTH1) as hitherto best characterised family member (*Fig. 1*). MTH1 is encoded by *NUDT1* and hydrolyses the oxidised purine bases 8-oxo-dGTP, 2-oxo-(deoxy)adenosine triphosphate (2-oxo-(d)ATP) and 8-oxo-(deoxy)adenosine triphosphate (8-oxo-(d)ATP) to their corresponding monophosphates. To prevent DNA incorporation and genome instability, the corresponding monophosphates are rapidly degraded. Although MTH1 has the highest activity towards 2-oxo-dATP hydrolysis, due to the higher abundance of 8-oxo-dGTP, the hydrolysis of 8-oxo-dGTP is the most relevant mode of action of MTH1. MTH1 is therefore responsible for oxidised deoxynucleoside triphosphate (dNTP) pool sanitation and consequently, required for cell survival, especially under oxidative stress conditions [7,8].

Another NUDIX protein family member responsible for oxidised nucleotide sanitation is NUDT15, often referred to as MTH2. Similar to MTH1, NUDT15 is responsible for the hydrolysis of 8-oxo-(d)GTP albeit with lower activity. However, newer studies have revealed its preferred role as thiopurine metabolite hydrolase, thereby playing an important role in the anti-cancer efficacy of 6-thioguanine or 6-mercaptopurine, two standard-of-care treatments in leukaemia. More specifically, dephosphorylation of active thiopurine metabolites mediated through NUDT15 results in DNA incorporation prevention and a lack in cancer drug efficiency [9,10].

The family members NUDT5 and, to a lesser extent, NUDT9 are important key players in polyadenosine 5'diphosphoribose polymerase (PARP) activation in the DNA damage response as well as NAD⁺ pool recovery. Both NUDIX proteins catalyse the hydrolysis of modified nucleoside diphosphate esters such as adenosine 5'diphosphoribose (ADPR) resulting in ribose 5-phosphate and adenosine monophosphate (AMP), which is an important precursor for adenosine triphosphate (ATP) production [4,11]. Especially NUDT5 plays thus an important role in a multitude

of cellular processes such as cell proliferation, transcriptional regulation as well as chromatin remodelling [12].

Whereas several NUDIX family members are important regulators in DNA replication and energy metabolism, other members are important key players in RNA synthesis regulation. NUDT21 is a novel post-transcriptional regulator through its polyadenylation activity and important for RNA synthesis. In contrast, NUDT3, NUDT16 and Dcp2 (*NUDT20*) mediate mRNA degradation through their decapping activities [1,4].

Phylogenetic sequence analysis of both, the full length as well as the NUDIX fold domain of all NUDIX protein family members and available crystal structures revealed only recently the relationship between structure and activity by separating the family members into three general classes with the exception of the hitherto unstudied family member NUDT22 (*Fig. 1*). The three identified classes accurately represent the three main biological activities, diphosphoinositol polyphosphate phosphohydrolases (DIPP), NADH diphosphatases and diadenosine tetraphosphate (Ap_4A) binding proteins [4].

The upregulation of several NUDIX family members upon cellular stress and their genetic alterations in cancer versus normal tissue suggests a specific role of the protein superfamily in cancer and several family members are new and already established targets in cancer therapy (*Fig. 2*) [4,7,13]. The potential role of MTH1, NUDT2 and NUDT5 as anti-cancer target are discussed in the following (*Fig. 3*).

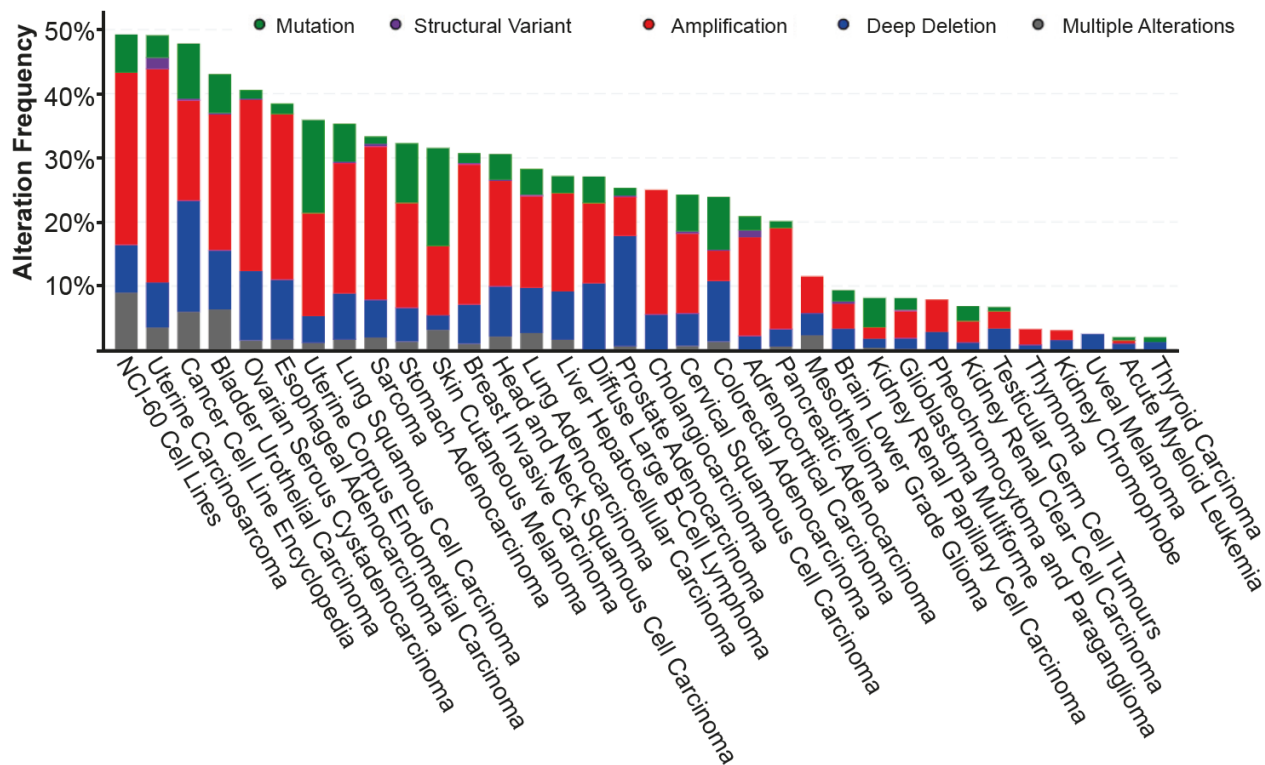


Figure 2. Overview of genetic alterations of NUDIX family members in cancer. Genetic alterations of all NUDIX family members in cancer were determined for selected subsets of The Cancer Genome Atlas (TCGA) and pan-cancer atlas data with cBioportal [14,15]. Mutations are displayed in green, structural variants in purple, amplifications in red, deep deletions in blue, and multiple alterations in grey.

In contrast to healthy tissue, cancer cells are especially prone to acquire malfunctioned redox regulation leading to reactive oxygen species (ROS) accumulation suggesting the importance of the NUDIX protein family member MTH1 for the prevention of free nucleotide and DNA damage due to oxidised nucleotide incorporation for cancer cell survival. Since *MTH1* genetic alterations as well as MTH1 protein expression was observed in several cancer tissues as determined by The Cancer Genome Atlas (TCGA) and Human Protein Atlas (HPA) analysis, targeting MTH1 was proposed as promising new strategy in cancer therapy (Fig. 3A) [14–16]. Several small molecule inhibitors were developed resulting in the identification of karonudib as most promising and potent MTH1 inhibitor in cancer cell and xenograft models, which is currently being evaluated based on its efficacy, safety and tolerability in leukaemia as well as patients with advanced solid malignancies in two clinical Phase I trials (NCT04077307, NCT03036228) [7,17–19].

Nevertheless, recent studies uncovered discrepancies in the proposed mode of action and target specificity of previously proposed specific and potent MTH1 inhibitors questioning the suitability of MTH1 as target in cancer therapy [20]. Whereas *MTH1* siRNA induced cytotoxicity in human drug resistant bladder cancer NTUB1/P, DLD1 and SW480 colorectal cancer cells, no cytotoxicity was observed upon *MTH1* depletion in osteosarcoma U2OS and human cervical HeLa suggesting context-specific effects [7,8,17,21]. In addition CRISPR-mediated *MTH1* knockout did not show impaired growth of SW480 cells questioning the previously proposed role of MTH1 in cancer [21].

When considering MTH1 small molecule inhibitors, controversial effects were mainly observed upon treatment with the inhibitors TH287, TH588 and (S)-crizotinib in cancer cell models. Even though the two first-in-class MTH1 inhibitors TH287 and TH588 were proposed to be target specific and to induce cytotoxicity via MTH1 inhibition through 8-oxo-guanine incorporation into the DNA, cytotoxic effects could not be rescued by *MTH1* overexpression and their activity towards tubulin polymerisation inhibition was uncovered as main mode of action *in vitro* only recently [7,22]. Another study confirmed off-target effects of TH588 and proposed potential off-target effects of (S)-crizotinib based on observed cytotoxicity in *MTH1* siRNA transfected U2OS cells [21]. One reason for the observed off-target effects of MTH1 inhibitors besides their previously considered target specificity and their proposed mode of action through 8-oxoguanine incorporation could be the use of modified comet assay to assess 8-oxoguanine incorporation. If tested molecules act through ROS induction production thereby, raising the content of oxidised nucleotides in the DNA, the observed increase in genomic 8-oxoguanine could be induced *in situ* through off-target activity rather than on-target activity [20].

However, the effects of *MTH1* depletion as well as inhibition were assessed in a multitude of different cancer and non-cancer cell lines with different concentrations and siRNA sequences making the comparison between individual studies challenging and the potential role of MTH1 as anti-cancer target has to be further investigated.

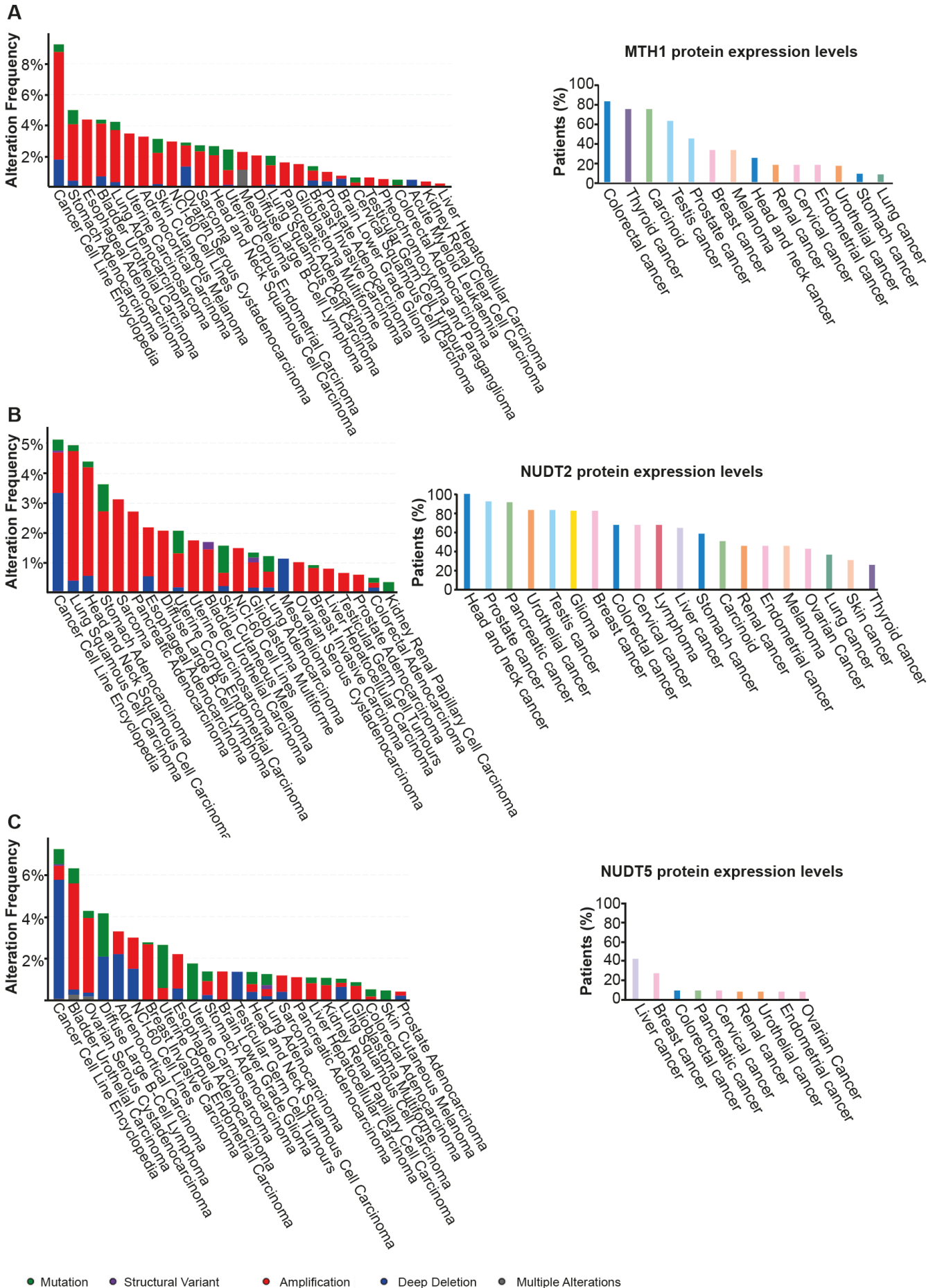


Figure 3. MTH1, NUDT2 and NUDT5 expression alterations in cancer. **A** *MTH1* genetic expression alterations in cancer based on The Cancer Genome Atlas (TCGA) (left). Overview of *MTH1* protein expression levels based on the Human Protein Atlas (HPA) stained with *MTH1* antibody HPA012636 (right). **B** Genetic expression alterations (left) as well as protein expression levels (right) of *NUDT2* based on analysis of TCGA and HPA (*NUDT2* antibody CAB004684), respectively. **C** Overview of *NUDT5* genetic alterations based on TCGA (left) as well as protein expression levels according HPA analysis (right, *NUDT5* antibody HPA019827) in cancer. For genetic alteration frequency determination, TCGA and pan-cancer atlas studies, NCI-60 cell lines and Cancer Cell Line Encyclopedia were selected and analysed with cBioPortal [14, 15]. Mutations are shown in green, structural variants in purple, amplifications in red, deep deletions in blue, and multiple alterations in grey, respectively. Figures showing protein expression levels were adapted from humanproteinatlas.org [16].

Another example of targeting the NUDIX protein family in cancer is the targeting of *NUDT5* with small molecule inhibitors in breast cancer [11]. *NUDT5* is especially high expressed in breast cancer tissue and associated with poor prognosis due to its role in cell proliferation, migration and invasion suggesting a promising new strategy to interfere with ADP-ribose metabolism as well as progesterin-dependent gene regulation through *NUDT5* inhibition [11, 12, 23]. More specifically, recent studies have identified *NUDT5* as a key player in nuclear ATP synthesis in breast cancer after stimulation with either oestrogen or progesterone leading to first, the synthesis of ADPR from poly(ADP-ribose) (PAR) by poly(ADP-ribose) glycohydrolase (PARG), which can then be transformed to ATP by *NUDT5* if a biphosphate is present [13]. Since ATP acts as co-factor of oestrogen and progesterone and both hormones have been linked to breast cancer development and growth, it is not surprising that high levels of *NUDT5* induce ATP-dependent breast cancer proliferation, chromatin remodelling and transcriptional changes resulting in poor prognosis in breast cancer patients [13, 24]. Targeting *NUDT5* is thus suggested to be especially interesting in patients with high *NUDT5* expressing and/or ER⁺ breast cancer since small molecule *NUDT5* inhibitors disrupt nuclear ATP synthesis thereby inhibiting hormone signalling and consequently cancer growth [11, 13]. Even though recent studies mainly focussed on the role of *NUDT5* as potential target in breast cancer, analysis of TCGA and HPA data revealed the presence of *NUDT5* genetic alterations as well as *NUDT5* protein expression in cancer in general suggesting that the described nuclear ATP synthesis mediated by *NUDT5* might also play additional hormone-independent roles in other malignancies (Fig. 3C). Both, target validation to better understand *NUDT5*'s role in cancer and non-cancer, and the suitability of targeting *NUDT5* with the developed small molecule inhibitors in breast cancer has thus to be further evaluated [11].

The Ap₄A hydrolase NUDT2 is another family member with a proposed role in breast cancer proliferation, invasion and metastasis. Recent studies have shown the correlation between the overexpression of *NUDT2* with poor clinical outcome in breast carcinoma patients suggesting its exploitation as both, prognostic factor as well as target in breast cancer therapy [25]. In addition, both genetic alterations as well as protein expression was observed in several cancer tissues when analysing NUDT2 RNA sequencing as well as protein expression TCGA and HPA data (*Fig. 3B*). However, NUDT2 is one of the less studied NUDIX proteins demonstrating the need of further research to better understand its mechanism as well as its potential role in cancer development and therapy.

The above examples of MTH1, NUDT5 and NUDT2 together with the observed gene expression alterations of other family members in cancer demonstrate the need for further exploration of other family members as targets in cancer therapy [4]. Due to the still limited knowledge of the exact biological functions of most of the NUDIX protein family members except MTH1, further research is required to uncover their specific roles in cancer and non-cancer metabolism.

1.1.2 NUDT22 is a UDP-glucose hydrolase

NUDT22 is an unstudied family member of the NUDIX protein superfamily. With the identification of guanosine diphosphate (GDP)-D-mannose as substrate of the *Arabidopsis thaliana* NUDT22 sequence homolog, the unique catalytic activity of human NUDT22 towards uridine diphosphate (UDP)-glucose and galactose was discovered in a nucleoside diphosphate (NDP)-sugars substrate screen. Interestingly, even though other NUDIX protein family members such as NUDT14 were previously reported to be involved in UDP-glucose and -galactose hydrolysis, it was recently shown that NUDT22's catalytic activity outperforms and is distinct among all NUDIX family members [26]. NUDT22 exhibits its catalytic hydrolase activity towards both, UDP-glucose as well as UDP-galactose resulting in the synthesis of uridine monophosphate (UMP) and, either glucose 1-phosphate (G1P) or galactose 1-phosphate (*Fig. 4B*) [26].

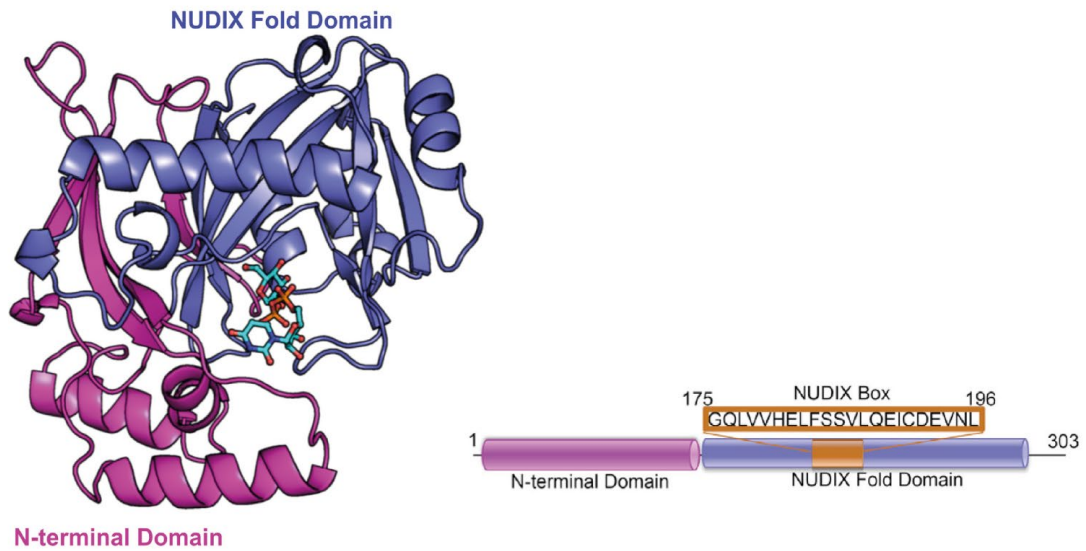
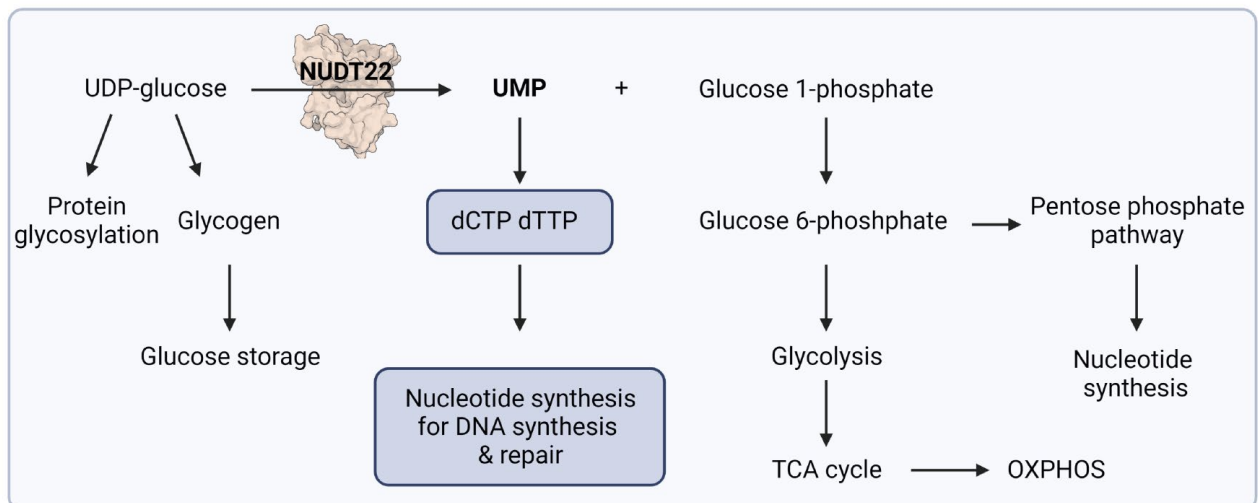
A**B**

Figure 4. NUDT22 is a UDP-glucose hydrolase. **A** Co-crystal structure of NUDT22 and uridine diphosphate (UDP)-glucose with N-terminal domain (magenta) and NUDIX fold (blue). Domain map of NUDT22 allocates NUDIX box (orange) in the NUDIX fold domain (blue). Adapted from Carter et al., 2018 [26]. **B** NUDT22 hydrolyses UDP-glucose to uridine monophosphate (UMP) and glucose 1-phosphate (G1P). UDP-glucose is required for glycogen synthesis, glucose storage and protein glycosylation. Both, UMP and G1P have roles in nucleotide synthesis and DNA replication and repair. G1P has additional roles in glycolysis and the TCA cycle. Figure was prepared with Biorender.com.

The identification of NUDT22's substrate specificity contributed to successfully solving the first crystal structures of NUDT22 alone as well as in complex with UDP-glucose (Fig. 4A). Both crystal structures confirmed the previously observed differences between NUDT22 and its family members in phylogenetic sequence analysis (Fig. 1A)

[4,26]. More specifically, NUDT22 inherits a partially conserved NUDIX fold domain; its structure however, contains an additional N-terminal fold, which is required for substrate binding and coordination and is unique among the NUDIX protein family. The NUDIX box motif is annotated to the residues AA175-197 located in the NUDIX fold and contains the two glutamine residues Glu189 and Glu193, which coordinate the divalent cation Mg^{2+} required for NUDT22 hydrolase activity (*Fig. 4A*) [26].

Even though the exact biological functions and significance of NUDT22 are largely unknown, the substrate of NUDT22, UDP-glucose as well as both, UMP and G1P, suggest important roles in a multitude of biological processes (*Fig. 4B*). UDP-glucose itself is directly required for both, protein glycosylation and glycogen synthesis, the latter being important for glucose storage as a quickly mobilised energy source upon high-energy required processes [27]. Glycogen storage has previously been identified in the liver and muscles but the distinct role of glycogen synthesis and storage in cancer has yet to be determined. However, recent studies suggest glycogen synthesis under high glucose conditions especially in hypoxic cancer cells as preparation for low nutrient and stress conditions and the consequent prevention of ROS formation and cell death. Furthermore, the transformation of glucose into glycogen, which is then further broken down for glycolysis, also known as glycogen shunt pathway, was proposed to be involved in tumour progression and metastasis [28].

UMP is the direct precursor for both pyrimidines deoxythymidine triphosphate (dTTP) and deoxycytidine triphosphate (dCTP), and therefore involved in DNA replication and repair processes as well as mRNA transcription. G1P can be further converted to glucose 6-phosphate (G6P) by phosphoglucosmutase (PGM) and is an important precursor for energy metabolism, oxidative phosphorylation as well as nucleotide synthesis through the pentose phosphate pathway (PPP) (*Fig. 4B*) [29–31]. More specifically G6P can directly enter glycolysis leading to the synthesis of the tricarboxylic acid (TCA) cycle precursor Acetyl Coenzyme A (Acetyl-CoA) via pyruvate production. The mitochondrial TCA cycle is an important pathway required for oxidative phosphorylation (OXPHOS) and ROS regulation (*Fig. 4B*) [29,30,32].

In addition, comparison of *NUDT22* gene expression in healthy versus tumour tissue by using RNA sequencing data of both, TCGA and HPA as well as NUDT22 protein expression in cancer tissue based on HPA, revealed the presence of NUDT22 in

several malignancies (*Fig. 5A/B*) [14–16]. More specifically, *NUDT22* mRNA was expressed in all 17 analysed carcinoma tissues, albeit at relatively low levels indicating low cancer specificity (*Fig. 5A*). The low cancer specificity based on *NUDT22* mRNA levels in cancer correlates with the low cancer cell line dependency as determined by the Cancer Dependency Map (DEPMAP) database. However, DEPMAP does not include non-cancer cell lines, which is especially important for the validation of a novel target in cancer therapy. Since *NUDT22* is a novel enzyme with a suggested role in nucleotide synthesis as well as energy metabolism, the effects of *NUDT22* depletion should be assessed in both, cancer and non-cancer cell lines to correctly assess *NUDT22* dependency in cancer. Large scale CRISPR/Cas9-based screens like DEPMAP often only run for a short amount of time, which could make it impossible for cancer or non-cancer cells to adapt to potential metabolic changes due to the loss of the corresponding gene and, consequently, protein of interest.

When comparing mRNA levels and protein levels of *NUDT22* in cancer, the presence of *NUDT22* mRNA levels could not be translated to *NUDT22* protein expression in cancer (*Fig. 5B*). Here, medium to high levels of *NUDT22* protein levels were detected in 9 out of 17 carcinoma types. However, protein levels of a maximum of 12 cancer patients of each carcinoma type were analysed, which could lead to a potential misinterpretation of the actual protein expression levels of *NUDT22* in cancer due to limited patient sample availability.

When considering genetic alterations of *NUDT22* in different cancer tissues, TCGA analysis of RNA sequencing data revealed the presence of *NUDT22* amplifications, mutations and deep deletions at different levels in cancer (*Fig. 5C*). Genetic alterations in cancer versus normal tissue play an important role in drug discovery processes and can contribute to target selection. For example, gene amplifications in cancer tissues could indicate a higher dependency or need for the target of interest in the specific cancer. *NUDT22* could thus play a role in pancreatic cancer, uterine carcinoma or prostate adenocarcinoma due to observed amplification frequencies. However, it could also mean that a certain chromosomal region was amplified and that the positive selection is due to other gene(s) on that region. In addition, genetic amplifications do not always translate into elevated protein expression levels and could therefore be misleading for target selection.

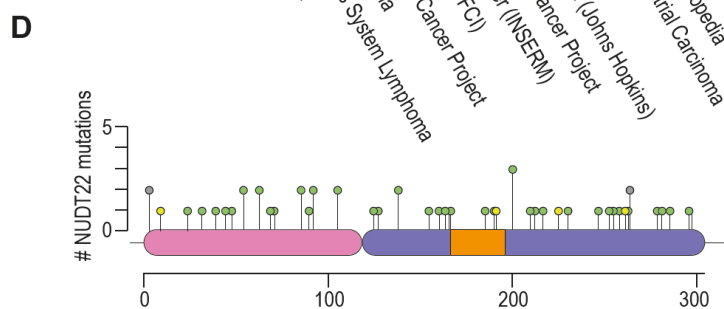
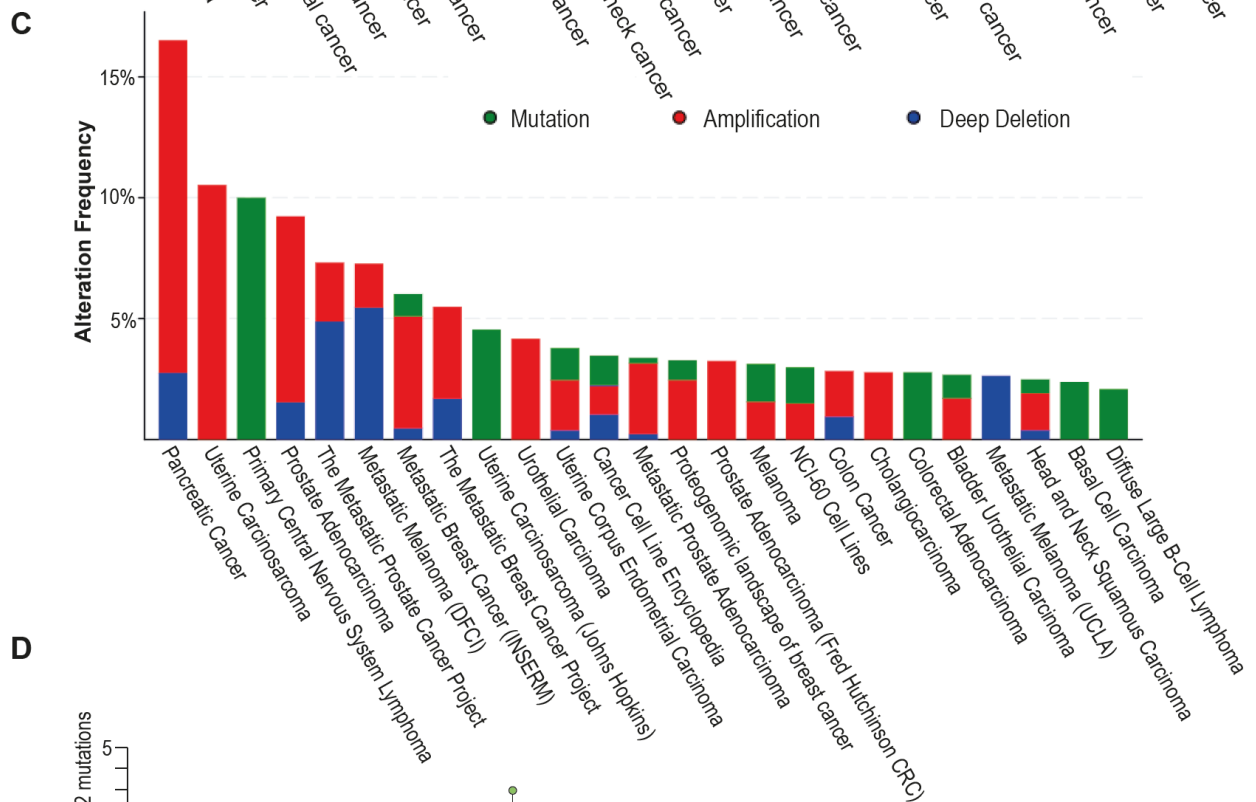
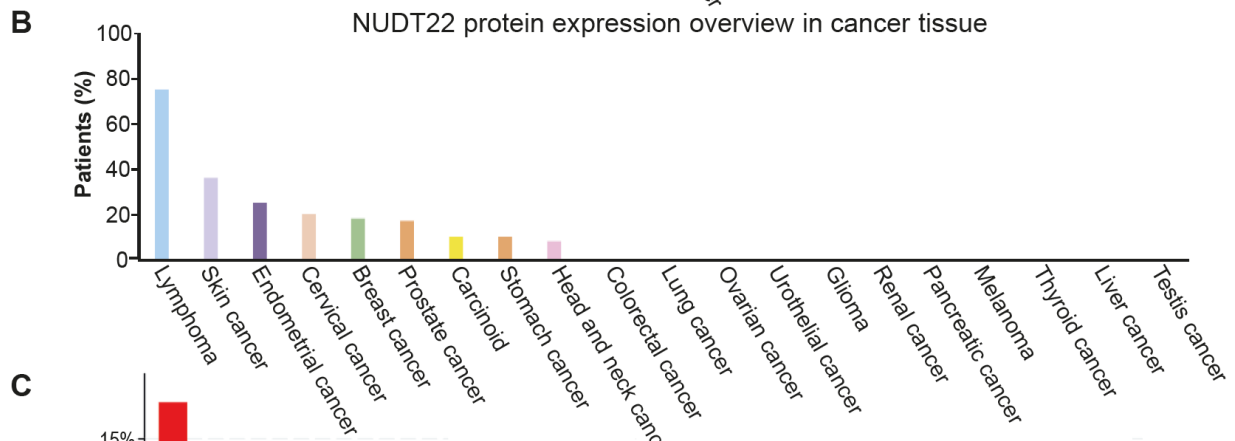
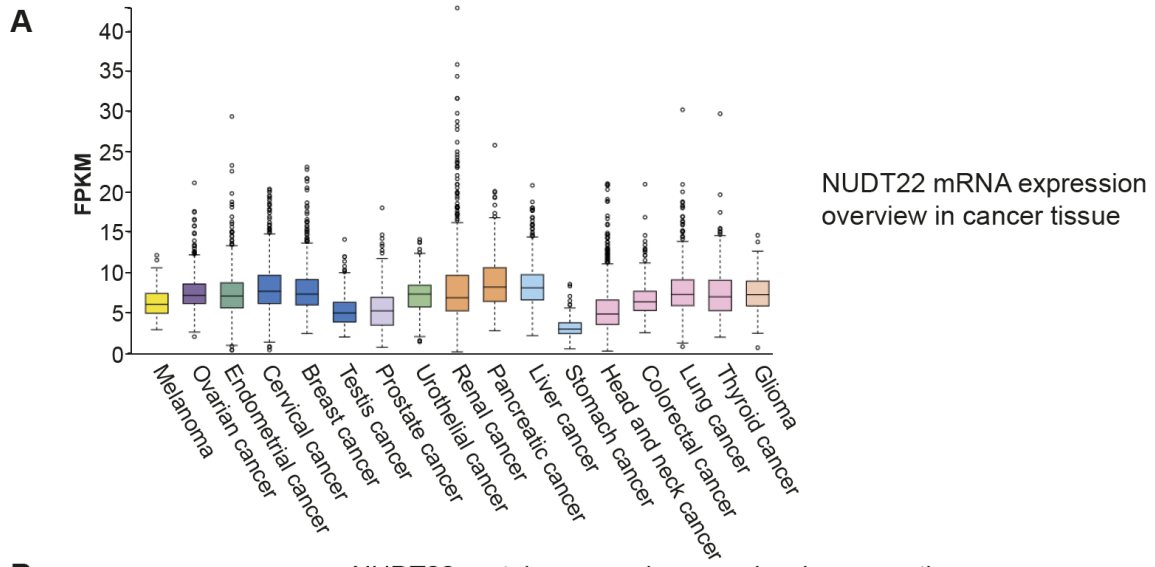


Figure 5. NUDT22 expression alterations in cancer. **A** *NUDT22* mRNA expression levels based on RNA-seq data of The Cancer Genome Atlas (TCGA) extracted from the Human Protein Atlas (HPA). RNA-seq data is presented in number Fragments Per Kilobase of exon per Million reads (FPKM). **B** *NUDT22* protein expression overview in cancer tissue based on the HPA. Protein expression of a maximum of 12 patients per cancer type were analysed and the percentage of patients with medium to high *NUDT22* protein levels are displayed in the bar chart. Figures displaying HPA data were adapted from humanproteinatlas.org and samples were stained with HPA039334 antibody [16] **C** Analysis of TCGA database with cBioportal revealed altered *NUDT22* expression levels in cancer [14,15]. Mutations are shown in green, amplifications in red and deep deletions in blue. **D** Lollipop scheme of *NUDT22* mutations allocated to specific regions of the protein structure with N-terminal domain (magenta), NUDIX fold (blue) and NUDIX box motif (orange) based on TCGA data and analysed with cBioPortal [14,15]. Green lollipop represents missense mutations with unknown significance, yellow lollipop splice mutations with unknown significance and grey lollipop truncating mutations with unknown significance.

Conversely, the presence of mutations or deep deletions could translate to differences or a lack in functionality of the gene of interest as well as changes in protein structure, which could impose difficulties in target validation and drug discovery. Especially mutations in regions involved in substrate binding or co-factor binding required for correct protein folding could lead to significant changes in protein functionality.

NUDT22 mutations are especially frequent in primary central nervous system lymphoma as well as uterine carcinoma. Deep deletions can be found in metastatic melanoma (*Fig. 5C*). Targeting *NUDT22* in these cancer tissues could therefore be less beneficial. When assessing the localisation of *NUDT22* mutations based on TCGA RNA sequencing data, several mutations are located in the N-terminal domain, NUDIX fold and NUDIX box motif albeit with unknown significance (*Fig. 5D*). Especially the mutations located in the N-terminal domain and in the NUDIX box motif, both required for correct substrate binding and therefore hydrolase activity, could indicate changes in protein conformation and catalytic activity.

Due to an increased need for nutrients and biomass, cancer cells can either upregulate or adapt different metabolic pathways to maintain fast cell proliferation. One example for the adaptation to a different pathway is the so-called Warburg Effect. Cancer cells acquire higher glucose uptake followed by a switch from TCA and OXPHOS towards glycolysis in presence of oxygen (aerobic glycolysis) to rapidly generate ATP and support biosynthesis of metabolites required for proliferation [29,33,34]. In addition, cancer cells can also adapt the more energy-efficient nucleoside salvage pathways for nucleotide synthesis and DNA replication to maintain cancer cell proliferation and survival [35].

Changes in nucleotide synthesis can lead to DNA replication stress and genome instability [36]. As metabolic pathway alterations as well as genome instability are described as hallmarks of cancer, changes in *NUDT22* gene expression levels as well as its involvement in a multitude of biological processes suggests the necessity to further explore its specific role in cancer and non-cancer [37–40].

1.2 Pyrimidine synthesis and cancer

This chapter includes the below listed published literature review with me as first author.

Walter, M.; Herr, P. Re-Discovery of Pyrimidine Salvage as Target in Cancer Therapy. *Cells* 2022, *11*, 739, doi:10.3390/cells11040739.

Re-Discovery of Pyrimidine Salvage as Target in Cancer Therapy

Melanie Walter  and Patrick Herr * 

Weston Park Cancer Centre, Department of Oncology and Metabolism, University of Sheffield, Sheffield S10 2RX, UK; mwalter3@sheffield.ac.uk

* Correspondence: p.herr@sheffield.ac.uk; Tel.: +44-114-215-9077

Abstract: Nucleotides are synthesized through two distinct pathways: de novo synthesis and nucleoside salvage. Whereas the de novo pathway synthesizes nucleotides from amino acids and glucose, the salvage pathway recovers nucleosides or bases formed during DNA or RNA degradation. In contrast to high proliferating non-malignant cells, which are highly dependent on the de novo synthesis, cancer cells can switch to the nucleoside salvage pathways to maintain efficient DNA replication. Pyrimidine de novo synthesis remains the target of interest in cancer therapy and several inhibitors showed promising results in cancer cells and in vivo models. In the 1980s and 1990s, poor responses were however observed in clinical trials with several of the currently existing pyrimidine synthesis inhibitors. To overcome the observed limitations in clinical trials, targeting pyrimidine salvage alone or in combination with pyrimidine de novo inhibitors was suggested. Even though this approach showed initially promising results, it received fresh attention only recently. Here we discuss the re-discovery of targeting pyrimidine salvage pathways for DNA replication alone or in combination with inhibitors of pyrimidine de novo synthesis to overcome limitations of commonly used antimetabolites in various preclinical cancer models and clinical trials. We also highlight newly emerged targets in pyrimidine synthesis as well as pyrimidine salvage as a promising target in immunotherapy.



Citation: Walter, M.; Herr, P. Re-Discovery of Pyrimidine Salvage as Target in Cancer Therapy. *Cells* **2022**, *11*, 739. <https://doi.org/10.3390/cells11040739>

Academic Editors: Laura Carrassa, Kumar Sanjiv and Maria Letizia Taddei

Received: 20 January 2022

Accepted: 18 February 2022

Published: 20 February 2022

Publisher's Note: MDPI stays neutral with regard to jurisdictional claims in published maps and institutional affiliations.



Copyright: © 2022 by the authors. Licensee MDPI, Basel, Switzerland. This article is an open access article distributed under the terms and conditions of the Creative Commons Attribution (CC BY) license (<https://creativecommons.org/licenses/by/4.0/>).

Keywords: nucleotide metabolism; cancer therapy; DNA replication; replication stress; pyrimidine salvage

1. Introduction

The essential building blocks of DNA, as well as RNA, consist of two classes of nucleotides, purines, and pyrimidines. Both nucleotides are composed of nucleobases such as the purine precursors adenine (A) and guanine (G), as well as the pyrimidine nucleobases thymine (T), cytosine (C), and uracil (U), respectively. These nucleobases are converted to nucleosides when linked to either ribose or deoxyribose, and nucleotides with the further addition of one to three phosphate groups to the purine or pyrimidine moiety.

Nucleotides are synthesized via two distinct pathways: the de novo synthesis, which utilizes amino acids and glucose, and the salvage pathway. The de novo biosynthesis of nucleotides is a highly energy-intensive multistep process using six to ten molecules of ATP per generated nucleotide and is the main source for nucleotide synthesis in non-malignant cells [1]. A multitude of dedicated enzymes regulates not only the generation of nucleosides but also maintains a fine balance in nucleotide pool composition through allosteric inhibitory mechanisms [2]. To maintain high proliferation, cancer cells can switch to the more energy-efficient nucleoside salvage pathways [1,3]. Whereas the role of purine salvage has been reviewed previously, the significance of pyrimidine salvage in cancer therapy has yet to be fully established [4–6].

With the discovery of pyrimidine de novo synthesis as an attractive target in cancer therapy more than two decades ago, various anti-cancer agents and pyrimidine analogs were developed and are still used in cancer therapy to date [7–10]. However, cancer cells can escape pyrimidine de novo synthesis inhibition by adapting the nucleoside salvage path-

ways leading to unsuccessful market approval of novel compounds as well as limitations of currently used anti-cancer agents [11–13].

Here we focus on pyrimidine synthesis in cancer therapy and discuss the recent re-discovery of targeting pyrimidine salvage to overcome observed limitations of currently used anti-cancer agents and pyrimidine analogs. Furthermore, we highlight co-targeting of pyrimidine de novo synthesis and salvage pathways as a novel strategy in cancer therapy.

2. Pyrimidine De Novo and Salvage Pathways

In mammalian cells, pyrimidines are derived through de novo synthesis as well as salvage pathways (Figure 1) [14,15]. Pyrimidine synthesis in healthy non-malignant fast proliferating cells relies predominantly on the de novo biosynthesis to maintain the demand of pyrimidines for successful DNA replication. In contrast, differentiated non-malignant cells use predominantly salvage pathways for the maintenance of pyrimidine synthesis [1,15].

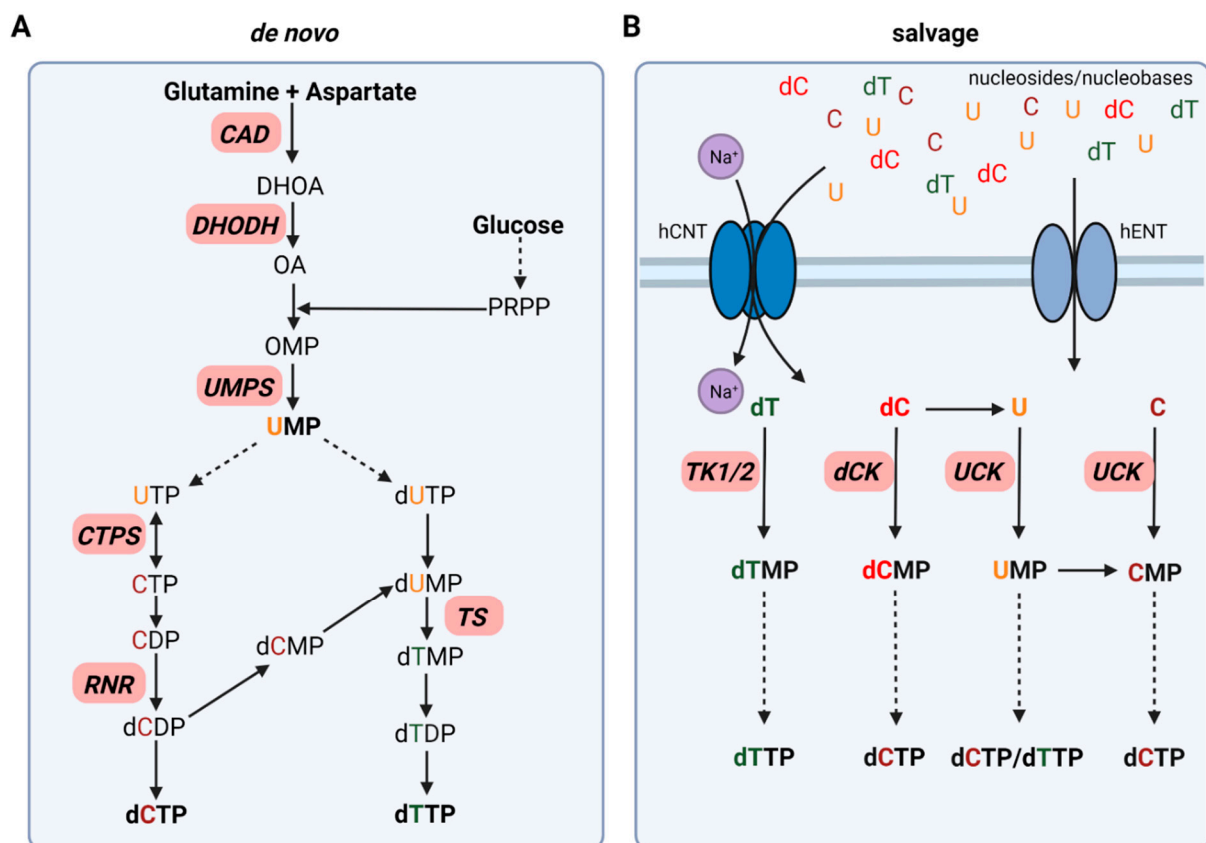


Figure 1. Simplified schematic of pyrimidine synthesis divided into de novo synthesis (A) and salvage pathways (B). Enzymes of interest for targeting approaches in cancer therapy are displayed in red. Solid arrows display direct steps in pyrimidine synthesis. Dashed arrows represent multiple steps leading to the synthesis of the corresponding pyrimidine. Created with [BioRender.com](https://www.biorender.com) (accessed on 20 January 2022).

Cancer cells have however frequently undergone metabolic rewiring to exploit the more energy-efficient pyrimidine salvage pathway to maintain faithful DNA replication in highly proliferating cells and, consequently, support genome integrity [1,15].

2.1. Pyrimidine De Novo Synthesis

Pyrimidine de novo synthesis requires glucose and the two amino acids glutamine and aspartate as starting points for the synthesis of both, deoxythymidine triphosphate (dTTP) and deoxycytidine triphosphate (dCTP). In the first committed step of pyrimidine

synthesis, the trifunctional enzyme CAD converts glutamine and aspartate to *N*-carbamoyl-aspartate and, dihydroorotate (DHOA) resulting in a pyrimidine ring formation. The mitochondrial membrane protein dihydroorotate dehydrogenase (DHODH) catalyzes the formation of orotate (OA), which is then transformed into orotidine monophosphate (OMP) upon addition of 5-phosphoribosyl-1-phosphate (PRPP). OMP is further metabolized to the main pyrimidine precursor uridine monophosphate (UMP) by UMP synthase (UMPS) (Figure 1A) [14].

For dCTP synthesis, UMP is phosphorylated to uridine triphosphate (UTP) via cytidine monophosphate kinase (CMPK) and nucleoside diphosphate kinase (NDPK) followed by the formation of CTP by the bidirectional CTP synthase (CTPS). After dephosphorylation of CTP to CDP by NDPK, CDP is further reduced to deoxycytidine diphosphate (dCDP) by ribonucleotide reductase (RNR). NDPK then catalyzes the formation of dCTP, which can then be incorporated in DNA (Figure 1A) [14].

In contrast to dCTP synthesis directly via RNR, dTTP synthesis is dependent on the formation of deoxythymidine diphosphate (dTDP) via deoxyuridine monophosphate (dUMP) formation. dUMP can be synthesized upon deoxyuridine triphosphate (dUTP) generation catalyzed by dUTPase, which is then dephosphorylated to dUMP. In addition, dUMP formation occurs upon the switch from dCMP to dUMP by deoxycytidylate deaminase (DCTD). Thymidylate synthase (TS), as well as deoxythymidine monophosphate (dTMP) kinase, are required to form dTMP and dTDP. NDPK phosphorylates dTDP to dTTP for DNA incorporation (Figure 1A) [14].

2.2. Pyrimidine Salvage Pathways

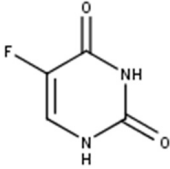
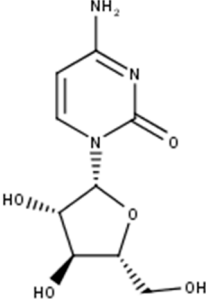
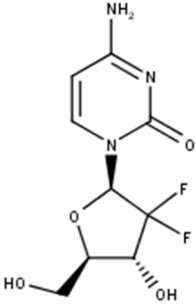
Pyrimidine salvage utilizes extracellular nucleosides and nucleobases via uptake from the bloodstream or intracellular recycled nucleic acids (UMP, CMP, TMP) derived from DNA and RNA degradation, to synthesize nucleotides for efficient DNA replication and repair as well as mRNA synthesis. Two different types of nucleoside transporter families have been identified: the Na⁺-dependent SLC28 family of concentrative nucleoside transporter (CNT) and the Na⁺-independent SLC29 family equilibrative nucleoside transporter (ENT) (Figure 1B) [16].

After cellular uptake, free pyrimidines are converted to their corresponding nucleoside and deoxynucleoside monophosphates (NMPs/dNMPs). Two enzyme classes are responsible for this process: deoxycytidine kinase (dCK) as well as the thymidine kinases (TKs) cytosolic thymidine kinase 1 (TK1) and mitochondrial thymidine kinase 2 (TK2). NMPs are then further phosphorylated to their corresponding deoxynucleoside triphosphates (dNTPs) as discussed above. Deoxycytidine (dC) can be converted to uracil (U) by cytidine deaminase (CDA), which is then further phosphorylated to UMP by UCK. In addition, this switch from C to U can also take place at the monophosphate level. DCTD, as mentioned previously, catalyzes the formation of UMP from CMP and, therefore, contributes to pyrimidine salvage (Figure 1B) [14].

3. Limitations of Targeting Pyrimidine De Novo Synthesis in Cancer

Pyrimidine synthesis and, more specifically, targeting the de novo pyrimidine synthesis pathways remains the backbone of cancer therapy for several decades. The hitherto most prominent group of anti-cancer agents are the so-called nucleoside analogs/anti-metabolites with 5-fluorouracil (5-FU), gemcitabine, and cytarabine as the most prominent pyrimidine analogs (Table 1) [17–20]. Nucleoside analogs are structurally similar to their physiological nucleoside counterparts and exhibit their mode of action either through incorporation into DNA or RNA or via inhibition of enzymes involved in the nucleotide de novo synthesis pathways.

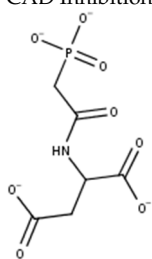
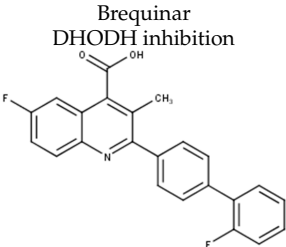
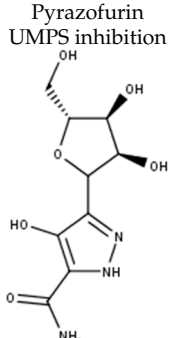
Table 1. Overview of pyrimidine de novo synthesis inhibitors used in cancer therapy.

Drug Name	Mode of Action	Current Use
5-Fluorouracil (Prodrugs: Floxuridine, capecitabine) 	Thymidylate synthase inhibition and RNA synthesis inhibition	Breast cancer Colon cancer Esophageal cancer Stomach cancer Pancreas cancer Head and neck cancer Premalignant skin cancer
Cytarabine (cytosine arabinoside) 	DNA incorporation	Acute myeloid leukemia (AML) Acute lymphocytic leukemia (ALL) Chronic myelogenous leukemia (CML) Lymphoma
Gemcitabine 	Inhibits ribonucleotide reductase (RNR) and DNA synthesis	Non-small cell lung cancer Gallbladder cancer Bladder cancer Breast cancer Ovarian Cancer Pancreatic cancer

The inhibition of CAD to impair pyrimidine de novo synthesis in the first committed step from glutamine was thought to be a promising strategy in cancer already in the early 1970s (Figure 1A). One of the most studied CAD inhibitors is *N*-(phosphonacetyl)-*L*-aspartate (PALA), which initially showed beneficial effects in vitro but failed in clinical studies later on (Table 2) [21–23].

In contrast to CAD inhibitors, several DHODH inhibitors including brequinar (BRQ) and teriflunomide as well as its prodrug leflunomide have reached market approval as immunosuppressive agents in rheumatoid arthritis and multiple sclerosis. As dihydroorotate dehydrogenase (DHODH) converts dihydroorotate to orotate in UMP de novo synthesis and antitumor properties were observed in several cancer tissues, the focus shifted towards DHODH as a target in cancer therapy (Figure 1A) [9,11,24]. Preliminary studies in vitro and in vivo showed promising results. However, the observed antitumor activity, as well as tumor growth inhibitory effects, could not be reproduced in Phase II clinical trials (Table 2) [25–29]. In recent years, multiple studies in different cancer cell and animal models, as well as patient-derived cancer cells and xenograft models, once again elucidated the importance of targeting DHODH alone or in combination with other anti-cancer agents. This renewed interest in DHODH has led to the development of new inhibitors as well as the re-discovery of BRQ and related agents. However, none of the novel nor already developed inhibitors has gained market approval for anti-cancer therapy so far [30–32].

Table 2. Overview of a selection of Phase II clinical trials of the CAD inhibitor PALA, the DHODH inhibitor Brequinar, and the UMPS inhibitor Pyrazofurin.

Drug Name and Mode of Action	Clinical Trials	Status	Observations and Side Effects
PALA CAD Inhibition 	<i>Kleeberg et al., 1982</i> Advanced breast cancer <i>Paridaens et al., 1982</i> Malignant melanoma	not approved	No response Mucocutaneous toxicity and diarrhea 7% complete response Mucocutaneous toxicity and ocular manifestations
Brequinar DHODH inhibition 	<i>Dodion et al., 1990</i> Metastatic colorectal cancer <i>Urba et al., 1992</i> Advanced squamous-cell carcinoma of the head and neck <i>Cody et al., 1993</i> Advanced breast cancer <i>Maroun et al., 1993</i> Advanced lung cancer <i>Moore et al., 1993</i> Advanced gastrointestinal cancer	not approved in cancer FDA-approved for rheumatoid arthritis and multiple sclerosis data	No response Severe toxicity, thrombocytopenia No response Moderate toxicity, thrombocytopenia, diarrhea 12% partial response Moderate toxicity 6% partial response Moderate toxicity, thrombocytopenia 3% response in colorectal carcinoma; 7% in gastric carcinoma; no response in pancreatic cancer Moderate toxicity; two treatment-related deaths
Pyrazofurin UMPS inhibition 	<i>Creagan et al., 1977</i> Advanced colorectal carcinoma <i>Nichols et al., 1978</i> Advanced breast cancer <i>Carroll et al., 1979</i> Advanced colorectal carcinoma	not approved	No response Nausea, vomiting, stomatitis No response Moderate to severe stomatitis, thrombocytopenia No response Normochromic normocytic anemia

Pyrazofurin is a nucleoside analog that inhibits the orotidine monophosphate decarboxylase function of UMPS and showed initially promising results in in vitro studies in several cancer cell lines (Figure 1A). Nevertheless, in the late 1970s, it has failed to proceed beyond Phase II clinical trials in several cancers due to lack of efficacy and severe toxicity (Table 2) [33–37].

Targeting thymidine synthase (TS) with 5-FU or its prodrug capecitabine remains the backbone of anti-cancer therapy with its greatest impact in the prolongation of overall survival in advanced colorectal cancer (Table 1; Figure 1A) [20,38]. After uptake into the cell, 5-FU is metabolized to its active metabolites fluorodeoxyuridine monophosphate (FdUMP), and fluorouridine triphosphate (FUTP). Whereas FUTP impairs RNA synthesis via its incorporation into mRNA, FdUMP covalently inhibits TS resulting in pyrimidine synthesis disruption and cancer cell death [20]. Even though 5-FU is still widely used in clinical practice, it comes with certain limitations such as low response rates as well as resistance in cancer patients [13,20].

One of the main reasons why initial in vitro findings of most inhibitors of the pyrimidine de novo synthesis could not be translated in clinical studies and the observed low response rates of cancer patients is the ability of cancer cells to exploit the more energy-efficient nucleoside salvage pathway to escape pyrimidine de novo synthesis inhibi-

tion [2,9,11,39–41]. Pyrimidine salvage utilizes free nucleosides present in the extracellular tumor environment to maintain efficient DNA replication and cell proliferation. Uridine concentrations in human plasma and serum range from 5–20 μM , which makes it the most dominant circulatory pyrimidine when compared to plasma levels of the other two pyrimidines cytidine and thymidine with 0.6 μM and 0.2 μM , respectively [42]. Uridine is not only the most prominent circulatory pyrimidine but also the most prominent nucleoside when compared with physiological purine plasma levels of approximately 0.5 μM for adenosine and 0.9 μM for guanosine [43,44]. This highlights the need for novel strategies targeting the pyrimidine salvage pathways.

4. Pyrimidine Salvage as Target in Cancer Therapy

Previous strategies to exploit pyrimidine de novo synthesis inhibition suffered mostly from the unsuccessful translation of in vitro and in vivo findings to clinical trials. The cell's ability to shift to pyrimidine salvage to maintain DNA replication and cell proliferation opened up a new field of novel targets in pyrimidine synthesis.

4.1. Nucleoside Transporter

Nucleoside transporters (NTs) are transmembrane proteins for the import and export of free nucleosides and nucleobases from the extracellular environment of cancer and non-cancer cells and, thus, are involved in nucleoside salvage (Figure 1B). NTs are members of the solute carrier protein family and are classified in two structural unrelated NT families; the human concentrative transporter (hCNT; SLC28) and the human equilibrative transporter family (hENT, SLC29). Substrate specificity, uptake efficiency, expression levels, and location of NTs vary between the different transporter families as well as between family members. Whereas hCNTs are Na^+ -dependent unidirectional nucleoside import pumps that transport nucleosides against their concentration gradients, hENTs function as bidirectional Na^+ -independent NTs [45–50].

Even though all three members of the CNT family transport uridine as well as both, hCNT1 and hCNT3 transport all pyrimidines; recent studies suggest the role of hCNTs as transceptors in nucleoside sensing and signal transduction instead of nucleoside homeostasis [51]. Together with the observed decrease or loss in hCNT1 expression in different tumors and the lack of currently developed hCNT inhibitors, nucleoside uptake and thus nucleoside homeostasis via hENTs remains the target of interest to inhibit pyrimidine uptake and therefore salvage in anti-cancer therapy [52,53]. Out of the four hENT family members, only hENT1 and hENT2 are widely expressed at cell plasma membranes of various tissues and both are required for pyrimidine transport [54]. Furthermore, hENT2 was identified as a key element to maintain the supply of nucleosides and nucleotides for DNA replication and cell cycle progression [55].

The two hENT transporters can be differentiated by their activity towards the nucleoside analog nitrobenzylmercaptapurine riboside (NBMPR), a potent hENT1 inhibitor and nucleoside analog (Figure 2A,D) [49].

Already in the 1980s and 1990s, the vasodilators dipyridamole and dilazep were identified to inhibit nucleoside transport via targeting hENT1 and, however less potent, hENT2 (Figure 2A,D) [56–58]. Even though targeting nucleoside uptake in combination with other cytotoxic agents was thought to be a promising anti-cancer strategy, clinical phase I studies did not show the desired efficacy, and targeting nucleoside uptake moved out of the focus [59–64]. Only recently, the potential of dipyridamole to reduce triple-negative breast cancer progression and metastasis in xenograft models was uncovered, which has to be further evaluated in clinical trials [65].

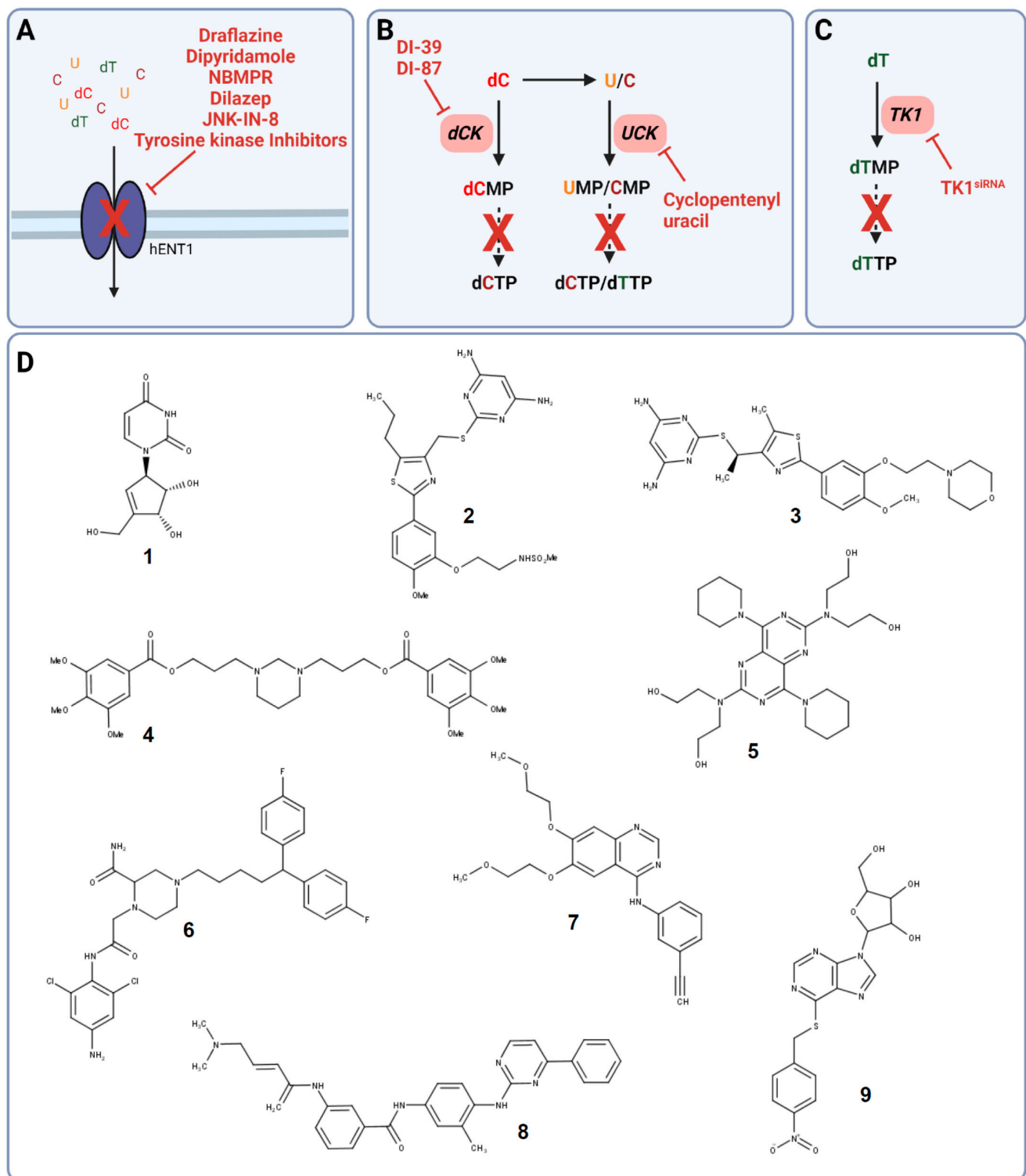


Figure 2. Targets in pyrimidine salvage and their corresponding inhibitors. (A) Inhibition of pyrimidine uptake transporter hENT1. (B) Targeting of either dCK with DI-39 and DI-87 or UCK with cyclopentenyl uracil. (C) Silencing of *TK1* with TK1siRNA leads to dTTP synthesis inhibition. (D) Chemical structures of cyclopentenyl uracil (1), DI-39 (2), DI-87 (3), the tyrosine kinase inhibitor erlotinib (4), dilazep (5), dipyridamole (6), draflazine (7), JNK-IN-8 (8), and nitrobenzylmercaptapurine riboside (NBMPR) (9). Solid arrows are direct steps and dashed arrows represent multiple steps in pyrimidine salvage. Created with [BioRender.com](https://www.biorender.com) (accessed on 20 January 2022).

The failure of dipyridamole in the clinics can be explained by its observed binding to serum protein α_1 -acid glycoprotein (AGP) causing insufficient target engagement and, therefore, the low response rate in vivo as well as in cancer patients [63,64]. To overcome the observed limitations, new chemically optimized hENT1 and hENT2 inhibitors were developed and identified. Structural analogs of the platelet aggregation and hENT1 inhibitor draflazine were developed to prolong the drug resiliency time leading to improved binding affinity as well as kinetic properties compared to dipyridamole and dilazep (Figure 2A,D) [66]. Furthermore, screens to assess off-target effects of tyrosine kinase inhibitors revealed the potential of several tyrosine kinase inhibitors such as lorlatinib, gefitinib, vandetanib, and erlotinib to not just inhibit their designated target but also hENT1 causing nucleotide transport inhibition in non-cancer and cancer cells (Figure 2A,D) [67–69]. In addition, hENT1 inhibition and, thus, impaired nucleoside uptake was observed upon treatment with the C-Jun N-terminal kinase (JNK) inhibitor JNK-IN-8 in pancreatic cancer cells demonstrating another potential drug class to target pyrimidine salvage in cancer (Figure 2A,D) [70].

4.2. Uridine-Cytidine Kinase and Deoxycytidine Kinase

After uptake of free uridine from the extracellular tumor environment, UCK phosphorylates uridine to UMP, the main precursor for dUTP, dCTP, and dTTP (Figure 1B). Whereas UCK is also required for the direct phosphorylation of cytidine, dCK phosphorylates deoxycytidine, representing another way to synthesize dCTP for DNA synthesis and replication (Figure 1B).

Uridine has been shown to have a significant role in countering pyrimidine de novo inhibition by several anti-cancer agents, leading to unsuccessful clinical trial outcomes. Already in the mid-1980s and early 1990s, targeting of UCK by small molecule inhibitors was proposed as a novel strategy in several cancers. Cyclopentenyl uracil was identified as a selective inhibitor for UCK, reducing the salvage of uridine and to lesser extent cytidine, making it an interesting candidate for use as chemotherapeutic (Figure 2B,D) [12,71].

However, even though cyclopentenyl uracil and other UCK and dCK inhibitors were identified and their potential use as anti-cancer agents was proposed, this approach was not followed up until recently with the discovery of the link between dCK and replication stress in acute lymphoblastic leukemia (ALL). The knockout of dCK and, therefore, impaired pyrimidine salvage in mouse models of hematological cancer, induced replication stress followed by S phase arrest and DNA damage in hematopoietic progenitors due to a decreased dCTP pool [2]. This observation resulted in the development of the small molecule dCK inhibitor DI-39, which induced replication stress in ALL cancer cell models through dCTP depletion (Figure 2B,D) [72].

Even though DI-39 showed promising results as a single agent and more prominently as combination therapy with other inhibitors of pyrimidine de novo synthesis in ALL cancer cells and mouse models, DI-39 has limited solubility and metabolic stability due to a short half-life in vivo leading to the development of additional dCK inhibitors with DI-87 being the most promising candidate (Figure 2B,D) [73,74]. The newly developed small molecule DI-87 showed promising pharmacological effects in vitro as well as in vivo ALL models [73].

4.3. Thymidine Kinases as a Prognostic Biomarker and Anti-Cancer Target

Thymidine kinases (TKs) convert free thymidine after its uptake from the extracellular matrix into thymidine monophosphate, which is then further phosphorylated and incorporated into the DNA (Figure 1B). There are two thymidine kinase genes in humans, encoding for the cytosolic cell-cycle dependent TK1 and the mitochondrial TK2. TK2 is continuously expressed in low amounts during the cell cycle whereas TK1 expression and abundance are increased in the S/G2 phase in proliferating cells [75,76]. TK1 expression is upregulated during the early stages of cancer development and elevated levels are detected in the serum of cancer patients making it an ideal biomarker [77–80]. Several studies showed that high

expression of *TK1* correlates with poor prognosis, reduced overall survival, and relapse in patients with lung, breast, or pancreatic cancer [81–83].

Silencing of *TK1* decreased cell proliferation in vitro and in vivo in pancreatic ductal adenocarcinoma (PDAC) cell lines suggesting the exploitation of *TK1* not just as a biomarker but also as a potential anti-cancer target (Figure 2C) [82]. In addition, *TK1* silencing in thyroid carcinoma cell lines caused a decrease in cell proliferation, invasion, and migration and induced apoptosis. These findings were supported by inhibition of tumor growth in thyroid carcinoma xenograft studies, further highlighting the role of *TK1* in cancer [84]. Strikingly, there are no *TK1* inhibitors for the use in cancer described in the literature so far.

With the recent discovery that *TK1* localizes to the plasma membrane of malignant cells only, *TK1* is now also considered a potential anti-cancer target suitable for immunotargeting [85,86]. Consequently, the effects of monoclonal antibodies targeting *TK1* were evaluated in lung, breast, colon, and prostate cancer cell models. The binding of *TK1* monoclonal antibodies to their corresponding *TK1* epitopes was observed in all cancer cell models but not in normal lymphocytes suggesting the suitability of anti-*TK1* antibodies as a highly specific targeting approach in malignant cells. Furthermore, monoclonal antibodies could potentially be exploited to detect *TK1* on tumor cells, and, therefore, determine tumor burden in cancer patients in a diagnostic approach. Furthermore, anti-*TK1* antibodies induced cytolysis of lung and breast cancer cells by effector cells demonstrating the potential to be used as immunotargeting agents to eliminate high *TK1* expressing tumor cells in cancer therapy [87]. However, this approach has not been evaluated in animal models so further studies are required to determine the translational aspect of targeting *TK1* with monoclonal antibodies in cancer.

In contrast to *TK1*, the mitochondrial thymidine kinase *TK2* has lower substrate specificity. In addition to phosphorylating thymidine, *TK2* can also phosphorylate deoxycytidine to dCMP the precursor for dCTP [88,89]. The deoxycytidine analog gemcitabine (2',2'-difluoro-2'-deoxycytidine; dFdC) is activated through the activity of another pyrimidine salvage pathway enzyme dCK via conversion to the monophosphate required for active gemcitabine metabolite formation [90]. However, a high level of dCTP leads to decreased cytotoxicity and anticancer activity of gemcitabine due to the negative feedback regulation of dCK activity [91]. Diminishing dCTP synthesis via *TK2* siRNA knockdown caused an increase in anti-proliferative activity of gemcitabine upon an increase in dCK levels in cervical carcinoma as well as breast cancer cell models in vitro. This effect was not observed upon the siRNA-induced knockdown of the pyrimidine de novo synthesis enzyme TS suggesting not just a potential role of *TK2* as an anti-cancer target but also its specific role in gemcitabine resistance [92].

5. Co-Targeting of Pyrimidine De Novo Synthesis and Salvage Pathways to Overcome Limitations of De Novo Synthesis Inhibitors

Uncovering the impact of pyrimidine salvage in the rescue of pyrimidine de novo synthesis inhibition as well as its potential as an anti-cancer target resulted in the rationalization of new strategies to co-target pyrimidine de novo synthesis and salvage pathways to overcome the limitations of targeting pyrimidine de novo inhibition alone already in the 1980s and 1990s [11,12]. Simultaneous inhibition of uridine salvage with cyclopentenyl uracil and pyrimidine de novo synthesis with the CAD inhibitor PALA increased cancer cell death in mouse models further highlighting the impact of nucleoside salvage on the efficacy of anti-cancer agents targeting de novo synthesis. Co-targeting pyrimidine salvage and de novo synthesis were therefore suggested to be beneficial in anti-cancer therapy [12]. As an example, co-targeting of DHODH with BRQ and nucleoside transport with dipyridamole increased the efficiency of DHODH in vitro and in vivo [11].

Even though preliminary results in vitro and in vivo demonstrated synergy of pyrimidine de novo synthesis and salvage inhibition leading to a beneficial response compared to pyrimidine de novo synthesis inhibition alone, this strategy was not followed up until recently.

5.1. Co-Targeting De Novo Pyrimidine Synthesis and Nucleoside Uptake

Even though anti-cancer agents targeting pyrimidine de novo synthesis via DHODH inhibition failed to prove their effectiveness in clinical trials, with advancing technologies and methodologies such as gene expression profiling and metabolomics, the importance of DHODH as a target in cancer was rediscovered. Consequently, an old approach to overcome the observed adaptations towards nucleoside salvage in cancer cells to escape growth inhibition was once again investigated [11].

Several studies proposed co-targeting DHODH with BRQ and nucleoside uptake via hENT1/2 with dipyridamole in different cancer cell models (Figure 3A). Synergistic effects were observed in colon cancer and pancreatic cancer cells [40,93,94]. However, the in vitro findings in colon cancer and pancreatic cancer cells could not be translated in in vivo xenograft cancer models due to no significant differences in tumor sizes after co-treatment with BRQ and dipyridamole compared to BRQ alone [40].

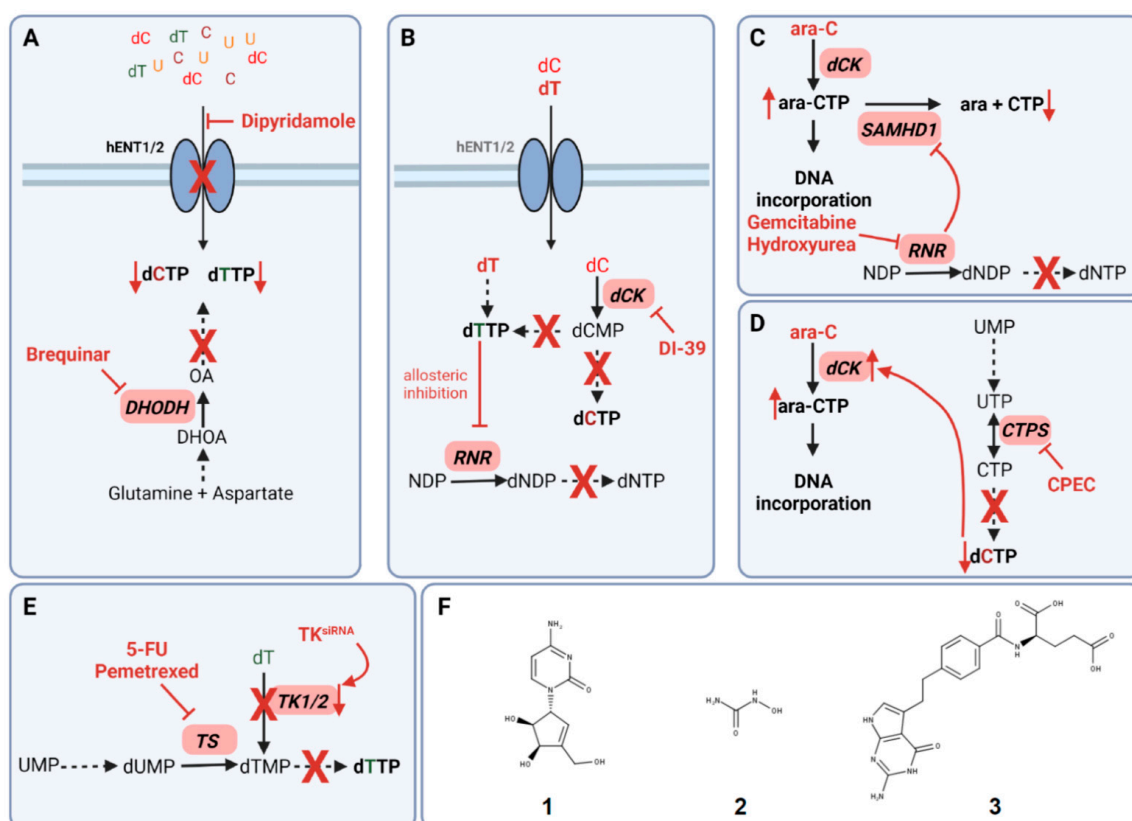


Figure 3. Principles of co-targeting pyrimidine de novo synthesis and salvage pathways. (A) Simultaneous targeting of pyrimidine uptake with dipyridamole and DHODH with brequinar. (B) Targeting of both, RNR via allosteric inhibition with TTP synthesized via dT addition, and dCK with DI-39. (C) RNR inhibition with gemcitabine or hydroxyurea results in non-allosteric inhibition of the ara-CTPase SAMHD1 leading to an increase in ara-CTP DNA incorporation. (D) CTPS inhibition with cyclopentenyl cytosine (CPEC) leads to an increase in dCK activity followed by increased ara-CTP DNA incorporation. (E) dTTP synthesis inhibition via co-targeting of TS with 5-fluorouracil (5-FU) or pemetrexed and siRNA knockdown of TK1/2. (F) Chemical structures of CPEC (1), hydroxyurea (2), and pemetrexed (3). Solid arrows represent direct steps in the pathway. Dashed arrows display multiple steps leading to metabolite synthesis. Created with [BioRender.com](https://www.biorender.com) (accessed on 20 January 2022).

DHODH was identified to be an effective target in *MYCN*-amplified neuroblastoma cell lines and mouse neuroblastoma models. However, in contrast to the combination of BRQ and dipyridamole, DHODH inhibition with BRQ did not cause the suppression of

proliferation and tumorigenicity of neuroblastoma cell lines when subjected to physiological uridine levels demonstrating again the need for co-targeting pyrimidine salvage. In addition, neuroblastoma growth was suppressed in animal models when subjected to co-treatment with BRQ and dipyridamole [94].

Synergistic effects of DHODH and hENT1/2 inhibition were also observed in acute myeloid leukemia (AML). Whereas the newly developed DHODH inhibitor MEDS433 had limited efficacy *in vitro* when subjected to physiological concentrations of uridine, combining DHODH inhibition and dipyridamole caused an increase in toxicity and, therefore, cell death in AML cells but not in non-cancer cells. High apoptotic rates were also observed in patient-derived primary AML cells suggesting the suitability of co-targeting DHODH and hENT1/2 in AML, which has to be further confirmed *in vivo* [93].

However, when combining pyrimidine *de novo* synthesis inhibitors with inhibitors of nucleoside uptake, the choice of *de novo* inhibitor is crucial. NTs and, more specifically, hENT1/2 are not only required for the uptake of free nucleosides and nucleobases but also the uptake of nucleoside analogs [53,95,96]. Consequently, nucleoside analogs such as gemcitabine that are depending on the uptake via hENT1/2 should not be used for combination therapy with dipyridamole or related compounds to maintain their activity and, thus efficacy in cancer therapy [95].

5.2. Co-Targeting of Ribonucleotide Reductase and Deoxycytidine Kinase

In pyrimidine *de novo* synthesis, ribonucleotide reductase is responsible for dCDP synthesis, which is then further converted to dCTP for DNA and RNA synthesis (Figure 1A). RNR activity can be impaired by either direct targeting with anti-cancer agents such as hydroxyurea or gemcitabine or via allosteric regulation upon dTTP levels (Figure 3B) [2,97]. More specifically, upon a high concentration of dTTP, RNR activity is inhibited through binding of dTTP to its regulatory site disabling CDP binding and, thus, interrupting dCTP *de novo* synthesis [2]. This regulation of RNR was exploited as a strategy in cancer therapy through the treatment with dT as a single dCTP-depleting agent via dTTP synthesis by TK1. However, clinical trials showed only limited efficacy due to the ability of cancer cells to exploit pyrimidine salvage for successful dCTP synthesis [2,98–100].

The ability of cancer cells to switch from pyrimidine *de novo* synthesis via RNR to pyrimidine salvage, to maintain efficient DNA synthesis, and to escape allosteric RNR inhibition with dT resulted in the development of a strategy to co-target RNR and the pyrimidine salvage enzyme dCK.

Simultaneous targeting of dCK with the small molecule inhibitor DI-39 and RNR with dT in acute lymphoblastic leukemia (ALL) cancer cells induced replication stress and apoptosis confirming synergy between *de novo* dCTP inhibition and pyrimidine salvage inhibition (Figure 2B). These findings were successfully translated to ALL *in vivo* models, where co-treatment with DI-39 and dT caused a decrease in tumor size with limited host toxicity [72].

These findings could also be replicated in glioblastoma cell lines. However, not all glioblastoma cell lines were sensitive towards simultaneous *de novo* pyrimidine synthesis and pyrimidine salvage inhibition highlighting the need for personalized treatment strategies for glioblastoma cancer patients. The effects of targeting dCTP *de novo* synthesis with DI-39 and salvage with dT could not be assessed *in vivo* due to poor blood–brain barrier penetration of both anti-cancer agents. To further investigate targeting both pyrimidine synthesis pathways in glioblastoma, alternatives for DI-39 and dT with good blood–brain barrier penetration abilities will have to be developed [101].

5.3. Co-Targeting of SAMHD1 and RNR to Sensitize Cells towards Cytarabine

With the discovery of the ara-CTPase activity of the dNTP triphosphohydrolase SAM and HD domain-containing protein-1 (SAMHD1) resulting in limited ara-C activity in SAMHD1⁺ cancer cells as well as xenograft models, SAMHD1 was proposed as a novel target in AML patients [102–104]. The deoxycytidine analog cytarabine (ara-C)

in combination with anthracyclines remains the standard of care in AML patients [105]. After cellular uptake, dCK converts ara-C to its active metabolite ara-CTP, which is then incorporated in DNA leading to DNA damage by perturbing DNA synthesis [106]. However, a lack in response followed by relapse and treatment failure is often observed through the unsuccessful accumulation of ara-CTP demonstrating the need for novel strategies in AML treatment in adults and children [105,106]. Several small-molecule SAMHD1 inhibitors were developed in silico and validated in enzymatic assays; however, none of them demonstrated cellular activity [107,108].

As small molecules failed to inhibit SAMHD1 in vitro, a novel approach was required to sensitize AML cancer cells and xenograft models to cytarabine. Successful targeting of SAMHD1 resulting in increased sensitivity of ara-C could be achieved with the simian immunodeficiency virus (SIV) protein Vpx in AML cell and xenograft models as well as in primary AML patient-derived blasts [103,109]. Vpx results in labeling SAMHD1 for proteasomal degradation and reduces SAMHD1 protein levels [110].

The recent discovery of RNR as a regulator of SAMHD1 activity enabled a novel strategy to overcome the limitations of ara-C. SAMHD1 ara-CTPase activity is dependent on dNTP binding to the regulatory site of the enzyme. Upon RNR inhibition, dNTP synthesis is disabled causing an imbalance in dNTP pools and a decrease in SAMHD1 activity. Pyrimidine RNR inhibitors such as hydroxyurea and gemcitabine were identified to improve ara-C efficacy in *SAMHD1* expressing in vitro and in vivo models as well as in primary patient-derived blasts ex vivo. Surprisingly, no synergistic effects of RNR inhibition with purine analogs and ara-C were observed demonstrating the importance of pyrimidine de novo synthesis in the response rates of AML patients to ara-C (Figure 3C,F) [109].

5.4. Targeting of CTPS to Potentiate Gemcitabine and Cytarabine DNA Incorporation

The two human CTPS isoforms, CTPS1 and CTPS2 interconvert UTP to the dCTP precursor CTP as the rate-limiting step in pyrimidine de novo synthesis for successful DNA synthesis to maintain cell proliferation (Figure 1A) [111,112]. Already in the 1970s and 80s, CTPS was suggested to be an attractive target in anti-cancer therapy due to its observed increase in activity leading to elevated CTP levels in lymphocytic and non-lymphocytic leukemia, liver as well as renal carcinoma, and in a variety of other cancers [113–115]. With the discovery of increased levels of CTPS1 in lymphoblastic as well as other cancer tissues compared to the unchanged levels of CTPS2 in malignant and healthy tissue, targeting CTPS1 has received renewed interest only recently [116–119]. More specifically, proteomics analysis of triple-negative breast cancer (TNBC) patient samples revealed an increased expression of CTPS1 compared to para-tumor tissue, which is accompanied by a decrease in disease-free and overall survival of TNBC patients with high levels of CTPS1. CTPS1 silencing in TNBC cancer cell lines decreased proliferation, migration, and invasion as well as increased apoptosis. Furthermore, a reduction in tumor growth was observed in TNBC xenografts upon CTPS1 silencing [116]. Consequently, selective targeting of CTPS1 with small molecules could be a promising new anti-cancer strategy.

The first identified CTPS inhibitor cyclopentenyl cytosine (CPEC) showed initially promising anti-tumor activity in human colon carcinoma, pediatric acute lymphocytic leukemia (ALL) as well as in patient-derived pediatric acute non-lymphocytic leukemia (ANLL) cells (Figure 3F) [120–123]. Furthermore, CTPS inhibition with CPEC caused a decrease in tumor burden in colon carcinoma and leukemia xenograft models [122,123].

Since ara-C and gemcitabine efficacy is strongly dependent on dCK activity and dCTP is a negative feedback regulator for dCK activity, co-targeting of CTPS with CPEC and either gemcitabine or ara-C was suggested to improve DNA incorporation of both pyrimidine analogs upon dCTP synthesis inhibition (Figure 3D) [90,106]. Inhibition of CTPS with CPEC increased ara-C activity followed by apoptosis induction in T lymphoblastic as well as human neuroblastoma cancer cells [124,125]. A similar effect was observed upon pre-treatment with CPEC followed by gemcitabine leading to increased dFdCTP incorporation accompanied by increased cytotoxicity in lymphocytic and myeloid leukemia cells [126].

Even though initial *in vitro* and *in vivo* studies targeting CTPS alone or in combination with cytidine analogs have shown promising results, the findings could not be translated into the clinics. Treatment of colon cancer patients with CPEC in a single Phase I study caused severe cardiovascular toxicity demonstrating the need for new selective CTPS inhibitors [127].

Structural binding analysis of co-crystal structures of the newly developed CTPS1 inhibitors R80 and R80 structural analogs revealed specific binding to CTPS1 and all R80 analogs were potent in enzymatic activity assays on recombinant CTPS1. However, their potential as anti-cancer agents targeting CTPS1 alone or in combination with other standard-of-care pyrimidine synthesis inhibitors must be further evaluated *in vitro* and *in vivo* [119].

5.5. Co-Targeting of Thymidine Synthase and Thymidine Kinases Sensitizes Cancer Cells towards Traditional Anti-Cancer Agents

The activity of both, cytosolic (TK1) and mitochondrial thymidine kinase (TK2), is upregulated by anti-cancer agents targeting thymidine synthase (TS) in the pyrimidine *de novo* synthesis pathways. Consequently, co-targeting of pyrimidine salvage via TKs and pyrimidine *de novo* synthesis via TS inhibition in different cancer cell models was suggested to improve the efficacy of traditional anti-cancer agents.

The inhibition of the TK-mediated pyrimidine salvage is currently only possible via siRNA-induced knockdown of the corresponding enzyme due to the lack of TK-specific inhibitors [84,92,128,129]. Knockdown of the mitochondrial thymidine kinase TK2 via siRNA increased the capacity of TS siRNA to sensitize cervical carcinoma cancer cells as well as breast epithelial adenocarcinoma cancer cells towards the active metabolite 5-fluorodeoxyuridine (5FUdR) of the traditional anti-cancer agent 5-FU. Interestingly, siRNA knockdown of the cytosolic thymidine kinase TK1 but not TK2 caused an increased effect of TS siRNA and increased sensitivity of both cell lines towards the TS targeting folate analog pemetrexed (Figure 3E) [129].

As TK1 is the predominant thymidine kinase present in normal proliferating cells as well as cancer cells, the role of mitochondrial cell-cycle independent TK2 in cancer must be further investigated. The potential of TK1 and TK2 as anti-cancer targets in combination with other pyrimidines *de novo* synthesis inhibitors has only been demonstrated *in vitro* so that further *in vivo* experiments are required to fully understand the potential effect of TKs in cancer.

6. Conclusions

Targeting nucleotide synthesis and, consequently, DNA synthesis remains the backbone of cancer therapy besides its limitations caused by the ability of cancer cells to adapt to nucleoside salvage pathways to maintain successful DNA replication.

In recent years, pyrimidine salvage gained new attention leading to the development of new inhibitors for already existing key players as well as to the discovery of novel enzymes involved in pyrimidine salvage. Combination therapy is the go-to in current anti-cancer therapy. This review opens a new perspective of combining inhibitors of pyrimidine salvage and *de novo* synthesis to overcome the limitations of traditionally used anti-cancer agents. We highlight current targets for the development of new inhibitors to improve overall survival and prognosis in cancer patients.

Even though the targeting of key players of pyrimidine salvage with both new and already established inhibitors alone or in combination with pyrimidine *de novo* synthesis showed promising results in cancer cell models, it must be further evaluated *in vivo* as well as in patients to uncover its full potential in cancer therapy.

We furthermore hypothesize that targeting of pyrimidine salvage could not just be of advantage in combination with *de novo* pyrimidine synthesis inhibition but also with other anti-cancer agents targeting different pathways such as cell cycle regulation or purine

metabolism in cancer. However, more research must be completed to identify potential co-targeting strategies in cancer.

Funding: This project has received funding from the European Union’s Horizon 2020 research and innovation program under the Marie Skłodowska-Curie grant agreement No 813284.

Conflicts of Interest: The authors declare no conflict of interest.

References

- Heiden, M.G.V.; Lunt, S.Y.; Dayton, T.L.; Fiske, B.P.; Israelsen, W.J.; Mattaini, K.R.; Vokes, N.I.; Stephanopoulos, G.; Cantley, L.C.; Metallo, C.M.; et al. Metabolic Pathway Alterations That Support Cell Proliferation. *Cold Spring Harb. Lab. Press* **2011**, *76*, 325–334. [[CrossRef](#)] [[PubMed](#)]
- Austin, W.R.; Armijo, A.L.; Campbell, D.O.; Singh, A.S.; Hsieh, T.; Nathanson, D.; Herschman, H.R.; Phelps, M.E.; Witte, O.N.; Czernin, J.; et al. Nucleoside Salvage Pathway Kinases Regulate Hematopoiesis by Linking Nucleotide Metabolism with Replication Stress. *J. Exp. Med.* **2012**, *209*, 2215–2228. [[CrossRef](#)] [[PubMed](#)]
- Heiden, M.G.V. Targeting Cancer Metabolism: A Therapeutic Window Opens. *Nat. Rev. Drug Discov.* **2011**, *10*, 671–684. [[CrossRef](#)] [[PubMed](#)]
- Yin, J.; Ren, W.; Huang, X.; Deng, J.; Li, T.; Yin, Y. Potential Mechanisms Connecting Purine Metabolism and Cancer Therapy. *Front. Immunol.* **2018**, *9*, 1697. [[CrossRef](#)] [[PubMed](#)]
- Townsend, M.H.; Robison, R.A.; O’Neill, K.L. A Review of HPRT and Its Emerging Role in Cancer. *Med. Oncol.* **2018**, *35*, 89. [[CrossRef](#)]
- Camici, M.; Garcia-Gil, M.; Pesi, R.; Allegrini, S.; Tozzi, M.G. Purine-Metabolising Enzymes and Apoptosis in Cancer. *Cancers* **2019**, *11*, 1354. [[CrossRef](#)]
- Mollick, T.; Lain, S. Modulating Pyrimidine Ribonucleotide Levels for the Treatment of Cancer. *Cancer Metab.* **2020**, *8*, 12. [[CrossRef](#)]
- Hertel, L.W.; Boder, G.B.; Kroin, J.S.; Rinzel, S.M.; Poore, G.A.; Todd, G.C.; Grindey, G.B. Evaluation of the Antitumor Activity of Gemcitabine (2’,2’-Difluoro-2’-Deoxycytidine). *Cancer Res.* **1990**, *50*, 4417–4422.
- Peters, G.J.; Sharma, S.L.; Laurensse, E.; Pinedo, H.M. Inhibition of Pyrimidine de Novo Synthesis by DUP-785 (NSC 368390). *Investig. New Drug* **1987**, *5*, 235–244. [[CrossRef](#)]
- Dexter, D.L.; Hesson, D.P.; Ardecky, R.J.; Rao, G.V.; Tippett, D.L.; Dusak, B.A.; Paull, K.D.; Plowman, J.; DeLarco, B.M.; Narayanan, V.L. Activity of a Novel 4-Quinolinecarboxylic Acid, NSC 368390 [6-Fluoro-2-(2’-Fluoro-1,1’-Biphenyl-4-Yl)-3-Methyl-4-Quinolinecarb Oxylic Acid Sodium Salt], against Experimental Tumors. *Cancer Res.* **1985**, *45*, 5563–5568.
- Peters, G.; Kraal, I.; Pinedo, H. In Vitro and in Vivo Studies on the Combination of Brequinar Sodium (DUP-785; NSC 368390) with 5-Fluorouracil; Effects of Uridine. *Br. J. Cancer* **1992**, *65*, 229–233. [[CrossRef](#)] [[PubMed](#)]
- Csyk, R.L.; Malinowski, N.; Marquez, V.; Zaharevitz, D.; August, E.M.; Moyer, J.D. Cyclopentenyl Uracil: An Effective Inhibitor of Uridine Salvage in Vivo. *Biochem. Pharmacol.* **1995**, *49*, 203–207. [[CrossRef](#)]
- Sasada, S.; Miyata, Y.; Tsutani, Y.; Tsuyama, N.; Masujima, T.; Hihara, J.; Okada, M. Metabolomic Analysis of Dynamic Response and Drug Resistance of Gastric Cancer Cells to 5-Fluorouracil. *Oncol. Rep.* **2013**, *29*, 925–931. [[CrossRef](#)] [[PubMed](#)]
- Evans, D.R.; Guy, H.I. Mammalian Pyrimidine Biosynthesis: Fresh Insights into an Ancient Pathway*. *J. Biol. Chem.* **2004**, *279*, 33035–33038. [[CrossRef](#)]
- Löffler, M.; Fairbanks, L.D.; Zameitat, E.; Marinaki, A.M.; Simmonds, H.A. Pyrimidine Pathways in Health and Disease. *Trends Mol. Med.* **2005**, *11*, 430–437. [[CrossRef](#)]
- Young, J.D.; Yao, S.Y.M.; Baldwin, J.M.; Cass, C.E.; Baldwin, S.A. The Human Concentrative and Equilibrative Nucleoside Transporter Families, SLC28 and SLC29. *Mol. Asp. Med.* **2013**, *34*, 529–547. [[CrossRef](#)]
- Wang, W.; Cui, J.; Ma, H.; Lu, W.; Huang, J. Targeting Pyrimidine Metabolism in the Era of Precision Cancer Medicine. *Front. Oncol.* **2021**, *11*, 684961. [[CrossRef](#)]
- Francia, R.D.; Crisci, S.; Monaco, A.D.; Cafiero, C.; Re, A.; Iaccarino, G.; Filippi, R.D.; Frigeri, F.; Corazzelli, G.; Micera, A.; et al. Response and Toxicity to Cytarabine Therapy in Leukemia and Lymphoma: From Dose Puzzle to Pharmacogenomic Biomarkers. *Cancers* **2021**, *13*, 966. [[CrossRef](#)]
- Toschi, L.; Finocchiaro, G.; Bartolini, S.; Gioia, V.; Cappuzzo, F. Role of Gemcitabine in Cancer Therapy. *Future Oncol.* **2005**, *1*, 7–17. [[CrossRef](#)] [[PubMed](#)]
- Longley, D.B.; Harkin, D.P.; Johnston, P.G. 5-Fluorouracil: Mechanisms of Action and Clinical Strategies. *Nat. Rev. Cancer* **2003**, *3*, 330–338. [[CrossRef](#)]
- Paridaens, R.; Mouridsen, H.T.; Palshof, T.; Cocconi, G.; van Oosterom, A.; Rotmensch, N.; Sylvester, R.; Heuson, J.C.; Rozenzweig, M. N-(Phosphonacetyl)-l-Aspartate (PALA) in Advanced Breast Cancer: A Phase II Trial of the EORTC Breast Cancer Cooperative Group. *Eur. J. Cancer Clin. Oncol.* **1982**, *18*, 67–70. [[CrossRef](#)]
- Collins, K.D.; Stark, G.R. Aspartate Transcarbamylase Interaction with the Transition State Analogue N-(Phosphonacetyl)-l-Aspartate. *J. Biol. Chem.* **1971**, *246*, 6599–6605. [[CrossRef](#)]

23. Kleeberg, U.R.; Mulder, J.H.; Rümke, P.; Thomas, D.; Rozenzweig, M. N-(Phosphonacetyl)-L-Aspartate (PALA) in Advanced Malignant Melanoma: A Phase II Trial of the EORTC Malignant Melanoma Cooperative Group. *Eur. J. Cancer Clin. Oncol.* **1982**, *18*, 723–726. [[CrossRef](#)]
24. Schwartzmann, G.; Peters, G.J.; Laurensse, E.; de Waal, F.C.; Loonen, A.H.; Leyva, A.; Pinedo, H.M. DUP 785 (NSC 368390): Schedule-Dependency of Growth-Inhibitory and Antipyrimidine Effects. *Biochem. Pharmacol.* **1988**, *37*, 3257–3266. [[CrossRef](#)]
25. Cody, R.; Stewart, D.; DeForni, M.; Moore, M.; Dallaire, B.; Azarnia, N.; Gyves, J. Multicenter Phase II Study of Brequinar Sodium in Patients with Advanced Breast Cancer. *Am. J. Clin. Oncol.* **1993**, *16*, 526–528. [[CrossRef](#)] [[PubMed](#)]
26. Moore, M.; Maroun, J.; Robert, F.; Natale, R.; Neidhart, J.; Dallaire, B.; Sisk, R.; Gyves, J. Multicenter Phase II Study of Brequinar Sodium in Patients with Advanced Gastrointestinal Cancer. *Investig. New Drug* **1993**, *11*, 61–65. [[CrossRef](#)] [[PubMed](#)]
27. Maroun, J.; Ruckdeschel, J.; Natale, R.; Morgan, R.; Dallaire, B.; Sisk, R.; Gyves, J. Multicenter Phase II Study of Brequinar Sodium in Patients with Advanced Lung Cancer. *Cancer Chemother. Pharmacol.* **1993**, *32*, 64–66. [[CrossRef](#)] [[PubMed](#)]
28. Urba, S.; Doroshow, J.; Cripps, C.; Robert, F.; Velez-Garcia, E.; Dallaire, B.; Adams, D.; Carlson, R.; Grillo-Lopez, A.; Gyves, J. Multicenter Phase II Trial of Brequinar Sodium in Patients with Advanced Squamous-Cell Carcinoma of the Head and Neck. *Cancer Chemother. Pharmacol.* **1992**, *31*, 167–169. [[CrossRef](#)] [[PubMed](#)]
29. Dodion, P.F.; Wagener, T.; Stoter, G.; Drozd, A.; Lev, L.M.; Skovsgaard, T.; Renard, J.; Cavalli, F. Phase II Trial with Brequinar (DUP-785, NSC 368390) in Patients with Metastatic Colorectal Cancer: A Study of the Early Clinical Trials Group of the EORTC. *Ann. Oncol.* **1990**, *1*, 79–80. [[CrossRef](#)] [[PubMed](#)]
30. Ladds, M.J.G.W.; van Leeuwen, I.M.M.; Drummond, C.J.; Chu, S.; Healy, A.R.; Popova, G.; Fernández, A.P.; Mollick, T.; Darekar, S.; Sedimbi, S.K.; et al. A DHODH Inhibitor Increases P53 Synthesis and Enhances Tumor Cell Killing by P53 Degradation Blockage. *Nat. Commun.* **2018**, *9*, 1107. [[CrossRef](#)] [[PubMed](#)]
31. Li, L.; Ng, S.R.; Colón, C.I.; Drapkin, B.J.; Hsu, P.P.; Li, Z.; Nabel, C.S.; Lewis, C.A.; Romero, R.; Mercer, K.L.; et al. Identification of DHODH as a Therapeutic Target in Small Cell Lung Cancer. *Sci. Transl. Med.* **2019**, *11*, eaaw7852. [[CrossRef](#)] [[PubMed](#)]
32. Sykes, D.B.; Kfoury, Y.S.; Mercier, F.E.; Wawer, M.J.; Law, J.M.; Haynes, M.K.; Lewis, T.A.; Schajnovitz, A.; Jain, E.; Lee, D.; et al. Inhibition of Dihydroorotate Dehydrogenase Overcomes Differentiation Blockade in Acute Myeloid Leukemia. *Cell* **2016**, *167*, 171–186.e15. [[CrossRef](#)]
33. Cadman, E.C.; Dix, D.E.; Handschumacher, R.E. Clinical, Biological, and Biochemical Effect of Pyrazofurin. *Cancer Res.* **1978**, *38*, 682–688. [[PubMed](#)]
34. Nichols, W.C.; Kvols, L.K.; Ingle, J.N.; Edmonson, J.H.; Ahmann, D.L.; Rubin, J.; O’Connell, M.J. Phase II Study of Triazinate and Pyrazofurin in Patients with Advanced Breast Cancer Previously Exposed to Cytotoxic Chemotherapy. *Cancer Treat. Rep.* **1978**, *62*, 837–839.
35. Dix, D.E.; Lehman, C.P.; Jakubowski, A.; Moyer, J.D.; Handschumacher, R.E. Pyrazofurin Metabolism, Enzyme Inhibition, and Resistance in L5178Y Cells. *Cancer Res.* **1979**, *39*, 4485–4490.
36. Carroll, D.S.; Kemeny, N.E.; Gralla, R.J. Phase II Evaluation of Pyrazofurin in Patients with Advanced Colorectal Carcinoma. *Cancer Treat. Rep.* **1979**, *63*, 139–140. [[PubMed](#)]
37. Creagan, E.T.; Rubin, J.; Moertel, C.G.; Schutt, A.J.; O’connell, M.J.; Hahn, R.G.; Reitemeir, R.J.; Frytak, S. Phase II Study of Pyrazofurin in Advanced Colorectal Carcinoma. *Cancer Treat. Rep.* **1977**, *61*, 491–493. [[PubMed](#)]
38. Twelves, C.; Scheithauer, W.; McKendrick, J.; Seitz, J.-F.; Hazel, G.V.; Wong, A.; Díaz-Rubio, E.; Gilbert, F.; Cassidy, J. Capecitabine versus 5-Fluorouracil/Folinic Acid as Adjuvant Therapy for Stage III Colon Cancer: Final Results from the X-ACT Trial with Analysis by Age and Preliminary Evidence of a Pharmacodynamic Marker of Efficacy. *Ann. Oncol.* **2012**, *23*, 1190–1197. [[CrossRef](#)] [[PubMed](#)]
39. Cadman, E.; Benz, C. Uridine and Cytidine Metabolism Following Inhibition of de Novo Pyrimidine Synthesis by Pyrazofurin. *Biochim. Biophys. Acta BBA-Nucleic Acids Protein Synth.* **1980**, *609*, 372–382. [[CrossRef](#)]
40. Cuthbertson, C.R.; Guo, H.; Kyani, A.; Madak, J.T.; Arabzada, Z.; Neamati, N. The Dihydroorotate Dehydrogenase Inhibitor Brequinar Is Synergistic with ENT1/2 Inhibitors. *ACS Pharmacol. Transl. Sci.* **2020**, *3*, 1242–1252. [[CrossRef](#)] [[PubMed](#)]
41. Kunos, C.A.; Ferris, G.; Pyatka, N.; Pink, J.; Radivoyevitch, T. Deoxynucleoside Salvage Facilitates DNA Repair During Ribonucleotide Reductase Blockade in Human Cervical Cancers. *Radiat. Res.* **2011**, *176*, 425–433. [[CrossRef](#)] [[PubMed](#)]
42. Karle, J.M.; Anderson, L.W.; Dietrick, D.D.; Cysyk, R.L. Determination of Serum and Plasma Uridine Levels in Mice, Rats, and Humans by High-Pressure Liquid Chromatography. *Anal. Biochem.* **1980**, *109*, 41–46. [[CrossRef](#)]
43. Traut, T.W. Physiological Concentrations of Purines and Pyrimidines. *Mol. Cell. Biochem.* **1994**, *140*, 1–22. [[CrossRef](#)]
44. Eells, J.T.; Spector, R. Purine and Pyrimidine Base and Nucleoside Concentrations in Human Cerebrospinal Fluid and Plasma. *Neurochem. Res.* **1983**, *8*, 1451–1457. [[CrossRef](#)] [[PubMed](#)]
45. Ritzel, M.W.; Yao, S.Y.; Huang, M.Y.; Elliott, J.F.; Cass, C.E.; Young, J.D. Molecular Cloning and Functional Expression of CDNAs Encoding a Human Na⁺-Nucleoside Cotransporter (HCNT1). *Am. J. Physiol. Cell Physiol.* **1997**, *272*, C707–C714. [[CrossRef](#)] [[PubMed](#)]
46. Ritzel, M.W.L.; Ng, A.M.L.; Yao, S.Y.M.; Graham, K.; Loewen, S.K.; Smith, K.M.; Ritzel, R.G.; Mowles, D.A.; Carpenter, P.; Chen, X.-Z.; et al. Molecular Identification and Characterization of Novel Human and Mouse Concentrative Na⁺-Nucleoside Cotransporter Proteins (HCNT3 and MCNT3) Broadly Selective for Purine and Pyrimidine Nucleosides (System Cib)*. *J. Biol. Chem.* **2001**, *276*, 2914–2927. [[CrossRef](#)] [[PubMed](#)]

47. Baldwin, S.A.; Beal, P.R.; Yao, S.Y.M.; King, A.E.; Cass, C.E.; Young, J.D. The Equilibrative Nucleoside Transporter Family, SLC29. *Pflügers Arch.* **2004**, *447*, 735–743. [[CrossRef](#)]
48. Griffiths, M.; Beaumont, N.; Yao, S.Y.M.; Sundaram, M.; Boumah, C.E.; Davies, A.; Kwong, F.Y.P.; Coe, I.; Cass, C.E.; Young, J.D.; et al. Cloning of a Human Nucleoside Transporter Implicated in the Cellular Uptake of Adenosine and Chemotherapeutic Drugs. *Nat. Med.* **1997**, *3*, 89–93. [[CrossRef](#)]
49. Griffiths, M.; Yao, Y.M.S.; Abidi, F.; Phillips, E.V.S.; Cass, E.C.; Young, D.J.; Baldwin, A.S. Molecular Cloning and Characterization of a Nitrobenzylthioinosine-Insensitive (Ei) Equilibrative Nucleoside Transporter from Human Placenta. *Biochem. J.* **1997**, *328*, 739–743. [[CrossRef](#)]
50. Ritzel, M.W.L.; Yaof, S.Y.M.; Ng, A.M.L.; Mackeyt, J.R.; Cass, C.E.; Young, J.D. Molecular Cloning, Functional Expression and Chromosomal Localization of a cDNA Encoding a Human Na⁺/Nucleoside Cotransporter (HCNT2) Selective for Purine Nucleosides and Uridine. *Mol. Membr. Biol.* **2009**, *15*, 203–211. [[CrossRef](#)]
51. Pastor-Anglada, M.; Pérez-Torras, S. Emerging Roles of Nucleoside Transporters. *Front. Pharmacol.* **2018**, *9*, 606. [[CrossRef](#)] [[PubMed](#)]
52. Gloeckner-Hofmann, K.; Guillén-Gómez, E.; Schmidtgen, C.; Porstmann, R.; Ziegler, R.; Stoss, O.; Casado, F.J.; Rüschoff, J.; Pastor-Anglada, M. Expression of the High-Affinity Fluoropyrimidine-Preferring Nucleoside Transporter HCNT1 Correlates with Decreased Disease-Free Survival in Breast Cancer. *Oncology* **2006**, *70*, 238–244. [[CrossRef](#)] [[PubMed](#)]
53. Pastor-Anglada, M.; Pérez-Torras, S. Nucleoside Transporter Proteins as Biomarkers of Drug Responsiveness and Drug Targets. *Front. Pharmacol.* **2015**, *6*, 13. [[CrossRef](#)] [[PubMed](#)]
54. Molina-Arcas, M.; Pastor-Anglada, M. Pharmacogenomics of Human Drug Transporters. In *Pharmacogenomics of Human Drug Transporters*; Ishikawa, T., Kim, R.B., König, J., Eds.; John Wiley & Sons, Inc.: New York, NY, USA, 2013; pp. 243–270. [[CrossRef](#)]
55. Grañé-Boladeras, N.; Spring, C.M.; Hanna, W.J.B.; Pastor-Anglada, M.; Coe, I.R. Novel Nuclear HENT2 Isoforms Regulate Cell Cycle Progression via Controlling Nucleoside Transport and Nuclear Reservoir. *Cell Mol. Life Sci.* **2016**, *73*, 4559–4575. [[CrossRef](#)] [[PubMed](#)]
56. Oates, J.A.; Wood, A.J.J.; FitzGerald, G.A. Dipyridamole. *N. Engl. J. Med.* **1987**, *316*, 1247–1257. [[CrossRef](#)] [[PubMed](#)]
57. Visser, F.; Vickers, M.F.; Ng, A.M.L.; Baldwin, S.A.; Young, J.D.; Cass, C.E. Mutation of Residue 33 of Human Equilibrative Nucleoside Transporters 1 and 2 Alters Sensitivity to Inhibition of Transport by Dilazep and Dipyridamole*. *J. Biol. Chem.* **2002**, *277*, 395–401. [[CrossRef](#)]
58. Wright, N.J.; Lee, S.-Y. Structures of Human ENT1 in Complex with Adenosine Reuptake Inhibitors. *Nat. Struct. Mol. Biol.* **2019**, *26*, 599–606. [[CrossRef](#)]
59. Remick, S.C.; Grem, J.L.; Fischer, P.H.; Tutsch, K.D.; Alberti, D.B.; Nieting, L.M.; Tombes, M.B.; Bruggink, J.; Willson, J.K.; Trump, D.L. Phase I Trial of 5-Fluorouracil and Dipyridamole Administered by Seventy-Two-Hour Concurrent Continuous Infusion. *Cancer Res.* **1990**, *50*, 2667–2672. [[PubMed](#)]
60. Markman, M.; Chan, T.C.K.; Cleary, S.; Howell, S.B. Phase I Trial of Combination Therapy of Cancer with N-Phosphanacetyl-L-Aspartic Acid and Dipyridamole. *Cancer Chemother. Pharmacol.* **1987**, *19*, 80–83. [[CrossRef](#)] [[PubMed](#)]
61. Budd, G.T.; Jayaraj, A.; Grabowski, D.; Adelstein, D.; Bauer, L.; Boyett, J.; Bukowski, R.; Murthy, S.; Weick, J. Phase I Trial of Dipyridamole with 5-Fluorouracil and Folinic Acid. *Cancer Res.* **1990**, *50*, 7206–7211.
62. Willson, J.K.; Fischer, P.H.; Remick, S.C.; Tutsch, K.D.; Grem, J.L.; Nieting, L.; Alberti, D.; Bruggink, J.; Trump, D.L. Methotrexate and Dipyridamole Combination Chemotherapy Based upon Inhibition of Nucleoside Salvage in Humans. *Cancer Res.* **1989**, *49*, 1866–1870.
63. Saravanan, K.; Barlow, H.C.; Barton, M.; Calvert, A.H.; Golding, B.T.; Newell, D.R.; Northen, J.S.; Curtin, N.J.; Thomas, H.D.; Griffin, R.J. Nucleoside Transport Inhibitors: Structure–Activity Relationships for Pyrimido[5,4-d]Pyrimidine Derivatives That Potentiate Pemetrexed Cytotoxicity in the Presence of A1-Acid Glycoprotein. *J. Med. Chem.* **2011**, *54*, 1847–1859. [[CrossRef](#)] [[PubMed](#)]
64. Curtin, N.J.; Newell, D.R.; Harris, A.L. Modulation of Dipyridamole Action by A1acid Glycoprotein Reduced Potentiation of Quinazoline Antifolate (CB3717) Cytotoxicity by Dipyridamole. *Biochem. Pharmacol.* **1989**, *38*, 3281–3288. [[CrossRef](#)]
65. Spano, D.; Marshall, J.-C.; Marino, N.; Martino, D.D.; Romano, A.; Scoppettuolo, M.N.; Bello, A.M.; Dato, V.D.; Navas, L.; Vita, G.D.; et al. Dipyridamole Prevents Triple-Negative Breast-Cancer Progression. *Clin. Exp. Metastasis* **2013**, *30*, 47–68. [[CrossRef](#)] [[PubMed](#)]
66. Vlachodimou, A.; Konstantinopoulou, K.; IJerman, A.P.; Heitman, L.H. Affinity, Binding Kinetics and Functional Characterization of Draflazine Analogues for Human Equilibrative Nucleoside Transporter 1 (SLC29A1). *Biochem. Pharmacol.* **2019**, *172*, 113747. [[CrossRef](#)] [[PubMed](#)]
67. Jouan, E.; Moreau, A.; Bruyere, A.; Alim, K.; Denizot, C.; Parmentier, Y.; Fardel, O. Differential Inhibition of Equilibrative Nucleoside Transporter 1 (ENT1) Activity by Tyrosine Kinase Inhibitors. *Eur. J. Drug Metab. Pharmacokinet.* **2021**, *46*, 625–635. [[CrossRef](#)]
68. Damaraju, V.L.; Scriver, T.; Mowles, D.; Kuzma, M.; Ryan, A.J.; Cass, C.E.; Sawyer, M.B. Erlotinib, Gefitinib, and Vandetanib Inhibit Human Nucleoside Transporters and Protect Cancer Cells from Gemcitabine Cytotoxicity. *Clin. Cancer Res.* **2014**, *20*, 176–186. [[CrossRef](#)] [[PubMed](#)]

69. Damaraju, V.L.; Weber, D.; Kuzma, M.; Cass, C.E.; Sawyer, M.B. Selective Inhibition of Human Equilibrative and Concentrative Nucleoside Transporters by BCR-ABL Kinase Inhibitors Identification of Key Hent1 Amino Acid Residues for Interaction with Bcr-Abl Kinase Inhibitors*. *J. Biol. Chem.* **2016**, *291*, 18809–18817. [[CrossRef](#)] [[PubMed](#)]
70. Abt, E.R.; Rosser, E.W.; Durst, M.A.; Lok, V.; Poddar, S.; Le, T.M.; Cho, A.; Kim, W.; Wei, L.; Song, J.; et al. Metabolic Modifier Screen Reveals Secondary Targets of Protein Kinase Inhibitors within Nucleotide Metabolism. *Cell Chem. Biol.* **2019**, *27*, 197–205.e6. [[CrossRef](#)] [[PubMed](#)]
71. Lim, M.I.; Moyer, J.D.; Cysyk, R.L.; Marquez, V.E. Cyclopentenyluridine and Cyclopentenylcytidine Analogs as Inhibitors of Uridine-Cytidine Kinase. *J. Med. Chem.* **1984**, *27*, 1536–1538. [[CrossRef](#)] [[PubMed](#)]
72. Nathanson, D.A.; Armijo, A.L.; Tom, M.; Li, Z.; Dimitrova, E.; Austin, W.R.; Nomme, J.; Campbell, D.O.; Ta, L.; Le, T.M.; et al. Co-Targeting of Convergent Nucleotide Biosynthetic Pathways for Leukemia Eradication. *J. Exp. Med.* **2014**, *211*, 473–486. [[CrossRef](#)]
73. Poddar, S.; Capparelli, E.V.; Rosser, E.W.; Gipson, R.M.; Wei, L.; Le, T.; Jung, M.E.; Radu, C.; Nikanjam, M. Development and Preclinical Pharmacology of a Novel DCK Inhibitor, DI-87. *Biochem. Pharmacol.* **2020**, *172*, 113742. [[CrossRef](#)] [[PubMed](#)]
74. Nomme, J.; Li, Z.; Gipson, R.M.; Wang, J.; Armijo, A.L.; Le, T.; Poddar, S.; Smith, T.; Santarsiero, B.D.; Nguyen, H.-A.; et al. Structure-Guided Development of Deoxycytidine Kinase Inhibitors with Nanomolar Affinity and Improved Metabolic Stability. *J. Med. Chem.* **2014**, *57*, 9480–9494. [[CrossRef](#)] [[PubMed](#)]
75. Arnér, E.S.J.; Eriksson, S. Mammalian Deoxyribonucleoside Kinases. *Pharmacol. Ther.* **1995**, *67*, 155–186. [[CrossRef](#)]
76. Herr, P.; Boström, J.; Rullman, E.; Rudd, S.G.; Vesterlund, M.; Lehtiö, J.; Helleday, T.; Maddalo, G.; Altun, M. Cell Cycle Profiling Reveals Protein Oscillation, Phosphorylation, and Localization Dynamics*. *Mol. Cell Proteom.* **2020**, *19*, 608–623. [[CrossRef](#)]
77. Alegre, M.M.; Weyant, M.J.; Bennett, D.T.; Yu, J.A.; Ramsden, M.K.; Elnaggar, A.; Robison, R.A.; O'Neill, K.L. Serum Detection of Thymidine Kinase 1 as a Means of Early Detection of Lung Cancer. *Anticancer Res.* **2014**, *34*, 2145–2151. [[PubMed](#)]
78. Alegre, M.M.; Robison, R.A.; O'Neill, K.L. Thymidine Kinase 1: A Universal Marker for Cancer. *Cancer Clin. Oncol.* **2013**, *2*, 159–167. [[CrossRef](#)]
79. O'Neill, K.L.; Zhang, F.; Li, H.; Fuja, D.G.; Murray, B.K. Thymidine Kinase 1—A Prognostic and Diagnostic Indicator in ALL and AML Patients. *Leukemia* **2007**, *21*, 560–563. [[CrossRef](#)] [[PubMed](#)]
80. Alegre, M.M.; Robison, R.A.; O'Neill, K.L. Thymidine Kinase 1 Upregulation Is an Early Event in Breast Tumor Formation. *J. Oncol.* **2012**, *2012*, 575647. [[CrossRef](#)] [[PubMed](#)]
81. Bagegni, N.; Thomas, S.; Liu, N.; Luo, J.; Hoog, J.; Northfelt, D.W.; Goetz, M.P.; Forero, A.; Bergqvist, M.; Karen, J.; et al. Serum Thymidine Kinase 1 Activity as a Pharmacodynamic Marker of Cyclin-Dependent Kinase 4/6 Inhibition in Patients with Early-Stage Breast Cancer Receiving Neoadjuvant Palbociclib. *Breast Cancer Res.* **2017**, *19*, 123. [[CrossRef](#)] [[PubMed](#)]
82. Zhu, X.; Shi, C.; Peng, Y.; Yin, L.; Tu, M.; Chen, Q.; Hou, C.; Li, Q.; Miao, Y. Thymidine Kinase 1 Silencing Retards Proliferative Activity of Pancreatic Cancer Cell via E2F1-TK1-P21 Axis. *Cell Prolif.* **2018**, *51*, e12428. [[CrossRef](#)] [[PubMed](#)]
83. Foekens, J.A.; Romain, S.; Look, M.P.; Martin, P.M.; Klijn, J.G. Thymidine Kinase and Thymidylate Synthase in Advanced Breast Cancer: Response to Tamoxifen and Chemotherapy. *Cancer Res.* **2001**, *61*, 1421–1425.
84. Liu, C.; Wang, J.; Zhao, L.; He, H.; Zhao, P.; Peng, Z.; Liu, F.; Chen, J.; Wu, W.; Wang, G.; et al. Knockdown of Thymidine Kinase 1 Suppresses Cell Proliferation, Invasion, Migration, and Epithelial–Mesenchymal Transition in Thyroid Carcinoma Cells. *Front. Oncol.* **2020**, *9*, 1475. [[CrossRef](#)] [[PubMed](#)]
85. Weigel, E.G.; Meng, W.; Townsend, M.H.; Velazquez, E.J.; Brog, R.A.; Boyer, M.W.; Weber, K.S.; Robison, R.A.; O'Neill, K.L. Biomarker Analysis and Clinical Relevance of TK1 on the Cell Membrane of Burkitt's Lymphoma and Acute Lymphoblastic Leukemia. *OncoTargets Ther.* **2017**, *10*, 4355–4367. [[CrossRef](#)]
86. Weigel, E.G.; Burrup, W.; Kovtun, R.; Velazquez, E.J.; Felsted, A.M.; Townsend, M.H.; Ence, Z.E.; Suh, E.; Piccolo, S.R.; Weber, K.S.; et al. Membrane Expression of Thymidine Kinase 1 and Potential Clinical Relevance in Lung, Breast, and Colorectal Malignancies. *Cancer Cell Int.* **2018**, *18*, 135. [[CrossRef](#)] [[PubMed](#)]
87. Velazquez, E.J.; Brindley, T.D.; Shrestha, G.; Bitter, E.E.; Cress, J.D.; Townsend, M.H.; Berges, B.K.; Robison, R.A.; Weber, K.S.; O'Neill, K.L. Novel Monoclonal Antibodies against Thymidine Kinase 1 and Their Potential Use for the Immunotargeting of Lung, Breast and Colon Cancer Cells. *Cancer Cell Int.* **2020**, *20*, 127. [[CrossRef](#)] [[PubMed](#)]
88. Munch-Petersen, B.; Cloos, L.; Tyrsted, G.; Eriksson, S. Diverging Substrate Specificity of Pure Human Thymidine Kinases 1 and 2 against Antiviral Dideoxynucleosides. *J. Biol. Chem.* **1991**, *266*, 9032–9038. [[CrossRef](#)]
89. Kierdaszuk, B.; Krawiec, K.; Kazimierczuk, Z.; Jacobsson, U.; Johansson, N.G.; Munch-petersen, B.; Eriksson, S.; Shugar, D. Substrate/Inhibitor Properties of Human Deoxycytidine Kinase (DCK) and Thymidine Kinases (Tk1 and Tk2) Towards the Sugar Moiety of Nucleosides, Including O'-Alkyl Analogues. *Nucleosides Nucleotides* **2006**, *18*, 1883–1903. [[CrossRef](#)]
90. Al-Madhoun, A.S.; Tjarks, W.; Eriksson, S. The Role of Thymidine Kinases in the Activation of Pyrimidine Nucleoside Analogues. *Mini Rev. Med. Chem.* **2004**, *4*, 341–350. [[CrossRef](#)]
91. Jansson, O.; Eriksson, S. Direct Photoaffinity-Labeling of Human Deoxycytidine Kinase with the Feedback Inhibitor DCTP. *Biochem. J.* **1990**, *269*, 201–205. [[CrossRef](#)]
92. Cresce, C.D.; Figueredo, R.; Rytelewski, M.; Vareki, S.M.; Way, C.; Ferguson, P.J.; Vincent, M.D.; Koropatnick, J. SiRNA Knockdown of Mitochondrial Thymidine Kinase 2 (TK2) Sensitizes Human Tumor Cells to Gemcitabine. *Oncotarget* **2015**, *6*, 22397–22409. [[CrossRef](#)] [[PubMed](#)]

93. Gaidano, V.; Houshmand, M.; Vitale, N.; Carrà, G.; Morotti, A.; Tenace, V.; Rapelli, S.; Sainas, S.; Pippione, A.C.; Giorgis, M.; et al. The Synergism between DHODH Inhibitors and Dipyridamole Leads to Metabolic Lethality in Acute Myeloid Leukemia. *Cancers* **2021**, *13*, 1003. [[CrossRef](#)]
94. Yu, Y.; Ding, J.; Zhu, S.; Alptekin, A.; Dong, Z.; Yan, C.; Zha, Y.; Ding, H.-F. Therapeutic Targeting of Both Dihydroorotate Dehydrogenase and Nucleoside Transport in MYCN-Amplified Neuroblastoma. *Cell Death Dis.* **2021**, *12*, 821. [[CrossRef](#)]
95. Spratlin, J.; Sangha, R.; Glubrecht, D.; Dabbagh, L.; Young, J.D.; Dumontet, C.; Cass, C.; Lai, R.; Mackey, J.R. The Absence of Human Equilibrative Nucleoside Transporter 1 Is Associated with Reduced Survival in Patients with Gemcitabine-Treated Pancreas Adenocarcinoma. *Clin. Cancer Res.* **2004**, *10*, 6956–6961. [[CrossRef](#)] [[PubMed](#)]
96. Zhang, J.; Visser, F.; King, K.M.; Baldwin, S.A.; Young, J.D.; Cass, C.E. The Role of Nucleoside Transporters in Cancer Chemotherapy with Nucleoside Drugs. *Cancer Metastasis Rev.* **2007**, *26*, 85–110. [[CrossRef](#)] [[PubMed](#)]
97. Baker, C.H.; Banzon, J.; Bollinger, J.M.; Stubbe, J.; Samano, V.; Robins, M.J.; Lippert, B.; Jarvi, E.; Resvick, R. 2'-Deoxy-2'-Methylenecytidine and 2'-Deoxy-2',2'-Difluorocytidine 5'-Diphosphates: Potent Mechanism-Based Inhibitors of Ribonucleotide Reductase. *J. Med. Chem.* **1991**, *34*, 1879–1884. [[CrossRef](#)]
98. Kufe, D.W.; Wick, M.M.; Moschella, S.; Major, P. Effect of High-dose Thymidine Infusions in Patients with Mycosis Fungoides. *Cancer* **1981**, *48*, 1513–1516. [[CrossRef](#)]
99. Kufe, D.W.; Beardsley, P.; Karp, D.; Parker, L.; Rosowsky, A.; Canellos, G.; Frei, E. High-Dose Thymidine Infusions in Patients with Leukemia and Lymphoma. *Blood* **1980**, *55*, 580–589. [[PubMed](#)]
100. Chiuten, D.F.; Wiernik, P.H.; Zaharko, D.S.; Edwards, L. Clinical Phase I-II and Pharmacokinetic Study of High-Dose Thymidine given by Continuous Intravenous Infusion. *Cancer Res.* **1980**, *40*, 818–822.
101. Laks, D.R.; Ta, L.; Crisman, T.J.; Gao, F.; Coppola, G.; Radu, C.G.; Nathanson, D.A.; Kornblum, H.I. Inhibition of Nucleotide Synthesis Targets Brain Tumor Stem Cells in a Subset of Glioblastoma. *Mol. Cancer Ther.* **2016**, *15*, 1271–1278. [[CrossRef](#)]
102. Herold, N.; Rudd, S.G.; Sanjiv, K.; Kutzner, J.; Bladh, J.; Paulin, C.B.J.; Helleday, T.; Henter, J.-I.; Schaller, T. SAMHD1 Protects Cancer Cells from Various Nucleoside-Based Antimetabolites. *Cell Cycle* **2017**, *16*, 1029–1038. [[CrossRef](#)] [[PubMed](#)]
103. Herold, N.; Rudd, S.G.; Ljungblad, L.; Sanjiv, K.; Myrberg, I.H.; Paulin, C.B.J.; Heshmati, Y.; Hagenkort, A.; Kutzner, J.; Page, B.D.G.; et al. Targeting SAMHD1 with the Vpx Protein to Improve Cytarabine Therapy for Hematological Malignancies. *Nat. Med.* **2017**, *23*, 256–263. [[CrossRef](#)] [[PubMed](#)]
104. Herold, N. Pharmacological Strategies to Overcome Treatment Resistance in Acute Myeloid Leukemia: Increasing Leukemic Drug Exposure by Targeting the Resistance Factor SAMHD1 and the Toxicity Factor Top2 β . *Expert Opin. Drug Discov.* **2020**, *16*, 7–11. [[CrossRef](#)] [[PubMed](#)]
105. Fernandez-Calotti, P.; Jordheim, L.P.; Giordano, M.; Dumontet, C.; Galmarini, C.M. Substrate Cycles and Drug Resistance to 1-Beta-D-Arabinofuranosylcytosine (AraC). *Leuk. Lymphoma* **2009**, *46*, 335–346. [[CrossRef](#)] [[PubMed](#)]
106. Kufe, D.; Spriggs, D.; Egan, E.M.; Munroe, D. Relationships among Ara-CTP Pools, Formation of (Ara-C)DNA, and Cytotoxicity of Human Leukemic Cells. *Blood* **1984**, *64*, 54–58. [[CrossRef](#)] [[PubMed](#)]
107. Hollenbaugh, J.A.; Shelton, J.; Tao, S.; Amiralaei, S.; Liu, P.; Lu, X.; Goetze, R.W.; Zhou, L.; Nettles, J.H.; Schinazi, R.F.; et al. Substrates and Inhibitors of SAMHD1. *PLoS ONE* **2017**, *12*, e0169052. [[CrossRef](#)] [[PubMed](#)]
108. Seamon, K.J.; Hansen, E.C.; Kadina, A.P.; Kashemirov, B.A.; McKenna, C.E.; Bumpus, N.N.; Stivers, J.T. Small Molecule Inhibition of SAMHD1 DNTPase by Tetramer Destabilization. *J. Am. Chem. Soc.* **2014**, *136*, 9822–9825. [[CrossRef](#)] [[PubMed](#)]
109. Rudd, S.G.; Tsesmetzis, N.; Sanjiv, K.; Paulin, C.B.; Sandhow, L.; Kutzner, J.; Myrberg, I.H.; Bunten, S.S.; Axelsson, H.; Zhang, S.M.; et al. Ribonucleotide Reductase Inhibitors Suppress SAMHD1 Ara-CTPase Activity Enhancing Cytarabine Efficacy. *EMBO Mol. Med.* **2020**, *12*, e10419. [[CrossRef](#)] [[PubMed](#)]
110. Schaller, T.; Pollpeter, D.; Apolonia, L.; Goujon, C.; Malim, M.H. Nuclear Import of SAMHD1 Is Mediated by a Classical Karyopherin α /B1 Dependent Pathway and Confers Sensitivity to VpxMAC Induced Ubiquitination and Proteasomal Degradation. *Retrovirology* **2014**, *11*, 29. [[CrossRef](#)] [[PubMed](#)]
111. van den Berg, A.A.; van Lenthe, H.; Kipp, J.B.A.; de Korte, D.; van Kuilenburg, A.B.P.; van Gennip, A.H. Cytidine Triphosphate (Ctp) Synthetase Activity during Cell Cycle Progression in Normal and Malignant t-Lymphocytic Cells. *Eur. J. Cancer* **1995**, *31*, 108–112. [[CrossRef](#)]
112. van Kuilenburg, A.B.P.; Meinsma, R.; Vreken, P.; Waterham, H.R.; van Gennip, A.H. Identification of a cDNA Encoding an Isoform of Human CTP Synthetase. *Biochim. Biophys. Acta BBA-Gene Struct. Expr.* **2000**, *1492*, 548–552. [[CrossRef](#)]
113. Williams, J.C.; Kizaki, H.; Weber, G.; MORRIS, H.P. Increased CTP Synthetase Activity in Cancer Cells. *Nature* **1978**, *271*, 71–73. [[CrossRef](#)]
114. Kizaki, H.; Williams, J.C.; Morris, H.P.; Weber, G. Increased Cytidine 5'-Triphosphate Synthetase Activity in Rat and Human Tumors. *Cancer Res.* **1980**, *40*, 3921–3927.
115. Ellims, P.H.; Gan, T.E.; Medley, G. Cytidine Triphosphate Synthetase Activity in Lymphoproliferative Disorders. *Cancer Res.* **1983**, *43*, 1432–1435. [[PubMed](#)]
116. Lin, Y.; Zhang, J.; Li, Y.; Guo, W.; Chen, L.; Chen, M.; Chen, X.; Zhang, W.; Jin, X.; Jiang, M.; et al. CTPS1 Promotes Malignant Progression of Triple-Negative Breast Cancer with Transcriptional Activation by YBX1. *J. Transl. Med.* **2022**, *20*, 17. [[CrossRef](#)] [[PubMed](#)]
117. Lin, Y.; Lin, L.; Fu, F.; Wang, C.; Hu, A.; Xie, J.; Jiang, M.; Wang, Z.; Yang, L.; Guo, R.; et al. Quantitative Proteomics Reveals Stage-Specific Protein Regulation of Triple Negative Breast Cancer. *Breast Cancer Res. Treat.* **2021**, *185*, 39–52. [[CrossRef](#)] [[PubMed](#)]

118. Martin, E.; Palmic, N.; Sanquer, S.; Lenoir, C.; Hauck, F.; Mongellaz, C.; Fabrega, S.; Nitschké, P.; Esposti, M.D.; Schwartzentruber, J.; et al. CTP Synthase 1 Deficiency in Humans Reveals Its Central Role in Lymphocyte Proliferation. *Nature* **2014**, *510*, 288–292. [[CrossRef](#)] [[PubMed](#)]
119. Lynch, E.M.; DiMattia, M.A.; Albanese, S.; van Zundert, G.C.P.; Hansen, J.M.; Quispe, J.D.; Kennedy, M.A.; Verras, A.; Borrelli, K.; Toms, A.V.; et al. Structural Basis for Isoform-Specific Inhibition of Human CTPS1. *Proc. Natl. Acad. Sci. USA* **2021**, *118*, e2107968118. [[CrossRef](#)] [[PubMed](#)]
120. Verschuur, A.C.; Gennip, A.H.V.; Leen, R.; Muller, E.J.; Elzinga, L.; Voûte, P.A.; Kuilenburg, A.B.P.V. Cyclopentenyl Cytosine Inhibits Cytidine Triphosphate Synthetase in Paediatric Acute Non-Lymphocytic Leukaemia a Promising Target for Chemotherapy. *Eur. J. Cancer* **2000**, *36*, 627–635. [[CrossRef](#)]
121. Verschuur, A.C.; Gennip, A.H.V.; Leen, R.; Meinsma, R.; Voute, P.A.; Kuilenburg, A.B.P.V. In Vitro Inhibition of Cytidine Triphosphate Synthetase Activity by Cyclopentenyl Cytosine in Paediatric Acute Lymphocytic Leukaemia. *Br. J. Haematol.* **2000**, *110*, 161–169. [[CrossRef](#)] [[PubMed](#)]
122. Moyer, J.D.; Malinowski, N.M.; Treanor, S.P.; Marquez, V.E. Antitumor Activity and Biochemical Effects of Cyclopentenyl Cytosine in Mice. *Cancer Res.* **1986**, *46*, 3325–3329. [[PubMed](#)]
123. Gharehbaghi, K.; Zhen, W.; Fritzer-Szekeres, M.; Szekeres, T.; Jayaram, H.N. Studies on the Antitumor Activity and Biochemical Actions of Cyclopentenyl Cytosine against Human Colon Carcinoma HT-29 in Vitro and in Vivo. *Life Sci.* **1998**, *64*, 103–112. [[CrossRef](#)]
124. Verschuur, A.C.; Gennip, A.H.V.; Leen, R.; Voûte, P.A.; Brinkman, J.; Kuilenburg, A.B.P.V. Cyclopentenyl Cytosine Increases the Phosphorylation and Incorporation into DNA of 1- β -D-arabinofuranosyl Cytosine in a Human T-lymphoblastic Cell Line. *Int. J. Cancer* **2002**, *98*, 616–623. [[CrossRef](#)] [[PubMed](#)]
125. Bierau, J.; van Gennip, A.H.; Leen, R.; Helleman, J.; Caron, H.N.; van Kuilenburg, A.B.P. Cyclopentenyl Cytosine Primes SK-N-BE(2)c Neuroblastoma Cells for Cytarabine Toxicity. *Int. J. Cancer* **2003**, *103*, 387–392. [[CrossRef](#)] [[PubMed](#)]
126. Verschuur, A.C.; Gennip, A.H.V.; Leen, R.; Kuilenburg, A.B.P.V. Increased Cytotoxicity of 2',2'-Difluoro-2'-Deoxycytidine in Human Leukemic Cell-Lines After a Preincubation with Cyclopentenyl Cytosine. *Nucleosides Nucleotides Nucleic Acids* **2004**, *23*, 1517–1521. [[CrossRef](#)]
127. Politi, P.M.; Xie, F.; Dahut, W.; Ford, H.; Kelley, J.A.; Bastian, A.; Setser, A.; Allegra, C.J.; Chen, A.P.; Hamilton, J.M.; et al. Phase I Clinical Trial of Continuous Infusion Cyclopentenyl Cytosine. *Cancer Chemother. Pharmacol.* **1995**, *36*, 513–523. [[CrossRef](#)]
128. Miran, T.; Vogg, A.T.J.; Moussaoui, L.E.; Kaiser, H.; Drude, N.; Felbert, V.; Mottaghy, F.M.; Morgenroth, A. Dual Addressing of Thymidine Synthesis Pathways for Effective Targeting of Proliferating Melanoma. *Cancer Med.* **2017**, *6*, 1639–1651. [[CrossRef](#)]
129. Cresce, C.D.; Figueredo, R.; Ferguson, P.J.; Vincent, M.D.; Koropatnick, J. Combining Small Interfering RNAs Targeting Thymidylate Synthase and Thymidine Kinase 1 or 2 Sensitizes Human Tumor Cells to 5-Fluorodeoxyuridine and Pemetrexed. *J. Pharmacol. Exp. Ther.* **2011**, *338*, 952–963. [[CrossRef](#)]

1.3 DNA replication stress and genome instability in cancer

Cancer is a multifactorial disease derived from uncontrolled and abnormal cell proliferation caused by various factors, which are described as Hallmarks of Cancer. One of the major hallmarks is genome instability deriving from several intrinsic and extrinsic factors leading to a disruption in DNA replication and the induction of DNA replication stress [40–42]. Consequently, a tightly regulated signalling network is crucial to maintain faithful DNA replication to avoid malignant transformation in dividing cells. This tightly regulated signalling network is orchestrated by the phosphatidylinositol-3 kinase-related kinase (PIKK) family including the serine/threonine kinases ataxia telangiectasia and Rad3 related (ATR), ataxia telangiectasia mutated (ATM) and DNA-protein kinase dependent catalytic subunit (DNA-PKcs) [43]. Errors in DNA replication cannot only lead to neoplastic development in early stages of tumorigenesis but can also be exploited as target in anti-cancer therapy.

Due to the potential role of NUDT22 in nucleotide synthesis, we will discuss the different signalling cascades responsible for DNA synthesis and repair upon DNA replication stress induction mediated through ATR and ATM with a focus on cancer. Furthermore, we highlight the targeting of pathways leading to DNA replication stress and the direct targeting of key players in the DNA replication stress response as strategy in cancer therapy.

1.3.1 DNA replication and DNA replication stress response

DNA replication in human combines DNA replication initiation, elongation and termination (*Fig. 6*). DNA replication is initiated in a two-step process starting at specific genomic regions, the so-called origins of replication. The first step involves the recognition of DNA replication sites, a process described as origin licensing. The second step involves DNA synthesis activation also known as origin firing [44].

All potential origins are licensed through loading of pre-replication complex proteins in G1 phase of the cell cycle. More specifically, origin recognition complex (ORC) followed by CDC6 and the DNA replication factor CDT1 bind to origins of replication thereby enabling the recruitment of the chromosome maintenance MCM helicase complex consistent of the six subunits MCM2-7 (*Fig. 6*). The assembly of the pre-

replication complex is tightly regulated to prevent re-replication during S-phase of the cell cycle [44]. For example, in human cells, to prevent further origin licensing before mitosis is finished, both ORC and CDC6 are rapidly degraded at the onset of S phase. In addition to rapid degradation, the biggest subunit of ORC, ORC1 is phosphorylated through CDK1/cyclin A to disable additional binding to replication sites [45].

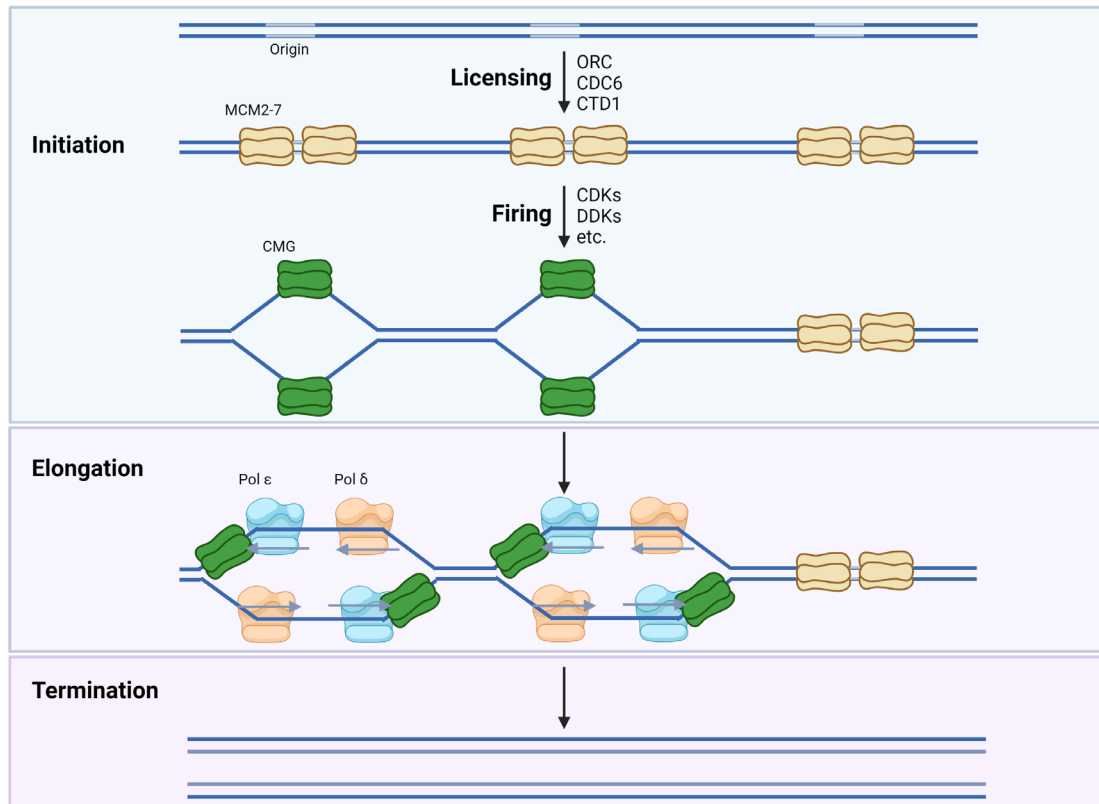


Figure 6. DNA replication. Simplified overview of DNA replication steps. DNA replication is initiated through loading of pre-replication complex proteins such as ORC, CDC6 and CTD1 thereby initiating the binding of the chromosome maintenance MCM helicase complex. DBF4-dependent kinases (DDKs) and cyclin-dependent kinases (CDKs) initiate origin firing through phosphorylation of MCM2-7 resulting in DNA unwinding and DNA replication fork generation. CDKs and DDKs furthermore mediate the recruitment of DNA replication proteins such as GINS and CDC45, which form together with MCM the CMG complex required for further unwinding of the DNA and DNA replication initiation. Through the binding of DNA polymerase ϵ and δ the DNA is elongated and eventually terminated. Figure is adapted from *Dewar et al., 2017* and created with Biorender.com [46].

During G1-S phase transition, pre-initiation complex assembly regulated through both, DBF4-dependent kinases (DDKs) and cyclin-dependent kinases (CDKs) initiate origin firing (*Fig. 6*). It should be added that, even though all origins of the replication unit are licensed, some origins remain silent and are not activated, which is suggested to be controlled by the activation of ATR and ATM followed by downstream pathways such

as cell cycle regulation by cell cycle checkpoint kinases. Origins chosen to be activated can differ from cell to cell in the same cell population uncoupling origin licensing from firing. Furthermore, there are three classes of origins present in cells. Flexible origins are the most common class and their activation varies from cell to cell. Constitutive origins represent the smallest class of origins and are characterised by their constant firing. The third class includes dormant origins, which are only activated in case of abnormal cell cycle progression following DNA damage and replication fork stalling thereby maintaining genome integrity [44].

The MCM helicase complex is activated through MCM2-7 phosphorylation mediated by CDKs and DDKs causing DNA unwinding and the activation of the MCM hexamer complex thereby inducing the formation of two functional DNA replication forks moving in opposite directions from the activated origin [44].

The activation of the MCM helicase complex activates and recruits additional proteins to the site of replication, which form part of the replisome protein complex required for DNA unwinding and elongation of the leading and lagging strand, the second step of DNA replication (*Fig. 6*). The functional helicase CMG complex present at each DNA replication fork includes the activated heterohexameric ring MCM helicase complex, the tetrameric GINS complex and CDC45 causing further unwinding of the DNA required for DNA synthesis [44]. Single stranded DNA (ssDNA) caused by DNA replication fork formation is immediately coated and thus stabilised by replication protein A (RPA). On the leading strand, DNA synthesis takes place through recruitment of proliferating cell nuclear antigen (PCNA) and DNA polymerase ϵ by replication factor A (RFA). Since DNA polymerases move in 5'-3' directions, elongation of the lagging strand requires the insertion of a short DNA/RNA primer sequence by DNA polymerase α . More specifically, DNA polymerase α consists of four subunits, with either primase or polymerase function. Subsequently, the primase subunits first insert a short RNA primer, which is elongated to approximately 8-10 nucleotides by the DNA polymerase subunit. This switch from primase to polymerase activity is initiated by the ATP-dependent replication factor C (RFC). Polymerase α is then removed by RFA followed by the recruitment of PCNA/DNA polymerase δ complex by RFC extending the primer and thereby forming short sequences of DNA, the so-called Okazaki fragments consistent of approximately 20-30 nucleotides in human. To

synthesise double stranded DNA (dsDNA) of the lagging strand, polymerase δ displaces the initiator primer into a 5' flap structure, which has to be cleaved by Flap endonuclease 1 (FEN1) or, in case of longer flap structures, by helicase-nuclease DNA synthesis defective protein for ligation with DNA ligase 1 regulated by PCNA [47].

In contrast to DNA replication initiation and elongation, the exact mechanisms and pathways leading to DNA replication termination have yet to be uncovered (*Fig. 6*). One suggested mechanism of DNA replication termination starts with the formation of supercoils due to overwinding of unreplicated DNA when DNA replication forks come too close to each other towards the end of the replicon, also known as convergence. An increase in supercoils ultimately causes a decrease in DNA replication fork speed and DNA replication in general. During convergence, supercoils can either be relaxed by DNA topoisomerases type I and type II or by clockwise rotation of DNA forks to the direction of fork movement resulting in the generation of pre-catenanes due to cross over of both replicated DNA strands. Pre-catenanes can then be removed by topoisomerase II. The eventual encounter of DNA replication forks terminates convergence, but does not cause DNA replication fork stalling due to by-pass of both CMG machineries. Once CMG is associated with dsDNA after gap filling between 3' end of the leading strand and the last Okazaki fragment of opposing DNA replication fork, the replisome is unloaded and MCM7 ubiquitylation is initiated. The last step of DNA replication termination is suggested to be catenane formation after unwinding of the final part of parental DNA double-helix, which have to be resolved by topoisomerases before chromosome segregation [46].

Even though DNA replication is a tightly regulated process to preserve genome integrity, it can be impaired by multiple intrinsic as well as extrinsic obstacles leading to a stop in DNA replication machinery progression accompanied by ssDNA formation and/or transient slowing or stalling of DNA replication forks. This process is better known as DNA replication stress. Extrinsic obstacles such as UV or ionizing radiation, chemotherapeutics or hypoxia can cause DNA replication stress and, more specifically, ssDNA breaks (SSBs). In contrast, intrinsic, also known as endogenous factors such as ROS formation, oncogene activation, uncontrolled origin firing, the disruption of nucleotide synthesis or misincorporation of nucleotides and nucleotide analogues can

lead to DNA replication stress and the formation of both, ssDNA as well as SSBs (Fig. 7) [48].

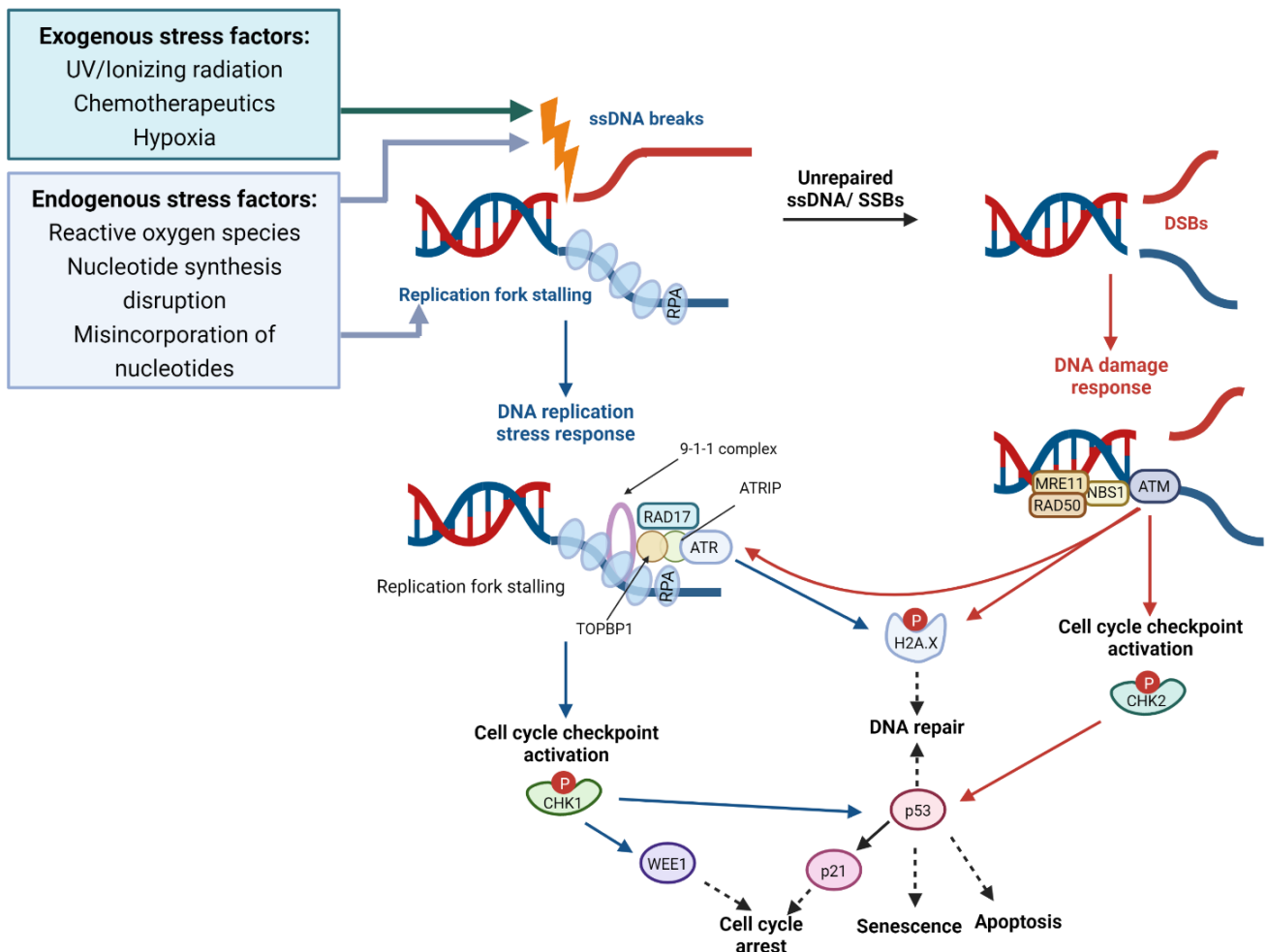


Figure 7. DNA replication stress. Simplified overview of DNA replication stress response with the focus on the ataxia telangiectasia and Rad3 related (ATR) and ataxia telangiectasia mutated (ATM) kinases. Exogenous and endogenous factors cause the formation of ssDNA breaks (SSBs) and/or stalling of DNA replication forks followed by ssDNA coating of RPA and DNA replication stress response induction (blue). Ataxia telangiectasia and RAD17 complexes are assembled at ssDNA sites. The activation of cell cycle checkpoint kinase 1 (CHK1) by ATR then prevents cell cycle progression to enable DNA replication fork reverse and restart for DNA replication resumption. If DNA replication forks cannot be reversed or in case of DNA replication fork collapse, the DNA damage response (red) is initiated upon recruitment of ATM, which phosphorylates the DNA damage repair factor H2A.X for DNA repair induction or the cell cycle checkpoint kinase 2 (CHK2). CHK1 and CHK2 activate p53 to either induce senescence, apoptosis or DNA repair or via, p21 activation, induce cell cycle arrest. Figure adapted from Ngoi et al., 2020 and created with Biorender.com [49].

ssDNA gaps formed at replication fork junctions derive as a result from polymerase and MCM helicase uncoupling from the DNA replication complex, and are characteristic at sides of stalled DNA replication forks [50,51]. RPA binds exposed

ssDNA, thereby initiating the DNA replication stress response to maintain correct DNA replication and to resolve DNA replication stress. More specifically, ssDNA coating by RPA results in the recruitment of the sensor proteins ATR-interacting protein (ATRIP), the Rad9-Hus1-Rad1 (9-1-1) DNA clamp complex, topoisomerase II binding protein (TOPBP1), and Ewing tumour-associated antigen 1 (ETAA1). This network of sensor proteins causes the stabilisation of stalled replication forks to ensure rapid restoring of DNA synthesis by the recruitment and activation of the central replication stress kinase ATR. ATR then induces the phosphorylation and therefore, activation of one of its downstream target, the main effector kinase checkpoint kinase 1 (CHK1) (*Fig. 7*) [52,53].

ATR signalling can regulate nucleotide pool levels via nucleotide *de novo* synthesis and, more specifically, ribonucleotide reductase (RNR) activity regulation through CHK1, or via the regulation of the pyrimidine salvage kinase deoxycytidine kinase (dCK) activity for DNA repair [54–56]. In case of reduced nucleotide levels, ATR phosphorylates and thus, activates the fanconi anaemia (FA) group D2 (FANCD2) associated with MCM replicative helicase to decrease DNA synthesis speed and prevent the formation of long ssDNA [51].

ATR-mediated activation of the DNA replication stress response also inhibits late-stage origin firing and further ssDNA generation, which would lead to RPA exhaustion and the collapse of DNA replication forks causing DNA double strand breaks (DSBs) [57]. In addition, the activation of the ATR-CHK1 signalling cascade can lead to cell cycle arrest through WEE1 activation resulting in a delay in G2-M transition through inhibition of CDKs (*Fig. 3*) [58]. Consequently, DNA replication forks can be either repaired or restarted for complete replication of the affected region and to repair DNA lesions before entering mitosis [59,60]. Alternatively, DNA replication can resume from so-called dormant origins, which are non-licensed origins that act as backup in case of replication fork stalling [48].

DNA replication stress is the major source for the formation of DSBs, the most cytotoxic DNA lesions. In case of prolonged fork stalling or the failure to resume DNA synthesis resulting in DNA replication fork collapse, DSBs are formed causing the initiation of another tightly regulated signalling cascade, the DNA damage response (DDR) [61–63]. DDR upon DSBs requires the recruitment and activation of the ataxia-

telangiectasia mutated (ATM) checkpoint kinase through interaction with the MRE11-RAD50-NBS1 (MRN) complex [64]. ATM then phosphorylates and therefore, activates the cell cycle checkpoint kinase 2 (CHK2), which then dissociates from the DNA damage sites to interact with multiple targets responsible for cell cycle progression, DNA repair and apoptosis (*Fig. 7*) [65].

In addition, the activation of ATM initiates the phosphorylation of histone variant H2A.X, one of the major DNA repair factors, to its active form γ H2A.X (*Fig. 7*) [66]. H2A.X is part of the nucleosome and is predominantly activated upon DSBs formation [66]. However, H2A.X can also participate in the surveillance of DNA replication through its activation by ATR upon SSBs formation induced by UV irradiation as well as the RNR inhibitor hydroxyurea (HU) [67].

Depending on the type of DNA damage, cells have acquired several pathways to repair DNA damage for successful DNA replication and to prevent genome instability. Base excision repair (BER) is a repair pathway involved in the correction of small base lesions deriving from deamination, oxidation or methylation without inducing significant changes in DNA helix orientation. After chromatin remodelling, damaged single bases are recognised by specific DNA glycosylases creating an abasic site. The endonuclease-generated gap can then either be repaired by DNA polymerase β in non-proliferative cells or polymerase δ/ϵ in proliferative cells followed by flap cleavage and ligation in case of oxidised and reduced sites. In case of single base sites, DNA polymerase β and ligation mediated by ligase 1 or ligase 3 in complex with XRCC1 are used for DNA damage repair [68]. In case of DNA helix distortion due to bulky lesions induced by exogenous sources such as UV radiation or chemotherapeutics, the damaged ssDNA segments can be repaired by nucleotide excision repair (NER). Here, the damaged sites are first removed by the two endonucleases XPF-ERCC1 and XPG followed by gap filling mediated by DNA polymerase δ and ϵ and ligase 1-initiated ligation. For the removal of mismatched nucleotides caused either during DNA replication or through exogenous factors such as hypoxia in the mismatch repair (MMR) pathway, either MSH2:MSH6 or MSH2:MSH3 recognise the DNA damage site followed by endonuclease-mediated cleavage. DSBs can either be repaired by non-homologous end joining (NHEJ) or homologous recombination (HR). Whereas HR requires a template for successful DNA repair, NHEJ repair DSBs by direct ligation

enabling faster DNA damage repair. More specifically, DSBs are recognised by the Ku70/Ku80 heterodimer inducing the recruitment of DNA-PKcs, XRCC4, DNA ligase 4 and other components for DNA damage repair to the damage site. In contrast, HR is a tightly regulated DNA damage repair process regulated by several co-factors such as BRCA1, BRCA2 and ATM, and less error prone due to the utilisation of a homologous template of the damaged DNA sites. 3' overhangs are created through 5'-to-3' nucleolytic degradation, which are immediately coated by RPA. RPA is displaced by RAD51, which mediates the localisation of the required sequence for DSB repair in the template DNA [68].

Similar to DNA repair activation through γ H2A.X upon both, SSBs and DSBs, the DNA replication stress response and the DDR are not separate pathways due to existing crosstalk between ATR and ATM especially during S and G2 phase of the cell cycle. In response to DSBs generated by irradiation ionisation, ATM-mediates DNA end resection to provide ssDNA for RPA coating and therefore, the activation of ATR/CHK1 signalling for DNA repair (*Fig. 7*) [69–71].

If DNA lesions persist and DNA replication does not resume, both ATR-CHK1 as well as the ATM-CHK2 signalling cascade can activate the tumour suppressor p53, which in turn induces several pathways to maintain genome integrity (*Fig. 3*). P53 activation can lead to both apoptosis and senescence, but it can also induce DNA repair pathways as well as cell cycle arrest. The p53-mediated activation of the tumour suppressor P21 and the retinoblastoma protein Rb, similar to WEE1, results in CDKs inhibition and consequently, cell cycle arrest through the prevention of G1/S and G2/M phase transition (*Fig. 7*) [72,73]. In addition, P21 can also interact with PCNA to prevent DNA replication *in vitro* [74].

1.3.2 Differences in DNA replication stress response in cancer

Precancerous and cancerous lesions are often associated with elevated levels of DNA replication stress to maintain high proliferation for cancer development and progression. Either, activation or overexpression of cancer promoting factors, the so-called oncogenes, frequently trigger DNA replication stress in cancer. The activation of oncogenes, another Hallmark of Cancer, can directly interfere with DNA replication by inducing changes in DNA replication fork speed and either origin licensing or firing, thereby inducing DNA replication stress. In addition, mutations or reduced expression

of tumour suppressors as well as cell cycle checkpoints and other key players in both, the DNA replication stress response and DDR, can lead to premature entry into mitosis and the replication of unrepaired DNA risking genome instability [75].

The three proto-oncogenes *K-RAS*, *H-RAS* and *N-RAS* of the RAS protein family belong to one of the best characterised and most often genetic altered oncogene family in cancer. These proteins act as GTPase signal transducers important for the regulation of cell metabolism, growth and survival [76]. Mutations often observed in cancer cells result in a constant activation of *RAS* and consequently, increased cell proliferation and metabolic reprogramming to escape cell death. Overexpressed oncogenic *RAS* promotes origin firing leading to asymmetric replication forks and the induction of DNA replication stress [77]. Furthermore, oncogenic *RAS* directly interacts with one of the RNR subunits responsible for nucleotide synthesis resulting in nucleotide pool depletion and the impairment of replication fork progression [78,79].

Another example of oncogenes responsible for DNA replication stress induction, are cyclin E1 and E2, the two members of the cyclin E protein family. In healthy cells, these proteins regulate DNA replication during G1/S phase through phosphorylation of DNA replication factors. In cancer cells, overexpression of *cyclin E* can result in either increased or reduced origin firing due to its interference with the pre-replication complex assembly during G1 phase of the cell cycle [80–82]. Cell cycle progression and consequently, DNA replication induction by cyclin E, requires the presence of the cell cycle progression regulators CDKs. CDKs are activated through the binding of cyclin to induce cell cycle progression leading to premature entry into mitosis and potential genome instability [83]. Similar to *RAS*, cyclin E overexpression can lead to hyperproliferation and therefore, nucleotide depletion causing DNA replication fork collapse and DSBs [36]. The generated one-ended DSBs can be repaired by break-induced replication (BIR) to maintain DNA replication and cell proliferation. DNA repair by BIR is, however associated with the induction of genomic rearrangements such as tandem duplications and copy number alterations, which can lead to genome instability and cancer development [84].

The MYC family consistent of the three members c-, l- and mMYC is another important key player in oncogenic-induced DNA replication stress with altered cMYC expression in more than 50% of cancers. In healthy cells, this family of transcription factors are

responsible for correct cell proliferation, differentiation and apoptosis induction [85]. Similar to *RAS* and *cyclin E* overexpression, activated MYC can interfere with origin firing through the interaction with cyclins/CDKs and the transcription factor E2F, thereby inducing DNA replication fork stalling followed by DNA replication fork collapse and DNA damage induction. [79,86].

Oncogene-induced DNA replication stress leads to the robust activation of DDR and irreversible cell cycle arrest, also known as oncogene-induced senescence (OIS). OIS is considered as a barrier for tumorigenesis but can be circumvented by often-observed gene expression alterations or mutations of key players of the DNA replication stress pathways as well as tumour suppressors [77,87]. Tumour suppressors act as counterparts to the cancer driving oncogenes, resulting in a barrier for oncogene-induced DNA replication stress and damage and the maintenance of genome stability. In later cancer stages, tumour suppressor genes often acquire either loss- or gain-of-function mutations, which potentially lead to a loss in oncogene-induced replication stress prevention and, more specifically, cell cycle progression of unrepaired DNA lesions, thereby causing genome instability. Mutations in the DDR kinase *ATM*, the tumour suppressor *TP53* and the ubiquitin-ligase encoding *MDM2* often observed in cancer lead to the escape of apoptosis as well as senescence, and thus, cell death in cancer [75]. Since *ATM* plays a key role in the initiation of DSBs repair after replication fork collapse and recruits the *TP53* product p53 to induce apoptosis or senescence upon unsuccessful DNA repair, both, *TP53* and *ATM* are often downregulated or acquire loss-of-function mutations in cancer cells. In contrast, p53 degradation and therefore, inactivation is dependent on ubiquitin ligase *MDM2* activity resulting in the often overexpression of *MDM2* in cancer cells to prevent cell death or senescence [88].

1.3.3 DNA replication stress as target in cancer therapy

In contrast to healthy cells, cancer cells experience high rates of DNA replication stress to maintain high proliferation rates for cancer cell survival. However, DNA replication stress can also be exploited in anti-cancer therapy by introducing additional DNA replication stress, leading to DNA damage in a catastrophic manner or by promoting cell cycle progression besides DNA replication fork disruption and, thereby inducing cancer cell death.

Many traditional cancer drugs act through DNA replication stress or DNA damage induction albeit not being their proposed mode of action during drug development. However, they mostly exhibit their action through direct DNA damage and/or the depletion of cellular resources for successful DNA replication such as nucleotides. One example of DNA replication stress inducing compounds by nucleotide depletion as well as DNA incorporation, are nucleoside analogues, which were already extensively reviewed in *Chapter 1.2*, with 5-fluorouracil (5-FU), gemcitabine and cytarabine as the most famous examples. Both, cytarabine and gemcitabine, are dC analogues competing with the natural occurring nucleotide dCTP for DNA incorporation, thereby inducing a delay or termination in DNA replication fork progression [89,90]. In addition, gemcitabine inhibits RNR, an enzyme involved in both purine and pyrimidine synthesis to reduce general nucleotide levels, whereas 5-FU only impairs the synthesis of dTTP via thymidine synthase (TS) inhibition [89,91]. Platinum-based compounds such as cisplatin and carboplatin as well as alkylating agents such as decarbazine and temozolamide induce DNA replication stress and damage based on either the generation of intra- or interstranded DNA base crosslinks and/or alkylation of DNA bases. Intra- and interstrand crosslinks as well as DNA adducts form physical barriers that cause the disruption in DNA replication machinery progression [92,93]. Other agents creating an obstacle for DNA replication are PARP as well as topoisomerase targeting agents, which cause the disruption of DNA synthesis and the induction of the DNA replication stress response and, in case of DSB formation, the activation of the DDR. Topoisomerase inhibitors directly damage DNA through the formation of stable protein-DNA complexes, thereby blocking DNA replication fork progression and often cause DSBs [94–96]. One of the proposed mechanisms for PARP inhibition is the trapping of PARP on DNA after PARP recruitment to ssDNA sites. This creates a physical barrier for SSB repair prevention causing potential DNA replication fork collapse and DSBs in cancer cells [97].

Even though the above-described DNA replication stress and damage inducing agents are still used in the clinics, they often come with limitations such as toxicity, lack in efficacy and tumour resistances due to the upregulation of key players in both, the DNA replication stress and DDR in cancer cells [98–100]. Therefore, in addition to amplifying DNA replication stress, the direct targeting of the S phase checkpoint response key players ATR and CHK1 was proposed to promote cell cycle progression

besides unrepaired ssDNA or DSBs, causing premature entry in mitosis and consequently, cancer-specific synthetic lethality [101]. After promising preclinical studies in several cancer models, multiple potent ATR and CHK1 inhibitors are currently assessed in Phase I and II clinical trials (*Table 1*) [102].

Table 1. Overview of a selection of Phase I and II clinical trials of inhibitors targeting key players in the DNA replication stress response alone or in combination with other DNA damage inducing agents. Inhibitors included in this table are targeting ataxia telangiectasia and Rad3 related (ATR), ataxia telangiectasia mutated (ATM) kinases, the cell cycle checkpoint kinase 1 (CHK1) or the gatekeeper of G2-arrest and cell cycle progression WEE1.

Drug name	Target	Clinical trials	
Ceralasertib (AZD6738)	ATR	In chronic myelomonocytic leukaemia (NCT03770429)	Phase I
		Combined with olaparib or carboplatin in advanced solid malignancies (NCT02264678)	Phase I/II
		With olaparib in recurrent ovarian cancer (NCT03462342)	Phase I/II
		With gemcitabine as combination therapy in cancer (ATRIUM) (NCT03669601)	Phase II
AZ20	ATM/ATR	-	
MK8776	CHK1	With cytarabine in acute leukaemia (NCT00907517) and relapsed acute myeloid leukaemia (NCT01970596)	Phase I/II
		With gemcitabine in solid tumours or lymphoma (NCT00779584)	Phase I
AZD7762	CHK1	Alone or with gemcitabine in advanced solid malignancies (NCT00413686)	Phase I
		Combined with gemcitabine in solid tumours and advanced solid malignancies (NCT00937664)	Phase I
Prexasertib	CHK1	In advanced solid tumours (NCT02514603/NCT02778126)	Phase I
		In combination with cytarabine or fludarabine in acute myeloid leukaemia (NCT02649764)	Phase I
		With olaparib in advanced solid tumours (NCT03057145)	Phase I

		Advanced solid tumours (NCT01748825)	Phase I
Adavosertib (MK-1775)	WEE1	With gemcitabine in ovarian, primary peritoneal, or fallopian tube cancer (NCT02101775)	Phase II
		With cisplatin in recurrent or metastatic head and neck cancer Carboplatin (NCT02196168)	Phase II

Since cancer cells can escape DNA damage induced by standard-of-care anti-cancer agents by upregulating key players in DDR, a novel strategy suggests the combination approach of ATR and/or CHK1 inhibition and standard-of-care DNA replication stress inducing agents. Preclinical studies in *BRCA*-mutant ovarian cancer cell and patient-derived xenograft models have shown an increase in sensitivity towards co-targeting of PARP with olaparib and either targeting CHK1 with MK8776 or ATR with AZD6738 (ceralasertib) alone or in combination [100].

In addition, combining gemcitabine with the ATR inhibitors ceralasertib as well as AZ20 increased cancer cell death in pancreatic cancer cell models at low concentrations and ceralasertib significantly prolonged survival in pancreatic ductal adenocarcinoma (PDAC) *in vivo* models [103,104]. The efficacy of gemcitabine could also be improved by co-treatment with the CHK1 inhibitor AZD7762 in aggressive KRAS-driven Lkb1-deficient lung adenocarcinoma *in vitro* and *in vivo* [105]. Simultaneous targeting of cell cycle checkpoints as well as pathways leading to DNA replication stress opens up promising new strategies to improve cancer patients' response and toxicity, which are currently evaluated in Phase I and II clinical trials in multiple cancers. For example, the ATR inhibitor AZD6738 is currently assessed in combination with carboplatin or olaparib for the treatment of advanced solid malignancies in a Phase I/II clinical trial. Moreover, a Phase I clinical trial assessing the CHK1 inhibitor prexasertib in combination with the nucleoside analogues cytarabine and fludarabine in AML opens up a promising new strategy for better prognosis in cancer patients (*Table 1*) [102].

Another proposed strategy to overcome observed limitations of standard-of-care anti-cancer agents involved in DNA replication stress and DDR induction is the targeting of the gatekeeper of G2-arrest, WEE1. Similar to ATR and CHK1 inhibitors, WEE1

inhibition leads to premature entry into mitosis by promoting G2-M phase transition besides uncompleted DNA replication causing mitotic catastrophe and cancer cell death [106]. Especially in p53-deficient cancers, which are more dependent on G2 cell cycle checkpoint due to the loss in G1-S phase checkpoint regulation, the inhibition of WEE1 was shown to be of advantage to promote cancer cell death in several preclinical studies as well as Phase II clinical trials with adavosertib (MK-1775) (*Table 1*) [106–109]. Adavosertib is currently the only WEE1 inhibitor assessed in clinical trials as monotherapy as well as in combination with other DDR targeting agents such as gemcitabine, cisplatin or carboplatin (*Table 1*) [109–112]. In addition, co-targeting of WEE1 with adavosertib and CHK1 in preclinical studies induced synergistic effects on cancer cell death *in vitro* as well as on tumour growth and survival in xenograft models *in vivo* suggesting the further exploration of combining WEE1 and CHK1 inhibition in cancer therapy [113–116].

Taken together, targeting of pathways impairing DNA replication as well as key players involved in the response to both, DNA replication stress and damage alone or in combination remains an important strategy in cancer therapy. Consequently, the identification of novel targets and combination approaches are necessary for better treatment strategies and improved prognoses for cancer patients.

1.4 Objectives

Our group previously identified *NUDT22*'s hydrolase activity towards UDP-glucose resulting in the generation of G1P as well as UMP [26]. Whereas G1P can directly enter glycolysis upon phosphorylation to G6P, UMP is a known precursor for the synthesis of the two pyrimidines, dCTP and dTTP. Furthermore, analysis of the TCGA revealed the presence of *NUDT22* genetic alterations in several cancer tissues suggesting a potentially specific role of *NUDT22* in cancer. Cancer cells are known to frequently have altered metabolism and increased activity of nucleotide metabolising enzymes has been identified in cancer [117]. Here, we hypothesise a role for *NUDT22* in pyrimidine synthesis that can be exploited as a novel target for the development of anti-cancer drugs.

To test this hypothesis, the following objectives have been set:

(1) to determine the role of *NUDT22* in pyrimidine synthesis in U2OS osteosarcoma and the non-cancer cell line hTERT-RPE1;

(2) to clarify the effects of *NUDT22* knockout (KO) on DNA replication stress in breast cancer MCF7 cells on their own as well as in combination with commonly used anti-cancer agents;

(3) to validate differences in tumour growth upon *NUDT22* KO in MCF7 xenograft models.

(4) to develop first-in-class small molecule *NUDT22* inhibitors by computer-aided drug design (CADD); and,

(5) to determine their biochemical activity, effects on DNA replication stress and cell proliferation; and to assess their target engagement with recombinant *NUDT22* protein and in cell lysate.

2. Materials and Methods

2.1 Antibodies

Primary and secondary antibodies were used in the following experiments accordingly (*Table 2*).

Table 2. Overview of antibodies used in western blot (WB), immunofluorescence (IF), DNA fibre and EdU incorporation experiments.

Antibody	Supplier	Catalogue number	Experiments and dilutions
NUDT22 (H-9)	SantaCruz Biotechnologies	sc-515491	WB (1 :1,000)
P53 (DO-1)	SantaCruz Biotechnologies	sc-126	WB (1 :1,000)
P21 (H-164)	SantaCruz Biotechnologies	sc-756	WB (1 :1,000)
SOD1	SantaCruz Biotechnologies	sc-17767	WB (1 :10,000)
ATM (11G12)	SantaCruz Biotechnologies	sc-53173	WB (1 :1,000)
P-ATM	SAB Signalway Antibody	12701	WB (1 :1,000)
β-Actin	Abcam, Dallas	ab8227	WB (1 :10,000)
γH2A.X	Millipore, Merck Life Science	05-636	WB (1 :1,000) IF (1 :1,000)
P-RPA	Bethyl Laboratories, Inc.	A300-245A	WB (1 :1,000)
RPA	Cell Signaling Technology	2208	WB (1 :1,000) IF (1 :1,000)
CHK1	Cell Signaling Technology	2G1D5	WB (1 :1,000)
pCHK1	Cell Signaling Technology	133D3	WB (1 :1,000)
CHK2	Cell Signaling Technology	3440S	WB (1 :1,000)

pCHK2	Cell Signaling Technology	2661S	WB (1 :1,000)
Starbright Blue 700 (mouse)	Bio-Rad Laboratories	12004158	WB (1 :10,000)
Starbright Red 520 (rabbit)	Bio-Rad Laboratories	12004161	WB (1 :10,000)
HRP (mouse)	Thermo Fisher Scientific	31430	WB (1 :10,000)
HRP (rabbit)	Abcam, Dallas	ab6721	WB (1 :10,000)
HRP (rat)	Sigma-Aldrich	A9037	WB (1:10,000)
Alexa Fluor-488 (mouse)	Thermo Fisher Scientific	A32723	DNA fibre (1:500) IF (1:1,000)
Alexa Fluor-488 (rat)	Thermo Fisher Scientific	A21208	IF (1:1,000)
Alexa Fluor 555 (rat)	Thermo Fisher Scientific	A21434	DNA fibre (1 :500)
Alexa Fluor-647 (mouse)	Thermo Fisher Scientific	A32728	IF (1 :1,000)
DAPI	Sigma-Aldrich	D9542	IF (1 :1,000) EdU (1 :1000)
Atto488	Sigma-Aldrich	41051	EdU (1 :1000)
Rat anti-BrdU	Abcam	ab6326	DNA fibre (1 :1,000)
Mouse anti-BrdU	BD Biosciences	347580	DNA fibre (1 :500)

2.2 Cell lines and culturing conditions

The osteosarcoma U2OS and the retinal pigment epithelial hTERT-RPE1 cell lines were originally purchased from the American Type Culture Collection (ATCC). Wild-type and *NUDT22* knockout U2OS and hTERT-RPE1 cells were cultured in Gibco™ Dulbecco's Modified Eagle Medium (DMEM) Glutamax (cat. no. 11965092, Thermo Fisher Scientific) supplemented with 10% fetal bovine serum (FBS), penicillin (60-100 µg/mL) and streptomycin (100 µg/mL).

The breast cancer cell line MCF7 was obtained from ATCC and wild-type and *NUDT22* knockout MCF7 cells were cultured in Lonza® or Gibco™ RPMI 1640 medium supplemented with 10% FBS, penicillin (60-100 µg/mL), streptomycin (100 µg/mL) and 2 mM L-glutamine.

All cells were grown in a humidified incubator at 37°C with 5% CO₂. The cells were regularly assessed for Mycoplasma contamination (MycoAlert, Lonza, Basel, Switzerland) and short-tandem repeat (STR) profiling was performed for cell line validation.

2.3 CRISPR/Cas9 gene editing

CRISPR/Cas9 gene editing was performed as described in the method section in the manuscript in *Chapter 3*. Briefly, *NUDT22* gene knockout (KO) in hTERT-RPE1 (*NUDT22* clones 1-5 and 2-1) and U2OS cells (*NUDT22* clones 1-2 and 3-6) was performed and single KO clones were selected by Patrick Herr in collaboration with Thomas Helleday at Karolinska Institute, Stockholm, Sweden. The gene editing in MCF7 cells was either performed in-house (KO3) or by Synthego (Redwood City, CA, USA), here described as KO14. SgRNA sequences were used as described in *Table 2* and NT sgRNA was used for respective control cells.

Table 3. sgRNA used for CRISPR/Cas9 gene editing in U2OS, hTERT-RPE1 and MCF7 cells.

U2OS/hTERT-RPE1	5'-AUCCUCUACAACCGGGUUCAGGG-3' 5'-GUCCCACUGGAGCGGCCCUAGGG-3' 5'-ACUUUAUUCUUGGAUUCGGUUGG-3'
MCF7 KO3	5'-CCGGCUAAAGGCCCAACCC-3'
MCF7 KO14 (Synthego)	5'-GACAAGGAAGUCAUCGGCUG-3'

The selection of transfected cells was performed with either puromycin (U2OS and hTERT-RPE1) or after transfection with Cas9-GFP (Sigma) by flow cytometry retaining the top-10% population (MCF7 KO3) performed by Patrick Herr and Victoria Cookson. Individual in-house and Synthego MCF7 KO clones were assessed based on the amplification of genomic DNA using Q5[®] Hot Start High-Fidelity DNA Polymerase (M0493L, New England Biolabs Inc., Ipswich, MA, USA) according to manufacturer's protocol with the following primer sequences: 5'-ATCCTGAGGTGACCTTGCT-3' and 5'-ACTAGCCACAGCCGATGA-3'. Gene editing was further assessed by performing T7 Endonuclease 1 Assay (M0302, New England Biolabs Inc.) followed by purification of selected PCR products with Monarch[®] PCR and DNA Cleanup kit (T1030L, New England Biolabs Inc.) and Sanger sequencing.

2.4 Growth curve

300 MCF7 control and KO cells were seeded per well in twelve replicates to a 96 well plate and incubated for 10 days in total. To assess cell viability, after each 24 hours, resazurin (sc-206037, Santa Cruz Biotechnology) was added and the fluorescence was measured at 560 nm Ex/590 nm EM after 3 hours using a Molecular Devices ID5 plate reader (Molecular Devices, San Jose, CA, USA).

2.5 Glutamine starvation

For glutamine starvation experiments, U2OS and hTERT-RPE1 control and KO cells were harvested and washed once in phosphate buffered saline (PBS) followed by resuspension in glutamine free Gibco[™] DMEM medium. First, dilution series of glutamine (2 mM – 7.8 μ M) in triplicate were spotted on 96 well cell culture plates. 2000 cells per well were seeded and incubated at 37°C. After 4 days, cell viability was assessed using Resazurin (sc-206037, Santa Cruz) and a Molecular Devices ID5 plate reader.

2.6 Drug exposure for cell viability assessment

To assess cell viability in U2OS and hTERT-RPE1 control and *NUDT22* KO cells, pyrazofurin (SML1502, Sigma-Aldrich) (200 μ M – 5 μ M), leflunomide (L5025, Sigma-Aldrich) (400 μ M – 10 μ M), brequinar (5.08321, Sigma-Aldrich) (200 μ M – 10 μ M), and hydroxyurea (H8627, Sigma-Aldrich) (5 mM – 0.05 mM) were used. Cell viability in U2OS control and *NUDT22* KO cells was assessed with *NUDT22* inhibitors A1- A3

(100 μ M – 0.05 μ M) and A3 - A6 (100 μ M – 1 μ M). Pyrazofurin (200 μ M – 2 μ M) as well as brequinar and leflunomide, at the same concentrations as in U2OS and hTERT-RPE1 cells, were used to assess cell viability in MCF7 control and *NUDT22* KO cells. All drugs were dispensed at a log₂ dilution series in triplicate on 384 assay well plates using a Tecan D300e dispenser (Tecan, Männedorf, Switzerland). 500 cells per well were seeded and incubated for 4 days. On day 4, cell viability was assessed by using Resazurin assay (sc-206037, Santa Cruz). Fluorescence intensity at 560 nm Ex/590 nm EM was read on a Molecular Devices ID5 plate reader. Data analysis was performed using GraphPad Prism.

2.7 Western blotting

Western blotting was performed according standard protocols. Briefly, cells were collected, washed in PBS and resuspended in RIPA lysis buffer (150 mM sodium chloride, 1.0% Triton X-100, 0.5% sodium deoxycholate, 0.1% sodium dodecyl sulfate, 50 mM Tris, pH 8.0) containing 1x cOmplete™ protease inhibitor cocktail (04693159001, Roche, Basel, Switzerland) and incubated on ice for 10 min for cell lysis. The cell lysate was then sonicated with a needle sonicator (Sonics Vibracell™, 20% amplitude, 3 cycles 1 sec ON-OFF). The samples were centrifuged at 10,000 x g for 3 min to remove cell debris and protein aggregates.

The protein concentration of the supernatant was determined by performing Pierce™ BCA Protein Assay (cat. no. 23225, Thermo Fisher Scientific) according manufacturer's protocol and the absorbance was read at 562 nm with an ID5 plate reader (Molecular Devices).

20 μ g of each sample in 1x Laemmli sample buffer (Bio-Rad Laboratories) supplemented with 10% β -mercaptoethanol was first boiled for 5 min at 95°C and then loaded on a 4-20% Mini-PROTEAN® TGX™ Precast Protein gel (Bio-Rad Laboratories). In addition, Precision Plus Protein™-Dual Color Standard marker (#1610374, Bio-Rad Laboratories) was loaded as molecular weight marker. For protein separation by SDS-PAGE, the gel was run in 1x Tris/Glycine Buffer (Bio-Rad Laboratories) followed by transfer to a nitrocellulose membrane using the Trans-Blot® Turbo™ transfer system (Bio-Rad Laboratories). After confirming the successful transfer by using Ponceau staining, the membrane was blocked for 1 hour in 3%

bovine serum albumin (BSA) in tris buffered saline + 0.05% Tween-20 (TBST). Primary antibodies were then added to the membrane and incubated overnight at 4°C. After washing the membrane in TBST, the corresponding secondary antibodies were added and incubated for 1 hour at room temperature. In case of goat anti-mouse/rabbit/rat IgG secondary HRP antibodies, protein bands were detected by chemiluminescence after adding enhanced chemiluminescent (ECL) substrate (#1705061, Bio-Rad Laboratories, #34094 and #34577, Thermo Scientific). The concentrations of primary and secondary antibodies used in our western blot experiments are listed in *Table 2*. ChemiDoc™ MP Imaging System (Bio-Rad Laboratories) was used to take images followed by processing and analysing the protein bands with the Image Lab Software (Bio-Rad Laboratories).

2.8 DNA fibre

Duplicates of 500,000 MCF7 control and KO cells as well as duplicates of 500,000 KO cells were seeded. In addition, 500,000 KO cells in duplicate were exposed to 500 µM uridine (U3750, Sigma-Aldrich) for 24 hours. The next day, one well of each MCF7 control, KO and KO + 500 µM uridine were pulse-labelled with 25 µM 5-chloro-2'-deoxyuridine (CldU) for 30 min, washed with warm PBS and pulse-labelled with 250 µM 5-iodo-2'-deoxyuridine (IdU) for 30 min. After washing labelled and unlabelled cells two times in ice-cold PBS, the cells were harvested and 125,000 cells/mL of each unlabelled and labelled control, KO and KO + uridine to a final cell count of 250,000 cells/mL were prepared for fibre spreading. Briefly, 2.5 µL of cell suspension were added to Superfrost Plus microscopy slides and incubated at room temperature for 6 min. 30 µL of lysis buffer (200 mM Tris-HCl pH 7.4, 50 mM EDTA and 0.5% SDS) were then added for 10 min followed by slide tilting at approximately 45°C for fibre spreading. DNA fibres were then air-dried for a minimum of 4 hours in the dark. The slides were fixed using methanol/acetic acid 3:1 for 10 min at room temperature, excess volume was removed and slides were air-dried for 30 min. The slides were then incubated at -20°C for 24 hours.

For staining, DNA fibres were denatured with 2.5 M HCl for precisely 1 hour at RT. After neutralising in PBS, blocking with 2% BSA in PBS + 0.1% Tween-20 was performed for 1 hour at RT. Next, rat anti-BrdU monoclonal antibody (1:1000, 2% BSA in PBS + 0.1% Tween-20; Abcam, ab6326) to detect CldU and mouse anti-BrdU monoclonal antibody (1:500, 2% BSA in PBS + 0.1% Tween-20; cat# 347580, BD

Biosciences, Franklin Lakes, NJ, USA) for IdU detection were added and incubated for 1 hour at 37°C. The slides were washed in PBS and fixed with 4% paraformaldehyde (PFA) at RT for 10 min. After another washing step, the slides were incubated with both, goat anti-rat Alexa Fluor 555 (1:500, 2% BSA in PBS + 0.1% Tween-20; Invitrogen, A21434) and goat anti-mouse Alexa Fluor 488 (1:500, 2% BSA in PBS + 0.1% Tween-20; Invitrogen, A32723) secondary antibodies at 4°C for 1 hour. The slides were then mounted using ProLong™ Gold antifade reagent (Invitrogen, cat# P36934) and stored overnight at 4°C.

DNA fibres were then examined using a 63x oil immersion objective of a LSM980 Airyscan2 confocal laser scanning microscope (Zeiss, Jena, Germany). At least 250 replication structures per experiment were counted and the lengths of red (AF 555) and green (AF 488) labelled DNA replication structures were measured using the ImageJ software (National Institutes of Health; <http://rsbweb.nih.gov/ij/>). To calculate DNA replication fork speed, measured lengths were converted into micrometers using the scale bars created by the microscope and divided by the pulse-labelling time. Graphpad Prism was used for statistical analysis of IdU and CldU speed.

2.9 EdU incorporation

2000 MCF7 control or *NUDT22* KO cells were treated with 0.1 μ M pyrazofurin for 4 days on 96 well imaging plates. The nucleoside analogue 5-ethynyl-2'-deoxyuridine (EdU) (10 μ M) was added for 20 min to all wells except a triplicate of both untreated MCF7 control and *NUDT22* KO cells, which was later used as threshold to calculate the percentage of EdU positive cells. Cells were then fixed in 4% PFA for 20 min followed by permeabilisation with PBS + 0.3% Triton X-100 for 10 min. For click reaction, the reaction mix was first prepared by adding the following reagents in the exact order: 4.30 mL PBS, 200 μ L CuSO₄ (100 mM), 5 μ L Atto488 (Sigma-Aldrich) and 500 μ L ascorbic acid (100 mM). 50 μ L of click reaction mix was added to each well and incubated for 30 min at RT. Cells were then washed three times in PBS and 50 μ L of DAPI (1:1000) were added for 10 min. After washing the cells in PBS three times 10 min, the cell plates were imaged at the CellDiscoverer7 (Zeiss). Data was analysed with Zen Blue (Zeiss) and statistical analysis was performed using Graphpad Prism.

2.10 Immunofluorescence and microscopy

DNA replication stress and DNA damage induction was determined by immunofluorescence imaging in U2OS and MCF7 wild-type and *NUDT22* KO cells alone or after treatment with pyrazofurin (50 μ M in U2OS; 20 μ M in MCF7), brequinar (80 μ M in MCF7) or leflunomide (20 μ M in MCF7). Briefly, 2000 cells per well were seeded and incubated for 4 days at 37°C on 96-well imaging plates. On day 4, cells were first washed in PBS followed by extraction while fixation with 4% PFA in PBS + 0.1% Triton X-100 for 20 min. The cells were then washed thrice in PBS for 10 min each. Cells were permeabilised using PBS + 0.3% Triton X-100 for 10 min followed by blocking with 3% BSA in PBS for 40 min. Primary antibodies γ H2A.X (1:1,000, 3% BSA in PBS) and RPA-32 (1:1,000, 3% BSA in PBS) were added and incubated at 4°C overnight. The next day, after washing in PBS + 0.05% Tween-20 thrice, both secondary antibodies, donkey anti-rat Alexa Fluor-488 (1:1,000, 3% BSA in PBS) and goat anti-mouse Alexa Fluor-647 (1:1,000, 3% BSA in PBS) were added simultaneously with DAPI (1:1,000, 3% BSA in PBS) and incubated for 60 min at room temperature. The cells were then washed 3 times in PBS for 10 min and high content images were taken using a Celdiscoverer7 (Zeiss). The data was then analysed with Zen blue (Zeiss) and statistical analysis was performed using Graphpad Prism.

2.11 Mouse xenograft study

The MCF7 mouse xenograft study to assess effects on tumour growth upon *NUDT22* KO was performed under supervision of Alanna Green and with support of Victoria Cookson. The study was performed in accordance with local guidelines and with Home Office approval under project licence PP9172663, University of Sheffield, UK. For the xenograft study, ten-week-old female NOD/SCID wild-type mice (Charles River, Kent, UK) were used and kept on a 12 h/12 h light/dark cycle with unlimited access to food and water. For the generation of luciferase transfected MCF7 (MCF7-GFP-Luc) cells, MCF7 cells were infected with LVP020 (Amsbio, Cambridge, MA, USA) followed by selection with 1 μ g/ml puromycin.

Each 800,000 cells in 20 μ l media and 10% Matrigel were injected intra-nipple (4&9) on each side and the drinking water was supplemented with 4 mg/L 17- β -estradiol. To assess tumour growth, 30 mg/kg of D-Luciferin (Invitrogen, UK) was injected s.c. and incubated for 5 min before imaging by ventral exposure with an IVIS Lumina II system

(Caliper Life Sciences, UK). Images were then analysed by first creating a region of interest (ROI) around the tumours in the Living Image software (PerkinElmer) resulting in the luminescence signal in radiance (photons/second).

2.12 Computational drug design and compound evaluation

2.12.1 Ligand source and compound database

The compound library for virtual screening including 276,517 small molecule structures as structure-data file (SDF) was obtained from the compound database “NCI/DTP Open Chemical Repository” (<http://dtp.cancer.gov>). The top-40 hit compounds were purchased from the same compound database with a purity of >95% as certified by the supplier (Developmental Therapeutics Program, National Cancer Institute, Bethesda, MD, USA).

16 Amide analogues of the, in the virtual docking identified, hit TH012008 and the six NUDT22 inhibitors A1, A2, A3, A4, A5 and A6 were synthesised and provided by Martin Scobie, Tobias Koolmeister and Thomas Helleday (Karolinska Institute, Stockholm, Sweden).

2.12.2 Computational protein preparation

After importing the co-crystal structure of NUDT22 and its substrate UDP-glucose (5LOR.pdb) from the protein data bank (pdb) into Schrödinger Suite 2019-3 (Schrödinger, Inc., New York, NY, USA), the crystal structure was processed with the Protein Preparation Wizard. Briefly, hydrogen bond orders were assigned, missing hydrogen bonds and side chains were added and water molecules beyond 5 Å of hetero groups were deleted followed by the creation of potential disulphide bonds. Protonation states of the amino acid residues were calculated due to hetero state generation at pH 7.0. Protonation states and added amino acid side chains were visually inspected and the most likely residue configuration was selected. The final step of protein preparation involved minimisation of hydrogens at pH 7.0 of the altered species followed by hydrogen bond assignment. Water molecules with less than three hydrogen bonds to non-waters were removed and the protein was minimised with the restrained minimisation tool until the positions of the heavy atoms were converged to a root-mean-square deviation (RMSD) of 0.30 Å.

2.12.3 *In silico* screen of NCI/DTP compound database

Before performing the *in silico* docking screen, a subset of structures included in the NCI/DTP compound library had to be generated by using a predefined Knime 4.0.1 filtering workflow [118]. Structures with common motifs of rapid elimination of swill (REOS) or Pan Assay Interference (PAINS) compounds were removed, followed by filtering the remaining compounds based on numeric outliers regarding SlogP and AMW [119–121]. The implemented filtering cascade reduced the original input compound database from 276,517 to 98,513 structures. The generated subset of compounds was then prepared for docking using the LigPrep wizard implemented in Schrödinger Suite 2019-3. LigPrep uses Epik to generate possible ionisation states at pH 7.0 ± 2.0 followed by potential tautomer generation. The generation of stereoisomers was restricted to four per structure yielding 199,705 structures for docking [122].

The ligand UDP-glucose was selected as centre for Glide docking grid generation and the virtual screen was performed with the, in Glide implemented, screening workflow [123–125]. The screening workflow consists of a cascade of three docking steps with increased accuracy (Glide HTVS → SP → XP). In this case, the top-10% ranked hits of each step were passed on to the next one resulting in the identification of a total of 500 compounds in the last docking step Glide XP. The 500 compounds were filtered based on uniqueness and whether they were available to purchase from the NCI/DTP compound database using another Knime 4.0.1 workflow [118]. The remaining structures were assessed based on REOS and PAINS as well as based on Lipinski's type descriptors leaving 261 compounds [121]. Visual inspection as well as sorting the compound subsection based on ascending ligand efficiency was used to select the top-40 compounds for further assessment based on their enzymatic activity.

2.12.4 Chemical optimisation of Compound A

For chemical optimisation of the identified starting point for the development of NUDT22 inhibitors amide coupling with TH012008 was performed. A subset of amines consisting of aliphatic and aromatic primary and secondary amines was selected in the chemical inventory database KLARA (Karolinska Institute, Stockholm, Sweden) by substructure searching in an Instant Jchem (IJC 20.8)-based database (Chemaxon). The identified amines were then imported into a separate IJC database for filtering based on the following criteria: no carboxylic acid, no hydroxyl group, minimum one ring, as well as REOS, PAINS, and the Lipinski's rule of 5 descriptors SlogP < 2.0 and AMW between 100 and 200 Da. The resulting structures were desalted and duplicates were eliminated using the RDKit nodes in Knime 4.2.1 [118].

One stereoisomer and no tautomers per amine structure were generated using the LigPrep wizard implemented in Schrödinger Suite 2020-1. Amide coupling with Compound 1 was performed followed by reaction-based enumeration of the generated amide Compound 1 analogues creating a Compound 1 amide library. Then, potential ionisation states at pH 7.0 ± 2.0 of all optimised Compound 1 analogues were determined using the Epik function in the LigPrep wizard resulting in the generation of potential tautomers and a maximum of four stereoisomers per amide.

For the virtual screen in Schrödinger Suite 2020-1, the co-crystal structure of NUDT22 5LOR was prepared as described above. A glide docking grid with the substrate UDP-glucose as centre for the docking procedure was selected and virtual docking was performed by using Glide SP without constraints. The top-100 identified compounds then entered Glide XP docking resulting in top-50 TH012008 amide derivatives. The top-20 amide analogues were selected based on both, visual inspection of the binding mode and position in the substrate-binding site of the protein and Ligand Efficiency. For enzymatic evaluation, 16 amide TH012008 amide derivatives were synthesised including six compounds directly identified in the virtual screen as well as 10 structural similar compounds to the previously identified top-20 analogues.

2.12.5 Enzyme activity assay

The determination of enzymatic activity of the top-40 identified compounds in the first docking screen on the NCI/DTP database, the chemically optimised amide analogues of TH012008 and NUDT22 inhibitors A1 - A6 was performed in collaboration with Ingrid Almlöf and Prof Thomas Helleday at Karolinska Institute, Stockholm, Sweden. Briefly, two stock solutions (10 mM and 0.05 mM) were prepared for each compound and then nano-dispensed in 11 concentrations (1:3 dilution series) to 384-well assay plates using Echo liquid handler (Labcyte, San Jose CA, USA). A final DMSO concentration of $\leq 1\%$ was achieved. A dilution series of a control substance was included on each assay plate as well as controls lacking the enzyme (negative control) or inhibitor (positive control) for quality control. After adding 20 μL per well of 15 nM NUDT22 and 10 U mL^{-1} alkaline phosphatase from bovine intestinal mucosa in assay buffer (100 mM Tris-acetate, 40 mM NaCl, 10 mM Mg-acetate, 1 mM DTT and 0.005% Tween-20), the plates were pre-incubated for 10 min. Then, 20 μL of UDP-galactose to a final concentration of 50 μM were added and incubated for 30 min at 22°C followed by adding 10 μL of malachite green assay reagent and incubating for another 15 min at 22°C. The absorbance was read at 630 nm using a Hidex Sense plate reader (Hidex, Turku, Finland). IC_{50} values were then calculated using the following equation $Y = Y_{\min} + (Y_{\max} - Y_{\min}) / (1 + 10^{(\log[\text{C}_{50} - X] * \text{Hillslope})})$ with Y equals the read absorbance at 630 nm and X log[compound].

2.12.6 Differential Scanning Fluorimetry

Differential Scanning Fluorimetry (DSF) was used to determine target engagement as previously described with slight adaptations [126]. Triplicates of TH012008 and each TH012008 amide analogue at a concentration of 100 μM , and inhibitor A3, A4, A5 and A6 at 10 μM , as well as a no protein control and DMSO only control were added to a 96-well clear bottom Bio-Rad qPCR plate. Next, 5 μM of isolated NUDT22 protein and 5X SPYRO[®] Orange (Sigma-Aldrich, Saint-Louis MO, USA) in DSF buffer (20 mM HEPES pH 7.5, 100 mM NaCl, 10 mM Mg-acetate, and 1 mM DTT) were added. The samples were then exposed to a temperature gradient from 20 to 95°C while measuring the fluorescence intensity every 1°C at 580 nm with an excitation wavelength of 465 nm in a Bio-Rad CFX96 Real-Time System (Bio-Rad, Hercules CA,

USA). Processing and analysing of the generated data were performed using the by Niesen et al. provided Excel analysis and GraphPad Prism templates [126].

2.12.7 Cellular Thermal Shift Assay

Cellular Thermal Shift Assay (CETSA) was performed to assess the target engagement of A1, A2, A3, A4, A5 and A6 in U2OS cell lysate [127]. On the day of the experiment, 6×10^6 osteosarcoma U2OS cells were collected and washed once in PBS followed by resuspension in 1x Tris-buffered saline (TBS) with Halt™ protease inhibitor cocktail (cat. no. 78429, Thermo Fisher Scientific) at $80 \mu\text{L}/1 \times 10^6$ cells. Cell lysis was performed by freeze-thaw cycles of three times 3 minutes each in liquid nitrogen followed by water bath at 37°C . To remove cellular debris, the cell lysate was centrifuged at $17,000 \times g$ at 4°C for 20 min.

For target engagement assessment of all six NUDT22 inhibitors, $200 \mu\text{L}$ of supernatant was then either treated with $0.5 \mu\text{L}$ DMSO or $25 \mu\text{M}$ of inhibitor. To assess target engagement of inhibitors A1, A2, and A3, each $20 \mu\text{L}$ of DMSO or NUDT22i treated samples were transferred to 8 individual PCR strip tubes and heated at 8 different temperatures (37.0°C , 40.9°C , 43.3°C , 46.2°C , 48.9°C , 50.9°C , 53.2°C , and 57.0°C). To perform CETSA in cell lysate with inhibitors A3, A4, and A5, first the melting temperature T_m of NUDT22 was assessed. $20 \mu\text{L}$ of cell lysate were transferred to their corresponding PCR strip tubes and each sample was heated at its designated temperature (37 , 40 , 43 , 46 , 49 , 52 , 55 , 58 , 61 , 64 , and 67°C) in a T100 Thermal Cycler (Bio-Rad Laboratories) for 3 min. For inhibitors A3, A4, A5 and A6, the control DMSO sample was heated at 37°C , whereas the second DMSO sample as well as the inhibitor cell lysate samples were heated at 48°C , the previously identified T_m of NUDT22, for 3 min in a T100 Thermal Cycler (Bio-Rad Laboratories).

Following the heating step, the samples were centrifuged at $17,000 \times g$ for 20 min at 4°C to remove cellular debris and protein aggregates and prepared for western blotting. The western blot was performed according to the standard protocol described in *Chapter 2.6* with slight adaptations. Protein separation was performed via SDS-PAGE with 4-20% Criterion™ TGX™ Precast Midi protein gels (Bio-Rad Laboratories). Anti-NUDT22 (1:1,000 in 3% BSA in TBST) was used to detect NUDT22 protein stabilisation upon inhibitor binding and anti-SOD1 (1:10,000 in 3% BSA in TBST) was

used as loading control. After visualisation of the protein bands with ChemiDoc™ MP Imaging System (Bio-Rad Laboratories), the western blots were processed and analysed with the Image Lab Software (Bio-Rad Laboratories). For analysis of target engagement of all six inhibitors, NUDT22 protein expression intensity was first normalised to SOD1 protein expression intensity. In case of A1, A2, and A3 non-linear regression analysis in GraphPad Prism 8.0 (GraphPad, San Diego, CA, USA) was used to determine a shift in T_m of NUDT22 upon inhibitor binding. For inhibitors A3, A4, A5, and A6, which were heated at the specific T_m of NUDT22, the represented values are relative to NUDT22 band intensity of the DMSO control at 37°C.

2.12.8 Immunofluorescence and microscopy

To assess DNA damage induction in MCF7 cells, 10 μ M of each A3, A4, A5 and A6 (10 mM) were dispensed in triplicate on a Cellcarrier™-384 (PerkinElmer, Waltham, MA, USA) plate using the Tecan D300 plate dispenser. 500 cells per well were seeded and incubated for 4 days at 37°C. On day 4, cells were first washed for 2 times in PBS followed by extraction while fixation with 4% PFA in PBS + 0.1% Triton X-100 for 20 min. The cells were then washed twice in PBS for 10 min each. Cells were permeabilised using PBS + 0.3% Triton X-100 for 10 min followed by blocking with 3% BSA in PBS for 40 min. The primary antibody γ H2A.X (1:1,000, 3% BSA in PBS) was then added and incubated at 4°C overnight. The next day, the cells were washed three times in PBS + 0.05% Tween-20 followed by simultaneous incubation with DAPI (1:1,000, 3% BSA in PBS) and the secondary mouse antibody Alexa 647 (1:1,000, 3% BSA in PBS) for 60 min at room temperature. The cells were then washed 3 times in PBS for 10 min and high content images were taken using a CellDiscoverer7 (Zeiss). The data was then analysed with Zen blue (Zeiss).

2.13 Statistical analysis

All statistical analysis was performed using GraphPad prism 8 (GraphPad, San Diego, CA, USA). For comparison between two groups, the data were first analysed based on whether the data points were following a normal distribution. If the data points followed a normal distribution, unpaired two-tailed students t-test was used to assess statistical significance. If data points did not follow a normal distribution, two-tailed Mann-Whitney test was used instead. Results were considered as statistical significant with * p -value < 0.05, ** p -value < 0.01, *** p -value < 0.001, and **** p -value < 0.0001.

3. NUDT22 promotes cancer growth through pyrimidine salvage

This chapter includes the below listed manuscript with me as sole main contributor. The manuscript was a collaborative work between Patrick Herr and myself at the University of Sheffield as well as Thomas Helleday at Karolinska Institute, Stockholm, Sweden and my specific contributions are described below.

Walter M, Mayr F, Hanna BMF, Cookson V, Mortusewicz O, Helleday T, Herr P; NUDT22 promotes cancer growth through pyrimidine salvage. Partially published as preprint (<https://doi.org/10.21203/rs.3.rs-1491465/v1>) and currently under review at Nature Oncogene.

3.1 Context of research and contributions

3.1.1 Context of research

Targeting nucleotide synthesis and, more specifically, pyrimidine synthesis has remained the backbone of cancer therapy for more than 50 years and remains a key area of interest in the development of novel anti-cancer agents affecting DNA replication and cancer cell survival [128]. Disruption of nucleotide synthesis, and thus, the inaccurate supply of nucleotides at replication forks can further intensify oncogene-induced DNA replication stress and genome instability [36]. Since cancer cells can switch to the more energy-efficient salvage pathways to maintain high cell proliferation, the understanding of nucleotide synthesis in cancer is crucial for target identification and the development of novel therapy strategies [35,128].

We previously reported a unique UDP-glucose hydrolase activity for NUDT22 resulting in the synthesis of the pyrimidine precursor UMP and G1P suggesting a potential role of NUDT22 in both nucleotide synthesis for DNA replication, and energy metabolism and biomass production [26].

In this work, we elucidated the role of NUDT22 in nucleotide synthesis and its potential exploitation as anti-cancer target. We established that NUDT22 is directly regulated by p53 upon cell stress leading to increased pyrimidine salvage from UDP-glucose. We propose that NUDT22 prevents DNA replication stress and maintains cell growth by promoting pyrimidine synthesis in cancer cells. *NUDT22* depletion reduces

nucleotide pools with concomitant reduction in DNA replication fork speed and S phase progression leading to DNA replication stress and genome instability. Furthermore, we suggest that targeting *NUDT22* has high potential in cancer therapy due to the, upon *NUDT22* KO, increase in sensitivity towards pyrimidine *de novo* synthesis inhibition *in vitro* as well as due to reduced tumour growth *in vivo*.

3.1.2 Contributions

My main contribution to this work involved the assessment of the effects of *NUDT22* in response to cellular stress and on cell growth in U2OS, hTERT-RPE1 and MCF7 breast cancer cells. More specifically, Patrick Herr and Bishoy Hanna performed CRISPR/Cas9 knockout in U2OS and hTERT-RPE1 cells in collaboration with Thomas Helleday at Karolinska Institute, Stockholm, Sweden. Patrick Herr and Florian Mayr assessed the transcriptional regulation of *NUDT22* at Karolinska Institute. The in-house generation and profiling of the CRISPR/Cas9 knockout in MCF7 cells was carried out by myself with help from Patrick Herr and Victoria Cookson. I performed western blot as well as immunofluorescence microscopy experiments to determine DNA replication stress and damage and determined cell viability upon treatment with several anti-cancer agents and upon glutamine starvation with support by Patrick Herr. Oliver Mortusewicz performed DNA fibre experiments to assess effects on DNA replication fork speed in U2OS cells at Karolinska Institute. I developed the DNA fibre method to assess DNA replication fork speed in MCF7 cells as well as EdU incorporation determination to assess effects on S phase progression here at the University of Sheffield. I performed gene expression analysis of the Trans Cancer Genome Atlas (TCGA) as well as Genomic Tissue Expression (GTEx) databases. The MCF7 mouse xenograft experiment was supervised by Alanna Green and a joint effort between Patrick Herr, Victoria Cookson and myself. The writing of the manuscript was a collaborative effort between myself and Patrick Herr.

3.2 Manuscript

1 **Title:**

2 NUDT22 promotes cancer growth through pyrimidine salvage

3

4 **Authors:**

5 Melanie Walter¹, Florian Mayr², Bishoy Magdy Fekry Hanna², Victoria Cookson¹, Oliver

6 Mortusewicz², Thomas Helleday² and Patrick Herr^{1*}

7

8

9 **Affiliations:**

10 ¹Weston Park Cancer Centre, Department of Oncology and Metabolism, University of
11 Sheffield, Sheffield S10 2RX, UK

12

13 ²Science for Life Laboratory, Department of Oncology and Pathology, Karolinska Institute,
14 171 76 Stockholm, Sweden

15

16 *Correspondence to: p.herr@sheffield.ac.uk

17

18

19

20

21

22

23

24

25

1 **Abstract**

2 The NUDIX hydrolase NUDT22 converts UDP-glucose into glucose-1-phosphate and
3 the pyrimidine nucleotide uridine monophosphate¹. Glucose-1-phosphate is an important
4 metabolite for energy and biomass production through glycolysis and nucleotides required for
5 DNA replication are produced through energetically expensive de novo or energy-efficient
6 salvage pathways^{2,3}.

7 Here, we describe p53-regulated pyrimidine salvage through NUDT22-dependent
8 hydrolysis of UDP-glucose to maintain cancer cell growth and to prevent replication stress in
9 U2OS osteosarcoma and MCF7 breast cancer cells. *NUDT22* expression is consistently
10 elevated in cancer tissues indicating an increased dependency and *NUDT22* transcription is
11 induced under starvation, oncogenic stress, and DNA damage directly through p53.
12 CRISPR/Cas9 knockout of *NUDT22* induces growth retardation, S-phase delay, and slower
13 DNA replication fork speed. Uridine supplementation rescues replication fork progression and
14 alleviates replication stress. Conversely, *NUDT22* deficiency sensitizes both, U2OS and MCF7
15 cells to de novo pyrimidine synthesis inhibition in vitro and reduces cancer growth in MCF7
16 xenograft models in vivo. In conclusion, NUDT22 maintains pyrimidine supply in cancer cells.
17 Depletion of NUDT22 leads to genome instability and targeting NUDT22 therefore has high
18 potential for therapeutic applications in cancer therapy.

19

20

21

22

23

24

25

1
2
3
4
5
6
7
8
9
10
11
12
13
14
15
16
17
18
19
20
21
22
23
24
25

Introduction

Genetic instability in cancer is often caused by oncogene-induced replication stress^{4,5}, which is in part a consequence of an inaccurate supply of deoxynucleotides (dNTPs) at replication forks^{6,7}. Targeting the dNTP supply through anti-folates, thymidylate synthetase (TYMS) or ribonucleotide reductase (RNR) inhibitors has remained the backbone for anticancer treatments for over half a century, and provoking replication stress through inhibition of PARP or other DNA repair proteins remains a key area for future cancer therapies⁸. Thus, understanding dNTP synthesis pathways is important for our ability to identify novel cancer vulnerabilities.

We recently reported that the NUDIX family gene *NUDT22* encodes a UDP-glucose hydrolase that converts UDP-glucose to uridine-monophosphate (UMP) and glucose-1-phosphate (G1P)¹. Nudix family proteins were found to have a wide range of substrates⁹ and were previously suggested as anticancer targets^{10,11}. However, phylogenetic sequence analysis revealed *NUDT22* as a significant outlier¹², and any biological role of this enzyme has yet to be uncovered.

1 **Materials and Methods**

2 **Antibodies (s. Chapter 2.1)**

3 NUDT22 (H-9; sc-515491, Santa Cruz Biotechnology, Dallas, TX, US), β -Actin (ab8227,
4 Abcam, Dallas, TX, USA), p53 (DO-1; sc-126), cMyc (C-33; sc-42), P21 (H-164; sc-756),
5 γ H2A.X (Millipore 05-636, Merck Life Science, UK Limited, Gillingham, UK), RPA (cs 2208,
6 Cell Signalling Technology, Danvers, MA, USA), 53BP1 (ab36823), pCHK2 (cs2661S),
7 CHK2 (cs3440S), pCHK1 (cs133D3), CHK1 (cs2G1D5), P-RPA (A300-245A, Bethyl
8 Laboratories, Inc., Montgomery, TX, USA), GFP (ab290), ATM (11G12, sc-53173), P-ATM
9 (SAB #12701, SAB Signalway Antibody, Greenbelt, Maryland, USA), Alexa Fluor-488
10 (Thermo Fisher Scientific, Paisly, UK), Alexa-Fluor-647, DAPI (Thermo Fisher Scientific),
11 mouse & rabbit IRDye conjugated ab 680/800 (Licor Biosciences, Lincoln, Nebraska, USA),
12 mouse & rabbit Starbright conjugated ab 520/700 (Biorad, Watford, UK), mouse-hrp (31430,
13 Thermo Fisher Scientific) & rabbit-hrp (ab6721).

14

15 **Cell culture (s. Chapter 2.2)**

16 All cells were grown at 37°C containing 5% CO₂, in a humidified incubator. U2OS and
17 hTERT-RPE1 cells were grown in DMEM Glutamax with 10% FBS, penicillin (60-100 μ g/ml),
18 and streptomycin (100 μ g/ml). HA1EBs were grown in DMEM with 10% FBS, penicillin (60-
19 100 μ g/ml), streptomycin (100 μ g/ml), BJ-MYC^{ER} in DMEM/F12 without phenol red with 10%
20 FBS, penicillin (60-100 μ g/ml), streptomycin (100 μ g/ml) and HCT116 in McCoy's 5a with
21 10% FBS, penicillin (60-100 μ g/ml), and streptomycin (100 μ g/ml). MCF7 cells were grown
22 in RPMI with 10% FBS, penicillin (60-100 μ g/ml), and streptomycin (100 μ g/ml) (Thermo
23 Fisher Scientific). Cells were regularly checked for Mycoplasma contamination (MycoAlert,
24 Lonza, Basel, Switzerland). All cell lines were validated using short-tandem repeat (STR)

1 profiling. For glucose and glutamine starvation cells were washed twice in warm PBS, and
2 DMEM containing 10% FBS without glucose/glutamine was added for the indicated times.

3

4 **Immunofluorescence and microscopy (s. Chapter 2.10)**

5 Immunostaining was performed according to standard protocols in 96 well imaging plates and
6 high-content imaging was performed with an ImageXpress XLS (Molecular Devices, San Jose,
7 CA, USA) or a Celldiscoverer7 (Zeiss, Oberkochen, Germany). The data were analyzed with
8 CellProfiler-3.0.0 or Zen blue (Zeiss). For quantitative DNA damage foci analysis, >500 nuclei
9 per condition were analysed.

10

11 **Molecular cloning and plasmids**

12 pIRES2-EGFP-p53 WT was a gift from Dylan Taatjes (Addgene plasmid # 49242)¹³. The
13 *NUDT22* reporter was cloned by PCR amplification of the genomic region
14 GRCh38:11:64224628:64227818:1 and ligated into pGL4.10 (Promega, Southampton, UK).
15 The transfection control was CMV-driven control luciferase (pGL4.75-CMV-hRluc). PG13-
16 luc (wt p53 binding sites) was a gift from Bert Vogelstein (Addgene plasmid # 16442)¹⁴.
17 sgRNA for *NUDT22* knockout in U2OS and hTERT-RPE1 cells was cloned into pX330-U6-
18 Chimeric_BB-CBh-hSpCas9, a gift from Feng Zhang (Addgene plasmid # 42230)¹⁵.

19

20 **Gene editing (s. Chapter 2.3)**

21 For *NUDT22* gene knockout in U2OS and hTERT-RPE1 cells the following sgRNA sequences
22 were used: #1: 5'-AUCCUCUACAACCGGGUUCAGGG-3'; #2: 5'-
23 GUCCCACUGGAGCGGCCCUAGGG-3'; #3 5'-ACUUUAUUCUUGGAUUCCGUUGG-
24 3'. Transfected cells were selected with puromycin. Genomic DNA from individual knockout
25 clones was amplified with primers flanking the sgRNA recognition sites 5'-

1 CGAGTCTACAGGAATCTTCTTTGTGG-3' and 5'-CCAAGTCACTTGTCTGCC-3'. The
2 same primers were used for sequencing. For *NUDT22* gene knockout in MCF7 cells, the
3 following sgRNAs were used: 5'-CCGGCUAAAGGCCCAACCC-3' (Sigma
4 HSPD0000120767) for MCF7 KO3 and 5'-GACAAGGAAGUCAUCGGCUG-3' (Synthego,
5 Menlo Park, CA, USA) for MCF7 KO14. Cells were transfected with Cas9-GFP (Sigma) and
6 selected by FACS for the top 10% GFP+ cell population. gDNA from positive clones was
7 extracted and sequenced using the following primers: 5'-ATCCTGAGGTGACCTTGCT-3'
8 and 5'-ACTAGCCACAGCCGATGA-3'. NT sgRNA and the identical selection process was
9 used for the respective control cells.

10

11 **Dual Luciferase assay**

12 For the Dual-Luciferase® Assay (Promega), U2OS cells were seeded and transfected on a
13 10 cm dish. Transfection was conducted using jetPEI® (Polyplus, Biopark, Illkirch, France)
14 with a total amount of 5 µg DNA comprised of 9 parts *NUDT22-luc2*-pGL4.10 and 1 part
15 *CMV-hRluc*-pGL4.75. Cells were reseeded on a 96-well plate after 24 h. For analysis cells were
16 washed with PBS. Then, 20 µl of Passive Lysis Buffer was added, and the plate was incubated
17 for 15 min at room temperature on a rocking device. Then, 15 µl of the cell lysate of each well
18 was transferred onto an opti-96-well plate, and the plate was read with the dual luciferase
19 setting on a Hidex Sense plate reader (Hidex, Turku, Finland).

20

21 **Cell transfection**

22 Cells were seeded in 12-well plates, and the siRNA pool (ON-Target plus SMARTpool,
23 Dharmacon) was transfected to a final concentration of 5 nM according to the manufacturer's
24 protocol (INTERFERin, Polyplus). *p53* (L-003329-00-0005), *HK2* (L-006735-00-0005).
25 AllStars negative control siRNA (Qiagen, Hilden, Germany) was used as a control siRNA.

1 **Drug exposure (s. Chapter 2.5 and 2.6)**

2 Drugs were spotted using a Tecan D300e dispenser (Tecan, Mannedorf, Switzerland) at the
3 following concentrations with log₂ dilution series. pyrazofurin (SML1502, Sigma-Aldrich)
4 (200 μM - 5 μM for U2OS and hTERT-RPE1; 200 μM – 2 μM for MCF7), MPA (M5255,
5 Sigma-Aldrich) (100 μM - 0.05 μM), 6MP (38171, Merck) (100 μM - 0.05 μM), glutamine
6 starvation (2 mM-7.8 μM), brequinar (5.08321 Sigma-Aldrich) (200 μM -10 μM), and
7 leflunomide (L5025, Sigma-Aldrich) (400 μM - 10 μM), hydroxyurea (H8627, Sigma-Aldrich)
8 (5 mM-0.05 mM). Five hundred cells per well were seeded on 384-well cell culture plates, and
9 viability was assessed with a resazurin assay and read on a Hidex Sense or Molecular Devices
10 ID5 plate reader after 4 days. Uridine (U3750, Sigma-Aldrich) rescue was performed at a
11 concentration of 500 μM for 24 h. Doxorubicine (D1515, Sigma-Aldrich), actinomycin D
12 (A1410, Sigma-Aldrich), olaparib (AZD2281, Selleckchem), camptothecin (C9911, Sigma-
13 Aldrich), nutlin3a (SML0580, Sigma-Aldrich).

14

15 **Western blotting (s. Chapter 2.7)**

16 Western blotting was carried out following standard protocols with Bio-Rad SDS gradient gels
17 and the Trans-Blot Turbo transfer system (Bio-Rad). Cells were lysed in RIPA buffer for 20
18 minutes on ice in the presence of protease inhibitor cocktail (Roche, Basel, Switzerland)
19 followed by sonication with a needle sonicator (Hielscher UP100H (Teltow, Germany); 70%
20 amplitude; 0.7 cycles; 3 cycles). Images were taken with a LI-COR Odyssey FC or Biorad
21 Chemidoc MP.

22

23 **RNA Extraction and Quantitative RT-PCR**

24 Total mRNA was isolated from cells with the Direct-zol RNA Mini Prep kit (Zymo Research,
25 Irvine, CA, USA) or ReliaPrep (Promega) according to the manufacturer's instructions, and

1 cDNA was generated with the QuantiTect Reverse Transcription kit (Qiagen) or iScript (Bio-
2 Rad). qRT-PCR was performed using SYBR Green (Invitrogen/Life Technologies; Bio-Rad)
3 and the reactions were performed on a Rotor-Gene Q (Qiagen) and Bio-Rad CFX96 qRT-PCR
4 machine. β -Actin was used as a normalization control. Relative gene expression changes were
5 calculated using the $\Delta\Delta C_t$ method. Primers used are: *NUDT22* (5'-
6 GGCAGCTGGTGGTACATGA-3'; 5'-GTCTCATTTCGGGCGATG-3'), *β -Actin* (5'-
7 CCTGGCACCCAGCACAAT-3'; 5'-GGGCCGGACTCGTCATACT-3'), *cMYC* (5'-
8 TCGGATTCTCTGCTCTCCT-3'; 5'-CCTCATCTTCTTGTTCCTCCTC-3'), *p53* (5'-
9 CTTTCCACGACGGTGACA-3'; 5'-TCCTCCATGGCAGTGACC-3'), *CCNE* (5'-
10 CTCCAGGAAGAGGAAGGCAA-3'; 5'-TCGATTTTGGCCATTTCTTCA-3')¹⁶, *GRP78*
11 (5'-CATCAAGTTCTTGCCGTTCA-3'; 5'-TCTTCAGGAGCAAATGTCTTTGT-3'), *HRAS*
12 (5'-GCGATGACGGAATATAAGCTG-3'; 5'-TCAATGACCACCTGCTTCC-3'), *HK2* (5'-
13 TCCCCTGCCACCAGACTA-3'; 5'-TGGACTTGAATCCCTTGGTC-3'), *TKI* (5'-
14 CAGCTTCTGCACACATGACC-3'; 5'-CGTCGATGCCTATGACAGC-3'), *DCK* (5'-
15 ATATGAAAGTCTGGTTGAAAAGGTC-3'; 5'-AAAGCTGAAGTATCTGGAACCATT-
16 3'), *DHODH* (5'-GCGTGGAGACACCTGAAAA-3'; 5'-TCAGGTAGGAGGCGAAGAGA-
17 3'), *UMPS* (5'-GCATGAAACCAGAATTTCTTCAC-3'; 5'-
18 ACTGTTGGCCAAGATTATCTCC-3'), *TYMS* (5'-CCCAGTTTATGGCTTCCAGT-3'; 5'-
19 GCAGTTGGTCAACTCCCTGT-3'), *RNR* (5'-TGGACCTCTCCAAGGACATT-3'; 5'-
20 GGCTAAATCGCTCCACCA-3')

21

22 **ChIP-qPCR**

23 U2OS cells were transfected with plasmids encoding for GFP alone or p53-IRES-GFP. After
24 24 h, the cells were processed for ChIP according to¹⁷. qPCR was performed as described
25 previously with primers for *P21*¹⁸ and the *NUDT22* 5' CpG region fwd: 5'-

1 CCAGACTTGCCCAAGGTC-3'; rev: 5'-CCATGTCCCCCAAACC-3'. Fold enrichment was
2 calculated over the input control and relative to the IgG mock IP.

3

4 **DNA Fibre assay (s. *Chapter 2.8*)**

5 Cells were exposed to either DMSO or 500 μ M uridine for 24 hours, pulse-labelled with 25
6 μ M CldU for 30 min, washed with medium and pulse-labelled with 25 μ M IdU for U2OS and
7 hTERT-RPE1 cells or 250 μ M IdU for MCF7 cells for 30 min. Labelled cells were harvested
8 and DNA fibre spreads were prepared as described elsewhere¹⁹. CldU was detected by
9 incubating acid-treated fibre spreads with rat anti-BrdU monoclonal antibody (AbD Serotec;
10 cat# MCA2060; and Abcam; ab6326), whereas IdU was detected using mouse anti-BrdU
11 monoclonal antibody (BD Biosciences; cat# 347580) for 1 hour at 37°C. Slides were fixed with
12 4% PFA and incubated with goat anti-rat Alexa Fluor 555 or goat anti-mouse Alexa Fluor 488
13 for 1-2 hours at 4°C. Fibres were examined using a Zeiss (Jena, Germany) LSM780 or LSM980
14 Airyscan2 confocal laser scanning microscope with a 63x oil immersion objective. For
15 quantification of replication structures, at least 250 structures were counted per experiment.
16 The lengths of red (AF 555) and green (AF 488)-labelled patches were measured using the
17 ImageJ software (National Institutes of Health; <http://rsbweb.nih.gov/ij/>) and arbitrary length
18 values were converted into micrometers using the scale bars created by the microscope.

19

20 **EdU incorporation (s. *Chapter 2.9*)**

21 U2OS and hTERT-RPE1 cells were treated with 50 μ M pyrazofurin for 4 days, and MCF7
22 cells were treated with 0.1 μ M pyrazofurin for 4 days in 96-well plates. EdU (10 μ M) was
23 added for 20 min. Cells were fixed in 4% PFA and permeabilized in 0.3% Triton X-100. The
24 click reaction was performed as follows: 859 μ l PBS, 40 μ l CuS04 (100 mM), 1 μ l Atto 488
25 (Sigma-Aldrich), and 100 μ l 100 mM ascorbic acid for 30 min at RT. Cells were then washed

1 and imaged at the ImageXpress XLS (Molecular Devices) or Celldiscoverer7 (Zeiss). Data
2 were analyzed with CellProfiler-3.0.0 or Zen Blue (Zeiss).

3

4 **Statistical analysis (s. *Chapter 2.13*)**

5 Unpaired two-tailed Student's t-test was used for comparisons between two groups. When the
6 data points did not follow a normal distribution, a two-tailed Mann-Whitney test was
7 performed. All statistical analyses were performed using GraphPad Prism. All experiments
8 were repeated at least 3 times.

9

10 **LC-MS nucleotide measurements**

11 Measurements were carried out at Creative Proteomics (Shirley, NY, USA). To each cell pellet
12 100 μ L of water was added. Cells were lysed on a MM 400 mill mixer with the aid of two
13 metal balls at a shaking frequency of 30 Hz for 1 min. Then, 400 μ L of methanol was then
14 added to each tube and the samples were homogenized again for 1 min twice, followed by
15 sonication for 1 min in an ice-water bath. The samples were placed at -20 °C for 30 min before
16 centrifugal clarification at 21,000 g and 5 °C for 5 min. The clear supernatants were collected.
17 The protein pellets were used for the protein assay using the standard Bradford procedure.
18 Serially diluted, mixed standard solutions of dNTPs were prepared at the concentrations of
19 0.0002 to 10 μ M in an internal standard solution containing ¹³C or D-labeled ATP, GTP and
20 UTP. Twenty microliters of the supernatant of each sample solution was mixed with 180 μ L
21 of the same internal standard solution. Ten-microliter aliquots of the sample solutions and the
22 standard solutions were injected onto a C18 UPLC column (2.1*100 mm, 1.8 μ m) for UPLC-
23 MRM/MS runs with (-) ion detection on a Waters Acquity UPLC system coupled to a Sciex
24 QTRAP 6500 Plus MS instrument, with the use of a tributylamine formate solution (solvent
25 A) and acetonitrile (solvent B) as the mobile phase for gradient elution with an efficient

1 gradient of 5% to 50% B in 20 min at 0.30 mL/min and 50 °C. Concentrations of the detected
2 analytes were calculated with internal standard calibration by interpolating the constructed
3 linear regression curves of individual compounds, with the analyte-to-internal standard peak
4 area ratios measured from the sample solutions in each assay.

5

6 **In vivo studies (s. *Chapter 2.11*)**

7 Ten-week-old female NOD/SCID wild-type mice (Charles River, Kent, UK) kept on a 12-h/12-
8 h light/dark cycle with free access to food and water were used in this study, and the study was
9 carried out in accordance with local guidelines and with Home Office approval under project
10 licence PP9172663, University of Sheffield, UK. MCF7-GFP-Luc cells were generated by
11 infection with LVP020 (amsbio) and selected with 1 µg/ml puromycin.

12 On day 0 800.000 cells in 20 µl Media, 10% Matrigel were injected on either side intra nipple
13 (4&9). The drinking water was supplemented with 4mg/L 17-β-estradiol. Tumour growth was
14 monitored in live mice using an IVIS Lumina II system (Caliper Life Sciences, UK). Here, 30
15 mg/kg of D-Luciferin (Invitrogen, UK) was injected s.c. 5 min before imaging. Mice were
16 imaged by ventral exposure. Images were analyzed in Living Image software by creating a
17 region of interest (ROI) around the tumor(s); luminescence signal was acquired in radiance
18 (photons/second).

19

20

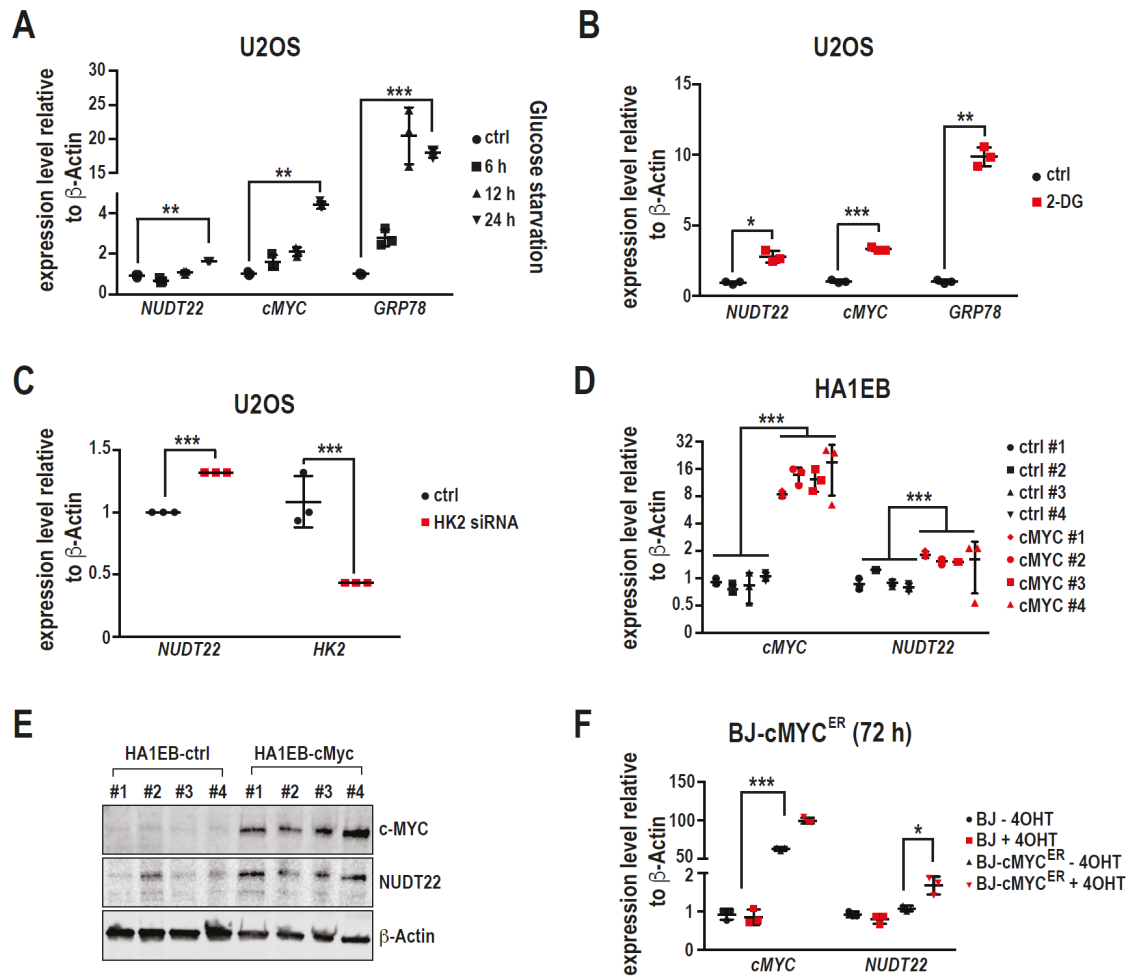
1 **Results**

2 ***NUDT22* is induced by cellular stress**

3 Both metabolic products of *NUDT22* activity, UMP and G-1-P, are generated from
4 UDP-glucose, originating from extracellular glucose. To interrogate the effects of constant
5 glucose flux on *NUDT22* expression we subjected cultured cells to glucose starvation.
6 Indicative of a potentially common regulation of glucose metabolism and *NUDT22* we detected
7 continuous increase in *NUDT22* expression alongside known glucose response genes *cMyc* and
8 *GRP78* (Fig. 1A). Similarly, blocking glycolysis through inhibition of the glucose
9 phosphorylating enzyme hexokinase 2 (HK2) with 2-deoxy-D-glucose (2-DG) (Fig. 1B), or
10 RNAi-mediated depletion of HK2 (HK2^{siRNA}) (Fig. 1C) resulted in a significant upregulation
11 of *NUDT22*.

12 Glucose starvation is known to induce *cMYC* expression, resulting in the activation of
13 genes involved in nucleotide metabolism, glucose uptake, and the serine biosynthesis
14 pathway²⁰, a critical mechanism for cancer cell survival²¹. Furthermore, *cMYC* overexpression
15 leads to replication stress, as a result of nucleotide shortage²². To investigate whether the
16 elevated expression of *NUDT22* after interference with glycolysis was directly regulated
17 through *cMYC*, we used cells with constitutively high²³ (Fig. 1D, E) and tamoxifen-induced
18 (4-OHT) short-term *cMYC* activation²⁴ (Fig. 1F). qRT-PCR analysis revealed that both
19 systems led to a significant increase in *NUDT22* expression. This is, however, not due to
20 oncogenic stress in general, as overexpression of the *CCNE*²⁵ and *HRAS*^{V12}²⁴ oncogenes had
21 no effect on *NUDT22* expression (Supplementary Fig. 1A, B).

22



1

2 **Fig. 1. A** Increased *NUDT22* gene expression after glucose starvation for 6, 12 and 24 h (*NUDT22*
3 $P=0.0082$; *cMYC* $P=0.0021$; *GRP78* $P=0.0006$). **B** Increased *NUDT22* gene expression after inhibition
4 of HK2 with 2-DG (*NUDT22* $P=0.0254$; *cMYC* $P=0.0001$; *GRP78* $P=0.0016$). *cMYC* and *GRP78* are
5 positive controls. **C** Increased *NUDT22* gene expression after HK2 depletion with siRNA (HK2
6 $P=0.006$; *NUDT22* $P<0.001$). **D** Elevated *NUDT22* gene expression in four independent HA1EB-
7 *cMYC* clones measured by qPCR (*NUDT22* $P=2.4 \times 10^{-8}$; *cMYC* $P=7.48 \times 10^{-7}$). **E** *cMYC*-overexpressing
8 cells induced *NUDT22* protein expression. **F** *cMYC*-induced *NUDT22* gene expression (*cMYC*
9 $P=0.0006$; *NUDT22* $P=0.0346$). P-values were calculated by paired t-test. Data are presented as the
10 mean values with SD and all experiments were repeated at least 3 times.

11 Transcriptional analysis by qRT-PCR and western blotting was performed by Patrick Herr and Florian
12 Mayr at Karolinska Institute (Stockholm, Sweden).

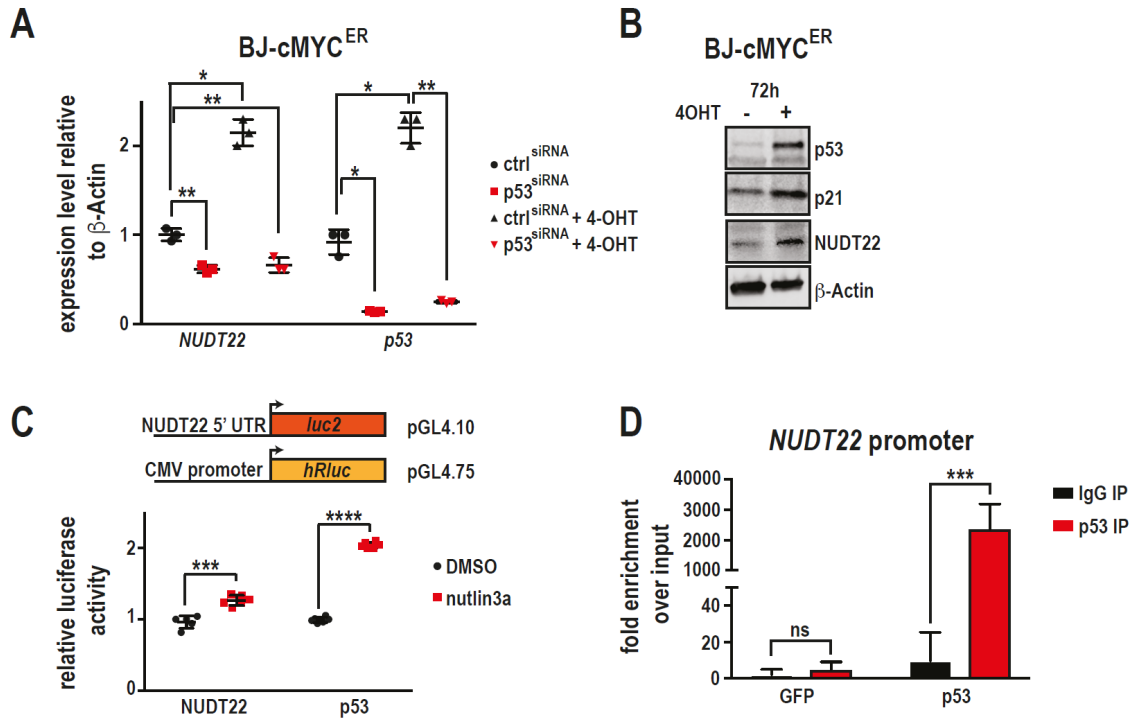
1 ***NUDT22* is a direct p53 target**

2 cMYC overexpression was previously shown to induce *p53*, *p21* and senescence²⁴. In
3 a largely opposing role to cMYC in glucose metabolism, glycolysis is tightly regulated by p53,
4 controlling the transcription of the glucose transporters *GLUT1* and *GLUT4* and reducing the
5 expression of *HK2*²⁶ and 6-phosphofrukto-2-kinase 3 (*PFKFB3*), thereby decreasing glycolysis
6 in favour of the pentose phosphate pathway (PPP)²⁷. Nucleotide synthesis, on the other hand,
7 is promoted through expression of the RNR gene *p53R2* directly by p53²⁸, and p53 was shown
8 to promote DNA replication and prevent replicative stress²⁹.

9 To test whether *NUDT22* expression is directly regulated by cMYC or rather through
10 p53, we depleted *p53* with RNAi (*p53^{siRNA}*) in cMYC-overexpressing cells. Strikingly, the
11 cMYC-induced expression of *NUDT22* was completely dependent on p53 (Fig. 2A), and direct
12 cMyc overexpression led to stabilized p53, p21 and *NUDT22* (Fig. 2B). This is also consistent
13 with the delay in the expression of *NUDT22* after cMYC activation (Supplementary Fig. 2A-
14 C) and increased *p53* expression after 2-DG exposure or *HK2^{siRNA}* (Supplementary Fig. 2D, E).
15 Furthermore, Nutlin3a-mediated p53 stabilization³⁰ led to induction of *NUDT22* in p53-
16 proficient cells only (Supplementary Fig. 2F) and direct overexpression of *p53*¹³ was sufficient
17 to induce the expression of *NUDT22* (Supplementary Fig. 2G).

18 Nutlin3a exposure of cells transfected with a *NUDT22* luciferase reporter construct
19 (*NUDT22-luc2*) further confirmed our findings, again indicating direct activation of the
20 *NUDT22* promoter by p53 (Fig. 2C). Finally, we confirmed direct p53 binding in the *NUDT22*
21 promoter region by chromatin immunoprecipitation followed by qRT-PCR (Fig. 2D and
22 Supplementary Fig. 2H).

23



1

2 **Fig. 2. A** The depletion of *p53* abolished the cMYC-mediated activation of *NUDT22* in BJ-MYC^{ER}
 3 cells (*NUDT22* P=0.0086; P=0.0119; P=0.0046; *p53* P=0.012; P=0.0146; P=0.0022), as measured by
 4 qRT-PCR. **B** Stabilized p53 and p21 and increased NUDT22 protein expression in BJ-MYC^{ER} cells. **C**
 5 Relative luciferase levels of the *NUDT22* reporter after stabilization of p53 with Nutlin3a in U2OS cells
 6 (*NUDT22* P=0.0003, *p53* P=0.0001). **D** qPCR for the 2 kb CpG 5' region of the *NUDT22* gene after
 7 ChIP with a p53(DO1) antibody in U2OS cells. GFP served as a transfection control (P=0.008). P-
 8 values were calculated by paired t-test. Data are presented as the mean values with SD and all
 9 experiments were repeated at least 3 times.

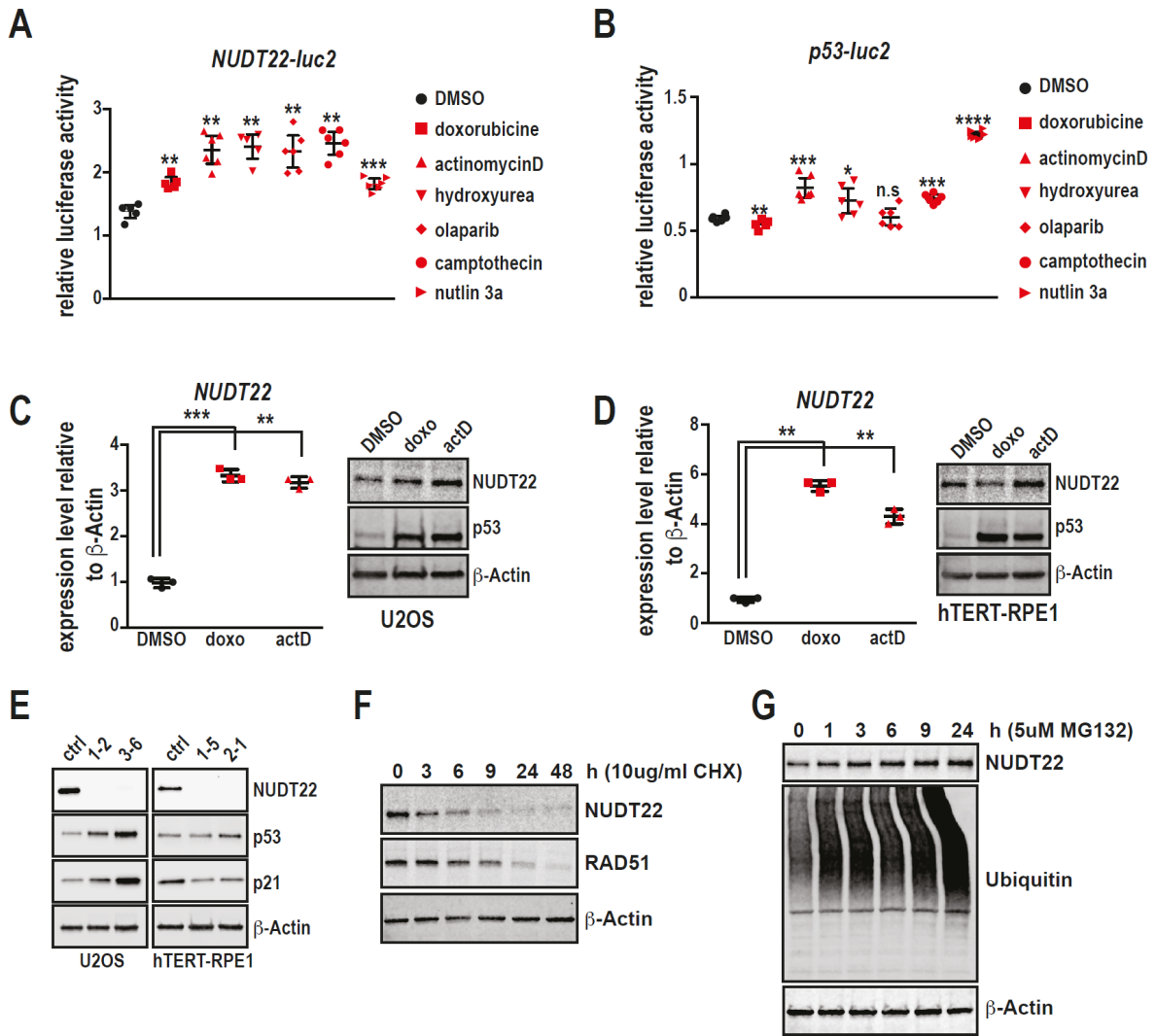
10 Experimental work was performed by Patrick Herr and Florian Mayr.

11

12

1 To test whether activation of p53 by different means would also influence *NUDT22*
2 expression we exposed U2OS cells carrying *NUDT22*-luc or *p53*-luc reporters to a spectrum
3 of chemotherapeutic drugs, which led to a significant increase in both (Fig. 3A, B). This was
4 again recapitulated after actinomycin D and doxorubicine exposure of U2OS and hTERT-
5 RPE1 cells, correlating with the stabilization of p53 (Fig. 3C, D). Importantly, *NUDT22* KO
6 U2OS cells already have increased p53 and p21 levels compared to their respective controls,
7 indicating elevated levels of metabolic stress and suggesting a p53-mediated positive feedback
8 loop regulating *NUDT22* expression. This was, however, not observed in hTERT-RPE1
9 fibroblasts (Fig. 3E). Consistent with a role for *NUDT22* in acute situations where
10 nucleotide/energy shortage requires immediate salvage of pyrimidines and G1P, *NUDT22*
11 itself has a very short half-life and is cleared through proteasomal degradation (Fig. 3F, G).
12

1



2

3 **Fig. 3. A** DNA damaging agents induce transcriptional activation of the *NUDT22* reporter in U2OS
 4 cells after treatment with corresponding anti-cancer agents for 24 h. **B** The p53-luciferase reporter
 5 served as a control. Drug concentrations: doxorubicine (doxo) 5 μ M, actinomycin D (actD) 5 nM,
 6 hydroxyurea (HU) 2 mM, olaparib 10 μ M, camptothecin 10 μ M, nutlin3a 2 μ M (P-values calculated to
 7 DMSO control (*NUDT22*): doxo P=0.0094; actD P=0.0036; HU P=0.0088; olaparib P=0.0042; CPT
 8 P=0.0021; nutlin3a P=0.0003. (*p53*) doxo P=0.0068; actD P=0.0008; HU P=0.0344; olaparib P=ns;
 9 CPT P=0.0003; nutlin3a p<0.0001). **C** U2OS and **D** hTERT-RPE1 cells were treated with doxorubicin
 10 and actinomycin D for 24 h. *NUDT22* gene expression was increased in both cell lines. This is
 11 consistent with the stabilization of p53 protein as determined by western blotting (C: doxo P=0.0013;

1 actD P=0.0013, **D**: doxo P=0.0004; actD P=0.0021). **E** *NUDT22* CRISPR/Cas9 knockout increases p53
2 stability and activity in U2OS cells but not hTERT-RPE1 cells. **F** *NUDT22* protein levels were
3 significantly reduced after 6 h of translation inhibition with 10 µg/ml CHX in U2OS osteosarcoma cells.
4 RAD51 served as a positive control. **G** *NUDT22* protein levels accumulate after proteasome inhibition
5 with 5 µM MG132 in U2OS cells. P-values are calculated by paired t-test in GraphPad Prism. Data are
6 shown as the mean with SD and all experiments were repeated at least 3 times.
7 Dual luciferase assay as shown in Fig. 3A and B as well as determination of *NUDT22* and p53 protein
8 expression by western blot in Fig. 3C, D, F and G were performed by Patrick Herr. Patrick Herr and
9 Bishoy Hanna generated CRISPR/Cas9 *NUDT22* KO U2OS and hTERT-RPE1 cells. I determined
10 *NUDT22*, p53 and p21 levels in U2OS and hTERT-RPE1 cells by western blotting as shown in Fig.
11 3E.

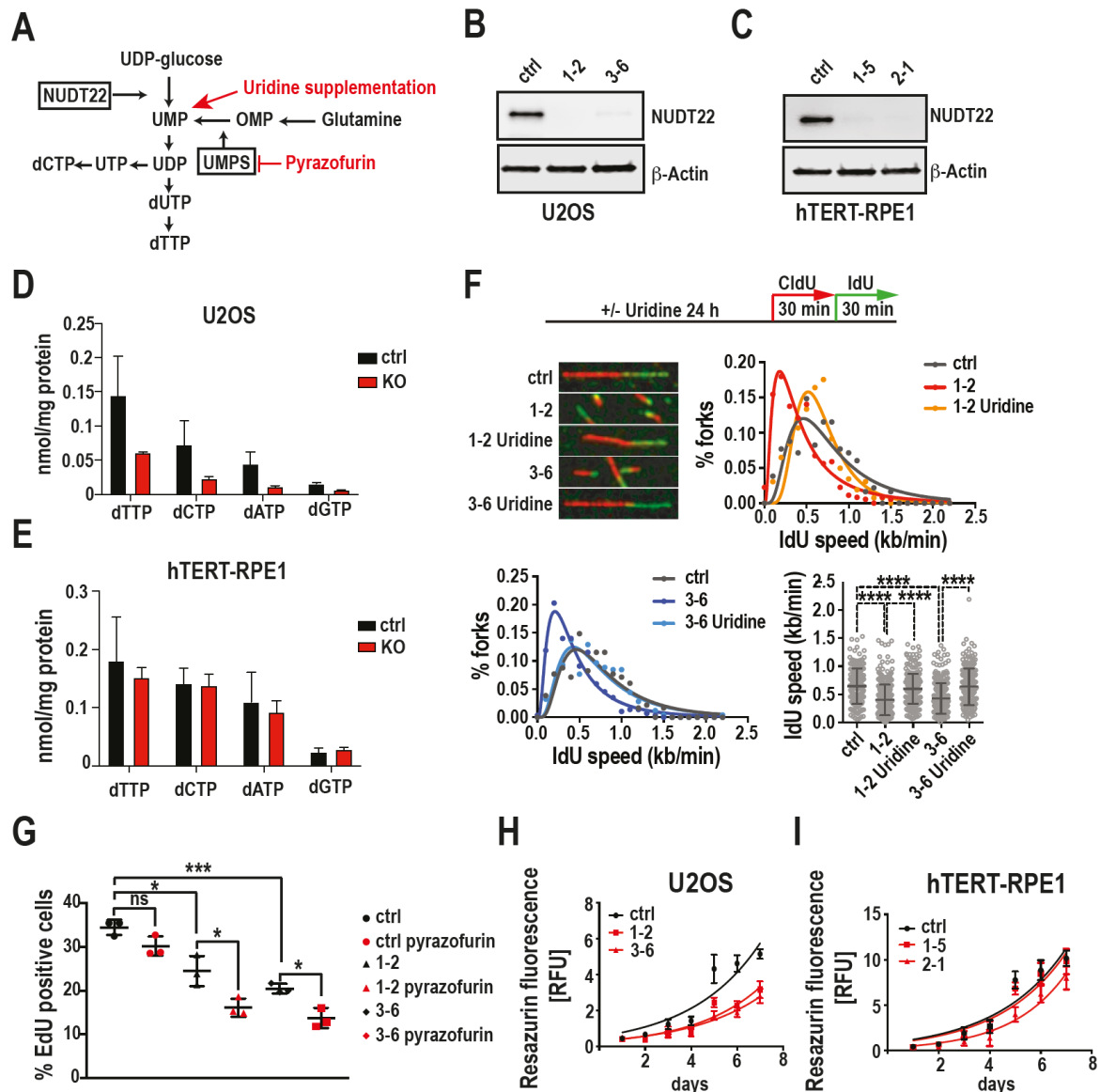
12

13 ***NUDT22* prevents replication stress**

14 Our biochemical data suggest that *NUDT22* generates the pyrimidine synthesis
15 precursor UMP from UDP-glucose¹ (Fig. 4A). We therefore aimed to determine the biological
16 significance of *NUDT22* for dNTP production and DNA replication in cells. To compare the
17 cellular role of *NUDT22* in cancer and fibroblast cell lines we generated U2OS osteosarcoma
18 and hTERT-RPE1 retina pigment epithelial *NUDT22* KO cell lines (Fig. 4B, C). dNTP pool
19 measurements by LC-MS confirmed that *NUDT22* KO U2OS cells had reduced levels of all 4
20 dNTPs but only marginal changes were observed in hTERT-RPE1 cells (Fig. 4D, E). The
21 reduction in intracellular dNTPs in *NUDT22* KO U2OS cells was reflected in a significantly
22 reduced DNA replication fork speed. To test whether the reduced replication fork speed in
23 *NUDT22* KO cells is a consequence of attenuated UMP production, we supplemented *NUDT22*
24 KO cells with uridine. Supporting our hypothesis, uridine supplementation completely restored
25 replication fork speed, demonstrating that the lack of *NUDT22*-dependent hydrolysis of UDP-
26 glucose to UMP is required for normal replication fork progression (Fig. 4F and Supplementary

1 Fig. 3A). The attenuated replication fork speed is further reflected by reduced EdU
2 incorporation during S-phase (Fig. 4G and Supplementary Fig. 3B) and a generally slower
3 proliferation speed in *NUDT22* KO U2OS but not hTERT-RPE1 cells (Fig. 4H, I).

4 These findings prompted us to hypothesize that *NUDT22* controls a novel pyrimidine
5 salvage pathway and might therefore synergise with de novo pyrimidine synthesis (Fig. 4A).
6 A key enzyme in the de novo synthesis of pyrimidines from glutamine is uridine
7 monophosphate synthetase (UMPS), which converts orotidine 5'-phosphate to UMP³¹.
8 Inhibition of UMPS with pyrazofurin³² caused a further reduction in EdU incorporation in
9 *NUDT22* KO cells progressing through S-phase (Fig. 4G and Supplementary Fig. 3B),
10 demonstrating that *NUDT22* is involved in a complementary pathway for UMP generation.



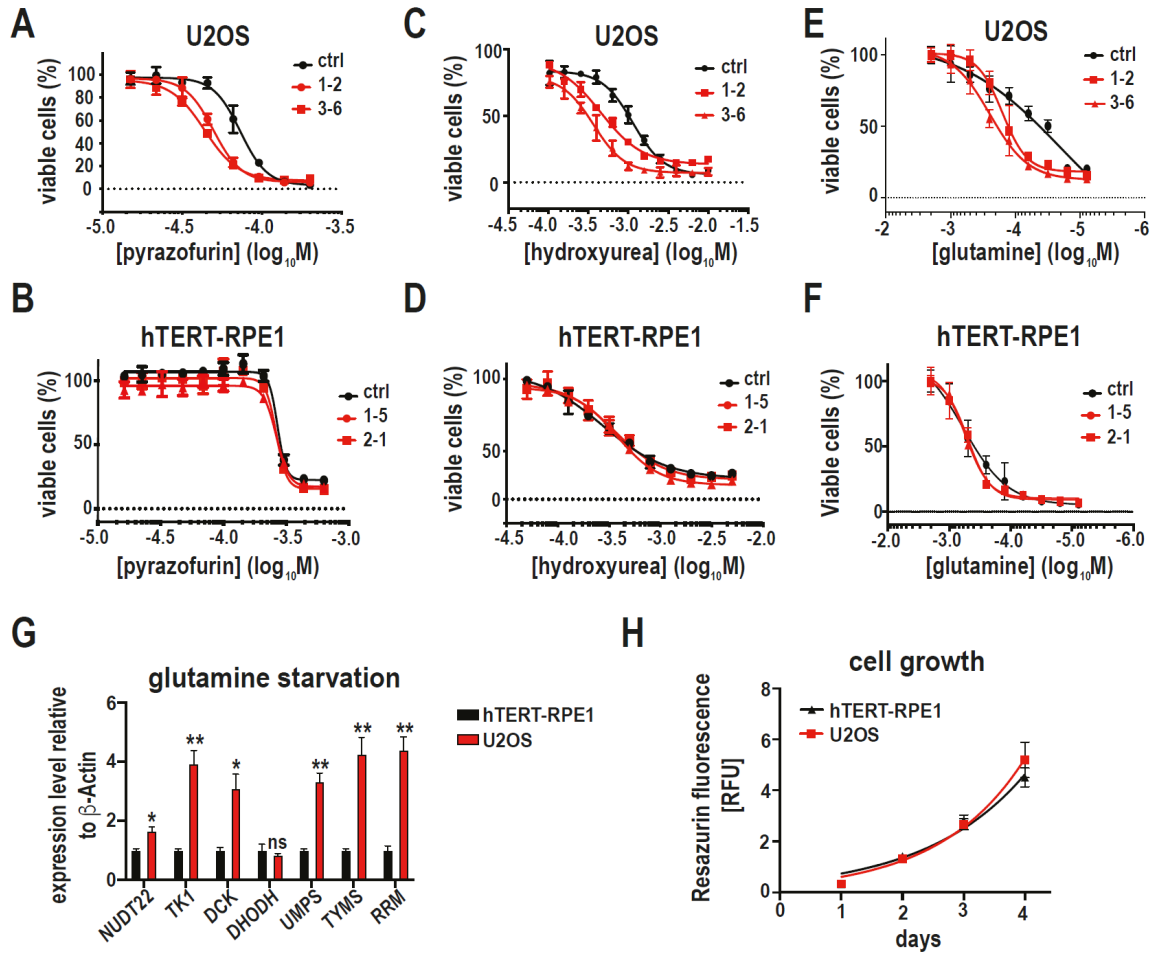
1
2 **Fig. 4.** A *NUDT22* hydrolyses UDP-glucose to UMP as a pyrimidine salvage pathway. De
3 novo UMP synthesis from glutamine can be inhibited by the nucleoside analogue pyrazofurin
4 or rescued with uridine supplementation. B Two independent U2OS (1-2; 3-6) and C hTERT-RPE1
5 (1-5; 2-1) *NUDT22* knockout (KO) clones were generated. D Nucleotide pool levels are decreased in
6 U2OS *NUDT22* KO cells but E unchanged in hTERT-RPE1 *NUDT22* KO cells compared to the
7 corresponding ctrl cell lines. Nucleotide pool levels were determined by LC-MS in collaboration with
8 Creative Proteomics. F *NUDT22* KO (1-2 and 3-6) in U2OS cells reduces DNA replication fork speed,
9 which was rescued by uridine supplementation. Replication fork speed in ctrl and *NUDT22* KO cells
10 was assessed by CldU and IdU incorporation in DNA fibre assay. At least 250 DNA fibre structures

1 were counted per experiment. This experiment was performed by Oliver Mortusewicz at Karolinska
2 Institute, Stockholm, Sweden. **G** *NUDT22* KO delays S phase progression in U2OS cells with and
3 without pyrazofurin treatment for 4 days. The percentage of EdU-positive cells was quantified by
4 immunofluorescence microscopy (ctrl::1-2 P=0.0109; ctrl::3-6 P=0.0003; 1-2 DMSO::1-2 pyrazofurin
5 P=0.0227; 3-6 DMSO::3-6 pyrazofurin P=0.0109). P-values were calculated by unpaired t-test. Errors
6 as the mean with SD. **H** *NUDT22* U2OS KO clones have slower growth rates compared to their controls.
7 **I** *NUDT22* KO in hTERT-RPE1 cells does not induce changes in growth rates. All experiments were
8 repeated at least 3 times.

9

10 These findings further suggest that *NUDT22* KO cells might be especially sensitive to
11 pyrazofurin. Exposure of *NUDT22* KO cells and their respective controls to pyrazofurin in
12 dose-response survival assays revealed a clear sensitization in U2OS but not hTERT-RPE1
13 cells (Fig. 5A, B). Similar combinatorial effects were observed after inhibition of RNR with
14 hydroxyurea (HU) (Fig. 5C, D) or by starving cells from the de novo pyrimidine precursor
15 glutamine (Fig. 5E, F), phenocopying the effect of pyrazofurin exposure and further supporting
16 a shortage in nucleotide supply in *NUDT22*-deficient cells. Interestingly, glutamine starvation
17 led to the upregulation of key pyrimidine biosynthesis enzymes and *NUDT22*, especially in
18 U2OS cells (Fig. 5G).

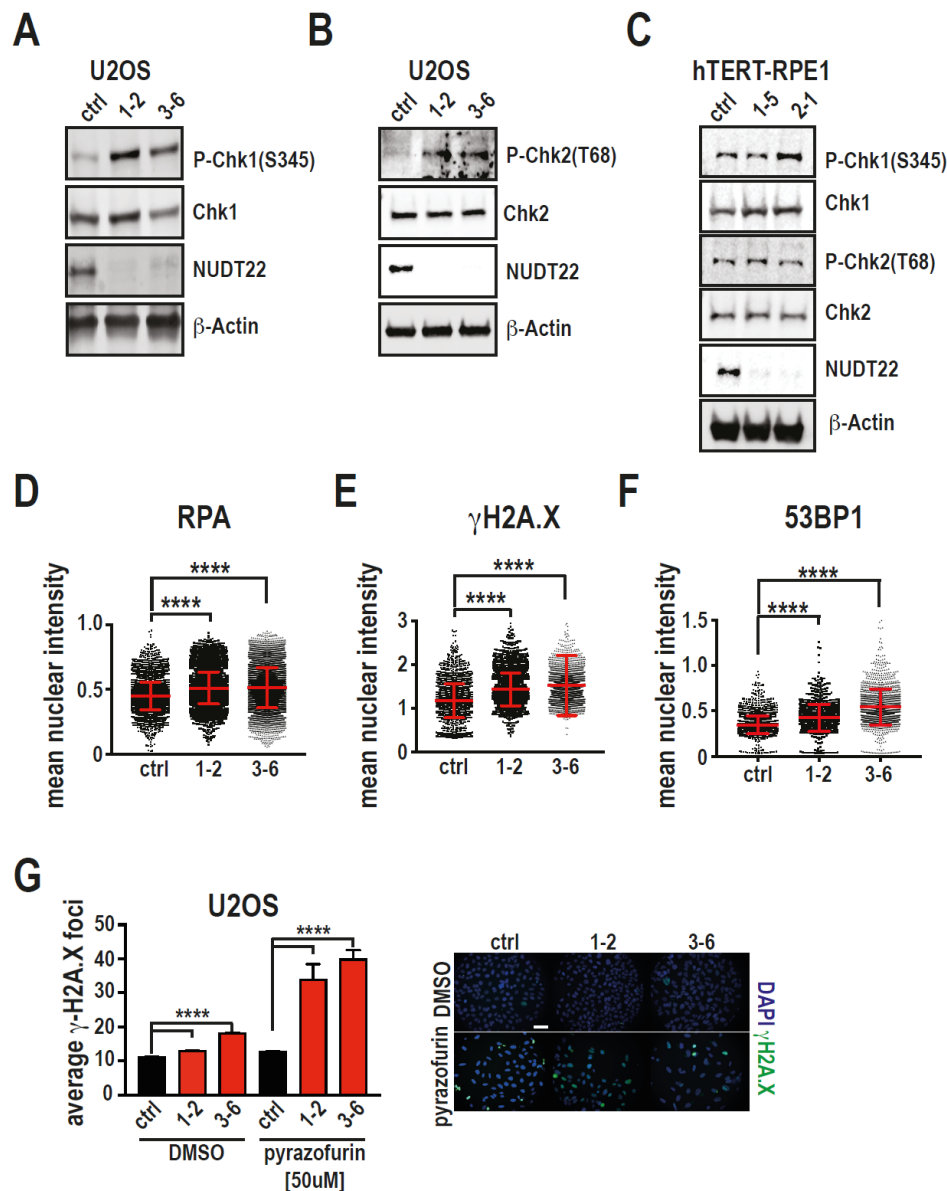
19 Pyrazofurin was shown to also affect purine biosynthesis³³. We therefore tested whether
20 the observed combinatorial effects are specifically related to a deficiency in pyrimidine
21 synthesis. Inhibition of purine synthesis with MPA or 6-MP did not increase the sensitivity of
22 *NUDT22* KO U2OS or hTERT-RPE1 cells, further supporting a specific role for *NUDT22* in
23 pyrimidine biosynthesis (Supplementary Fig. 3C, D). Importantly the difference in response
24 between U2OS and hTERT-RPE1 cells is not attributable to differential proliferation rates of
25 the two cell lines (Fig. 5 H).



1
 2
 3
 4
 5
 6
 7
 8
 9
 10

Fig. 5. Dose response curves of ctrl and *NUDT22* KO U2OS cells exposed to **A** pyrazofurin, **C** hydroxyurea and **E** after glutamine starvation for 4 days. Dose response curves of ctrl and *NUDT22* KO hTERT-RPE1 cells exposed to **B** pyrazofurin, **D** hydroxyurea and **F** after glutamine starvation for 4 days. **G** Gene expression levels of pyrimidine synthesis genes after 24 h of glutamine starvation relative to β-actin. Statistical analysis between hTERT-RPE1 and U2OS cells (*NUDT22* P=0.0135; *TK1* P=0.0071; *DCK* P=0.0132; *DHODH* P=ns; *UMPS* P=0.004; *TYMS* P=0.01; *RNR* P=0.0026). P-values were calculated by paired t-test. Data are presented as the mean values with SD. **H** Growth rate comparison between U2OS and hTERT-RPE1 cells. All experiments were repeated at least 3 times.

1 Nucleotide deficiency and reduced replication fork progression are often associated
 2 with replication stress. Consistent with the reduction in pyrimidine synthesis, we observed
 3 increased cell cycle checkpoint activation in *NUDT22* KO U2OS but not hTERT-RPE1 cells
 4 (Fig. 6A-C) and an increase in markers for replication stress (RPA) and DNA damage
 5 (γ H2A.X, 53BP1) (Fig.6 D-F), which was further increased when combined with low doses of
 6 pyrazofurin (Fig. 6G).



7
 8 **Fig. 6. A, B** Cell cycle checkpoint activation (P-Chk1 and P-Chk2) in *NUDT22* KO U2OS cells (1-2
 9 and 3-6). **C** No significant cell cycle checkpoint activation in *NUDT22* KO hTERT-RPE1 cells (1-5

1 and 2-1). **D** Increased single stranded DNA (nuclear RPA intensity) and DNA damage (nuclear γ H2A.X
2 **E** and 53BP1 **F** intensity) in U2OS *NUDT22* KO cells (1-2 and 3-6) compared to U2OS ctrl cells as
3 determined by immunofluorescence imaging. **G** Quantification of γ H2A.X DNA damage foci in ctrl
4 and *NUDT22* KO U2OS cells with and without pyrazofurin ($P < 0.0001$). P-values were calculated by
5 the Mann-Whitney test. Data are presented as the mean values with SEM. All experiments were
6 repeated at least 3 times.

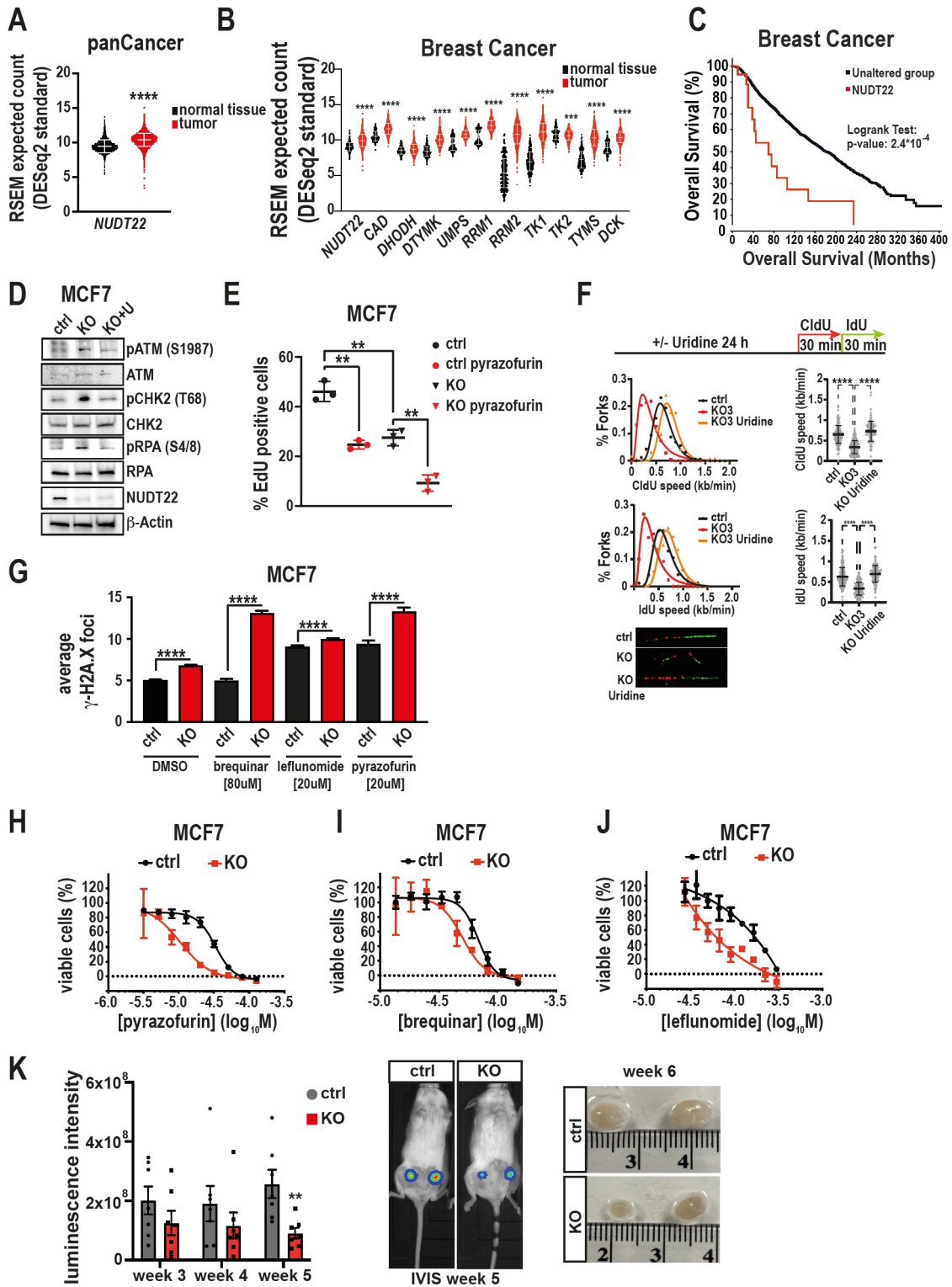
7

8 ***NUDT22* deficiency reduces cancer growth**

9 To better understand the overall significance of *NUDT22* in cancer, we interrogated the
10 TCGA and GTEx databases for differential gene expression of *NUDT22* and other genes
11 involved in pyrimidine biosynthesis. Pan-cancer analysis clearly indicated increased *NUDT22*
12 expression levels in cancer tissue compared with normal tissue (Fig. 7A). This pattern was
13 further reinforced in breast cancer, with all major pyrimidine metabolism enzymes following
14 the same trend (Fig. 7B). This correlates with the previously described role of other members
15 of the NUDIX protein superfamily in breast cancer³⁴. In addition, breast cancer patients³⁵ with
16 *NUDT22* alterations have a worse prognosis in overall survival (Fig. 7C). To test whether our
17 results in U2OS cells also translate in breast cancer cells we generated *NUDT22* KO MCF7
18 cells. Similar to *NUDT22* KO U2OS cells, *NUDT22* KO MCF7 cells exhibited an increase in
19 the phosphorylation of replication stress markers, which was rescued by uridine
20 supplementation (Fig. 7D). *NUDT22* KO MCF7 cells also had reduced growth rates
21 (Supplementary Fig. 4A) and reduced EdU incorporation compared to control cells, which was
22 further exaggerated by UMPS inhibition with pyrazofurin (Fig. 7E and Supplementary Fig.
23 4B). The reduced replication fork speed observed in U2OS cells was again recapitulated in
24 *NUDT22* KO MCF7 cells, which was rescued by uridine supplementation (Fig. 7F and
25 Supplementary Fig. 4C). *NUDT22* KO MCF7 cells have increased DNA damage (γ H2A.X),
26 further exaggerated by low doses of DHODH (brequinar, leflunomide) and UMPS

1 (pyrazofurin) inhibitors (Fig. 7G), and *NUDT22* KO MCF7 cells were significantly sensitized
2 to inhibition of UMPS and DHODH (Fig. 7H-J).

3 To transfer our findings into an orthotopic mouse breast cancer xenograft model, we
4 injected engineered *luc2 NUDT22* KO MCF7 cells into female NOD/SCID mice and monitored
5 tumour growth by IVIS imaging in live animals. Recapitulating our data on cultured cells,
6 *NUDT22* KO MCF7 cells grew significantly slower than the control cells over the course of
7 the experiment (Fig. 7K). These findings underscore the significance of *NUDT22* for cancer
8 cell growth in vivo with a functional tumour microenvironment and access to nutrients through
9 vascularization.



1

2 **Fig. 7.** A RSEM expected count analysis of *NUDT22* expression in the panCancer TCGA and GTEx
 3 datasets ($P < 0.0001$; Mann-Whitney test, mean with SD). B RSEM expected count analysis of
 4 pyrimidine metabolism gene expression in breast cancer TCGA and GTEx datasets ($P < 0.0001$; Mann-
 5 Whitney test, mean with SD). C Overall survival of breast cancer patients with *NUDT22* gene

1 alterations (TCGA). **D** Cell cycle checkpoint activation of ctrl and *NUDT22* KO MCF7 cells was
2 rescued by uridine supplementation. **E** *NUDT22* KO MCF7 cells have reduced EdU incorporation,
3 which is further reduced by pyrazofurin (0.1 μ M) exposure for 4 days. **F** Reduced replication fork speed
4 in *NUDT22* KO MCF7 cells can be rescued by uridine supplementation. At least 250 DNA fibre
5 structures were counted per experiment. **G** *NUDT22* KO MCF7 cells have increased γ H2A.X foci
6 formation, which was further increased with brequinar (80 μ M), leflunomide (20 μ M) and pyrazofurin
7 (20 μ M) treatment for 24h ($P < 0.0001$). P-values were calculated by the Mann-Whitney t-test. Data are
8 shown as the mean with SD. **H** Dose-response curves of ctrl and *NUDT22* KO MCF7 cells treated with
9 pyrazofurin, **I** brequinar and **J** leflunomide for 4 days. **K** In vivo mammary cancer xenograft model
10 with ctrl and *NUDT22* KO MCF7 cells. *Luc2*⁺ ctrl and *Luc2*⁺ *NUDT22* KO MCF7 cells were injected
11 into mammary fat pads of 7 ten-week old female NOD/SCID wild-type mice per cell line and imaged
12 weekly for six weeks ($P < 0.0023$; Mann-Whitney test, mean with SEM). All experiments were repeated
13 at least 3 times.

14

15

1 **Discussion**

2 Taken together, we present evidence that NUDT22 is a previously unknown important
3 regulator of a cellular salvage pathway that appears to be of special significance in cancer. We
4 show that cancer tissues have elevated levels of *NUDT22* and that *NUDT22* expression is
5 regulated by p53 following metabolic stress, cMYC overexpression, and DNA damage, all of
6 which cause depletion of the nucleotide pool. We show that *NUDT22*-deficient cancer cells
7 have lower nucleotide pools and display hallmarks of replication stress, such as reduced
8 replication fork speed, delayed S-phase progression, cell cycle checkpoint activation, increased
9 DNA damage and single-stranded DNA.

10 Nucleotide salvage through recycling from intermediates in the degradative pathway is
11 an energy-efficient way to generate nucleotides. While pyrimidines have been shown to be re-
12 phosphorylated inside the cell through DCK and TK1³⁶, no true pyrimidine salvage pathway
13 has been described to date that resembles the well-known purine salvage pathway around the
14 *HPRT* gene that has been exploited extensively therapeutically and as a biological tool³⁷. Co-
15 targeting of pyrimidine salvage and de novo synthesis for cancer therapy has recently received
16 renewed attention, and our data suggest that targeting pyrimidine de novo synthesis combined
17 with NUDT22 inhibition might be an interesting novel therapeutic approach in the future. Our
18 data that glutamine starvation synergizes with *NUDT22* KO in U2OS cells (Fig. 3f) therefore
19 further supports this idea. UDP-glucose, the substrate for NUDT22, has been linked to
20 metastatic progression of lung cancer cells by directly interfering with translation of the EMT-
21 promoting gene *SNAI1*³⁸. Inhibition/deletion of NUDT22 could therefore potentially suppress
22 the metastatic potential and simultaneously increase the DNA damage burden in cancer cells
23 by reducing UMP and keeping UDP-glucose levels high (Fig. 1c, d).

24 There seems to be a distinct difference in the level of dependence on NUDT22 in
25 different cell types. We consistently observed much more severe effects in the cancer cell lines

1 (U2OS and MCF7) than in the fibroblast cell line (hTERT-RPE1). It is tempting to hypothesize
2 that this difference may be due to an increased metabolic demand in cancer, which is also
3 suggested by the increased *NUDT22* expression in cancer tissues but needs to be further
4 investigated. Although the majority of phenotypes in *NUDT22* KO could be rescued by uridine
5 supplementation and are clearly directly attributable to UMP, and therefore pyrimidine,
6 deficiency, the significance of G-1-P generated by *NUDT22* for the maintenance of cellular
7 growth in fast proliferating cancer cells needs to be addressed. The attack on nucleotide
8 synthesis through a complementary salvage pathway, which cancer cells seem to be more
9 reliant on, might prove advantageous over previous nucleoside inhibitors. Finally, our in vivo
10 findings provide a clear rationale for the preclinical translation of targeting *NUDT22* in cancer.

11

12 **Acknowledgements**

13 We would like to thank Adam Throup and Scott Allen for discussions and critical reading of
14 the manuscript and Jaime Espinoza-Ruiz and Jiri Bartek for HRasV12 and BJ-cMycER cell
15 lines. We also thank Alanna Green for supervision of the animal study.

16

17 **Author contributions**

18 P.H., M.W. and T.H. designed the experiments. P.H., M.W., F.M., O.M., V.C. and B.M.F.H
19 performed the experiments. P.H., M.W., and T.H. wrote the manuscript. All authors read and
20 approved the manuscript.

21 **Competing interests**

22 The authors declare no competing interests.

23

1 **Data availability statement**

2 The datasets generated during and/or analysed during the current study are available from the
3 corresponding author on reasonable request.

4

5 **Funding**

6 This work was funded by the Swedish Research Council, Swedish Cancer Society, the Swedish
7 Pain Relief Foundation and the Torsten and Ragnar Söderberg Foundation (TH). The Weston
8 Park Cancer Centre (PH, MW). The European Union’s Horizon 2020 research and innovation
9 programme under the Marie Skłodowska-Curie grant agreement no.722729 (BMFH) and
10 no.813284 (MW).

11

12

1 **References**

2

3 1 Carter M, Jemth A-S, Carreras-Puigvert J, Herr P, Carranza MM, Vallin KSA *et al.* Human
4 NUDT22 Is a UDP-Glucose/Galactose Hydrolase Exhibiting a Unique Structural Fold.
5 *Structure/Folding and Design* 2018; 26: 295-303.e6.

6 2 Aird KM, Zhang R. Nucleotide metabolism, oncogene-induced senescence and cancer.
7 *Cancer Letters* 2015; 356: 204–210.

8 3 Walter M, Herr P. Re-Discovery of Pyrimidine Salvage as Target in Cancer Therapy. *Cells*
9 2022; 11: 739.

10 4 Halazonetis TD, Gorgoulis VG, Bartek J. An oncogene-induced DNA damage model for
11 cancer development. *Science* 2008; 319: 1352–1355.

12 5 Bartkova J, Rezaei N, Liontos M, Karakaidos P, Kletsas D, Issaeva N *et al.* Oncogene-
13 induced senescence is part of the tumorigenesis barrier imposed by DNA damage
14 checkpoints. *Nature* 2006; 444: 633–637.

15 6 Jones RM, Mortusewicz O, Afzal I, Lorvellec M, García P, Helleday T *et al.* Increased
16 replication initiation and conflicts with transcription underlie Cyclin E-induced replication
17 stress. *Oncogene* 2012; 32: 3744–3753.

18 7 Bester AC, Roniger M, Oren YS, Im MM, Sarni D, Chaoat M *et al.* Nucleotide Deficiency
19 Promotes Genomic Instability in Early Stages of Cancer Development. *Cell* 2011; 145: 435–
20 446.

21 8 Dobbelstein M, Sørensen CS. Exploiting replicative stress to treat cancer. *Nature*
22 *Publishing Group* 2015; 14: 405–423.

23 9 McLennan AG. Substrate ambiguity among the nudix hydrolases: biologically significant,
24 evolutionary remnant, or both? *Cellular and molecular life sciences : CMLS* 2012; 70: 373–
25 385.

26 10 Gad H, Koolmeister T, Jemth A-S, Eshtad S, Jacques SA, Ström CE *et al.* MTH1
27 inhibition eradicates cancer by preventing sanitation of the dNTP pool. *Nature* 2014; 508:
28 215–221.

29 11 Huber KVM, Salah E, Radic B, Gridling M, Elkins JM, Stukalov A *et al.* Stereospecific
30 targeting of MTH1 by (S)-crizotinib as an anticancer strategy. *Nature* 2014; 508: 222–227.

31 12 Carreras-Puigvert J, Zitnik M, Jemth A-S, Carter M, Unterlass JE, Hallström B *et al.* A
32 comprehensive structural, biochemical and biological profiling of the human NUDIX
33 hydrolase family. *Nature Communications* 2017; 8: 1–17.

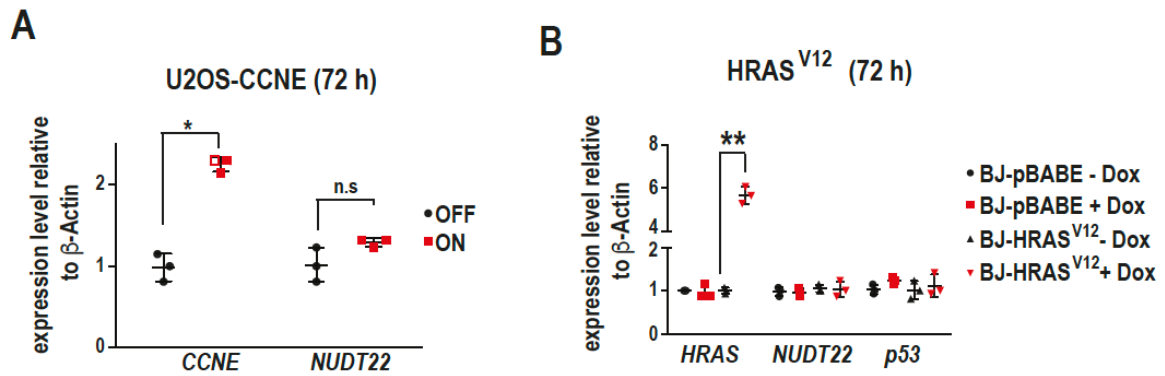
- 1 13 Lin S-C, Karoly ED, Taatjes DJ. The human Δ Np53 isoform triggers metabolic and gene
2 expression changes that activate mTOR and alter mitochondrial function. *Aging Cell* 2013;
3 12: 863–872.
- 4 14 el-Deiry WS, Tokino T, Velculescu VE, Levy DB, Parsons R, Trent JM *et al.* WAF1, a
5 potential mediator of p53 tumor suppression. *Cell* 1993; 75: 817–825.
- 6 15 Cong L, Ran FA, Cox D, Lin S, Barretto R, Habib N *et al.* Multiplex genome engineering
7 using CRISPR/Cas systems. *Science* 2013; 339: 819–823.
- 8 16 Span PN, Tjan-Heijnen VCG, Manders P, Beex LVAM, Sweep CGJF. Cyclin-E is a
9 strong predictor of endocrine therapy failure in human breast cancer. *Oncogene* 2003; 22:
10 4898–4904.
- 11 17 Carey MF, Peterson CL, Smale ST. Chromatin Immunoprecipitation (ChIP). *Cold Spring*
12 *Harbor Protocols* 2009; 2009: pdb.prot5279-pdb.prot5279.
- 13 18 Mattia M, Gottifredi V, McKinney K, Prives C. p53-Dependent p21 mRNA Elongation Is
14 Impaired when DNA Replication Is Stalled. *Molecular and cellular biology* 2007; 27: 1309–
15 1320.
- 16 19 Henry-Mowatt J, Jackson D, Masson J-Y, Johnson PA, Clements PM, Benson FE *et al.*
17 XRCC3 and Rad51 Modulate Replication Fork Progression on Damaged Vertebrate
18 Chromosomes. *MOLCEL* 2003; 11: 1109–1117.
- 19 20 Li B, Simon MC. Molecular Pathways: Targeting MYC-induced Metabolic
20 Reprogramming and Oncogenic Stress in Cancer. *Clinical Cancer Research* 2013; 19: 5835–
21 5841.
- 22 21 Sun L, Song L, Wan Q, Wu G, Li X, Wang Y *et al.* cMyc-mediated activation of serine
23 biosynthesis pathway is critical for cancer progression under nutrient deprivation conditions.
24 *Cell Research* 2015; 25: 429–444.
- 25 22 Murga M, Campaner S, Lopez-Contreras AJ, Toledo LI, Soria R, Montaña MF *et al.*
26 Exploiting oncogene-induced replicative stress for the selective killing of Myc-driven tumors.
27 *Nature structural & molecular biology* 2011; 18: 1331–1335.
- 28 23 Sanjiv K, Hagenkort A, Calderón-Montaña JM, Koolmeister T, Reaper PM, Mortusewicz
29 O *et al.* Cancer-Specific Synthetic Lethality between ATR and CHK1 Kinase Activities.
30 *CELREP* 2016; 14: 298–309.
- 31 24 Maya-Mendoza A, Ostrakova J, Kosar M, Hall A, Duskova P, Mistrik M *et al.* Myc and
32 Ras oncogenes engage different energy metabolism programs and evoke distinct patterns of
33 oxidative and DNA replication stress. *Molecular Oncology* 2015; 9: 601–616.
- 34 25 Jones RM, Mortusewicz O, Afzal I, Lorvellec M, a PG iacute, Helleday T *et al.* Increased
35 replication initiation and conflicts with transcription underlie Cyclin E-induced replication
36 stress. *Nature Publishing Group* 2012; 32: 3744–3753.

- 1 26 Flöter J, Kaymak I, Schulze A. Regulation of Metabolic Activity by p53. *Metabolites*
2 2017; 7: 21.
- 3 27 Franklin DA. p53 coordinates DNA repair with nucleotide synthesis by suppressing
4 PFKFB3 expression and promoting the pentose phosphate pathway. *Nature Publishing*
5 *Group* 2016; : 1–13.
- 6 28 Tanaka H, Arakawa H, Yamaguchi T, Shiraishi K, Fukuda S, Matsui K *et al.* A
7 ribonucleotide reductase gene involved in a p53-dependent cell-cycle checkpoint for DNA
8 damage. *Nature* 2000; 404: 42–49.
- 9 29 Klusmann I, Rodewald S, Müller L, Friedrich M, Wienken M, Li Y *et al.* p53 Activity
10 Results in DNA Replication Fork Processivity. *CELREP* 2016; 17: 1845–1857.
- 11 30 Vassilev LT, Vu BT, Graves B, Carvajal D, Podlaski F, Filipovic Z *et al.* In Vivo
12 Activation of the p53 Pathway by Small-Molecule Antagonists of MDM2. *Science* 2004;
13 303: 844–848.
- 14 31 Wittmann JG, Heinrich D, Gasow K, Frey A, Diederichsen U, Rudolph MG. Structures of
15 the Human Orotidine-5'-Monophosphate Decarboxylase Support a Covalent Mechanism and
16 Provide a Framework for Drug Design. *Structure* 2008; 16: 82–92.
- 17 32 Cadman E, Benz C. Uridine and cytidine metabolism following inhibition of de novo
18 pyrimidine synthesis by pyrazofurin. *Biochimica et biophysica acta* 1980; 609: 372–382.
- 19 33 Worzalla JF, Sweeney MJ. Pyrazofurin inhibition of purine biosynthesis via 5-
20 aminoimidazole-4-carboxamide-1-beta-D-ribofuranosyl 5'-monophosphate
21 formyltransferase. *Cancer Research* 1980; 40: 1482–1485.
- 22 34 Wright RHG, Beato M. Role of the NUDT Enzymes in Breast Cancer. *Int J Mol Sci* 2021;
23 22: 2267.
- 24 35 Györfy B, Lanczky A, Eklund AC, Denkert C, Budczies J, Li Q *et al.* An online survival
25 analysis tool to rapidly assess the effect of 22,277 genes on breast cancer prognosis using
26 microarray data of 1,809 patients. *Breast cancer research and treatment* 2010; 123: 725–731.
- 27 36 Austin WR, Armijo AL, Campbell DO, Singh AS, Hsieh T, Nathanson D *et al.*
28 Nucleoside salvage pathway kinases regulate hematopoiesis by linking nucleotide
29 metabolism with replication stress. *The Journal of experimental medicine* 2012; 209: 2215–
30 2228.
- 31 37 Townsend MH, Robison RA, O'Neill KL. A review of HPRT and its emerging role in
32 cancer. *Med Oncol* 2018; 35: 89.
- 33 38 Wang X, Liu R, Zhu W, Chu H, Yu H, Wei P *et al.* UDP-glucose accelerates SNAI1
34 mRNA decay and impairs lung cancer metastasis. *Nature* 2019; : 1–22.

35

3.3 Supplementary material

Supplementary Fig. 1

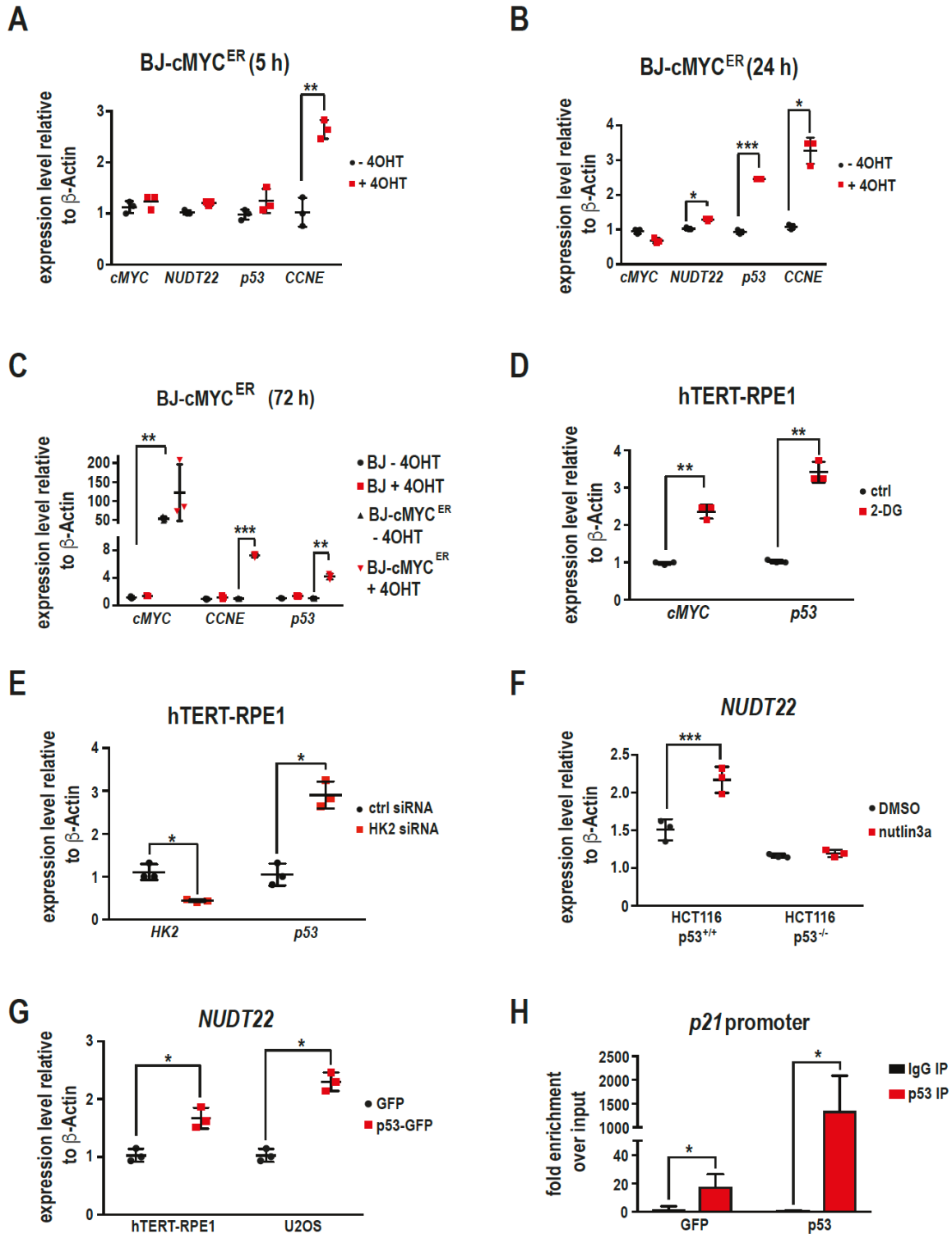


Supplementary Fig. 1

A Overexpression of *CCNE* had no significant effect on the expression of *NUDT22* (*CCNE* $P=0.0126$).

B Overexpression of *HRAS*^{V12} had no effect on either *NUDT22* or *p53* expression ($P=0.0028$). P-values were calculated by paired t-test. Data are shown as the mean with SD.

Supplementary Fig. 2

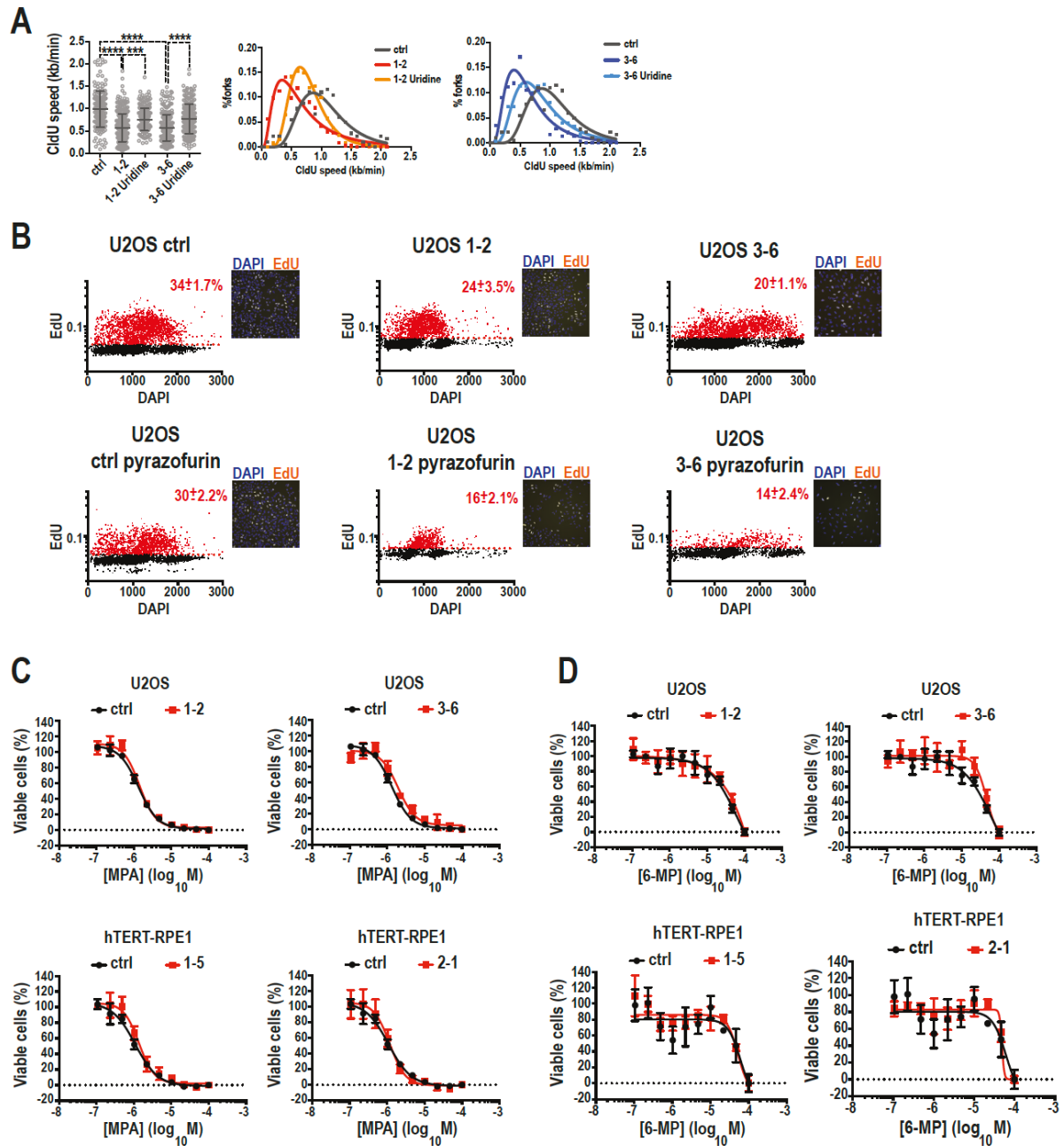


Supplementary Fig. 2

A Short-term activation of cMYC induced expression of the direct target gene *CCNE* ($P=0.0089$) but not of *NUDT22* or *p53*. **B** Increased expression of both *NUDT22* and *p53* after cMYC^{ER} activation with

tamoxifen (4-OHT) for 24 h (*NUDT22* P=0.038; *p53* P=0.0006; *CCNE* P=0.01). **C** Activation of *cMYC^{ER}* (4-OHT) for 72 h increased the expression of *CCNE* and *p53* (*cMYC* P=0.0041; *CCNE* P=0.0007; *p53* P=0.0047). **D** The exposure of hTERT-RPE1 cells to 2-DG for 48 h induced *cMYC* and *p53* expression (*cMYC* P=0.0037; *p53* P=0.0033). **E** Increased *p53* expression after *HK2^{siRNA}* transfection (*HK2* P=0.0314; *p53* P=0.0234). **F** Nutlin3a exposure induced *NUDT22* expression only in the *p53^{+/+}* HCT116 cell line and not in the isogenic *p53^{-/-}* HCT116 cell line (*NUDT22* P=0.001). **G** Increased *NUDT22* expression after *p53* overexpression (hTERT-RPE1 P=0.0314; U2OS P=0.0144). **H** qPCR for the *P21* promoter after ChIP with a p53(DO1) antibody. GFP served as a transfection control, (*P21* P=0.034 and 0.033). P-values were calculated by paired t-test. Data are presented as the mean values with standard deviation.

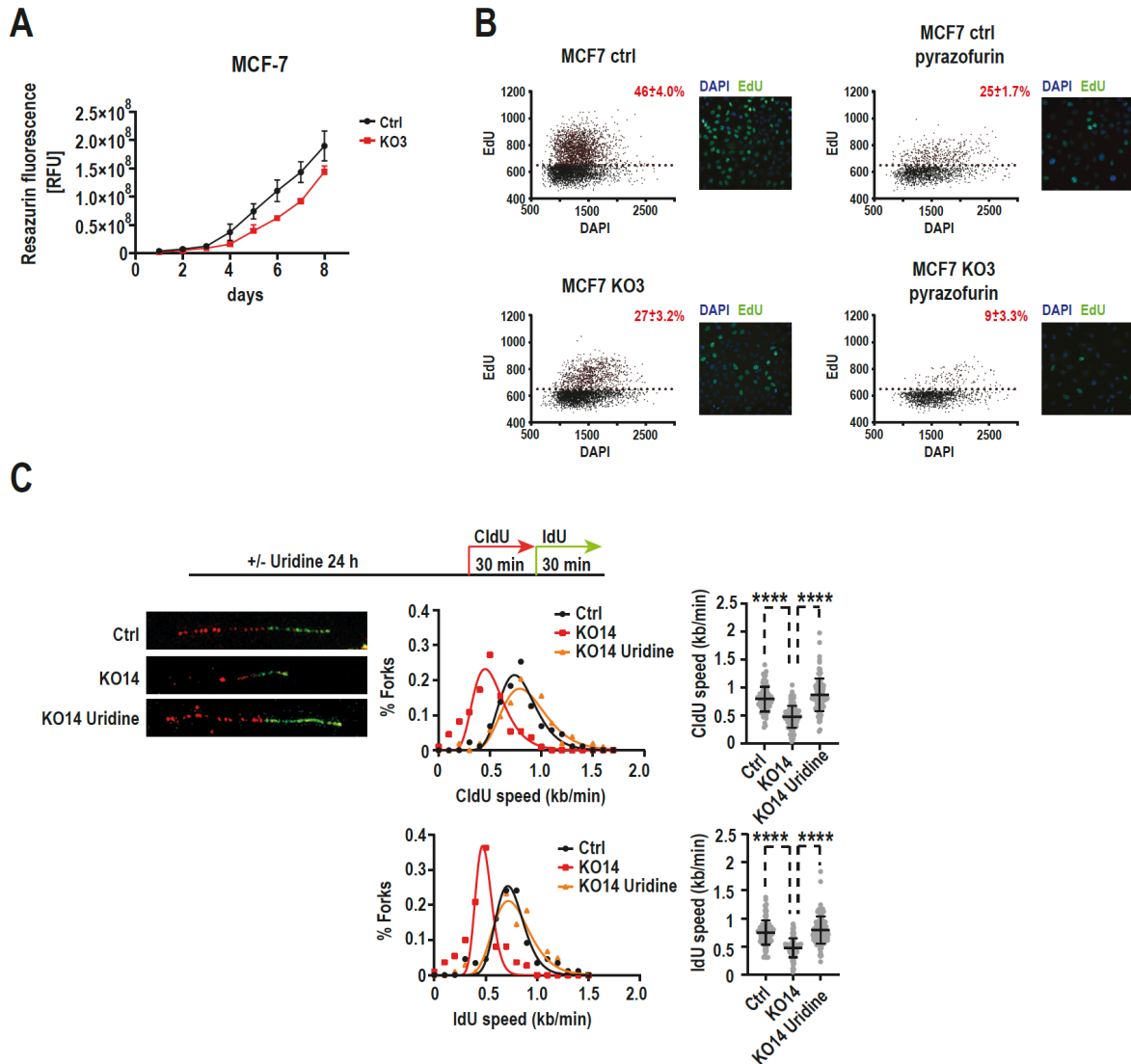
Supplementary Fig. 3



Supplementary Fig. 3

A Replication fork speed (CldU incorporation) in ctrl and *NUDT22* KO cells. **B** Quantification of the percentage of EdU-positive cells (ctrl::1-2 $P=0.0109$; ctrl::3-6 $P=0.0003$; 1-2 DMSO::1-2 pyrazofurin $P=0.0227$; 3-6 DMSO::3-6 pyrazofurin $P=0.0109$). P-values were calculated by unpaired t-test. Errors as the mean with SD) and representative images. **C** Dose response curves of ctrl and *NUDT22* KO U2OS and hTERT-RPE1 cells exposed to MPA and **D** 6-MP for 96 h.

Supplementary Fig. 4



Supplemental Fig. 4

A MCF7 *NUDT22* KO cells grew slower than their parental control cells. B *NUDT22* KO MCF7 cells have reduced EdU incorporation, which is further reduced by pyrazofurin exposure C Reduced replication fork speed in *NUDT22* KO14 MCF7 cells can be rescued by uridine supplementation.

4. Development of NUDT22 small molecule inhibitors with computer-aided drug design

4.1 Introduction

Improving overall survival and prognosis of cancer patients relies on the discovery of novel anti-cancer agents targeting well-established and newly emerging drug targets with exquisite specificity. Drug discovery pipelines usually start with the identification and validation of a suitable molecular target. Physical and virtual screening is then used to identify active drug candidates, the so-called hits, followed by lead optimisation. More specifically, hit compounds are transformed into biologically active lead compounds through optimising physicochemical properties to identify drug candidates for preclinical development. The best drug candidate enters clinical trials and, if successful, the market (Fig. 8) [129].

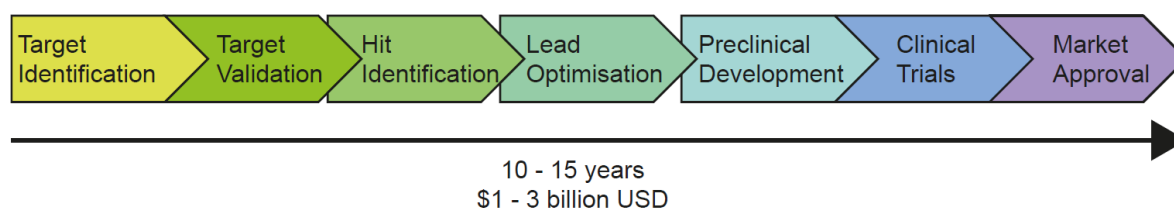


Figure 8. Drug discovery pipeline. Drug discovery starts with the identification and validation of a drug target followed by hit identification. Hit –to-lead optimisation results in the identification of one or several drug candidates entering preclinical development and, if successful, clinical trials. Drug development from target identification until market approval lasts on average around 10 – 15 years and costs \$1 – 3 billion USD.

Developing a new drug from identification until market approval is a highly time and cost intensive process with an average duration of 12 years and a cost of approximately \$1 - 3 billion USD [130,131].

The use of high throughput screening (HTS) as go-to starting point for hit identification in drug discovery programs especially in pharmaceutical industry is one of the reasons for the long and expensive drug development process. In HTS, a library of chemical synthesised drug-like compounds is assessed based on the potential to interact with a given target to identify hits for further hit-to-lead optimisation [132].

The introduction of computer-aided drug design (CADD) and the possibility to analyse millions of molecules through virtual screening even before their chemical synthesis enabled a faster and more cost-effective approach for the identification of promising new small molecules [133,134]. With the discovery of the HIV protease inhibitor Viracept as first drug identified in a structure-based virtual screen in 1997, computational tools moved into the spotlight for successful drug discovery [135]. Since then, several anti-cancer agents identified with CADD approaches such as the hepatocellular growth factor c-MET and anaplastic lymphoma kinase (ALK) inhibitor crizotinib have received market approval and are used in cancer therapy today [130,136].

However, in comparison to HTS, chemical synthesis of the compounds identified in virtual screens adds another potentially time-consuming step towards hit identification. Whereas all compounds in HTS are already chemically synthesised and are being assessed on their drug-likeness and biochemical activity towards the target of interest, compounds identified with computational tools have to be synthesised prior to their actual activity assessment for hit identification. Chemical synthesis of the compounds identified in virtual screens is often time-consuming and can be limited due to chemical resources and storage capacities posing a risk to potential hit elimination even before biochemical assessment [133].

A robust biochemical assay close to the target's activity is required for either hit selection in HTS or hit identification of compounds pre-selected in virtual screens. The development of such an assay can be challenging and can pose another time and cost-intensive step to drug discovery. In contrast to HTS, where compounds are usually only assessed in single concentrations, in CADD, due to the pre-selection of potential hits, the biochemical assay can be used to directly determine the half maximal inhibitory concentration (IC_{50}) for hit selection, which is usually done at a later step in HTS-based drug discovery [137,138].

Another parameter to consider when deciding on performing a virtual screen on a defined compound database to identify hit candidates is the restriction to only being able to exploit one protein crystal structure for molecular docking at the time. The availability of a well-defined and characterised protein structure and/or ligand is crucial to be successful in CADD. In contrast, HTS can also be utilised in case of targets

without well-defined crystal structures and hit identification can be performed on a broad range of targets at the same time [132].

In addition, virtual screening only predicts the binding of ligands to the target by using mathematical calculations based on the position of the compound in the active site of the target protein and both, protein and ligand confirmations are only estimated representations of their corresponding natural forms. To be successful in CADD, the selection and careful preparation of the virtual ligand database as well as target protein crystal structure is of high importance to be able to translate computational findings into biochemical and biological hit identification [139].

The rapid growth of computational tools, however, led to more and more accurate predictions of ligand-protein interactions and a higher success rate in identifying a promising starting point as well as, in later stages, enabling hit-to-lead optimisation for the development of novel anti-cancer agents. Several virtual screening approaches are available with structure-based and ligand-based drug discovery as the most prominent among others. Whereas ligand-based drug discovery exploits molecular similarity, which means structural information obtained from active ligands in case of no available 3D target structure, structure-based drug design relies on a known and well-defined protein structure to identify interaction patterns between ligands and receptor-protein [130].

In settings with more limited resources such as academia and smaller biotechnological companies, computational tools can be used to speed up and reduce costs to identify novel promising drug compounds. In addition, computational tools potentially reduce *in vitro* and *in vivo* studies through simulation and prediction of essential factors such as bioavailability, activity, toxicity and overall efficacy [134].

4.1.1 Aims

Here we exploited our previously solved co-crystal structure of NUDT22 and its substrate UDP-glucose to perform an *in silico* structure-based screen on an open access compound database to identify novel starting points for the development of first-in-class NUDT22 inhibitors [26]. Hit-to-lead optimisation was performed, resulting in a subset of lead compounds. We further evaluated the identified leads based on their enzymatic activity and target engagement towards recombinant NUDT22 protein.

4.2 Results

4.2.1 *In silico* screening of NCI/DTP to identify starting point for NUDT22 inhibitors

For the identification of potential NUDT22 interactors for further chemical optimisation, we performed a molecular docking study of the co-crystal structure of NUDT22 bound to its substrate UDP-glucose (5LOR.pdb, *Fig. 9*) on the NCI/DTP compound database in Schrödinger Suite 2019-3 (*Fig. 10; Chapter 2.12*).

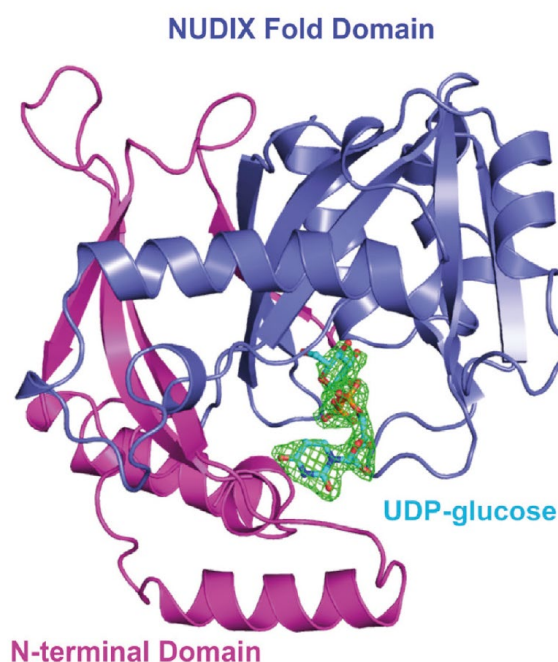


Figure 9. Co-crystal structure of NUDT22 with its substrate UDP-glucose (5LOR.pdb). UDP-glucose is located in the active site located in between the N-terminal domain and NUDIX fold domain of NUDT22. Adapted from Carter et al., 2018 [26].

In preparation for the virtual screen, we generated a subset of 98,513 compounds by implementing a filtering cascade to identify drug-like and novel compounds for successful hit identification. Firstly, we eliminated small molecules with reactive and interfering groups, so-called PAINS and REOS using a predefined Knime filtering workflow (*Fig. 10*) [118]. PAINS compounds are often associated with high reactivity as well as non-specific interactions with proteins in both virtual screens and bioactivity assays leading to frequent hitters in drug discovery processes [120]. In contrast to PAINS, the REOS filter selects compounds with functional groups that cause virtual

screen and/or assay interference and that usually have poor ADMET (absorption, distribution, metabolism, excretion and toxicity) properties [119]. Secondly, we applied a chemical property filter excluding compounds with a molecular weight (AMW) > 300 Da and filtered the compounds based on SlogP < 3.0, an important parameter to predict hydrophobicity and consequently, cell permeability (*Fig. 10*). Even though larger molecules tend to have higher mathematically calculated binding affinities, the so-called docking scores (DScores), due to stronger molecular interactions with residues in the active site of the target protein, smaller molecules are usually preferred as starting points for the development of drug candidates. Smaller molecules can be optimised by adding new groups to the chemical scaffold without the risk of violating Lipinski's Rule of 5, a rule used to assess drug-likeness of small molecules based on chemical properties [121,140].

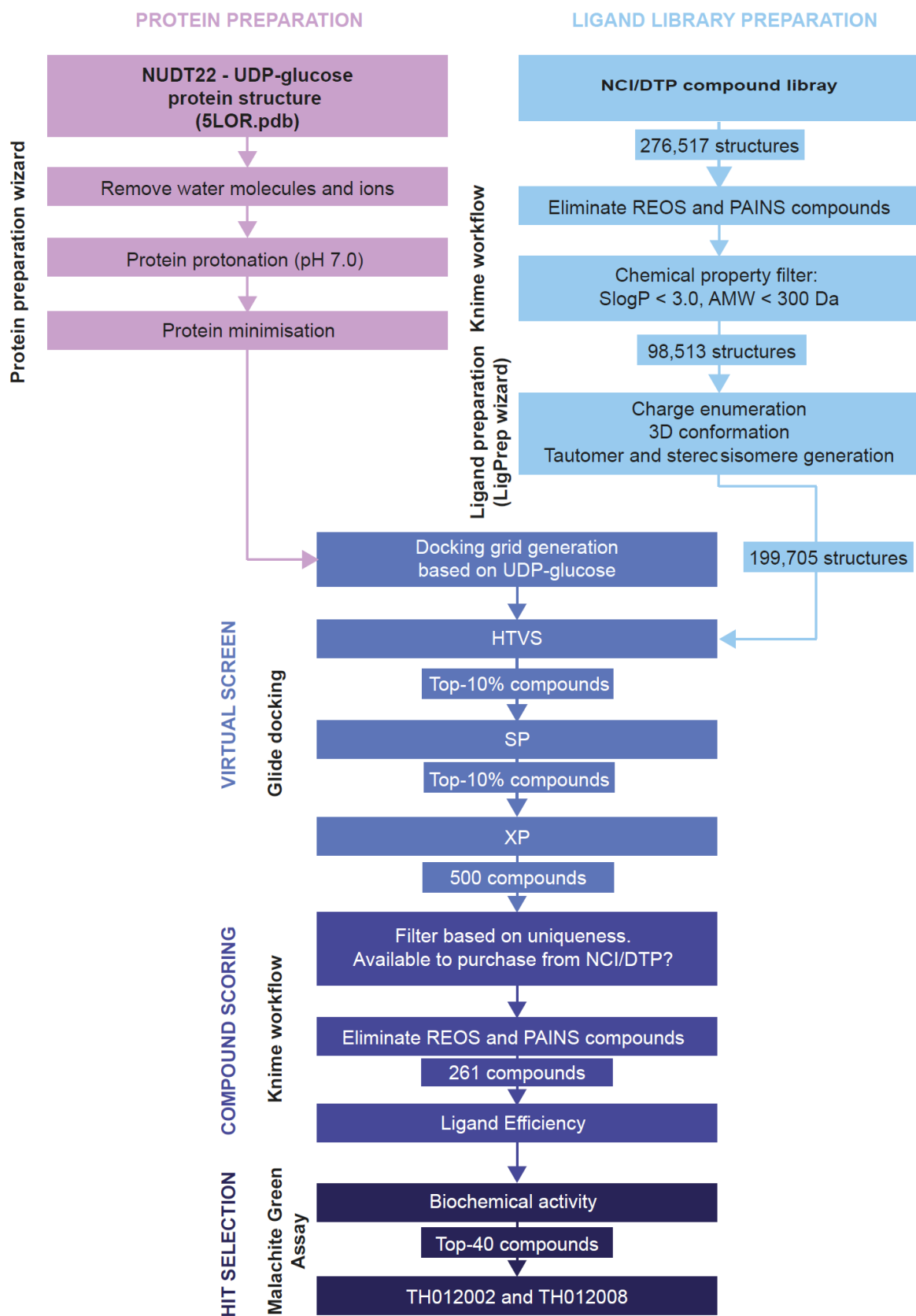


Figure 10. Virtual screen workflow leading to the identification of the two hit compounds TH012002 and TH012008. Briefly, before performing the virtual screen, the protein was prepared using the protein preparation wizard implemented in Schrödinger Suite 2019.3. A ligand library was prepared based on the National Cancer Institute/Developmental Therapeutics Program (NCI/DTP) compound database by eliminating potential interfering compounds (REOS and PAINS) from the 276,517 structures followed by filtering based on the chemical descriptors molecular weight (AMW) and SlogP with Knime 4.0.1. The remaining 98,513 structures were then further prepared based on their protonation states and 3D conformation, and potential tautomers and stereoisomers were generated using LigPrep implemented in Schrödinger Suite 2020.1 generating a total of 199,705 structures for virtual docking. A Glide docking grid was defined based on UDP-glucose in the ligand binding site of the prepared NUDT22 protein structure (5LOR.pdb) followed by performing the virtual docking screen consisting of a cascade of three docking steps with increased accuracy (Glide HTVS → SP → XP). The top-500 compounds were then filtered based on uniqueness and availability to purchase from the NCI/DTP compound database followed by eliminating potential REOS and PAINS compounds. After sorting the remaining structures based on ascending ligand efficiency, the top-40 compounds were selected for further assessment based on their enzymatic activity. Two hit compounds, TH012002 and TH012008, were identified to inhibit recombinant NUDT22 protein in the Malachite Green activity assay.

To identify all representative states of each structure, i.e. protonation states, 3D conformation, tautomers and stereoisomers, the remaining 98,513 compounds were further prepared using the LigPrep wizard implemented in Schrödinger Suite 2019-3, which generated 199,705 structures for the actual docking procedure (*Fig. 10*).

After importing the co-crystal structure of NUDT22 5LOR (5LOR.pdb) from the protein databank to Schrödinger Suite 2019-3, we first processed the protein to obtain the most accurate 3D conformation as a high-quality starting point for the docking process (*Fig. 10*) [134]. The prepared compounds entered the virtual Glide docking screen comprised of a cascade of three docking steps with increased accuracy resulting in the identification of 500 possible NUDT22 interactors. The determined docking scores (DScores), where lower is better, ranged from -12.34 to -6.1 kcal/mol.

To narrow down the top-500 compounds, we filtered them based on duplicates, compounds that were unavailable for purchase of the NCI/DTP compound database, and REOS as well as PAINS compounds (*Fig. 10*) [141]. This yielded 261 ligands with corresponding DScores in between -12.03 and -6.31 kcal/mol. As next step, we sorted the 261 compounds based on ascending Ligand Efficiency (LE) [20–22].

The consideration of LE is a valuable tool to overcome the earlier described selection of higher AMW compounds due to their often-occurring higher DScores instead of smaller compounds, which are more favourable for hit-to-lead optimisation in drug

discovery. LE predicts the binding affinity of each individual non-hydrogen atom in a chemical structure under consideration of both, the binding affinity DScore and AMW. It therefore normalises binding affinities for a better comparison of individual ligands in hit as well as lead selection processes [142–144].

The LE ranged from 0.21 to 0.72 kcal mol⁻¹, where the lower the more potent. After narrowing down the list of compounds based on their chemical structure and their position in the binding site of NUDT22, we again sorted the list based on ascending LE. A selection of top-40 commercially available compounds with a LE ranging from 0.41 to 0.60 kcal mol⁻¹ with corresponding DScores in between -8.98 and -6.31 kcal mol⁻¹ was further evaluated based on biochemical activity (*Fig. 10*).

4.2.2 Biochemical evaluation of top compounds identified in *in silico* screen

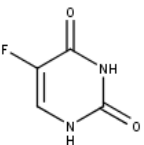
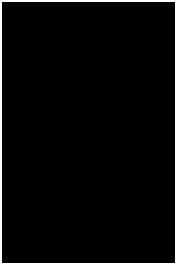
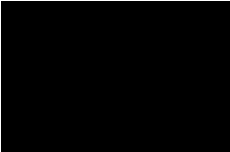
For further experimental evaluation of the top-40 compounds, we performed a high throughput-biochemical assay based on the malachite green assay approach on recombinant NUDT22 protein (*Fig. 10; Chapter 2.12.5*). This assay was performed in collaboration with Ingrid Almlöf and Thomas Helleday at Karolinska Institute, Stockholm, Sweden. The principle of the malachite green assay is based on the colorimetric determination of inorganic phosphate due to complex formation of the brown coloured Malachite Green with phosphomolybdate at a lower pH resulting in a colorimetric change towards green colour and consequently, a shift of the absorption maximum [145]. As NUDT22 only hydrolyses UDP-glucose and –galactose to UMP and the corresponding sugar 1-phosphate, alkaline phosphatase was added for inorganic phosphate generation. In addition, due to UDP impurities in the UDP-glucose samples leading to background signal in the performed malachite green assay approach, we used UDP-galactose as substrate to assess biochemical activity of our identified compounds [26].

Out of the top-40 compounds, two hits, TH012002 and TH012008 were identified to inhibit NUDT22 each with an IC₅₀ of > 650 µM. Both identified hits have similar DScores of -7.61 kcal mol⁻¹ and -7.19 kcal mol⁻¹ and LE of 0.59 kcal mol⁻¹ and 0.51 kcal mol⁻¹, respectively (*Table 4*). Considering chemical properties, TH012002 has an AMW of 188.16 Da, SlogP of -1.68 and a topological polar surface area (TPSA) of 70 Å². In contrast, TH012008 has an AMW of 210.21 Da, a SlogP of 0.58 and a TPSA of

107 Å². Both compounds have two hydrogen bond donors (HBD) and five hydrogen bond acceptors (HBA) as part of their chemical structure (*Table 4*).

Due to the similarity of TH012002 to the established nucleoside analogue 5-FU, which has shown to be inactive towards NUDT22 inhibition in a previously performed biochemical screen, we decided to continue with the pyrimidothione TH012008 for further chemical optimisation to potentially increase its relatively weak activity towards NUDT22 inhibition (*Table 4*) [91].

Table 4. Overview of 5-Fluorouracil and the two identified hit compounds TH012002 and TH012008.

	MW [Da]	SlogP	TPSA [Å ²]	HBD	HBA	Binding Affinity [kcal mol ⁻¹]	Ligand Efficiency [kcal mol ⁻¹]	IC50
5-Fluorouracil								
	130.08	-0.9	58	3	2	-	-	-
TH012002								
	188.16	- 1.68	70	2	5	- 7.61	0.59	> 625 μM
TH012008								
	210.21	0.58	107	2	5	- 7.19	0.51	> 625 μM

4.2.3 *In silico* Hit optimisation

As TH012008 only exhibited weak NUDT22 inhibitory activity in the previous performed biochemical assay approach, we suggested the chemical optimisation of the identified scaffold to improve the potency towards NUDT22 inhibition. The carboxylic acid residue of TH012008 is an ideal starting point for chemical optimisation through amide bond formation so that we performed *in silico* enumeration of amine derivatives of the in-house chemical library KLARA (Karolinska Institute, Stockholm, Sweden) (Fig. 11; Chapter 2.12.4) [146,147].

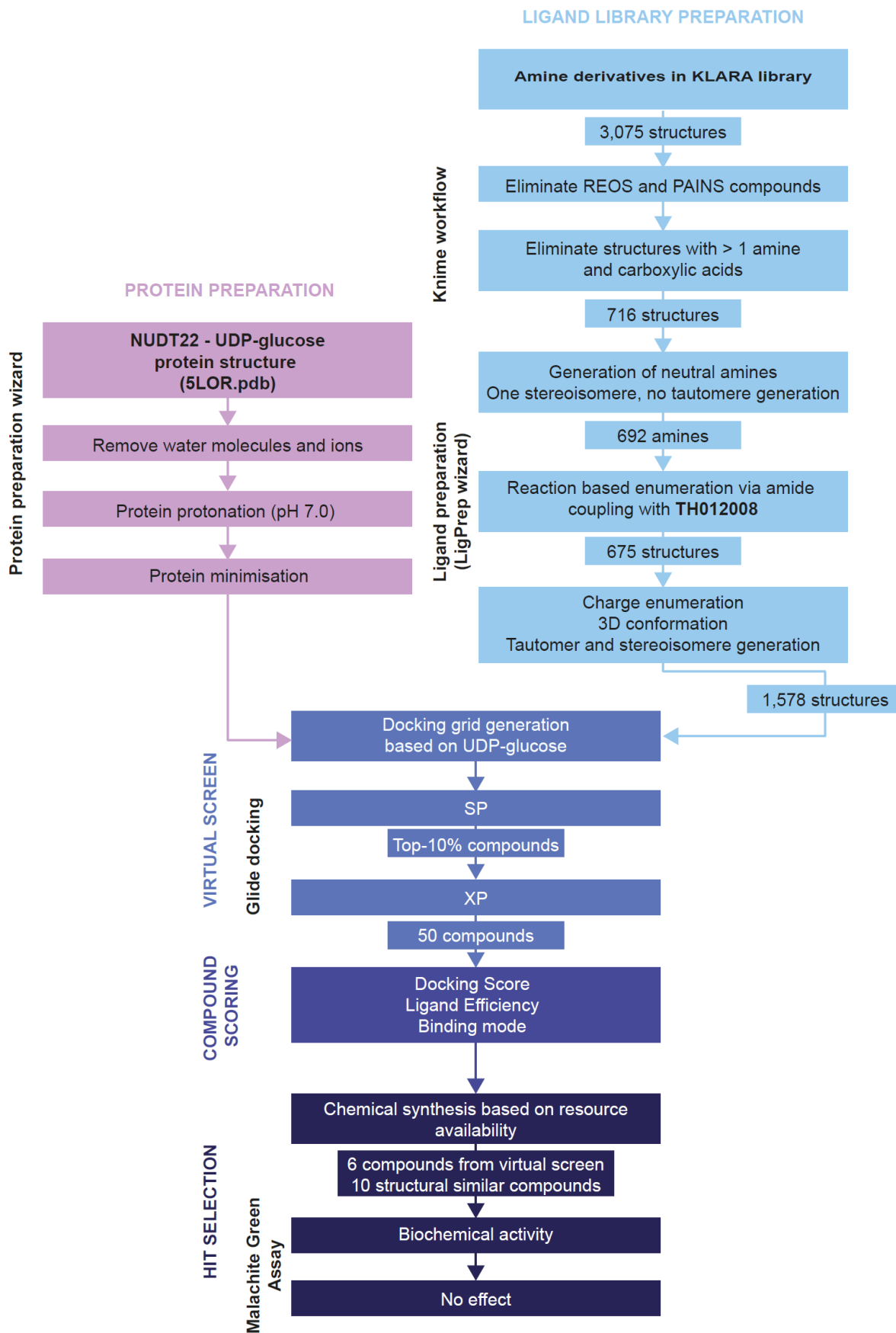


Figure 11. Chemical optimisation of TH012008 by amide coupling and second virtual screen to identify TH012008 analogues with improved activity towards NUDT22. We performed *in silico* enumeration of amine derivatives of the in-house chemical library KLARA. 3,075 aliphatic and aromatic primary amines were identified by substructure search followed by a Knime filtering workflow removing derivatives with > 1 amine, carboxylic acids as well as REOS and PAINS structures. 716 amines were then desalted, neutralised and one stereoisomere but no tautomere were generated followed by ligand preparation with LigPrep implemented in Schrödinger Suite 2020-1 retaining 692 amines. Amide coupling with TH012008 was then performed via reaction-based enumeration resulting in a TH012008 amide library of 675 substructures. The TH012008 amide library was prepared in LigPrep via charge enumeration, stereoisomere/tautomere and 3D conformation generation for virtual docking. NUDT22 protein in complex with UDP-glucose was prepared using the, in Schrödinger Suite 2020-1 implemented Protein Preparation wizard and the Glide docking grid was selected based on ligand binding site. Virtual docking was then performed resulting in 50 compounds, which were scored based on docking score, ligand efficiency and binding mode compared to UDP-glucose. The top-6 identified compounds as well as 10 structural similar compounds were chemically synthesised and their biochemical activity was assessed in the Malachite Green assay approach with recombinant NUDT22 protein. None of the identified TH012008 amides did show an effect towards recombinant NUDT22 inhibition.

We identified 3,075 aliphatic and aromatic primary amines by substructure search in an IJC-based database followed by a Knime filtering cascade including the elimination of derivatives containing more than one amine, carboxylic acids as well as PAINS and REOS compounds resulting in a total of 716 amines. After desalting, neutral amines with only one stereoisomer as well as no tautomers were prepared using the LigPrep wizard implemented in Schrödinger Suite 2020-1 retaining 692 amines. A reaction-based enumeration with TH012008 was performed via amide coupling generating an amide library consisting of 675 TH012008 amide derivatives (*Fig. 11*).

To assess their interaction potential with NUDT22, we performed another *in silico* docking screen on the prepared and optimised NUDT22 co-crystal structure 5LOR.pdb. For the actual docking screen, the 675 amides were again prepared using LigPrep to yield 1,578 structures, which were then docked using Glide SP and XP docking. 50 unique amides were selected based on their binding mode assessment in the active site of NUDT22. The top-50 compounds had calculated LE in between 0.27 and 0.40 kcal mol⁻¹, and DScores ranging from -9.16 to -7.16 kcal mol⁻¹ for further experimental evaluation. Out of the top-50 TH012008 amide derivatives, six compounds were synthesised in addition to 10 structural similar compounds based on reagent availability (*Fig. 11*).

4.2.4 Binding interactions of TH012008 and its amide derivatives with NUDT22

To evaluate the identified TH012008 amide analogues, we assessed their position in the binding site of NUDT22 compared to the natural substrate UDP-glucose *in silico* (Fig. 12).

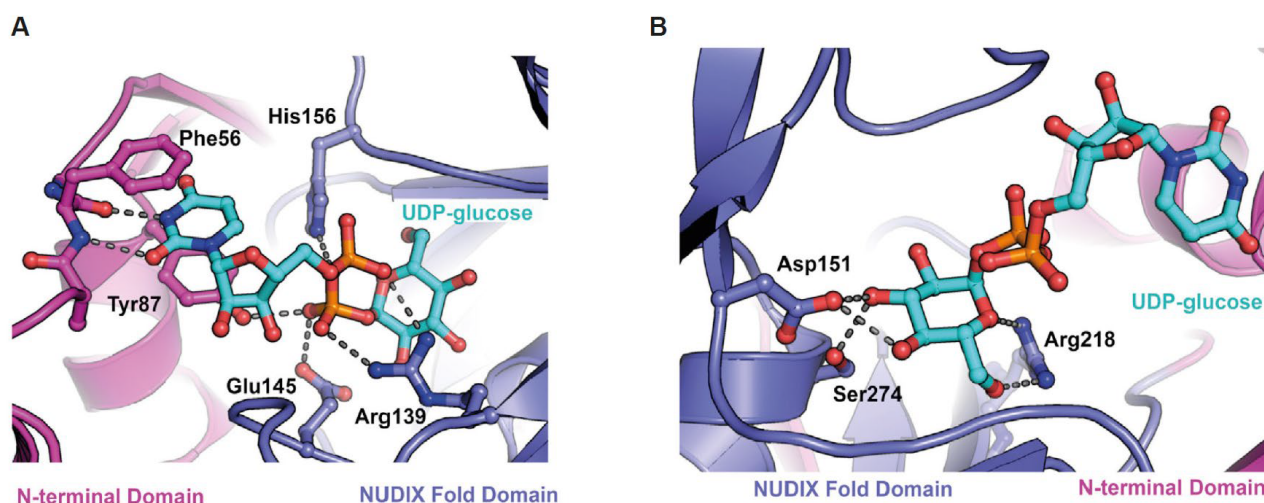


Figure 12. Binding model of NUDT22 with UDP-glucose and TH012008. **A** The uracil moiety of UDP-glucose is positioned between the two aromatic amino acids Tyr87 and Phe56 of the N-terminal domain forming π - π interactions coordinated by additional hydrogen bonding with Phe56. A complex hydrogen bond network formed between Tyr87, Glu145 and Arg139 and the β -phosphate as well as another hydrogen bond formed between His156 and the oxygen forming a bridge between the uracil moiety and the diphosphate moiety in the NUDIX fold domain. **B** Glu145 Asp151, Ser274 and Arg218 coordinate glucose moiety binding in the NUDIX fold of NUDT22. Figure A and B are adapted from *Carter et al., 2018 [26]*. **C** and **D** The pyrimidothiophene scaffold of TH012008 is stacked (blue) between Tyr87 and Phe56 and additional hydrogen bonds (yellow) are formed between the carboxyl- and amino-moieties and Phe56 in the N-terminal domain. Additional hydrogen bonds are formed between the carboxyl-moiety and Ala144 as well as Arg139 coordinating ligand binding. A salt bridge (purple) is formed between Arg139 and the negatively charged oxygen of the carboxyl moiety of TH012008.

Similar to the uracil moiety of UDP-glucose, the pyrimidothiophene scaffold of TH012008 and its amide analogues is positioned between the two aromatic amino acids Tyr87 and Phe56 in the flexible loop of the N-terminal domain of NUDT22 forming π - π interactions, also known as aromatic stacking. The scaffold is further coordinated by hydrogen bond (H-bond) formation between the carboxyl- and amine-moieties of the pyrimidine ring and the amino acid backbone of Phe56 (*Fig. 12; Table 5*).

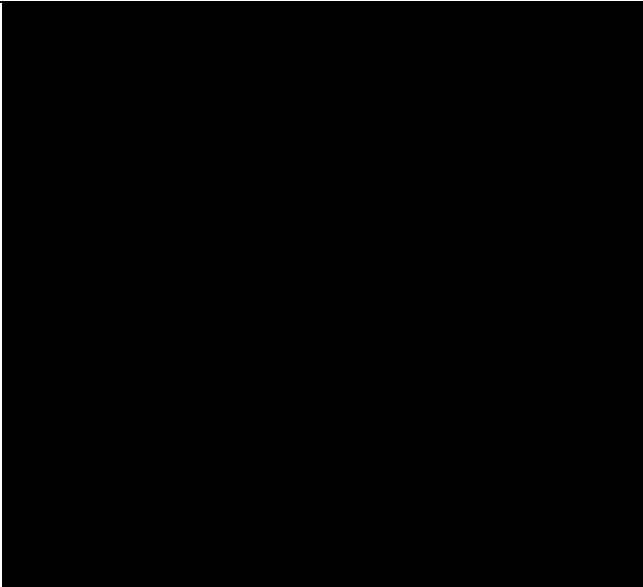
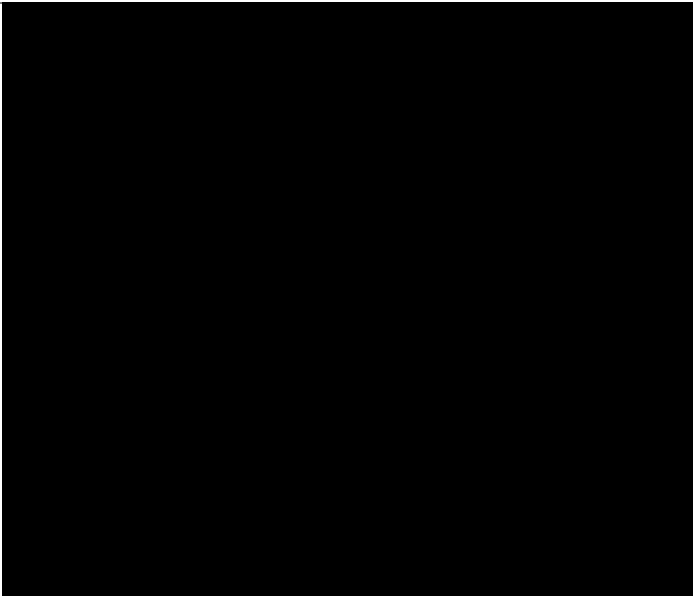
In the case of TH012008, the carboxylic acid residue forms H-bonds between the carboxylic oxygen and the basic amino acid Arg139 as well as the negatively charged oxygen and the aliphatic amino acid Ala144. The negatively charged oxygen further interacts via salt bridge with Arg139. The carboxylic oxygen of all TH012008 analogues except TH012565 and TH012568 establishes H-bonds with Ala144, but no salt bridges are formed (*Fig. 12C,D; Table 5*).

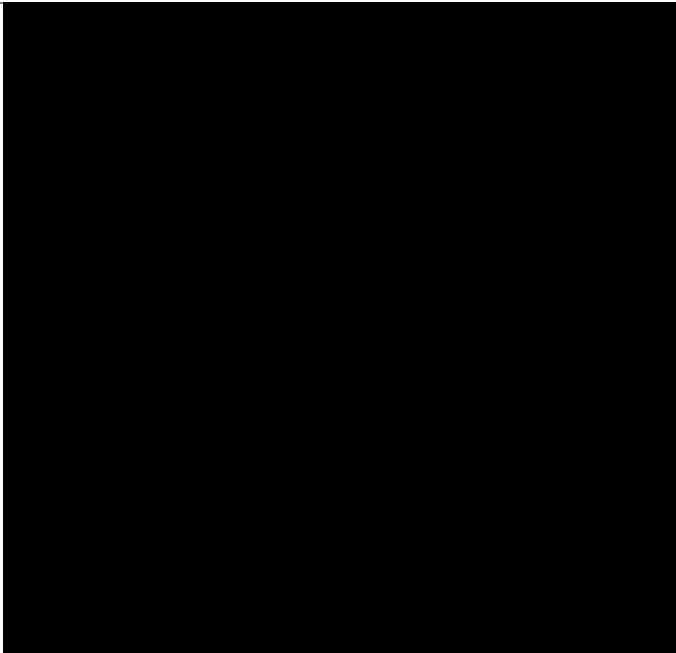
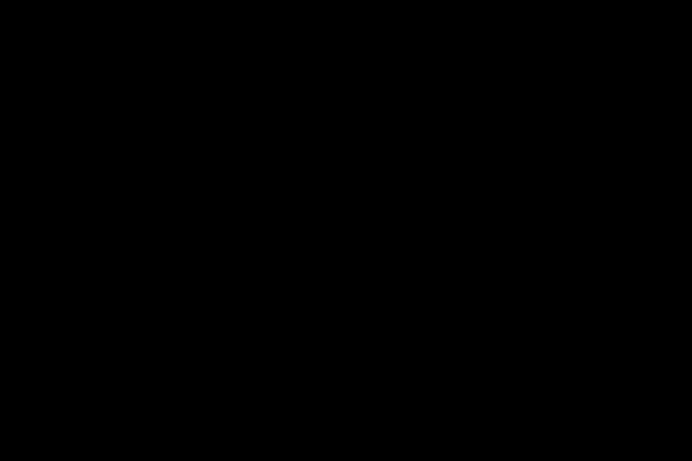
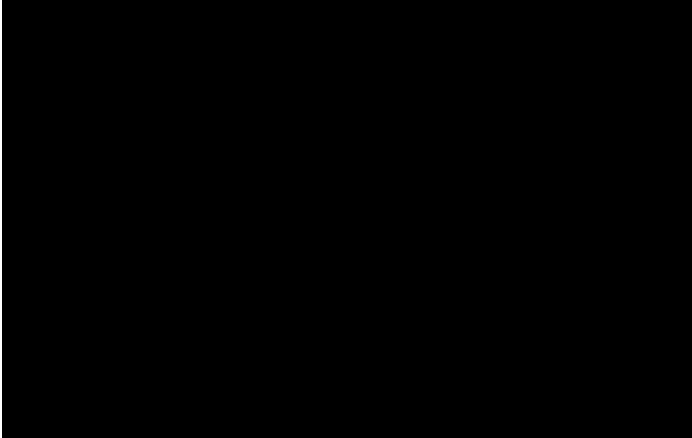
The amide residues of TH012556, TH012558, TH012560 and TH012565 are coordinated via salt bridges with the acidic amino acids Glu189, Glu193 and Glu247. A further direction occurs via H-bond formation between the amine residues with either Glu189, Glu193 or Glu247 (*Table 5*).

Two salt bridges between the amide residue and Glu189 and Asp151 coordinate TH012568. The amide residue of TH012564 does not form any salt bridges, but is directed by H-bond formation with Ser140 (*Table 5*).

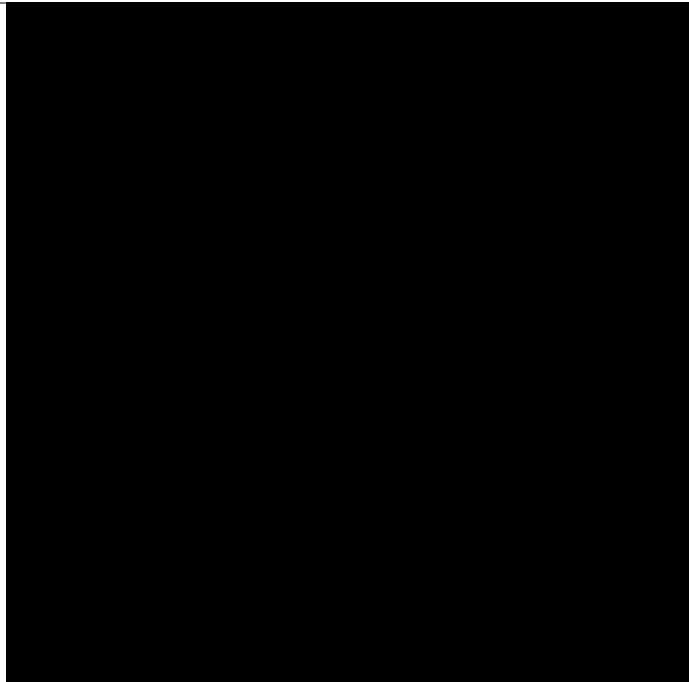
Table 5. . Binding affinity, ligand efficiency and ligand interactions of TH012008 and its amide analogues identified in the virtual docking screen.

π - π interactions are displayed in green, hydrogen bonds (H-bonds) in pink arrows and salt bridges in purple.

Compound	Binding Affinity [kcal mol ⁻¹]	Ligand Efficiency [kcal mol ⁻¹]	2D-Interactions	Amino acids involved in interactions
TH012008	- 7.19	0.51		Phe 56 Tyr 87 Arg 139 Ala 144
TH012556	- 9.16	0.37		Phe 56 Tyr 87 Ala 144 Glu 189 Glu 193 Glu 247

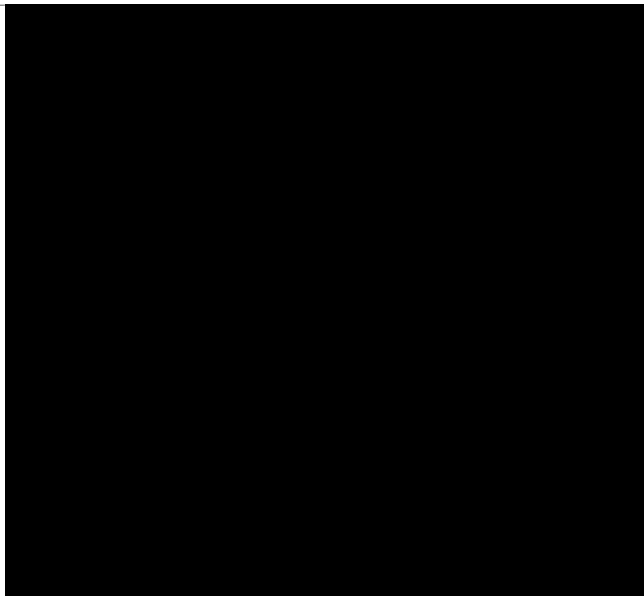
TH012558	- 8.87	0.37		Phe 56 Tyr 87 Ala 144 Glu 189 Glu 193 Glu 247
TH012560	- 8.76	0.40		Phe 56 Tyr 87 Ala 144 Glu 189 Glu 193 Glu 247
TH012564	- 7.89	0.34		Phe 56 Tyr 87 Ser 140 Ala 144

TH012565 - 8.22 0.32



Phe 56
Tyr 87
Glu 193
Glu 189
Glu 247

TH012568 - 8.23 0.33

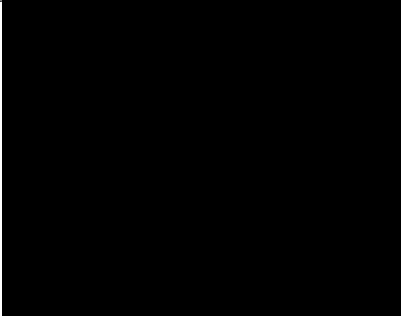
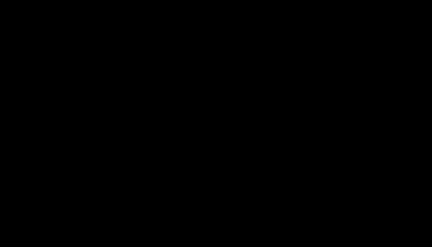
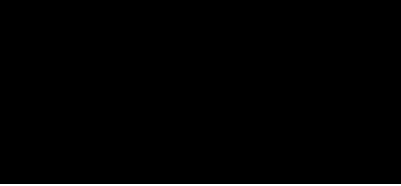



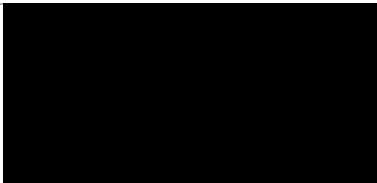
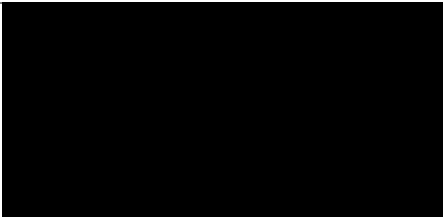
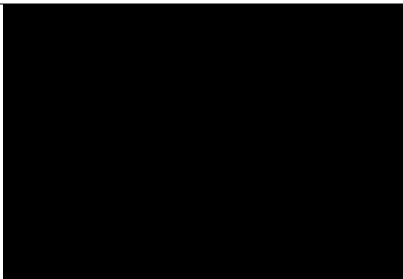
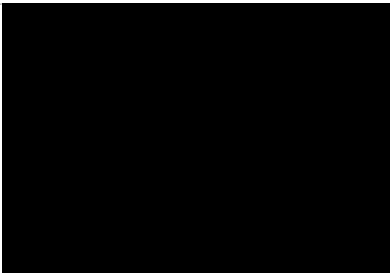
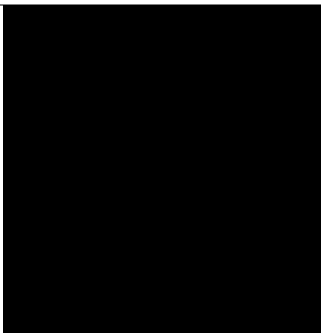
Phe 56
Tyr 87
Asp 151
Glu 189

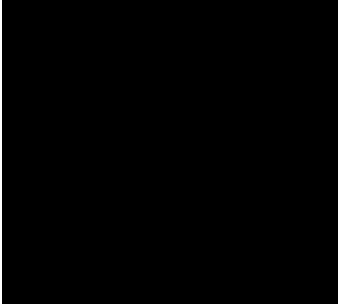
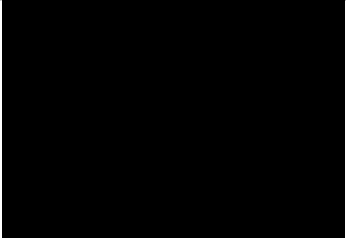
4.2.5 Enzymatic activity of TH012008 amide derivatives

The synthesised TH012008 amide derivatives were evaluated based on their enzymatic activity towards recombinant NUDT22 protein in the above-described Malachite Green Assay approach (Fig. 11; Chapter 2.12.4). Based on chemical optimisation, we were expecting an increase in potency compared to TH012008. However, none of the TH012008 analogues showed an inhibitory effect towards NUDT22 protein in the performed enzymatic assay (Table 6). The compounds were assessed in the highest possible concentration range based on their stock concentrations of either 10 or 50 mM with a DMSO content < 1% as limiting factor. If no effect was observed in the highest possible concentration, the IC₅₀ has, thus, to be > 125 µM (10 mM) or > 625 µM (50 mM), respectively.

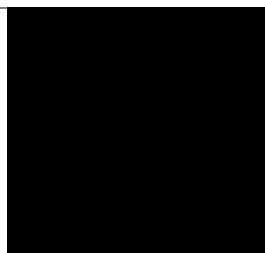
Table 6. IC₅₀ and chemical structures of TH012008 amide analogues. IC₅₀ determination was performed by Ingrid Almlöf at Karolinska Institutet, Stockholm, Sweden.

	Compound	IC ₅₀
TH012556		No effect, IC ₅₀ > 625 µM
TH012557		No effect, IC ₅₀ > 625 µM
TH012558		No effect, IC ₅₀ > 125 µM

TH012559		No effect, IC50 > 625 µM
TH012560		No effect, IC50 > 125 µM
TH012561		No effect, IC50 > 125 µM
TH012562		No effect, IC50 > 125 µM
TH012564		No effect, IC50 > 125 µM
TH012565		No effect, IC50 > 125 µM

TH012567		No effect, IC50 > 625 µM
TH012568		No effect, IC50 > 125 µM
TH012669		No effect, IC50 > 125 µM
TH012670		No effect, IC50 > 125 µM
TH012671		No effect, IC50 > 125 µM
TH012673		No effect, IC50 > 125 µM

TH012725



4.2.6 Target engagement of TH012008 amide derivatives

Next, we assessed the ability of TH012008 and its amide analogues to stabilise NUDT22 protein over a defined temperature gradient and therefore, to directly engage their target. We used the so-called differential scanning fluorimetry (DSF) approach to detect changes in the protein unique melting temperature (T_m) upon inhibitor binding (*Chapter 2.12.6*) [126]. When exposed to a temperature gradient above T_m , the protein starts to unfold resulting in the exposure of hydrophobic sites of the protein structure. The Sypro Orange fluorescent dye can then bind to these sites causing an increase in fluorescent signal.

Neither TH012008 nor any of the further optimised amide analogues significantly stabilised recombinant NUDT22 protein and consequently, did not induce a shift in T_m when compared to DMSO (*Fig. 13*).

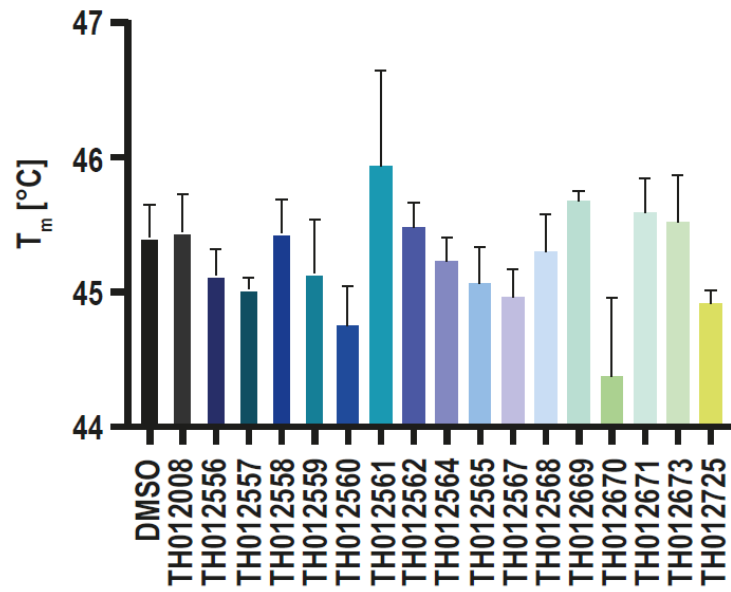


Figure 13. NUDT22 stabilisation upon NUDT22 inhibitor binding. Target engagement assessment of TH012008 and analogues with differential scanning fluorimetry (DSF). Isolated NUDT22 protein was treated with 100 μ M NUDT22 inhibitors and T_m was calculated. Data are means \pm SEM of three biological replicates and represent one of three independent experiments. $p > 0.05$; unpaired t-test analysis.

4.3 Discussion

For the identification of potential small molecule NUDT22 inhibitors, we exploited our previously identified co-crystal structure of NUDT22 and its substrate UDP-glucose to perform a virtual docking screen on the open access compound database provided by DTP/NCI [26]. This database includes more than 200,000 small molecules and has been exploited for molecular docking studies before [148–150]. In addition, several molecules provided by DTP/NCI has served as starting points for the development of anti-cancer agents such as entrectinib, ivosidenib and lorlatinib, which are currently used in anti-cancer therapy [130].

For the structure-based virtual screen on our preselected compound library and NUDT22, the docking site was set based on the binding site of the natural ligand UDP-glucose. We applied a ligand-grid without the implementation of restriction factors to avoid the biased interpretation of ligand-target binding due to lower flexibility. Out of 500 compounds identified in the virtual screen, the most promising top-40 compounds were selected and further evaluated based on their biochemical activity in the previously described malachite green assay. We identified two hits, TH012002 and TH012008 that inhibited recombinant NUDT22, albeit in the high micromolar range ($> 625 \mu\text{M}$) (*Table 4*). Considering ligand-target interaction metrics, both hits do not differ in their corresponding binding affinity nor LE metrics. Comparison of drug-like molecules with an average AMW of 500 Da and K_i of 10 nM identified in drug screenings performed by Pfizer revealed an average LE of $0.29 \text{ kcal mol}^{-1}$ per non-hydrogen atom and $\text{LE} \leq 0.3$ is usually considered as a good indicator for candidate selection in drug discovery [137,142]. Due to their relatively small AMW and low number of non-hydrogen atoms, TH012002 and TH012008 have $\text{LE} > 0.3$ (*Table 4*).

TH012002 and TH012008 are relatively small compounds ($< 250 \text{ Da}$) and follow Lipinski's Rule of 5 parameters such as $\text{HBD} < 5$ and $\text{HBA} < 10$. However, both hits differ in their TPSA and SlogP, which are important parameters to assess permeability and solubility of a molecule (*Table 4*). Since TPSA predicts the polarity of a compound, it is associated with membrane transport and therefore, the uptake and circulation of a small molecule. In contrast, SlogP is an important parameter for lipophilicity and solubility assessment of small molecules. Ideal small molecule drugs should have a $\text{SlogP} < 5$ and a $\text{TPSA} \leq 140 \text{ \AA}^2$ for optimal drug-likeness [121]. As our identified hits

did not exceed a TPSA of 140 \AA^2 nor SlogP of 5, they were ideal starting points for hit-to-lead optimisation. Due to the structural similarities of TH012002 to the nucleoside analogue 5-FU, we decided to proceed with TH012008 [91]. In addition, compounds with similar scaffolds to the pyrimidothiophene scaffold of TH012008 have been identified to be potent inhibitors of various enzymes involved in cancer further suggesting the potential of TH012008 for lead optimisation [151–153].

TH012008 consists of a pyrimidothiophene scaffold attached to a carboxylic acid residue. The replacement of carboxylic acids, the so-called bioisosteric replacement, is a prominent strategy in hit-to-lead optimisation. Carboxylic acids are replaced by surrogate structures such as primary amines to improve physicochemical properties, molecular ligand-protein interactions and activity of the parent compound [147]. Thus, we suggested replacing the carboxylic acid residue with primary aliphatic and aromatic amines for a second virtual screen to identify TH012008 amide analogues with improved activity to inhibit NUDT22. We identified 50 amides with improved DScores and increased, and consequently, improved LE compared to the parent compound TH012008.

We selected the top-20 compounds for biochemical evaluation. However, based on a shortage of chemical resources, we could only synthesise six compounds and included 10 structurally similar compounds to the top-20 identified ones for chemical synthesis and further assessment of their potential activity to inhibit recombinant NUDT22.

Understanding binding mechanisms of small molecules to the active site of the target protein is crucial to assess their potential as lead compounds for further biochemical and preclinical assessment. Comparing the parent compound TH012008 to its optimised amide analogues showed that in all cases, the pyrimidothiophene scaffold was positioned in the flexible loop in the N-terminal domain of NUDT22. Due to the similarity of our identified scaffold to pyrimidines, we were not surprised to find π - π interactions between the aromatic amino acids Phe56 and Tyr87 to be responsible for pharmacophore coordination (*Table 5*). These interactions are common in nucleotide-receptor interactions responsible for the correct orientation directed by aromatic amino acids in the active sites of the corresponding protein [154,155].

In contrast to TH012008, additional chemical interactions such as H-bonds and salt bridges formed with several amino acid residues in the active site of NUDT22 are responsible for the coordination of the different amide residues of the corresponding TH012008 amide analogues (*Table 5*). H-bonds are usually generated due to electrostatic attraction between a so-called H-bond acceptor and H-bond donor. More specifically, a weak bond is formed between a hydrogen atom attached to an electronegative atom, the H-bond donor, and another electronegative atom, i.e. oxygen, nitrogen, or fluorine, the H-bond acceptor. Due to the specificity and directionality of H-bonds, these interactions are important in receptor-ligand recognition and for correct ligand-binding [156]. In comparison, salt bridges are the strongest interactions in proteins or protein and ligands, and are formed by combining electrostatic interactions and H-bond formation. In the case of ligand-receptor interaction, positively and negatively charged residues can built salt bridges. More specifically, the aliphatic amino acids Asp and Glu can form a bond with positively charged residues. Basic amino acids such as Lys and Arg interact via salt-bridge formation with negatively charged residues of either, other amino acids in the protein structure or a ligand [157].

When comparing the interaction pattern of the carboxyl group of TH012008, no salt bridge was formed between Arg139 and the carboxylic oxygen in the TH012008 amide analogues, the additional interactions present in the Nudix fold domain are the reason for the improved binding affinity of the TH012008 analogues compared to TH012008 (*Fig. 12*).

Based on the improved binding affinity due to increased or stronger chemical interactions of the TH012008 amide analogues, we expected an increase in potency compared to the previously identified hit in our biochemical activity assay. Surprisingly, the chemical optimisation of TH012008 did not lead to an increase in potency towards NUDT22. In fact, none of the TH012008 analogues identified in the virtual screen and chemically synthesised showed any activity towards recombinant NUDT22 inhibition (*Table 6*). In contrast to the virtual screen, in which UDP-glucose was used to define the binding site for molecular docking, when assessing inhibitory activity in the biochemical assay approach, our identified NUDT22 inhibitors have to compete with the natural substrate UDP-galactose to bind and therefore, inhibit NUDT22 activity.

More specifically, a higher activity, which means a lower IC_{50} or inhibitory constant (K_i) towards NUDT22 compared to its natural ligand is required for compounds to be identified as potent NUDT22 inhibitors. We used an UDP-galactose concentration of 50 μ M in our approach, which corresponds to the experimentally determined Michaelis-Menten constant (K_m), the substrate concentration at which the enzymatic rate is half of its maximal value [26]. For future experiments, the determination of changes in K_m for UDP-galactose upon NUDT22 inhibitor treatment could be crucial for the successful development of new NUDT22 inhibitors.

In addition, a co-crystal structure of UDP-galactose as ligand instead of UDP-glucose could be of advantage for the identification of novel NUDT22 inhibitors. For correct catalytic activity of an enzyme, the substrate induces a conformational change of the active site of the protein [131]. As NUDT22 hydrolyses both, UDP-glucose and -galactose, for catalytic activity, its active site has to be correctly aligned based on the substrate. This means that the amino acid positions in the binding site of NUDT22 slightly differ depending on the presence of either of the natural ligands. As we selected the hit compounds as well as optimised TH012008 amide analogues based on ligand-grid generation around UDP-glucose, the identified small molecules might not bind effectively to NUDT22 in the presence of UDP-galactose in the biochemical approach.

To confirm whether our compounds could be active without the presence of a natural substrate, we assessed TH012008 and its analogues based on their ability to stabilise isolated NUDT22 protein over a defined temperature gradient upon inhibitor binding. Neither the biochemically active hit TH012008 nor any of its amide analogues engaged with NUDT22 directly confirming the loss in activity based on amide formation (*Fig. 13*).

The failure of amide formation to improve TH012008 activity could be explained by comparing chemical interactions of the biological ligand UDP-glucose in the active site of NUDT22 (*Fig. 13*). Whereas our compounds formed a strong π - π , salt bridge and H-bond interaction network with several amino acids also involved in UDP-glucose binding, UDP-glucose forms strong chemical interactions with an increased number of amino acids in the active site. More specifically, the uracil moiety is positioned in a similar way between the two aromatic amino acids Tyr87 and Phe56 compared to our

developed NUDT22 inhibitors. However, Tyr87, Arg139, Glu145 and His165 coordinate the phosphate and diphosphate moieties of UDP-glucose, whereas the carboxyl-residue of our developed compounds only interacted with Arg139. In addition, the glucose part of the natural ligand forms a strong network with Glu145, Asp151, Arg218 and Ser274 of the Nudix fold domain of the protein [26].

Being successful in virtual drug design strongly depends on the quality of the protein used for molecular docking. X-ray protein structure determination is usually the way forward for a high quality starting point for structure-based drug discovery and a resolution of $< 3.5 \text{ \AA}$ is beneficial to succeed in hit identification [158]. In our case, NUDT22 was co-crystallised with its natural ligand UDP-glucose with all residues fully visible in the active site of the protein and a resolution of 2.19 \AA [26].

For protein crystallisation, choosing the appropriate organism for recombinant protein expression is important. In our case, NUDT22 protein was expressed in a bacterial expression system. Although these systems are efficient due to quick expression and scale up especially for simpler proteins, bacteria are incapable of performing mammalian-like posttranslational modifications (PTMs), which are important for a biological active conformation of a protein [159]. Even though there are several computational approaches available to map PTMs after protein crystallisation, parts of the protein could still be wrongly aligned or missing [160]. To increase the accuracy of a human NUDT22 protein crystal structure for drug discovery purposes, several other protein expression systems could be used to obtain a functional, correctly folded and aligned NUDT22 protein and co-crystal structure. To preserve PTMs, the use of mammalian protein expression systems such as human embryonic kidney (HEK293) or Chinese hamster ovary (CHO) cells with intact posttranslational machinery could be of advantage. However, protein expression in mammalian cells can be time-consuming and often results in non-homologous protein mixtures due to different glycosylation sites imposing a challenge for protein crystallisation and, consequently, correct alignment of the protein crystal structure. Similar to mammalian protein expression systems, the use of insect cells transfected with a previously generated baculovirus vector transfection construct could be of advantage to yield a functional protein with PTMs present for protein crystallisation. Both mammalian and insect protein expression systems use viral transfection of the required gene construct, which

can result in the release of proteases upon transfection thereby risking protein quality due to protein degradation as well as the synthesis of non-human by-products [161,162]. An alternative approach could therefore be the use of cell-free protein expression systems, which utilise whole cell extracts with components required for translation, transcription and PTMs. Upon addition of the gene template and cofactors such as nucleotides, the corresponding protein can be synthesised albeit in relatively low quantity imposing another challenge for protein crystallisation and the use for future enzymatic characterisation of the protein or potential inhibitors [163].

In addition, during co-crystallisation processes, co-factors important for the right alignment of the active site of the protein could be missing causing a misinterpretation of the biological conformation of the protein [133]. In our case, NUDT22 activity is strongly dependent on its co-factor Mg^{2+} that coordinates the two amino acids Glu189 and Glu193 [26]. The used co-crystal structure of NUDT22 for the identification of potential small molecule inhibitors does not include the co-factor Mg^{2+} , which could cause a wrong 3D conformation of the protein after protein preparation for virtual docking of our compound database. More specifically, it could also cause an inaccurate positioning of amino acids in the active site, which are involved in ligand binding. In our case, most of the TH012008 analogues formed salt bridges with both Glu189 and Glu193, which are responsible for co-factor binding and could be positioned differently in the biological form of NUDT22 causing the observed lack in activity of all compounds. Therefore, solving a novel NUDT22 co-crystal structure with both UDP-glucose and the co-factor Mg^{2+} could be of advantage for the identification of potential NUDT22 inhibitors with CADD.

In addition, computational approaches only use approximations to predict confirmations of ligands and proteins and often result in the calculation of inaccurate binding energies that cannot be translated into biochemical activity. One way to improve CADD is the inclusion of positive and negative controls of known ligands to estimate the binding, and consequently, the potential of new compounds to be suitable for hit-to-lead development. Protein 3D structures co-crystallised with established drug-like ligands tend to be more successful in identifying potential drug candidates compared to co-crystal structures with natural ligands [134]. For future studies, the use of the co-crystal structure of NUDT22 with our unpublished inhibitor A3 could lead

to better starting points for the development of novel NUDT22 inhibitors compared to the used co-crystal structure of NUDT22 and its natural ligand UDP-glucose.

Alternatively, we could exploit our developed malachite green assay in a high throughput approach to determine bioactive compounds based on already established and chemically synthesised drug-like molecules to identify novel starting points and scaffolds for the development of small molecule NUDT22 inhibitors.

In conclusion, we identified a novel starting point, the pyrimidothiophene TH012008, for the development of NUDT22 inhibitors by computer-aided drug design. However, hit-to-lead optimisation by amine coupling did not cause an increase in biochemical activity nor direct target engagement and further chemical optimisation is required for the successful development of a novel NUDT22 inhibitor series.

5. Evaluation of first-in-class NUDT22 inhibitors

5.1 Introduction

Recently, due to late stage failures in drug discovery based on a lack in molecular understanding of target modulation by small molecules on disease phenotypes, the use of highly specific chemical probes has become the preferred choice for target validation purposes [164,165]. Chemical probes can give insights into the function of genes and proteins as well as their physiological and pathophysiological roles in cell and preclinical animal models. Consequently, they are key players in both, validating potential new targets for therapeutic intervention alone or in combination with often-used gene editing techniques as well as to assess the druggability of a desired target.

To be successful in target validation with a chemical probe, considering the so-called four pillars of survival *in vitro* as well as *in vivo* was suggested to lead to a better understanding of the effects of target perturbation in relation with relevant pharmacological modulation leading to the desired disease phenotype (Fig. 14).

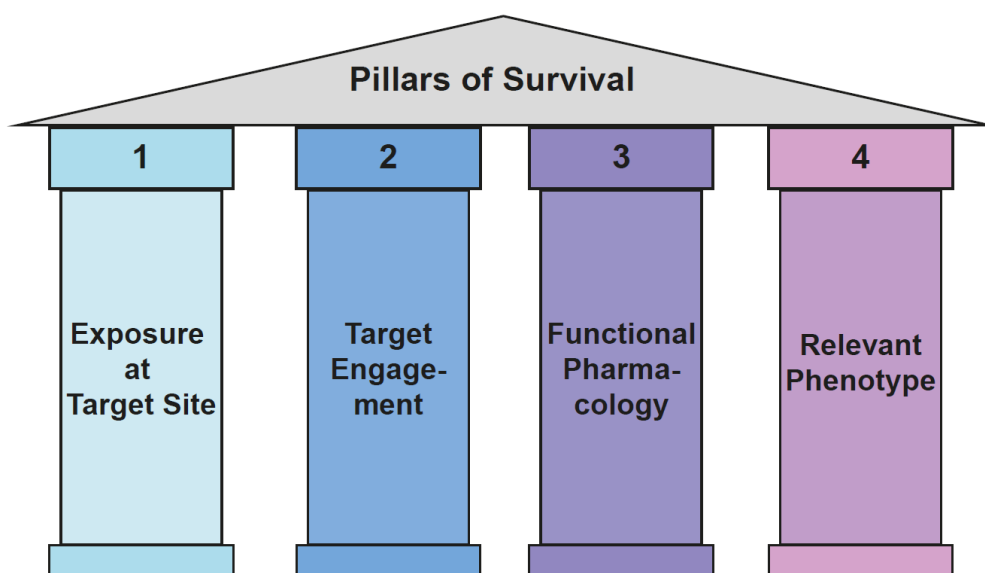


Figure 14. Four pillars of survival for target validation with a chemical probe. Pillar 1 covers the necessity of drug exposure at the target of interest. Pillar 2 includes selectivity assessment of the chemical probe in relation to target engagement, which is an important parameter for Pillar 4, the assessment of the relevant phenotype. Pillar 3 describes the assessment of functional pharmacology of a drug.

Pillar 1 describes the necessity of chemical probe exposure at the target site, which is crucial to observe a response in the selected cell or animal model. To understand on-versus off-target effects and to assess selectivity of a chemical probe, pillar 2 includes the assessment of target engagement, thereby confirming the observed phenotype upon targeting the desired protein and contributing to the interpretation of the biological function of a target. Pillars 3 and 4 cover the assessment of functional pharmacology and of specific effects of target perturbation in a relevant human disease model, which can be further supported by using patient-derived samples [166].

Subsequently, chemical probes developed for target validation purposes should be potent in biochemical assays (< 100 nM) and cellular assays (< 1 μ M) and highly selective based on demonstrated cellular target engagement. Cell permeability as well as optimal aqueous solubility for optimal drug exposure at the target site is another requirement for the successful exploitation of a chemical probe in target validation. The access to multiple chemical classes of highly selective and potent chemical probes as well as the availability of inactive probes as negative control are of advantage to confirm on-target activity [164,167].

This concept should not only be considered for the development of conventional small molecule enzyme inhibitors but also for the newer protein degrading agents such as proteolysis targeting chimera (PROTAC). PROTACs are heterobifunctional molecules that induce intracellular proteolysis through linking a small molecule protein ligand to an E3 ubiquitin ligase ligand, thereby inducing a ternary complex required for ubiquitination of the protein of interest. However, due to the often not ideal physicochemical properties such as their high lipophilic nature, higher polar surface area, molecular weight and number of rotatable bonds, PROTACs can fail to enter the cell and reach their target of interest. The utilisation of the four pillars of survival can therefore be crucial for candidate selection for both, target validation and therapeutic intervention keeping in mind the differences between protein inhibition and degradation. Similar to conventional small molecule enzyme inhibitors, PROTACs need to occupy and engage their target directly to induce the desired pharmacological response (Pillar 2). Even though PROTACs do not cause protein stabilisation, the determination of target engagement is still of necessity to avoid off-target effects and to determine target specificity. More specifically, highly specific and selective

PROTACs should engage not only the protein of interest and E3 ligase but should form a ternary complex required for ubiquitination. Different phenotypes (Pillar 4) upon protein degradation compared to protein inhibition should be considered when assessing PROTACs with the four pillars of survival model. Protein inhibition only inhibits a specific function of the protein but other potential catalytic interactions independent of the target site could still be present. On the other hand, protein degradation not only interferes with the function of a protein in downstream signalling cascades but also removes potential protein-protein interactions and other catalytic activities [168].

In comparison with protein degrading agents and gene editing techniques such as CRISPR/Cas9 or interfering RNA (RNAi), conventional enzyme inhibiting probes can be used for the functional and selective inhibition of a target protein, thereby preserving protein-protein interactions. Both, knockdown with either small hairpin RNA (shRNA) or siRNA as well as gene KO with CRISPR/Cas9 result in the complete removal of the target protein and risks the wrong interpretation of a phenotype due to multiple effects through disturbed protein complexes. However, using an allosteric inhibitor as chemical probe can also induce conformational changes in the protein structure risking the loss in essential protein-protein interaction [169].

Although the development of a chemical probe is a time- and cost-intensive process, once developed, it can be used as a more controlled approach to directly inhibit the target of interest compared to the delayed knockdown observed upon RNAi as well as the time-intensive process of generating CRISPR/Cas9 KO cell lines [169,170].

Both, gene editing with RNAi as well as CRISPR/Cas9 can result in off-target effects. Even though on-target efficacy and specificity of gene KO and knockdown can be directly evaluated on mRNA and protein level, the direct determination of potential off-target effects of either RNAi or CRISPR/Cas9 remains limited. Due to potential sequence homologies of shRNA or siRNA and physiological RNA encoding for other proteins than the target, RNAi can lead to undesired gene knockdown and the misinterpretation of an observed phenotype [169]. In contrast, the introduction of mutations, translocations, deletions or insertions at undesired genomic sites can cause off-target effects during CRISPR/Cas9 gene editing [171].

Since chemical probes are also limited by potential off-target effects, the combination with RNAi or CRISPR/Cas9 is the preferred approach to validate a novel target for therapeutic exploitation as well as to determine potential biological functions of a target gene or protein. Hence, the parallel use of several techniques can limit the risk of wrong interpretation of observed phenotypes [164,169].

In addition, chemical probes can also contribute in developing relevant biochemical and biological screening cascades for the selection of potential drug molecules in drug discovery. Consequently, the development of chemical probes targeting NUDT22 is crucial for further target validation to understand how NUDT22 can be exploited in cancer therapy. We used both structure-based and ligand-based computer-aided drug design approaches to maximise our chances for the identification of potent and selective NUDT22 inhibitors (NUDT22i). We performed a second virtual screen on an in-house chemical library comprised of approximately 8,000 compounds by targeting the UDP-glucose binding site of NUDT22. In addition, a NUDIX family selectivity panel identified Inhibitor A, which originated from our NUDT15 project, as a 19 μ M NUDT22 inhibitor and was selected for ligand-based drug discovery by structure-activity relationship (SAR) expansion. The combination of both approaches identified inhibitors A1 - A3 as potent NUDT22 inhibitors with IC_{50} s of 30, 17 and 10 nM, respectively.

5.1.1 Aims

Here, we evaluate the biochemical as well as cellular effects of inhibitors A1 - A3 as well as the chemically optimised inhibitors A4 - A6 on cell proliferation, target engagement with recombinant protein or in cell lysate and induction of DNA replication stress.

5.2 Results

5.2.1 Effect of inhibitors A1, A2 and A3 exposure on enzymatic activity and cell viability

Since all three developed NUDT22i A1, A2 and A3 were active in the previously performed optimised malachite green assay with IC_{50} s in the nanomolar range, we assessed their effects on cell viability in both, the U2OS control (ctrl) and *NUDT22* KO clones (1-2 and 3-6) by using the Resazurin assay approach (Chapter 2.6). However, none of the tested NUDT22i induced significant changes in cell viability in neither, the control nor the KO clones in the low concentration range (Fig. 15). In addition, exposure with the top concentration of 100 μ M caused only a partial reduction in cell viability. More specifically, 100 μ M of A1 and A2 reduced the percentage of viable cells to approximately 65% in all tested cell lines. In contrast to A1 and A2, the two U2OS *NUDT22* KO cell lines 1-2 and 3-6 were less sensitive towards inhibitor A3 when compared to U2OS control. Top-concentrations of A3 reduced viable cell levels to 30% in U2OS control compared to 80% in *NUDT22* KO clone 1-2. In addition, treatment with A3 did not induce any changes on cell viability in U2OS *NUDT22* KO clone 3-6 (Fig. 15).

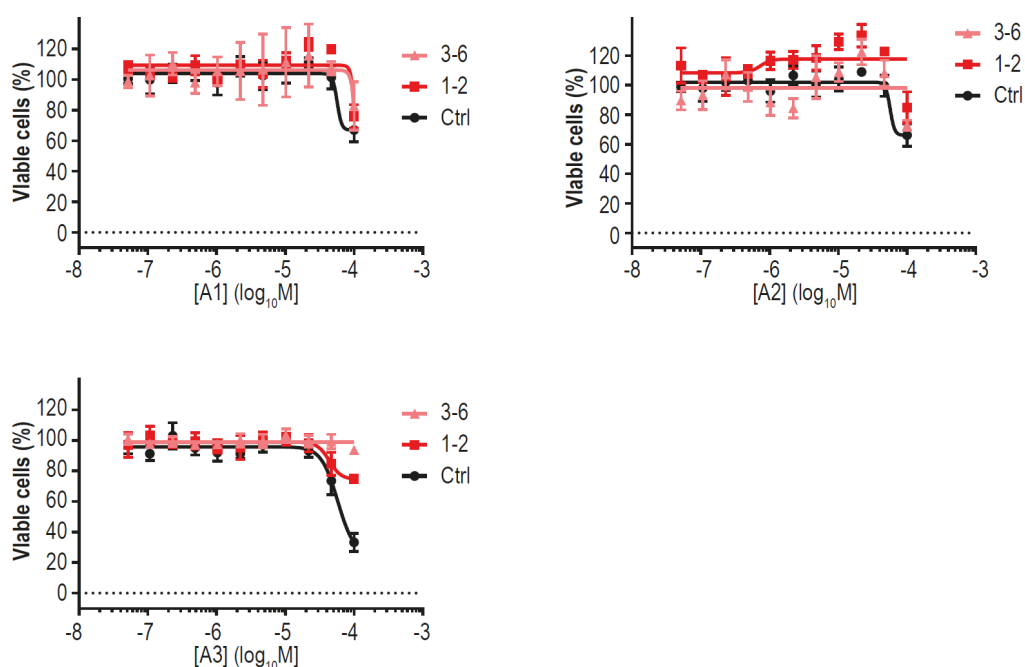


Figure 15. . Exposure with inhibitors A1, A2 and A3 reduced cell viability only at top concentrations. Changes in cell viability after exposure with A1, A2 and A3 (100 μ M – 0.05 μ M) in U2OS Ctrl and *NUDT22* KO cells for 4 days was assessed using Resazurin assay. Data are shown as means \pm standard deviation of three biological replicates and represent one of three independent experiments.

5.2.2 Target engagement of NUDT22 inhibitors A1, A2 and A3

Since treatment with all three NUDT22i only induced changes in cell viability at high concentrations, we assessed whether A1, A2 and A3 actively reach and bind their desired target NUDT22 in a cellular setting using the so-called CETSA approach in U2OS cell lysate (*Chapter 2.12.7*). CETSA can detect changes in the protein inherited melting temperature T_m , and consequently a stabilisation of the desired target upon inhibitor binding when exposed to a defined temperature gradient [127].

Since we did not use target engagement assessment to determine dose-response relationships but rather whether our developed compounds reach and stabilise their target, we chose 25 μM , a concentration 1000x higher than the biochemical determined IC_{50} s, which is sufficient for protein saturation.

After incubation with 25 μM of each NUDT22i, all three developed compounds stabilised NUDT22 protein when considering the visualised protein bands (*Fig. 7*). However, only treatment with A3 resulted in a significant shift of ΔT_m of 0.9°C and, more specifically, from 46.9 to 47.7°C ($p < 0.05$, *Fig. 7C*).

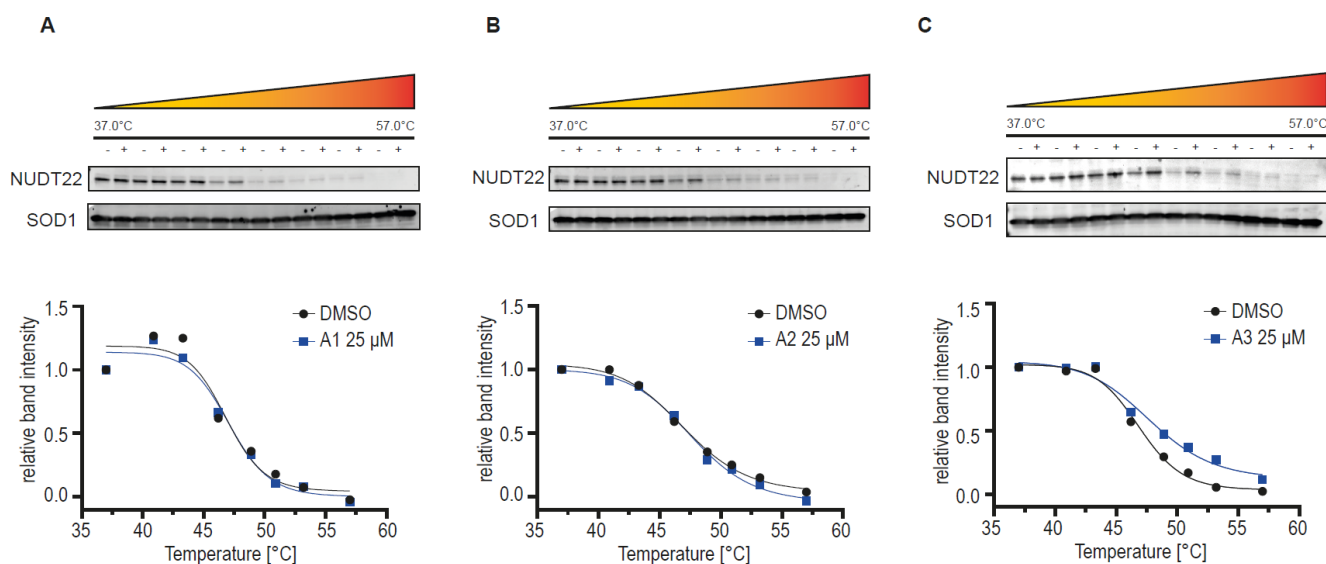


Figure 16. Inhibitor A3 stabilises NUDT22 in U2OS cell lysate. The cellular thermal shift assay (CETSA) was used to assess target engagement for A1, A2 and A3 in U2OS cell lysate. **A** Inhibitor A1 does not significantly stabilise NUDT22 ($p > 0.05$). **B** No NUDT22 stabilisation over a defined temperature gradient was observed upon treatment with inhibitor A2 ($p > 0.05$). **C** Inhibitor A3 induces a thermal shift of ΔT_m 0.8°C and engages its target directly ($*p < 0.05$). Data represents one experiment out of three individual experiments. Linear regression analysis was performed to assess statistical significance after normalisation of NUDT22 protein intensities to the loading control SOD1.

5.2.3 Dose-response evaluation of Inhibitor 4, 5 and 6

Even though A3 did only marginally impair cell viability in either, U2OS control or the two *NUDT22* KO clones in the previous used concentration range, due to its ability to stabilise *NUDT22* and therefore, directly engage its target, we proposed its further chemical optimisation performed in collaboration with Thomas Helleday at Karolinska Institute, Stockholm, Sweden. Briefly, additional chemical residues were added to the A3 scaffold resulting in an increased molecular weight, thereby proposing improved compound binding in the active site of *NUDT22*. The chemical optimisation resulted in the identification of three novel *NUDT22*i A4, A5 and A6 with improved biochemical activity and IC_{50} s of 7, 5 and 4 nM, respectively (Fig. 17).

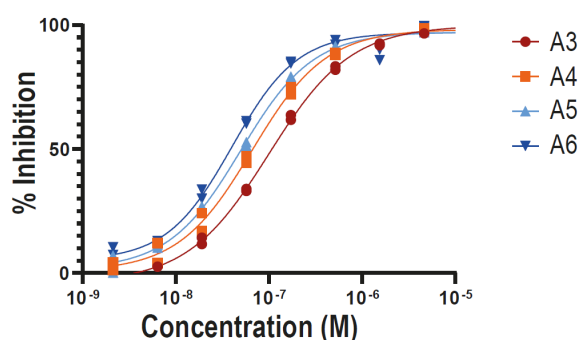


Figure 17. Inhibitors A3, A4, A5 and A6 are potent *NUDT22* inhibitors. The adapted malachite green assay (Chapter 2.11.4) was performed by Ingrid Almlöf at Karolinska Institute, Sweden and used to assess recombinant *NUDT22* protein inhibition of A3 and the chemically optimised *NUDT22* inhibitors A4, A5 and A6. Inhibitor A3 inhibits *NUDT22* at 10 nM, whereas A4, A5 and A6 have IC_{50} s of 7, 5 and 4 nM, respectively.

Further dose response analysis of the newly identified *NUDT22*i and A3 in control versus *NUDT22* KO U2OS cells, however did not cause an increase in sensitivity except at high concentrations compared to A1 and A2 (Fig. 18). The top-concentration of 100 μ M of A4 and A6 reduced viable cell levels in all three tested cell lines to 30% and 20%, respectively. In addition, a decrease in cell viability was observed starting at a concentration of 40 μ M of A3, A4 and A5 compared to the previously observed start upon a concentration of 50 μ M of A1 and A2 (Fig. 18). None of the tested cell lines was sensitive towards exposure with A5 even at top-concentrations (Fig. 18).

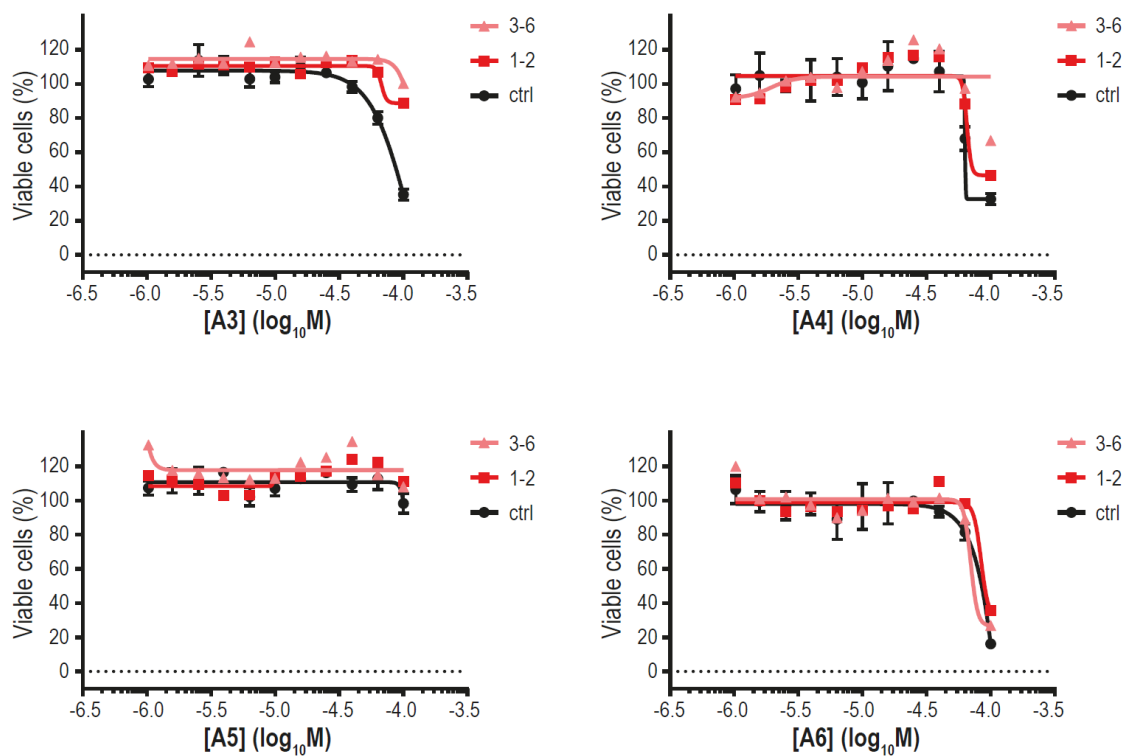


Figure 18. Effects of A3, A4, A5 and A6 on cell viability. Dose response of NUDT22 inhibitors A3, A4, A5 and A6 ($100 \mu M - 1 \mu M$) in U2OS ctrl and *NUDT22* KO clones was assessed by Resazurin assay (*Chapter 2.6*). Data represent means \pm standard deviation of three biological replicates and one of two independent experiments is shown.

5.2.4 Target engagement of NUDT22 inhibitors A3, A4, A5 and A6

To determine whether the chemically optimised NUDT22i A4, A5 and A6 bind and reach their desired target NUDT22 more efficiently than A3, two different target engagement approaches, DSF with isolated NUDT22 protein as well as CETSA in U2OS cell lysate were performed (*Chapter 2.12.6 and 2.12.7*).

Similar to the previously performed CETSA, we chose 10 μM , a concentration 1000x higher than the IC_{50} s of each compound as well as 2x the used protein concentration of 10 μM , to establish target engagement of A3, A4, A5 and A6 on protein level.

No significant differences in recombinant NUDT22 protein stabilisation were observed in between the four identified NUDT22i A3, A4, A5 and A6. All four inhibitors engaged NUDT22 and induced a significant thermal shift of ΔT_m of approximately 3°C when compared to the DMSO control (*Fig. 19A*).

To assess NUDT22 stabilisation on a cellular level, we first identified an optimal screening temperature of 48°C by assessing NUDT22 levels with SOD1 as loading control by western blot after subjecting U2OS cell lysate to a defined temperature gradient (*Fig. 19B*). All four NUDT22i, A3, A4, A5 and A6, significantly stabilised NUDT22 at 48°C in U2OS cell lysate, thereby confirming our previous findings in recombinant protein (*Fig. 19C*). The highest NUDT22 stabilisation, and therefore, protein binding was observed with 25 μM of A6, which did not induce a reduction in NUDT22 stabilisation levels compared to DMSO control at 37°C. After incubation with inhibitor A3, 75% of NUDT22 were still stabilised followed by A4, with 55% stabilised NUDT22 levels. Inhibitor A5 also engaged with NUDT22 as determined by 38% stabilised NUDT22 at 48°C. However, compared to the remaining stabilised NUDT22 levels of 27% of the DMSO control at 48°C, inhibitor A5 induced the least NUDT22 stabilisation, and consequently, has the lowest target engagement among all 4 tested NUDT22i (*Fig. 19C*).

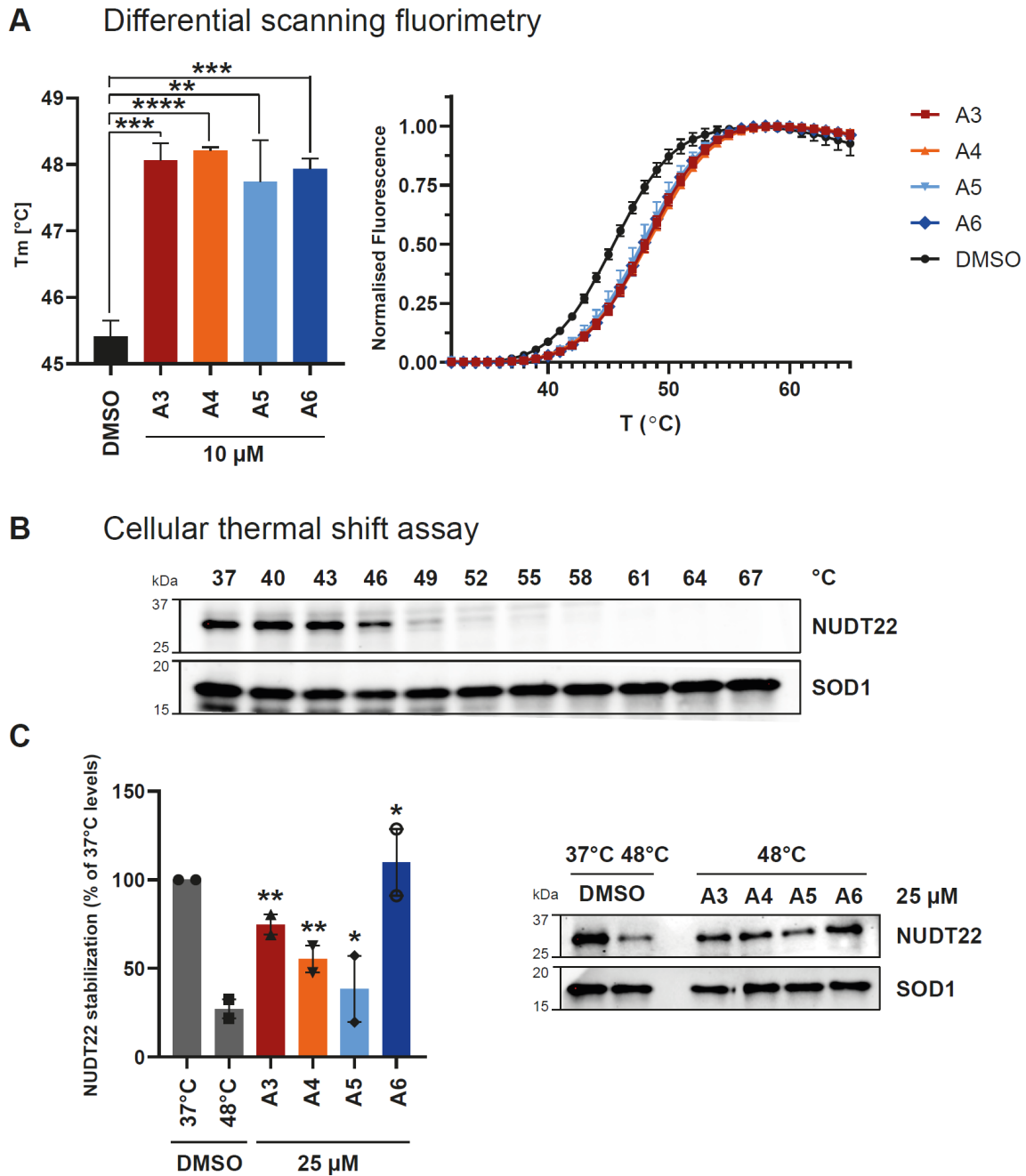


Figure 19. Inhibitor A3, A4, A5, and A6 directly engage NUDT22. **A** Thermal stabilisation of recombinant NUDT22 by NUDT22 inhibitors as determined by Differential Scanning Fluorimetry (DSF). Left, isolated NUDT22 protein was treated with 10 μ M NUDT22 inhibitors and T_m was calculated. Right, normalised fluorescence data of DMSO control versus NUDT22 inhibitors. Data are means \pm SEM of three biological replicates and represent one of three independent experiments. $**p < 0.01$, $***p < 0.001$, $****p < 0.0001$; unpaired t-test analysis. **B** Thermal melting curve to identify the ideal temperature for determining cellular target engagement of NUDT22 inhibitors in U2OS cell lysate. **C** NUDT22 stabilisation at 48°C upon NUDT22 inhibitor binding in U2OS cell lysate measured with Cellular Thermal Shift Assay (CETSA). Values are relative to NUDT22 band intensity at 37°C and normalised to the loading control SOD1. The data shown are means \pm SEM and represent $n = 2$ experiments. $*p < 0.05$, $**p < 0.01$; one-way ANOVA.

5.2.5 Inhibitor A3, A4, A5 and A6 and DNA damage

Since NUDT22 is involved in pyrimidine synthesis and we observed an increase in DNA damage upon *NUDT22* KO in the osteosarcoma cell line U2OS as well as the breast cancer cell line MCF7, we assessed whether our developed NUDT22i A3, A4, A5 and A6 would lead to DNA damage induction (*Chapter 2.12.8*).

Treatment with 10 μ M of each NUDT22i in MCF7 cells significantly increased the number of phosphorylated and therefore, activated DNA damage marker H2A.X foci compared to DMSO control γ H2A.X foci numbers per cell (**** p value < 0.001). Interestingly, cells treated with A4 experienced the highest increase in γ H2A.X foci followed by inhibitor A3. In comparison, A5 and A6 only marginally increased γ H2A.X foci indicating the least DNA damage induction (*Fig. 20A*).

Since there was only a slight increase in γ H2A.X foci upon treatment with all four NUDT22i when analysing the data based on γ H2A.X foci/cell, we re-analysed the data by first determining the average number of γ H2A.X foci in DMSO control to serve as a background level to assess DNA damage induction. Subsequently, we calculated the percentage of nuclei with > 7 γ H2A.X foci in MCF7 cells treated with A3, A4, A5 or A6 (*Fig. 20B*). Interestingly, only inhibitor A4 caused significantly more nuclei with > 7 γ H2A.X foci compared to DMSO control (** p value < 0.01).

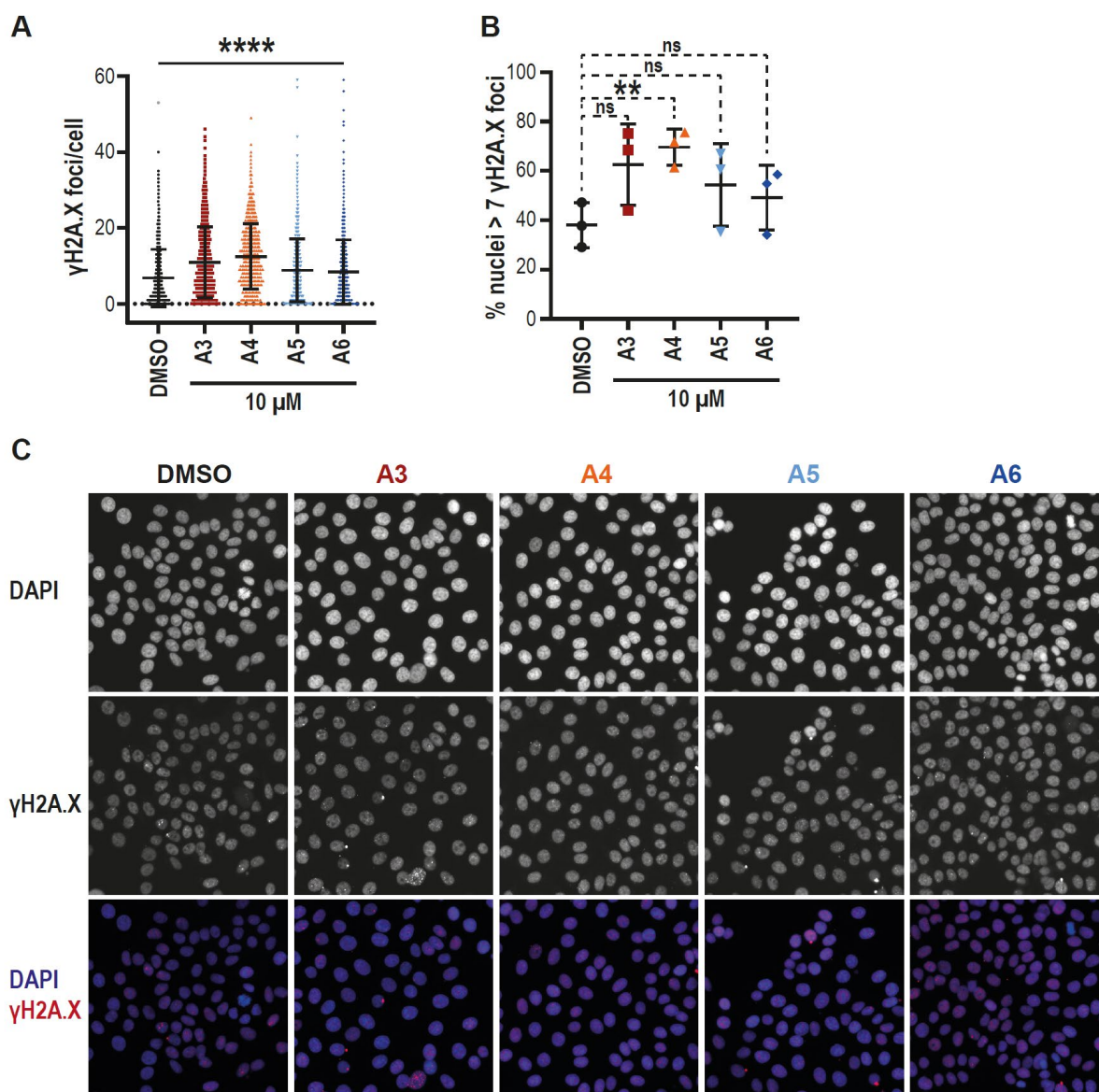


Figure 20. All four NUDT22 inhibitors induce DNA damage. **A** Treatment of MCF7 breast cancer cells with 10 μM of either A3, A4, A5 or A6 increased $\gamma\text{H2A.X}$ foci per cell. At least 1500 cells were analysed, data are means \pm SD of three biological replicates and show one of two independent experiments. Statistical significance (**** $p < 0.001$) was calculated by Mann-Whitney test. **B** Only NUDT22 inhibitor A4 increased the percentage of nuclei with > 7 $\gamma\text{H2A.X}$ foci. Average $\gamma\text{H2A.X}$ foci numbers in DMSO controls (7) served as threshold to calculate the percentage of nuclei > 7 $\gamma\text{H2A.X}$ foci after inhibitor treatment. One data point represents the % of nuclei with > 7 foci of one well and data is shown as mean \pm SD. Statistical significance (** $p < 0.01$) was calculated with unpaired t-test. **C** Example images of MCF7 DMSO ctrl or treated with each of the four NUDT22 inhibitors stained for $\gamma\text{H2A.X}$ (red) and DAPI (blue).

5.3 Discussion

The involvement of NUDT22 in a novel pyrimidine salvage pathway, which is especially important in cancer cells compared to healthy cells, suggests the potential exploitation of NUDT22 as novel anti-cancer target and the need for the development of potent chemical probes to further validate its role in cancer [164].

We identified the potent NUDT22i A1, A2 and A3 by combining structure-based and ligand-based drug design, which we evaluated based on their effects on cell proliferation and cellular target engagement. Besides their half maximal inhibitory activities (IC_{50} s) in the low nanomolar range, only A3 was identified to induce both changes in cell viability in U2OS control cells, albeit at high concentrations, as well as NUDT22 protein stabilisation in cell lysate (*Fig. 15, Fig. 16C*). Since no effect on cell proliferation was observed upon A3 treatment in *NUDT22* KO cells, we hypothesised that A3 is specific towards NUDT22 inhibition and the ideal starting point for the development of a high affinity and selective chemical probe for NUDT22 target validation.

We therefore suggested the chemical optimisation of A3 resulting in the identification of the NUDT22i A4, A5 and A6 with improved activity towards recombinant NUDT22 protein inhibition (*Fig. 17*). Even though all four inhibitors still inherit the chemical scaffold of A3 and we hypothesised to have improved their activity in cell models, no major changes in cell viability were observed after treatment with any of the three optimised inhibitors (*Fig. 18*). Surprisingly, A5 did not induce any changes in cell viability besides its similarities in biochemical activity as well as chemical structure compared to the other four NUDT22i (*Fig. 18*). Since *NUDT22* KO in U2OS and MCF7 cells did not induce cell death but a reduction in cell proliferation (*Chapter 3, Fig. 4H and Supplementary Fig. 4A*), we did not expect to induce cell death upon treatment with our NUDT22i after 4 days. Moreover, if our developed inhibitors were directly targeting NUDT22, we would expect to see a decrease in cell viability in control cells to similar levels compared to *NUDT22* KO cells upon inhibitor treatment. However, the observed differences in sensitivities towards NUDT22 inhibition in control and the KO cell lines could be due to potential metabolic adaptations in response to *NUDT22* KO, which could lead to different phenotypes and, therefore, sensitivities compared to the control cells.

To determine whether the lack in sensitivity, except at high concentrations for A4 and A6, and lack in response for the NUDT22i A5 could be due to a decrease in target engagement, we assessed the ability of our compounds to stabilise NUDT22 in the biophysical DSF approach utilising recombinant NUDT22 protein as well as in CETSA in cell lysate. Target engagement assessment has been introduced in drug discovery only recently and is considered a valuable strategy for lead identification and optimisation purposes for the development of high quality and effective drug compounds [172]. Here, A3, A4, A5 and A6 stabilised recombinant NUDT22 protein and therefore, directly engaged NUDT22 in the protein-based DSF assay in a comparable manner recapitulating the similarities in biochemical inhibitory activity towards recombinant NUDT22 protein (*Fig. 19A, B*). However, these findings could not be translated into cellular target engagement. CETSA in U2OS cell lysate identified A6 as strongest NUDT22 stabilising agent followed by A3 and A4. Inhibitor A5 stabilised NUDT22 only marginally compared to DMSO control, which could be a reason for the observed lack in sensitivity in the cellular dose response experiments (*Fig. 19C*).

Our proposed mode of action to induce DNA damage via NUDT22 inhibition involves nucleotide synthesis disruption followed by DNA replication stress and DNA damage induction as observed upon *NUDT22* KO especially in cancer cells (*Chapter 3*). Even though at relatively high concentrations, all four NUDT22i, A3, A4, A5 and A6, induced DNA damage in MCF7 breast cancer cells with inhibitor A4 as most potent compound when considering the number of foci per nuclei (*Fig. 20A*). However, only treatment with inhibitor A4 resulted in a statistically significant increased percentage of nuclei with more than average γ H2A.X foci levels of DMSO control cells (*Fig. 20B*). Therefore, it is unsure whether NUDT22i A3, A5 or A6 are able to induce DNA damage and further experiments are required to confirm the observed increase in γ H2A.X foci numbers upon NUDT22i exposure (*Fig. 20*). Assessing DNA damage induction upon NUDT22 inhibition with our developed inhibitors should also be performed in MCF7 *NUDT22* KO cells to preclude potential off-target effects as main reason for the observed increase in γ H2A.X foci and therefore, DNA damage.

Nonetheless, we did not determine whether our developed NUDT22i actively engage NUDT22 in live cells. Accordingly, we cannot conclude whether the observed effects

on cell proliferation and DNA damage induction are results from direct targeting of NUDT22 or due to off-target effects. Consequently, further target engagement assessment in live cells has to be performed to confirm the successful development of selective NUDT22 targeting agents.

Since our previous studies showed some activity towards the hydrolysis of both UDP-glucose and -galactose upon high concentrations of the NUDIX family member NUDT5, we should also assess target specificity of our compounds in a NUDIX selectivity panel [26]. Even though the protein structure of NUDT22 differs from the structures of other NUDIX protein family members through an additional N-terminal fold required for substrate, especially interactions with NUDT15 should be ruled out due to the use of Inhibitor A, which was previously identified to inhibit NUDT15, as starting point for the development of our NUDT22 inhibitor series [26].

In conclusion, we identified inhibitor A3 followed by A4 and A6 as potential chemical probes to proceed with the validation of NUDT22 as anti-cancer target. However, further research is required to assess the cellular activity as well as selectivity of our developed compounds towards NUDT22.

6. General discussion

Even though targeting nucleotide synthesis and the DNA damage response has remained the backbone of cancer therapy for several decades; the identification of new targets is crucial to overcome limitations. These include a lack in efficacy, side effects and resistances often observed in cancer patients receiving dNTP synthesis interfering and therefore, DNA replication stress inducing agents [128]. Our previously performed work identified a distinct UDP-glucose hydrolase activity for NUDT22 resulting in the generation of both, the pyrimidine precursor UMP and G1P, an important intermediate in energy metabolism and biomass generation through glycolysis and the TCA cycle [26]. Since NUDT22 gene expression alterations are present in several cancers, we hypothesised a potential role of NUDT22 in cancer. However, neither the biological function of NUDT22 nor its genomic regulation has been identified previously [4,26].

In this work, we investigated the role of NUDT22 in pyrimidine synthesis and its transcriptional regulation in cancer and non-cancer cell models followed by the characterisation of NUDT22 as potential anti-cancer target in breast cancer cell and xenograft models. The second part of our work focused on the identification, development and enzymatic and cellular evaluation of chemical probes for further target validation as well as for subsequent exploitation as potential anti-cancer agents through virtual screens on our previously solved co-crystal structure of NUDT22 and its substrate UDP-glucose.

6.1 Transcriptional regulation of *NUDT22* by p53 in cancer

The first aim of this work was to determine how *NUDT22* expression is regulated in cancer and non-cancer cells. We observed an increase in *NUDT22* gene expression upon cellular stress induced by either glucose starvation, glycolysis inhibition or the overexpression of the oncogene cMYC (*Chapter 3, Fig. 1*). However, no increase in *NUDT22* gene expression was observed upon overexpression with the two oncogenes *CCNE* and *HRAS*, which are both known to be involved in DNA replication stress induction in cancer cells suggesting that *NUDT22* gene regulation is not dependent on oncogenic stress *per se* (*Chapter 3 Supplementary Fig. 1A, B*). We identified the direct regulation of NUDT22 through p53 and, moreover, a p53-mediated positive feedback loop regulating *NUDT22* gene expression upon induction of metabolic stress, which

was exclusively present in the two *NUDT22* KO osteosarcoma (U2OS) clones but not in hTERT-RPE1 fibroblasts (*Chapter 3, Fig. 2, 3 and Supplementary Fig. 2*).

Conversely, *NUDT22* was expressed in the p53-deficient cell line HCT116 suggesting additional inputs regulating *NUDT22* expression, which remain to be identified (*Chapter 3 Supplementary Fig. 2F*). Based on eukaryotic promoter database search (epd.epfl.ch), we identified the hypoxia-inducible factor 1- α (HIF1 α) as one potential candidate to be involved in transcriptional *NUDT22* regulation. HIF1 α is an important adaptive regulator in response to hypoxia, thereby inducing the transcriptional modulation of multiple key metabolic pathways such as glycolysis and the TCA cycle to overcome reduced oxygen levels and maintain sufficient ATP production [173]. Moreover, the potential role of *NUDT22* in both glycolysis as well as TCA and OXPHOS regulation through the production of G1P strengthen the potential regulation of *NUDT22* expression by HIF1 α in response to oxidative stress, which has to be investigated further.

However, the transcriptional regulation of *NUDT22* by p53 upon metabolic stress has to be further determined to consider the exploitation of *NUDT22* as anti-cancer target in the future. *TP53* is the most frequent mutated tumour suppressor leading to either gain-of-function or loss-of-function mutations in more than 50% of cancer [75,174]. Thus far, we limited our mechanistic studies to the two cancer cell lines with wild-type p53, U2OS and MCF7, to generate *NUDT22* KO clones to exclude the p53 mutational status from the initial characterisation of the biological function of *NUDT22*. It was recently shown that mutant P53 (mtP53) regulates nucleotide pool levels to maintain cancer cell proliferation by inducing a switch towards nucleoside salvage through dCK upregulation in several mtp53 breast cancer cell lines [175]. Since *NUDT22* is involved in nucleotide synthesis, and more specifically, pyrimidine synthesis, it is important to further assess the effects of different p53 mutations on the expression and biological activity of *NUDT22* in a larger number of cell models including cell lines with either P53 gain-of-function or loss-of-function mutations. If we observe different responses of cell lines based on p53-status, the mutational status of p53 could then be used as a potential biomarker to stratify patient populations that will be responsive and benefit from targeting *NUDT22*.

6.2 Biological function of NUDT22 in cancer versus non-cancer cell lines

Since our previously performed biochemical studies suggested the generation of the pyrimidine precursor UMP upon hydrolysis of UDP-glucose catalysed by NUDT22, the next part of our work aimed at the identification of the biological function of NUDT22 in nucleotide synthesis and DNA replication in cancer and non-cancer cells [26].

NUDT22 KO in the osteosarcoma cell line U2OS but not in the non-cancer fibroblasts hTERT-RPE-1 reduced both purine and pyrimidine pool levels, which was reflected by reduced DNA replication fork speed and reduced cell proliferation. DNA replication fork speed could be restored through uridine supplementation, thereby rescuing pyrimidine synthesis via the direct production of UMP (*Chapter 3, Fig. 4*). Together with the observed synergy between glutamine starvation and *NUDT22* KO in U2OS cells, we propose the role of NUDT22 in pyrimidine synthesis and the discovery of a novel pyrimidine salvage pathway independent of *de novo* synthesis to maintain DNA replication and repair (*Fig. 21*). Whereas the purine salvage pathway mediated by *HRPT* has been described extensively and is already exploited in cancer therapy, no real pyrimidine salvage pathway besides the re-phosphorylation of extracellular derived pyrimidines has been described to date underlining the importance of our discovery [117,176].

An internal standard calibration consisting of the three nucleotides ATP, GTP, and UTP was used to assess changes in nucleotide levels upon *NUDT22* KO. Consequently, CTP and TTP levels were predicted based on biological abundances in relation to the directly detected concentrations of ATP, GTP and UTP. Another quantitative method for the direct detection of changes in pyrimidine levels upon *NUDT22* KO could be beneficial to confirm our observed findings as well as the proposed role of NUDT22 in pyrimidine salvage. One proposed method could be the combination of enzymatic and click reactions for the specific quantification of all four canonical dNTPs (dATP, dTTP, dGTP, and dCTP) in microplate format. More specifically, dNTP-specific oligonucleotide templates are pre-annealed with a biotin-labelled primer sequence. They are then added to the corresponding sample together with DNA polymerase and an excess amount of either 5-ethynyl-dUTP or C8-alkyne-dCTP, which is specific for dTTP quantification. During the following DNA polymerase

reaction, the specific oligonucleotide template-predefined amount of molecules of alkyne-modified dNTPs is incorporated per molecule of incorporated dNTP. After pulldown of the oligonucleotides and removal of the template, the biotin-labelled strands with incorporated 5-ethynyl-dUTP or C8-alkyne-dCTP are conjugated to an azide-fluorophore probe via click chemistry and the fluorescence intensity can be measured using a plate reader. Consequently, due to the specific templates for each canonical dNTP, the concentration of dATP, dTTP, dGTP and dCTP can be quantified in relation to alkyne-modified dNTP incorporation [177].

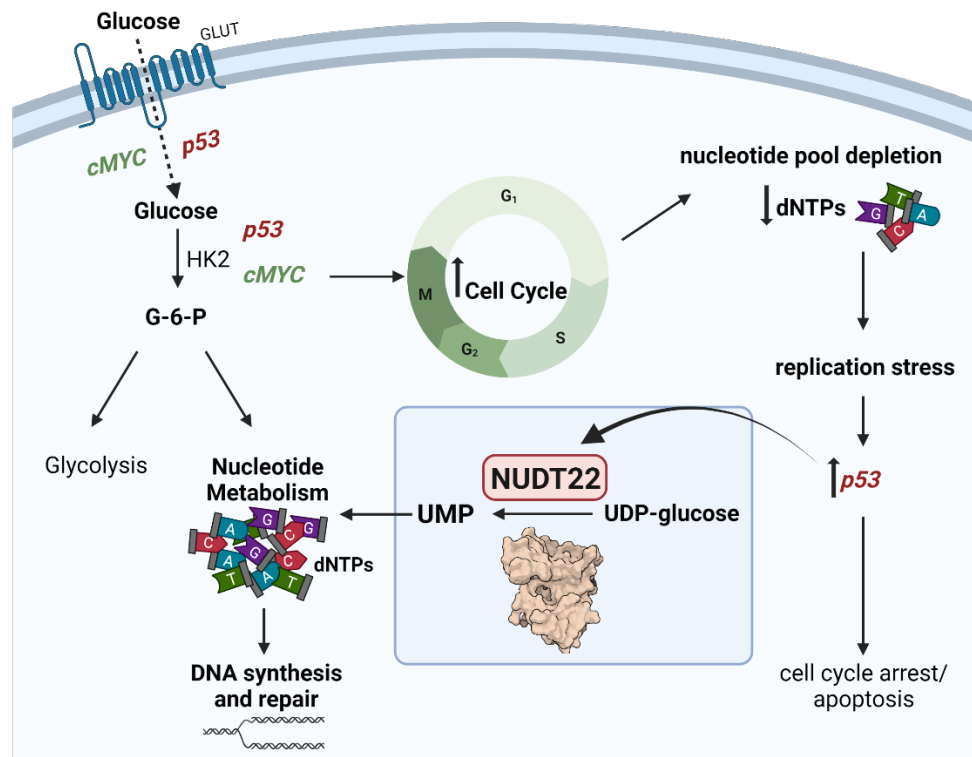


Figure 21. NUDT22 mediates a novel pyrimidine salvage pathway. In healthy cells, glucose transporters (GLUT) are responsible for the uptake of glucose into the cell, which is further phosphorylated to glucose 6-phosphate (G6P) by hexokinase 2 (HK2) and regulated by both cMYC and p53. G6P can directly enter glycolysis or synthesise nucleotides via the pentose phosphate pathway (PPP) for DNA synthesis and repair. Upon glucose starvation or in response to cellular stress, p53 activates cMYC resulting in an upregulation in cell cycle progression followed by nucleotide depletion and replication stress induction. Replication stress induces p53, which in turn promotes either cell cycle arrest and apoptosis or NUDT22 upregulation. NUDT22 then hydrolyses UDP-glucose to UMP to maintain nucleotide synthesis and DNA synthesis and repair.

Nevertheless, we observed DNA replication stress and damage induction, activation of cell cycle checkpoint kinases as well as a delay in S phase progression upon *NUDT22* KO in both, U2OS osteosarcoma and MCF7 breast cancer cells (*Chapter 3, Fig. 6; 7D, E, F*). Since a disruption in nucleotide synthesis or changes in nucleotide pool levels are both intrinsic factors contributing to DNA replication fork stalling, and consequently, cell cycle arrest, our observed findings further endorse the role of *NUDT22* to maintain pyrimidine levels for DNA replication and cell proliferation.

Although *NUDT22* KO decreased both purine and pyrimidine levels, we only observed an increase in sensitivity of U2OS *NUDT22* KO cells towards anti-cancer agents interfering with pyrimidine *de novo* but not purine synthesis (*Chapter 3, Fig. 5 A-E, 7 H-J, Supplementary Fig. 3C, D*). Nevertheless, a potential impact of *NUDT22* KO on purine synthesis cannot be ruled out based on the second, *NUDT22*-mediated, UDP-glucose hydrolase product G1P. G1P is the precursor of G6P, an important metabolite for both purine and pyrimidine synthesis via the PPP.

Cancer cells often experience changes in metabolism through deregulated glucose and amino acid uptake as well as changes in glycolysis and TCA cycle regulation to maintain cancer cell proliferation and survival. Similar to the DNA replication stress and DNA damage response, targeting these metabolic pathway alterations provides a promising strategy in cancer therapy [37]. G1P to G6P conversion catalysed by PGM was proposed as requirement in cancer cells to maintain cell proliferation in response to nutritional stress such as changes in glucose levels [178]. Since G6P is an important metabolite in glycolysis and therefore, energy and biomass generation, *NUDT22* might play an important role in other metabolic pathways [29]. We identified, in fact, increased *NUDT22* levels upon the inhibition as well as depletion of hexokinase 2 (HK2), which is required for glucose phosphorylation in the first step of glycolysis (*Chapter 3, Fig. 1B, C*) [29,32]. However, this work did not involve establishing the importance of G1P derived from *NUDT22*-mediated UDP-glucose hydrolase in glycolysis and other metabolic pathways such as the TCA cycle.

In addition, besides its role in glycogen synthesis and glycosylation, the biological significance of UDP-glucose in both nucleotide synthesis and energy metabolism has yet to be determined. Stable isotope labelling in combination with liquid chromatography – mass spectrometry (LC-MS) to determine metabolic flux could be

exploited to understand the importance of UDP-glucose hydrolysis via NUDT22 in cancer versus non-cancer cells [179].

Furthermore, UDP-glucose has been linked to metastatic progression in lung cancer cells through interference with translation of the epithelial-mesenchymal transition (EMT) factor *SNAI1* as well as in breast cancer mouse models upon knockout of UDP-glucose 6-dehydrogenase (UGDH) [180,181]. In contrast, a reduced synthesis in UDP-glucose through UDP-glucose pyrophosphorylase 2 (UGP2) depletion and consequently reduced glycogen synthesis has shown to be beneficial in PDAC cell and xenograft models [182]. However, NUDT22 inhibition, thereby impairing downstream processes from UDP-glucose could still be beneficial in cancer and, especially for the suppression of tumour metastasis, which has to be further investigated in cancer cell and xenograft models.

To establish the biological function of NUDT22 in cancer and non-cancer, we used CRISPR/Cas9 to create *NUDT22* knockout in cancer and non-cancer cells. Even though CRISPR/Cas9 is well established and routinely used in basic research, off-target effects through Cas9-mediated DNA cleavage at unspecific sites can cause the introduction of mutations at unwanted genomic loci [171]. Off-target effects can also be introduced through translocations, deletions or inversions, which can lead to chromosomal rearrangements [183]. Nevertheless, the risk of unwanted off-target effects decreases with the quality of the designed single guided RNA (sgRNA) as well as the use of multiple sgRNA's, thereby observing similar phenotypes [184]. For the generation of our *NUDT22* KO clones in U2OS, hTERT-RPE1 and MCF7, we used several different sgRNA's that were designed to target the first exon to disrupt the gene early on and used a non-targeting sgRNA in each cell line as negative control. We assessed on-target specificity by confirming the KO with PCR and western blotting followed by Sanger sequencing to verify that the intended region had been deleted. Although we observed a similar response upon *NUDT22* KO in U2OS as well as MCF7 cells compared to both control cell lines, we cannot exclude the potential risk of off-target effects at other sites than the target gene. Off-target effects can be assessed by performing a rescue experiment of the KO. More specifically, KO cells are transfected with a wild-type plasmid and phenotypic rescue/reversal is assessed. To study the significance of the enzymatic function for the observed phenotype, a catalytic

dead rescue construct with point mutations encoding for amino acids that are necessary for enzymatic activity, can be design and transfected.

We see similar effects on cell proliferation and DNA replication fork speed, ssDNA as well as DNA damage accumulation, and an increase in sensitivity towards pyrimidine *de novo* synthesis inhibition upon *NUDT22* KO in the two cancer cell lines U2OS and MCF7 with a total of 5 different sgRNA's. In contrast, the non-cancer cell line hTERT-RPE1 seems to be less affected by a loss in UMP synthesis via *NUDT22* suggesting a difference in *NUDT22* dependency in different cell lines. Since we also observed an increase in *NUDT22* expression in cancer compared to normal tissues, the higher dependency on *NUDT22* in cancer cells could be attributed to a higher demand of metabolites, and, more specifically, nucleotides to maintain DNA replication in fast proliferating cancer cells. This however, has to be further evaluated in a bigger subset of cancer and non-cancer cell lines based on either *NUDT22* KO or after the successful development of a highly specific and active chemical probe. In case we can confirm a higher dependency towards *NUDT22*-mediated pyrimidine salvage in cancer cells, selective targeting of *NUDT22* could be a promising new strategy in cancer with limited effects in healthy tissue.

6.3 *NUDT22* as target in breast cancer

Pyrimidine *de novo* synthesis remains a frequently exploited target in cancer therapy besides often observed limitations such as side effects, resistance and lack in efficacy partly caused by the switch of cancer cells towards the more energy efficient pyrimidine salvage pathways. Accordingly, co-targeting pyrimidine *de novo* synthesis as well as pyrimidine salvage kinases was proposed to improve response rates in cancer patients [128]. Due to the discovery of a novel pyrimidine salvage pathway mediated by *NUDT22* in combination with the observed increase in sensitivity towards pyrimidine *de novo* synthesis inhibition in *NUDT22* KO cancer cells, we evaluated the suitability of *NUDT22* as anti-cancer target as well as the co-targeting of *NUDT22* and pyrimidine *de novo* synthesis in this part of the work.

Based on the observed increase in *NUDT22* expression in breast cancer versus healthy tissue as well as a decrease in overall survival in breast cancer patients with altered *NUDT22* levels, we focussed on the evaluation of *NUDT22* as potential breast cancer target (*Chapter 3, Fig. 7B, C*). Similar to the increase in *NUDT22* levels, we

also observed an increase in gene expression levels of other enzymes involved in pyrimidine synthesis (*Chapter 3, Fig. 7B*). Even though gene expression alterations do not necessarily translate into changes in activity or dependency of the corresponding protein, the general increase in the expression of key players in pyrimidine synthesis could, however support our hypothesis to co-target pyrimidine *de novo* synthesis and salvage in breast cancer.

In addition to the increased sensitivity towards pyrimidine *de novo* synthesis inhibition, we observed a further increase in DNA damage induction upon dihydroorotate dehydrogenase (DHODH) and uridine monophosphate synthetase (UMPS) inhibition in *NUDT22* KO MCF7 cells (*Chapter 3, Fig. 7G, H-J*). Low doses of pyrazofurin in *NUDT22* KO MCF7 cells induced an additional delay in S phase progression and supports our hypothesis that *NUDT22* is not only involved in a novel pyrimidine salvage pathway, but can also be targeted to improve the efficacy of pyrimidine *de novo* synthesis inhibition in breast cancer (*Chapter 3, Fig. 7E*).

To translate our *in vitro* findings into an *in vivo* model with functional tumour microenvironment and the access to biological concentrations of nutrients, we performed a MCF7 xenograft study with our previously engineered *NUDT22* KO and control cells. Initially, we had planned to include the treatment with either pyrazofurin or brequinar to observe effects on tumour growth upon co-targeting pyrimidine salvage and *de novo* synthesis *in vivo*. Due to the slow growth rate observed especially in *NUDT22* KO tumours, we were only able to measure the tumour growth over 6 weeks without including additional treatment with either of the inhibitors. However, we can conclude that based on the slower growth rates of tumours with *NUDT22* KO MCF7 cells, *NUDT22* is required for cancer cell growth *in vivo*, which provides a clear rationale for the preclinical translation of *NUDT22* in cancer (*Chapter 3, Fig. 7K*). Additional *in vivo* studies are required to confirm the increase in sensitivity of pyrimidine *de novo* synthesis upon *NUDT22* KO by carefully selecting additional cancer cell models to assess tumour growth and overall survival.

We selected the estrogen (ER) and progesterone receptor (PR) positive breast cancer cell line MCF7 to determine the suitability of *NUDT22* as target in breast cancer without consideration of the effect of hormone receptors or human epidermal growth factor receptor 2 (HER2) status on overall survival in breast cancer patients with altered

NUDT22 expression levels. Further gene expression database analysis should be performed to select breast cancer subsets, which are especially dependent on *NUDT22* for survival.

Since *NUDT22* expression is elevated in cancer in general, we propose the exploration of a wider cancer cell panel to assess the effects of either CRISPR/Cas9 *NUDT22* KO or *NUDT22* inhibition with a chemical probe to clarify the suitability of targeting *NUDT22* in additional cancer tissues.

6.4 Identification of first-in-class NUDT22 inhibitors to be used as chemical probes

Our work has demonstrated the suitability of NUDT22 as cancer target based on our *in vitro* and *in vivo* findings using CRISPR/Cas9 KO to assess the roles of NUDT22 in pyrimidine synthesis. However, due to the limitations of gene editing, in the next part of this work, we aimed at the development of a chemical probe targeting NUDT22 for further target validation as well as the potential use in anti-cancer therapy in the future (*Chapter 4, 5*).

We identified two individual NUDT22 inhibitor series starting from two independent compound libraries by performing virtual screens on our previously identified co-crystal structure of NUDT22 and its substrate UDP-glucose (5LOR.pdb). We used the open access NCI/DTP compound database consisting of more than 200,000 molecules, which we filtered based on different parameters such as the compound size to avoid larger molecules to enable further chemical optimisation and, thereby risking low binding affinities translating to lower activity in enzymatic assays for a fragment-based virtual screen (*Chapter 4*). Conversely, we used Inhibitor A with an IC_{50} of 19 μ M towards recombinant NUDT22 protein, as starting point for a ligand-based virtual screen in combination with a structure-based screen on an in-house chemical library for the development of the second inhibitor series (*Chapter 5*).

Comparing the enzymatic activity with IC_{50} s > 625 μ M of the two active hits, TH012006 and TH012008, identified in the first virtual screen with Inhibitor A explains the higher likelihood of failure to identify active compounds after chemical optimisation of TH012008 compared to the second inhibitor series. The availability of a potent probe to establish SAR for the development of new inhibitors with CADD has been exploited extensively and is the method of choice especially in hit and lead optimisation steps in drug discovery [134,185]. To identify the second NUDT22i series, we could assess the link between the chemical structure, the calculated binding affinity as well as biochemical activity, the so-called SAR, of inhibitor A to predict the activity of compounds identified in the structure-based screen on the in-house chemical library. In addition, we could also exploit SAR expansion to predict the effects of the exchange of chemical entities in or the addition of chemical groups to the chemical structure of

Inhibitor A on the biochemical activity leading to the identification of inhibitors A1, A2 and A3 with low nanomolar activity towards recombinant NUDT22 inhibition.

The proposed chemical optimisation of TH012008 through amide coupling did not result in improved biochemical activity besides improved binding affinity and LE calculated in the docking screen compared to TH012008. Since TH012008 is a relatively small molecule (210 Da) with low biochemical activity ($> 625 \mu\text{M}$), coupling of amines with AMW of 100 – 200 Da and TH12008 generated compounds with nearly double the molecular weight of the initial hit making SAR predictions not as effective in comparison to the ligand-based screen for the second NUDT22 inhibitor series.

Due to the missing biochemical activity confirmed by a lack in target engagement of the optimised TH012008 inhibitor series, we limited further evaluation on effects in cancer cells as well as target engagement with recombinant protein and in cell lysate to the second NUDT22i series (*Chapter 5*).

Even though all six identified NUDT22i, A1, A2, A3, A4, A5 and A6 have IC_{50}s in the low nanomolar range, effects on cell viability were missing (A1, A2, A5) or could only be observed upon exposure to the top concentrations of each inhibitor. One could argue that the relatively low effects on cell viability observed upon treatment with all compounds could be due to the unsuccessful uptake of the inhibitors into the cell, thereby not engaging with their target of interest. This might be the case for A1 and A2, which failed to stabilise NUDT22 upon a defined temperature gradient in cell lysate (*Fig. 16A, B*). Since we did not assess target engagement in live cells, we cannot confirm that our developed inhibitors are able to reach their target inside cancer cells. However, we did observe a significant but mild increase in $\gamma\text{H2A.X}$ and therefore, DNA damage upon treatment with all four NUDT22i, but especially with A4 (*Fig. 20*). We also observed DNA damage induction upon *NUDT22* KO in MCF7 cells suggesting that our inhibitors reach NUDT22 and consequently, reduce pyrimidine levels leading to DNA replication stress and damage. To confirm our findings, it would be interesting to determine the effects of NUDT22 inhibition with A3, A4, A5 and A6 on ssDNA induction, DNA replication fork speed as well as cell cycle progression.

In addition, as described in *Chapter 3*, *NUDT22* KO did not induce cancer cell death but reduced cell proliferation as well as tumour growth *in vitro* and *in vivo*.

Consequently, we were not surprised to observe no significant changes on cell viability upon treatment with our developed inhibitors, except at very high concentrations. The effects of *NUDT22* KO on cell proliferation and tumour growth could also indicate that *NUDT22* inhibition induces cytostatic rather than cytotoxic effects. In contrast to cytotoxic agents, cytostatic agents inhibit tumour growth through interfering with mechanisms required for successful cell division without inducing direct cell death and are therefore less prone to side effects such as toxicities on healthy cells [186]. Currently, several targeted therapies are being developed with suggested cytostatic effects to be used for disease maintenance and to prevent metastasis formation. However, cytotoxic effects cannot be ruled out completely as agents often act through both cytostatic and cytotoxic mechanisms depending on dose and exposure times. To establish whether novel compounds act through cytostatic or cytotoxic mechanism choosing the right *in vitro* and *in vivo* assays by assessing a wide range of concentrations, doses and exposure times is crucial [186].

In our performed growth curve experiments, we observed a reduction in cell proliferation speed upon *NUDT22* KO after 4 days (*Chapter 3, Fig. 4A and Supplementary Fig. 4A*). Hence, we suggest to either repeat our performed drug exposure experiments over a longer period of time or assess the effect of inhibitor A3, A4, A5 and A6 on cell viability in another approach such as the colony formation assay. The colony formation assay or also known as clonogenic assay assesses the effects on drug exposure on cell survival upon the ability of single cells to grow into a colony of more than 50 cells over an incubation period of one to three weeks and could therefore be an important asset for cellular evaluation of our *NUDT22i* [187].

In *Chapter 3*, we propose the co-targeting of *NUDT22* and pyrimidine *de novo* synthesis with already established antimetabolites due to the observed increase in sensitivity towards pyrimidine *de novo* synthesis inhibition upon *NUDT22* KO in the osteosarcoma as well as breast cancer cell line (*Chapter 3, Fig. 5A-E, 7H-J*). To validate the suitability of our developed *NUDT22i* A3, A4, A5 and A6 as chemical probes for further target validation and potential anti-cancer agents, we propose to combine our inhibitors with pyrimidine *de novo* synthesis interfering agents to recapitulate previous observed changes in cell viability and DNA replication stress and damage induction upon *NUDT22* KO.

One of the major limitations of our developed NUDT22i is the lack in demonstrated selectivity. Even though we confirmed target engagement of A3, A4, A5 and A6 with recombinant NUDT22 protein as well as in cell lysate, we have not demonstrated whether our compounds reach their target in live cells. Besides the proposed NUDIX selectivity panel in *Chapter 5*, other approaches are necessary to confirm high selectivity of our compounds towards NUDT22 in enzymatic as well as cellular assays. In *Chapter 6.2* discussed generation of NUDT22 kinase dead mutants with altered amino acids in the active site, thereby preventing UDP-glucose binding but retaining the protein conformation and its potential participation in protein complexes could also be of benefit for selectivity assessment of our developed NUDT22i. These mutants could be exploited to simulate inhibitor binding and therefore assessing changes on cell viability, DNA replication stress and damage induction, DNA replication fork speed and cell cycle progression alone or in combination with agents targeting pyrimidine synthesis. Nevertheless, it would be interesting to determine whether exposure with our developed probes would cause any effects, more specifically off-target effects, in these kinase dead mutants.

Moreover, if we can confirm cellular activity as well as target engagement in live cells, we could perform trans-proteomic profiling (TPP) by combining CETSA with LC-MS to detect the interactions of our chemical probe with NUDT22 as well as potential off-target binding. This would provide important insights towards the safety of our compounds for future use in preclinical and clinical development. The use of CETSA-MS and an active and selective chemical probe can also give insights into drug-induced stress responses as well as drug metabolism [188]. With the development of an active and highly selective chemical probe, we could therefore exploit CETSA-MS to uncover the role of NUDT22 in cancer and non-cancer cell metabolism for target validation.

Overall, in this chapter we provide three compounds, A3, A4 and A6, with the potential to be exploited as chemical probes for further validation of NUDT22. However, additional biological evaluation has to be performed to fully uncover the specificity as well as activity of our developed compounds in cancer and non-cancer cells. The successful development of a chemical probe provides a future asset for cancer therapy

especially in cancers with high dependencies on nucleoside salvage and glycolysis for cancer progression.

7. Conclusion and future perspectives

This thesis explored the biological function and significance of NUDT22 in nucleotide synthesis and its potential to be exploited as novel anti-cancer target with a focus on breast cancer. We identified a novel, p53-regulated, pyrimidine salvage pathway mediated by NUDT22 for DNA replication stress prevention and cancer cell survival. Cancer cells have been shown to switch to nucleoside salvage pathways to escape nucleotide *de novo* synthesis inhibition by standard-of-care cancer therapy. This work describes novel co-targeting strategies to improve drug efficacies with potential future impact on patient responses. In addition, the identification and development of chemical probes targeting NUDT22 lay the foundation for further target validation and the development of selective NUDT22i for cancer therapy. However, future research is required to uncover the significance of NUDT22 in other processes than nucleotide synthesis, to confirm the observed differences in dependencies of cancer and non-cancer cells, and to evaluate targeting NUDT22 alone or in combination with other anti-cancer agents in a broader subset of cancer cell and animal models.

Future experiments to establish NUDT22 as an anti-cancer target could involve:

- Determining effects on nucleotide synthesis, DNA replication and damage, cell cycle progression and DNA replication fork speed of *NUDT22* CRISPR/Cas9 KO on wider cancer and non-cancer cell line panel.
- Cell line panel could include cell lines with different *TP53* mutational status to assess effects of gain- or loss-of-function mutations on *NUDT22* expression and transcriptional regulation.
- Changes on dNTP levels upon *NUDT22* KO should be assessed in another approach such as the above described template-dependent nucleotide incorporation assay to confirm the observed changes in dNTP levels. This should also be done in a wider cancer and non-cancer cell line panel to confirm the observed changes between U2OS and the non-cancer fibroblasts hTERT-RPE1.

- Generation of NUDT22 kinase dead mutants to confirm observed effects of *NUDT22* KO with CRISPR/Cas9. This way, potential important protein-protein interactions could be maintained.
- Performing additional xenograft models to assess effects of *NUDT22* KO on tumour growth alone or in combination with pyrimidine *de novo* inhibition in other cancer subtypes based on effects observed in cancer and non-cancer cell line panel.
- Establishing the significance of NUDT22-mediated UDP-glucose hydrolysis in other pathways than pyrimidine synthesis. These pathways include glycolysis, TCA cycle, glycogen synthesis and protein glycosylation. A first step could be a metabolomics approach to assess changes in metabolites involved in pathways upon *NUDT22* CRISPR/Cas9 KO in cancer and non-cancer cell lines.
- Stable isotope labelling of UDP-glucose in combination with LC-MS could be performed to assess metabolic flux and to determine the so-far unknown significance of UDP-glucose.
- Assessing the potential transcriptional regulation of *NUDT22* by HIF1 α in response to oxidative stress due to the potential role of NUDT22 in glycolysis and the TCA cycle.
- Establishing the role of NUDT22-mediated hydrolysis of UDP-glucose in tumour metastasis by performing migration assays in cancer cell models or assessing metastatic potential in xenograft models.
- Generating a constitutive *NUDT22* KO mouse model to determine the role of NUDT22 *in vivo*.

For the development of potent first-in-class NUDT22 inhibitors to be used in target validation and as potential anti-cancer agents future steps include:

- NUDT22 recombinant protein expression in non-bacterial protein expression system to obtain a functional protein with required PTMs.
- Solving a novel co-crystal structure with UDP-glucose and the co-factor Mg²⁺, which is required for correct protein folding and catalytic activity. This structure could then be used for another virtual docking screen with already chemical synthesised and enzymatic as well as cellular evaluated compounds for compound optimisation. Alternatively, another virtual docking screen with a new

ligand library could be performed to obtain new hit candidates for a novel starting point for inhibitor design.

- Solving a co-crystal structure of NUDT22 with UDP-galactose as comparison to already existing structure in complex with UDP-glucose to determine changes in protein folding and NUDT22 inhibitor binding virtually.
- Developing an enzymatic activity assay with UDP-glucose instead of UDP-galactose for existing compounds to determine differences in activity upon different substrates, which could play a role in cell models.
- Assessing NUDT22i A3, A4, A5, and A6 based on their target engagement in live cells.
- Performing cell viability and proliferation assessment with NUDT22i A3, A4, A5, and A6 in cancer and non-cancer cells over an extended amount of time. Resazurin assay as well as colony formation assays could be used.
- If NUDT22i show target engagement in live cells and effects on cell viability and proliferation could be determined, assessing the effects of the compounds on DNA replication fork speed and cell cycle progression could be performed.
- Co-treatment with NUDT22i and pyrimidine *de novo* synthesis interfering agents to assess cell viability, proliferation and DNA damage induction and to recapitulate our previous findings upon *NUDT22* KO in U2OS and MCF7 cells
- Determining the effects of NUDT22 inhibition in NUDT22 kinase dead mutants to detect potential off-target effects.
- Trans-proteomic profiling by combining CETSA with LC-MS to detect NUDT22 target specificity and potential off-target effects could be performed with promising NUDT22 inhibitors.
- To detect changes in metabolites such as dNTPs or intermediates in glycolysis and TCA cycle upon NUDT22 inhibition, metabolomics could be performed.
- *In vivo* studies could be performed in case NUDT22i prove to be potent and target specific in cell models.

8. References

1. McLennan, A.G. The Nudix Hydrolase Superfamily. *Cell Mol Life Sci Cmls* 2006, *63*, 123–143, doi:10.1007/s00018-005-5386-7.
2. Bessman, M.J.; Frick, D.N.; O’Handley, S.F. The MutT Proteins or “Nudix” Hydrolases, a Family of Versatile, Widely Distributed, “Housecleaning” Enzymes*. *J Biol Chem* 1996, *271*, 25059–25062, doi:10.1074/jbc.271.41.25059.
3. Treffers, H.P.; Spinelli, V.; Belser, N.O. A Factor (or Mutator Gene) Influencing Mutation Rates in Escherichia Coli. *Proc National Acad Sci* 1954, *40*, 1064–1071, doi:10.1073/pnas.40.11.1064.
4. Carreras-Puigvert, J.; Zitnik, M.; Jemth, A.-S.; Carter, M.; Unterlass, J.E.; Hallström, B.; Loseva, O.; Karem, Z.; Calderón-Montaño, J.M.; Lindskog, C.; et al. A Comprehensive Structural, Biochemical and Biological Profiling of the Human NUDIX Hydrolase Family. *Nat Commun* 2017, *8*, 1541, doi:10.1038/s41467-017-01642-w.
5. Mildvan, A.S.; Xia, Z.; Azurmendi, H.F.; Saraswat, V.; Legler, P.M.; Massiah, M.A.; Gabelli, S.B.; Bianchet, M.A.; Kang, L.-W.; Amzel, L.M. Structures and Mechanisms of Nudix Hydrolases. *Arch Biochem Biophys* 2005, *433*, 129–143, doi:10.1016/j.abb.2004.08.017.
6. McLennan, A.G. Substrate Ambiguity among the Nudix Hydrolases: Biologically Significant, Evolutionary Remnant, or Both? *Cell Mol Life Sci* 2013, *70*, 373–385, doi:10.1007/s00018-012-1210-3.
7. Gad, H.; Koolmeister, T.; Jemth, A.-S.; Eshtad, S.; Jacques, S.A.; Ström, C.E.; Svensson, L.M.; Schultz, N.; Lundbäck, T.; Einarsdottir, B.O.; et al. MTH1 Inhibition Eradicates Cancer by Preventing Sanitation of the DNTP Pool. *Nature* 2014, *508*, 215–221, doi:10.1038/nature13181.
8. Huber, K.V.M.; Salah, E.; Radic, B.; Gridling, M.; Elkins, J.M.; Stukalov, A.; Jemth, A.-S.; Göktürk, C.; Sanjiv, K.; Strömberg, K.; et al. Stereospecific Targeting of MTH1 by (S)-Crizotinib as an Anticancer Strategy. *Nature* 2014, *508*, 222–227, doi:10.1038/nature13194.
9. Valerie, N.C.K.; Hagenkort, A.; Page, B.D.G.; Masuyer, G.; Rehling, D.; Carter, M.; Bevc, L.; Herr, P.; Homan, E.; Sheppard, N.G.; et al. NUDT15 Hydrolyzes 6-Thio-DeoxyGTP to Mediate the Anticancer Efficacy of 6-Thioguanine. *Cancer Res* 2016, *76*, 5501–5511, doi:10.1158/0008-5472.can-16-0584.
10. Carter, M.; Jemth, A.-S.; Hagenkort, A.; Page, B.D.G.; Gustafsson, R.; Griese, J.J.; Gad, H.; Valerie, N.C.K.; Desroses, M.; Boström, J.; et al. Crystal Structure, Biochemical and Cellular Activities Demonstrate Separate Functions of MTH1 and MTH2. *Nat Commun* 2015, *6*, 7871, doi:10.1038/ncomms8871.
11. Page, B.D.G.; Valerie, N.C.K.; Wright, R.H.G.; Wallner, O.; Isaksson, R.; Carter, M.; Rudd, S.G.; Loseva, O.; Jemth, A.-S.; Almlöf, I.; et al. Targeted NUDT5 Inhibitors Block Hormone Signaling in Breast Cancer Cells. *Nat Commun* 2018, *9*, 250, doi:10.1038/s41467-017-02293-7.
12. Wright, R.H.G.; Lioutas, A.; Dily, F.L.; Soronellas, D.; Pohl, A.; Bonet, J.; Nacht, A.S.; Samino, S.; Font-Mateu, J.; Vicent, G.P.; et al. ADP-Ribose-Derived Nuclear ATP Synthesis by NUDIX5 Is Required for Chromatin Remodeling. *Science* 2016, *352*, 1221–1225, doi:10.1126/science.aad9335.

13. Wright, R.H.G.; Beato, M. Role of the NUDT Enzymes in Breast Cancer. *Int J Mol Sci* 2021, 22, 2267, doi:10.3390/ijms22052267.
14. Cerami, E.; Gao, J.; Dogrusoz, U.; Gross, B.E.; Sumer, S.O.; Aksoy, B.A.; Jacobsen, A.; Byrne, C.J.; Heuer, M.L.; Larsson, E.; et al. The CBio Cancer Genomics Portal: An Open Platform for Exploring Multidimensional Cancer Genomics Data. *Cancer Discov* 2012, 2, 401–404, doi:10.1158/2159-8290.cd-12-0095.
15. Gao, J.; Aksoy, B.A.; Dogrusoz, U.; Dresdner, G.; Gross, B.; Sumer, S.O.; Sun, Y.; Jacobsen, A.; Sinha, R.; Larsson, E.; et al. Integrative Analysis of Complex Cancer Genomics and Clinical Profiles Using the CBioPortal. *Sci Signal* 2013, 6, p11, doi:10.1126/scisignal.2004088.
16. Uhlen, M.; Zhang, C.; Lee, S.; Sjöstedt, E.; Fagerberg, L.; Bidkhori, G.; Benfeitas, R.; Arif, M.; Liu, Z.; Edfors, F.; et al. A Pathology Atlas of the Human Cancer Transcriptome. *Science* 2017, 357, doi:10.1126/science.aan2507.
17. Berglund, U.W.; Sanjiv, K.; Gad, H.; Kalderén, C.; Koolmeister, T.; Pham, T.; Gokturk, C.; Jafari, R.; Maddalo, G.; Seashore-Ludlow, B.; et al. Validation and Development of MTH1 Inhibitors for Treatment of Cancer. *Ann Oncol* 2016, 27, 2275–2283, doi:10.1093/annonc/mdw429.
18. Oksvold, M.P.; Berglund, U.W.; Gad, H.; Bai, B.; Stokke, T.; Rein, I.D.; Pham, T.; Sanjiv, K.; Øy, G.F.; Norum, J.H.; et al. Karonudib Has Potent Anti-Tumor Effects in Preclinical Models of B-Cell Lymphoma. *Sci Rep-uk* 2021, 11, 6317, doi:10.1038/s41598-021-85613-8.
19. Hua, X.; Sanjiv, K.; Gad, H.; Pham, T.; Gokturk, C.; Rasti, A.; Zhao, Z.; He, K.; Feng, M.; Zang, Y.; et al. Karonudib Is a Promising Anticancer Therapy in Hepatocellular Carcinoma. *Ther Adv Med Oncol* 2019, 11, 1758835919866960, doi:10.1177/1758835919866960.
20. Samaranyake, G.J.; Huynh, M.; Rai, P. MTH1 as a Chemotherapeutic Target: The Elephant in the Room. *Cancers* 2017, 9, 47, doi:10.3390/cancers9050047.
21. Kettle, J.G.; Alwan, H.; Bista, M.; Breed, J.; Davies, N.L.; Eckersley, K.; Fillery, S.; Foote, K.M.; Goodwin, L.; Jones, D.R.; et al. Potent and Selective Inhibitors of MTH1 Probe Its Role in Cancer Cell Survival. *J Med Chem* 2016, 59, 2346–2361, doi:10.1021/acs.jmedchem.5b01760.
22. Kawamura, T.; Kawatani, M.; Muroi, M.; Kondoh, Y.; Futamura, Y.; Aono, H.; Tanaka, M.; Honda, K.; Osada, H. Proteomic Profiling of Small-Molecule Inhibitors Reveals Dispensability of MTH1 for Cancer Cell Survival. *Sci Rep-uk* 2016, 6, 26521, doi:10.1038/srep26521.
23. Zhang, H.; Zhang, L.-Q.; Yang, C.-C.; Li, J.; Tian, X.-Y.; Li, D.-N.; Cui, J.; Cai, J.-P. The High Expression of NUDT5 Indicates Poor Prognosis of Breast Cancer by Modulating AKT / Cyclin D Signaling. *Plos One* 2021, 16, e0245876, doi:10.1371/journal.pone.0245876.
24. Tong, X.-Y.; Quan, Y.; Zhang, H.-Y. NUDT5 as a Novel Drug Target and Prognostic Biomarker for ER-Positive Breast Cancer. *Drug Discov Today* 2020, 26, 620–625, doi:10.1016/j.drudis.2020.11.031.
25. Oka, K.; Suzuki, T.; Onodera, Y.; Miki, Y.; Takagi, K.; Nagasaki, S.; Akahira, J.; Ishida, T.; Watanabe, M.; Hirakawa, H.; et al. Nudix-type Motif 2 in Human Breast Carcinoma: A Potent Prognostic Factor Associated with Cell Proliferation. *Int J Cancer* 2011, 128, 1770–1782, doi:10.1002/ijc.25505.

26. Carter, M.; Jemth, A.-S.; Carreras-Puigvert, J.; Herr, P.; Carranza, M.M.; Vallin, K.S.A.; Throup, A.; Helleday, T.; Stenmark, P. Human NUDT22 Is a UDP-Glucose/Galactose Hydrolase Exhibiting a Unique Structural Fold. *Structure* 2018, *26*, 295–303.e6, doi:10.1016/j.str.2018.01.004.
27. Adeva-Andany, M.M.; González-Lucán, M.; Donapetry-García, C.; Fernández-Fernández, C.; Ameneiros-Rodríguez, E. Glycogen Metabolism in Humans. *Bba Clin* 2016, *5*, 85–100, doi:10.1016/j.bbacli.2016.02.001.
28. Dauer, P.; Lengyel, E. New Roles for Glycogen in Tumor Progression. *Trends Cancer* 2019, *5*, 396–399, doi:10.1016/j.trecan.2019.05.003.
29. Heiden, M.G.V.; Lunt, S.Y.; Dayton, T.L.; Fiske, B.P.; Israelsen, W.J.; Mattaini, K.R.; Vokes, N.I.; Stephanopoulos, G.; Cantley, L.C.; Metallo, C.M.; et al. Metabolic Pathway Alterations That Support Cell Proliferation. *Cold Spring Harb Sym* 2011, *76*, 325–334, doi:10.1101/sqb.2012.76.010900.
30. DeBerardinis, R.J.; Chandel, N.S. Fundamentals of Cancer Metabolism. *Sci Adv* 2016, *2*, e1600200, doi:10.1126/sciadv.1600200.
31. Najjar, V.A.; Pullman, M.E. The Occurrence of a Group Transfer Involving Enzyme (Phosphoglucomutase) and Substrate. *Science* 1954, *119*, 631–634, doi:10.1126/science.119.3097.631.
32. Heiden, M.G.V.; DeBerardinis, R.J. Understanding the Intersections between Metabolism and Cancer Biology. *Cell* 2017, *168*, 657–669, doi:10.1016/j.cell.2016.12.039.
33. Liberti, M.V.; Locasale, J.W. The Warburg Effect: How Does It Benefit Cancer Cells? *Trends Biochem Sci* 2016, *41*, 211–218, doi:10.1016/j.tibs.2015.12.001.
34. Heiden, M.G.V. Targeting Cancer Metabolism: A Therapeutic Window Opens. *Nat Rev Drug Discov* 2011, *10*, 671–684, doi:10.1038/nrd3504.
35. Aird, K.M.; Zhang, R. Nucleotide Metabolism, Oncogene-Induced Senescence and Cancer. *Cancer Lett* 2015, *356*, 204–210, doi:10.1016/j.canlet.2014.01.017.
36. Bester, A.C.; Roniger, M.; Oren, Y.S.; Im, M.M.; Sarni, D.; Chaoat, M.; Bensimon, A.; Zamir, G.; Shewach, D.S.; Kerem, B. Nucleotide Deficiency Promotes Genomic Instability in Early Stages of Cancer Development. *Cell* 2011, *145*, 435–446, doi:10.1016/j.cell.2011.03.044.
37. Pavlova, N.N.; Zhu, J.; Thompson, C.B. The Hallmarks of Cancer Metabolism: Still Emerging. *Cell Metab* 2022, doi:10.1016/j.cmet.2022.01.007.
38. Pavlova, N.N.; Thompson, C.B. The Emerging Hallmarks of Cancer Metabolism. *Cell Metab* 2016, *23*, 27–47, doi:10.1016/j.cmet.2015.12.006.
39. Negrini, S.; Gorgoulis, V.G.; Halazonetis, T.D. Genomic Instability — an Evolving Hallmark of Cancer. *Nat Rev Mol Cell Bio* 2010, *11*, 220–228, doi:10.1038/nrm2858.
40. Hanahan, D.; Weinberg, R.A. Hallmarks of Cancer: The Next Generation. *Cell* 2011, *144*, 646–674, doi:10.1016/j.cell.2011.02.013.
41. Hanahan, D. Hallmarks of Cancer: New Dimensions. *Cancer Discov* 2022, *12*, 31–46, doi:10.1158/2159-8290.cd-21-1059.

42. Hanahan, D.; Weinberg, R.A. The Hallmarks of Cancer. *Cell* 2000, *100*, 57–70, doi:10.1016/s0092-8674(00)81683-9.
43. Blackford, A.N.; Jackson, S.P. ATM, ATR, and DNA-PK: The Trinity at the Heart of the DNA Damage Response. *Mol Cell* 2017, *66*, 801–817, doi:10.1016/j.molcel.2017.05.015.
44. Fragkos, M.; Ganier, O.; Coulombe, P.; Méchali, M. DNA Replication Origin Activation in Space and Time. *Nat Rev Mol Cell Bio* 2015, *16*, 360–374, doi:10.1038/nrm4002.
45. Moiseeva, T.N.; Bakkenist, C.J. Regulation of the Initiation of DNA Replication in Human Cells. *Dna Repair* 2018, *72*, 99–106, doi:10.1016/j.dnarep.2018.09.003.
46. Dewar, J.M.; Walter, J.C. Mechanisms of DNA Replication Termination. *Nat Rev Mol Cell Bio* 2017, *18*, 507–516, doi:10.1038/nrm.2017.42.
47. Balakrishnan, L.; Bambara, R.A. Okazaki Fragment Metabolism. *Csh Perspect Biol* 2013, *5*, a010173, doi:10.1101/cshperspect.a010173.
48. Wilhelm, T.; Said, M.; Naim, V. DNA Replication Stress and Chromosomal Instability: Dangerous Liaisons. *Genes-basel* 2020, *11*, 642, doi:10.3390/genes11060642.
49. Ngoi, N.Y.; Sundararajan, V.; Tan, D.S. Exploiting Replicative Stress in Gynecological Cancers as a Therapeutic Strategy. *Int J Gynecol Cancer* 2020, *30*, 1224–1238, doi:10.1136/ijgc-2020-001277.
50. Byun, T.S.; Pacek, M.; Yee, M.; Walter, J.C.; Cimprich, K.A. Functional Uncoupling of MCM Helicase and DNA Polymerase Activities Activates the ATR-Dependent Checkpoint. *Gene Dev* 2005, *19*, 1040–1052, doi:10.1101/gad.1301205.
51. Berti, M.; Vindigni, A. Replication Stress: Getting Back on Track. *Nat Struct Mol Biol* 2016, *23*, 103–109, doi:10.1038/nsmb.3163.
52. Saldivar, J.C.; Cortez, D.; Cimprich, K.A. The Essential Kinase ATR: Ensuring Faithful Duplication of a Challenging Genome. *Nat Rev Mol Cell Bio* 2017, *18*, 622–636, doi:10.1038/nrm.2017.67.
53. Eykelenboom, J.K.; Harte, E.C.; Canavan, L.; Pastor-Peidro, A.; Calvo-Asensio, I.; Llorens-Agost, M.; Lowndes, N.F. ATR Activates the S-M Checkpoint during Unperturbed Growth to Ensure Sufficient Replication Prior to Mitotic Onset. *Cell Reports* 2013, *5*, 1095–1107, doi:10.1016/j.celrep.2013.10.027.
54. Beyaert, M.; Starczewska, E.; Neste, E.V.D.; Bontemps, F. A Crucial Role for ATR in the Regulation of Deoxycytidine Kinase Activity. *Biochem Pharmacol* 2016, *100*, 40–50, doi:10.1016/j.bcp.2015.11.022.
55. Zhang, Y.-W.; Jones, T.L.; Martin, S.E.; Caplen, N.J.; Pommier, Y. Implication of Checkpoint Kinase-Dependent Up-Regulation of Ribonucleotide Reductase R2 in DNA Damage Response*. *J Biol Chem* 2009, *284*, 18085–18095, doi:10.1074/jbc.m109.003020.
56. D’Angiolella, V.; Donato, V.; Forrester, F.M.; Jeong, Y.-T.; Pellacani, C.; Kudo, Y.; Saraf, A.; Florens, L.; Washburn, M.P.; Pagano, M. Cyclin F-Mediated Degradation of Ribonucleotide Reductase M2 Controls Genome Integrity and DNA Repair. *Cell* 2012, *149*, 1023–1034, doi:10.1016/j.cell.2012.03.043.

57. Toledo, L.I.; Altmeyer, M.; Rask, M.-B.; Lukas, C.; Larsen, D.H.; Povlsen, L.K.; Bekker-Jensen, S.; Mailand, N.; Bartek, J.; Lukas, J. ATR Prohibits Replication Catastrophe by Preventing Global Exhaustion of RPA. *Cell* 2013, *155*, 1088–1103, doi:10.1016/j.cell.2013.10.043.
58. Beck, H.; Nähse-Kumpf, V.; Larsen, M.S.Y.; O’Hanlon, K.A.; Patzke, S.; Holmberg, C.; Mejlvang, J.; Groth, A.; Nielsen, O.; Syljuåsen, R.G.; et al. Cyclin-Dependent Kinase Suppression by WEE1 Kinase Protects the Genome through Control of Replication Initiation and Nucleotide Consumption. *Mol Cell Biol* 2012, *32*, 4226–4236, doi:10.1128/mcb.00412-12.
59. Ge, X.Q.; Blow, J.J. Chk1 Inhibits Replication Factory Activation but Allows Dormant Origin Firing in Existing Factories. *J Cell Biology* 2010, *191*, 1285–1297, doi:10.1083/jcb.201007074.
60. Chen, Y.-H.; Jones, M.J.K.; Yin, Y.; Crist, S.B.; Colnaghi, L.; Sims, R.J.; Rothenberg, E.; Jallepalli, P.V.; Huang, T.T. ATR-Mediated Phosphorylation of FANCI Regulates Dormant Origin Firing in Response to Replication Stress. *Mol Cell* 2015, *58*, 323–338, doi:10.1016/j.molcel.2015.02.031.
61. Petermann, E.; Orta, M.L.; Issaeva, N.; Schultz, N.; Helleday, T. Hydroxyurea-Stalled Replication Forks Become Progressively Inactivated and Require Two Different RAD51-Mediated Pathways for Restart and Repair. *Mol Cell* 2010, *37*, 492–502, doi:10.1016/j.molcel.2010.01.021.
62. Cortez, D. Preventing Replication Fork Collapse to Maintain Genome Integrity. *Dna Repair* 2015, *32*, 149–157, doi:10.1016/j.dnarep.2015.04.026.
63. Macheret, M.; Halazonetis, T.D. Intragenic Origins Due to Short G1 Phases Underlie Oncogene-Induced DNA Replication Stress. *Nature* 2018, *555*, 112–116, doi:10.1038/nature25507.
64. Bosch, M. van den; Bree, R.T.; Lowndes, N.F. The MRN Complex: Coordinating and Mediating the Response to Broken Chromosomes. *Embo Rep* 2003, *4*, 844–849, doi:10.1038/sj.embor.embor925.
65. Zannini, L.; Delia, D.; Buscemi, G. CHK2 Kinase in the DNA Damage Response and Beyond. *J Mol Cell Biol* 2014, *6*, 442–457, doi:10.1093/jmcb/mju045.
66. Burma, S.; Chen, B.P.; Murphy, M.; Kurimasa, A.; Chen, D.J. ATM Phosphorylates Histone H2AX in Response to DNA Double-Strand Breaks*. *J Biol Chem* 2001, *276*, 42462–42467, doi:10.1074/jbc.c100466200.
67. Ward, I.M.; Chen, J. Histone H2AX Is Phosphorylated in an ATR-Dependent Manner in Response to Replication Stress*. *J Biol Chem* 2001, *276*, 47759–47762, doi:10.1074/jbc.c100569200.
68. Chatterjee, N.; Walker, G.C. Mechanisms of DNA Damage, Repair, and Mutagenesis. *Environ Mol Mutagen* 2017, *58*, 235–263, doi:10.1002/em.22087.
69. Cuadrado, M.; Martinez-Pastor, B.; Murga, M.; Toledo, L.I.; Gutierrez-Martinez, P.; Lopez, E.; Fernandez-Capetillo, O. ATM Regulates ATR Chromatin Loading in Response to DNA Double-Strand Breaks. *J Exp Medicine* 2006, *203*, 297–303, doi:10.1084/jem.20051923.
70. Myers, J.S.; Cortez, D. Rapid Activation of ATR by Ionizing Radiation Requires ATM and Mre11*. *J Biol Chem* 2006, *281*, 9346–9350, doi:10.1074/jbc.m513265200.

71. Jazayeri, A.; Falck, J.; Lukas, C.; Bartek, J.; Smith, G.C.M.; Lukas, J.; Jackson, S.P. ATM- and Cell Cycle-Dependent Regulation of ATR in Response to DNA Double-Strand Breaks. *Nat Cell Biol* 2006, 8, 37–45, doi:10.1038/ncb1337.
72. Taylor, W.R.; Stark, G.R. Regulation of the G2/M Transition by P53. *Oncogene* 2001, 20, 1803–1815, doi:10.1038/sj.onc.1204252.
73. Niculescu, A.B.; Chen, X.; Smeets, M.; Hengst, L.; Prives, C.; Reed, S.I. Effects of P21 Cip1/Waf1 at Both the G 1 /S and the G 2 /M Cell Cycle Transitions: PRb Is a Critical Determinant in Blocking DNA Replication and in Preventing Endoreduplication. *Mol Cell Biol* 1998, 18, 629–643, doi:10.1128/mcb.18.1.629.
74. Waga, S.; Hannon, G.J.; Beach, D.; Stillman, B. The P21 Inhibitor of Cyclin-Dependent Kinases Controls DNA Replication by Interaction with PCNA. *Nature* 1994, 369, 574–578, doi:10.1038/369574a0.
75. Macheret, M.; Halazonetis, T.D. DNA Replication Stress as a Hallmark of Cancer. *Annu Rev Pathology Mech Dis* 2015, 10, 425–448, doi:10.1146/annurev-pathol-012414-040424.
76. Pylayeva-Gupta, Y.; Grabocka, E.; Bar-Sagi, D. RAS Oncogenes: Weaving a Tumorigenic Web. *Nat Rev Cancer* 2011, 11, 761–774, doi:10.1038/nrc3106.
77. Micco, R.D.; Fumagalli, M.; Cicalese, A.; Piccinin, S.; Gasparini, P.; Luise, C.; Schurra, C.; Garre', M.; Nuciforo, P.G.; Bensimon, A.; et al. Oncogene-Induced Senescence Is a DNA Damage Response Triggered by DNA Hyper-Replication. *Nature* 2006, 444, 638–642, doi:10.1038/nature05327.
78. Aird, K.M.; Zhang, G.; Li, H.; Tu, Z.; Bitler, B.G.; Garipov, A.; Wu, H.; Wei, Z.; Wagner, S.N.; Herlyn, M.; et al. Suppression of Nucleotide Metabolism Underlies the Establishment and Maintenance of Oncogene-Induced Senescence. *Cell Reports* 2013, 3, 1252–1265, doi:10.1016/j.celrep.2013.03.004.
79. Maya-Mendoza, A.; Ostrakova, J.; Kosar, M.; Hall, A.; Duskova, P.; Mistrik, M.; Merchut-Maya, J.M.; Hodny, Z.; Bartkova, J.; Christensen, C.; et al. Myc and Ras Oncogenes Engage Different Energy Metabolism Programs and Evoke Distinct Patterns of Oxidative and DNA Replication Stress. *Mol Oncol* 2015, 9, 601–616, doi:10.1016/j.molonc.2014.11.001.
80. Ekholm-Reed, S.; Méndez, J.; Tedesco, D.; Zetterberg, A.; Stillman, B.; Reed, S.I. Deregulation of Cyclin E in Human Cells Interferes with Prereplication Complex Assembly. *J Cell Biology* 2004, 165, 789–800, doi:10.1083/jcb.200404092.
81. Jones, R.M.; Mortusewicz, O.; Afzal, I.; Lorvellec, M.; García, P.; Helleday, T.; Petermann, E. Increased Replication Initiation and Conflicts with Transcription Underlie Cyclin E-Induced Replication Stress. *Oncogene* 2013, 32, 3744–3753, doi:10.1038/onc.2012.387.
82. Liberal, V.; Martinsson-Ahlzén, H.-S.; Liberal, J.; Spruck, C.H.; Widschwendter, M.; McGowan, C.H.; Reed, S.I. Cyclin-Dependent Kinase Subunit (Cks) 1 or Cks2 Overexpression Overrides the DNA Damage Response Barrier Triggered by Activated Oncoproteins. *Proc National Acad Sci* 2012, 109, 2754–2759, doi:10.1073/pnas.1102434108.
83. Hughes, B.T.; Sidorova, J.; Swanger, J.; Monnat, R.J.; Clurman, B.E. Essential Role for Cdk2 Inhibitory Phosphorylation during Replication Stress Revealed by a Human Cdk2 Knockin Mutation. *Proc National Acad Sci* 2013, 110, 8954–8959, doi:10.1073/pnas.1302927110.

84. Costantino, L.; Sotiriou, S.K.; Rantala, J.K.; Magin, S.; Mladenov, E.; Helleday, T.; Haber, J.E.; Iliakis, G.; Kallioniemi, O.P.; Halazonetis, T.D. Break-Induced Replication Repair of Damaged Forks Induces Genomic Duplications in Human Cells. *Science* 2014, *343*, 88–91, doi:10.1126/science.1243211.
85. Duffy, M.J.; O’Grady, S.; Tang, M.; Crown, J. MYC as a Target for Cancer Treatment. *Cancer Treat Rev* 2021, *94*, 102154, doi:10.1016/j.ctrv.2021.102154.
86. Dominguez-Sola, D.; Ying, C.Y.; Grandori, C.; Ruggiero, L.; Chen, B.; Li, M.; Galloway, D.A.; Gu, W.; Gautier, J.; Dalla-Favera, R. Non-Transcriptional Control of DNA Replication by c-Myc. *Nature* 2007, *448*, 445–451, doi:10.1038/nature05953.
87. Bartkova, J.; Rezaei, N.; Liontos, M.; Karakaidos, P.; Kletsas, D.; Issaeva, N.; Vassiliou, L.-V.F.; Kolettas, E.; Niforou, K.; Zoumpourlis, V.C.; et al. Oncogene-Induced Senescence Is Part of the Tumorigenesis Barrier Imposed by DNA Damage Checkpoints. *Nature* 2006, *444*, 633–637, doi:10.1038/nature05268.
88. Lakin, N.D.; Jackson, S.P. Regulation of P53 in Response to DNA Damage. *Oncogene* 1999, *18*, 7644–7655, doi:10.1038/sj.onc.1203015.
89. Toschi, L.; Finocchiaro, G.; Bartolini, S.; Gioia, V.; Cappuzzo, F. Role of Gemcitabine in Cancer Therapy. *Future Oncol* 2005, *1*, 7–17, doi:10.1517/14796694.1.1.7.
90. Li, Z.; Guo, J.-R.; Chen, Q.-Q.; Wang, C.-Y.; Zhang, W.-J.; Yao, M.-C.; Zhang, W. Exploring the Antitumor Mechanism of High-Dose Cytarabine through the Metabolic Perturbations of Ribonucleotide and Deoxyribonucleotide in Human Promyelocytic Leukemia HL-60 Cells. *Molecules* 2017, *22*, 499, doi:10.3390/molecules22030499.
91. Longley, D.B.; Harkin, D.P.; Johnston, P.G. 5-Fluorouracil: Mechanisms of Action and Clinical Strategies. *Nat Rev Cancer* 2003, *3*, 330–338, doi:10.1038/nrc1074.
92. Fu, D.; Calvo, J.A.; Samson, L.D. Balancing Repair and Tolerance of DNA Damage Caused by Alkylating Agents. *Nat Rev Cancer* 2012, *12*, 104–120, doi:10.1038/nrc3185.
93. Xiong, Y.; Huang, B.-Y.; Yin, J.-Y. Pharmacogenomics of Platinum-Based Chemotherapy in Non-Small Cell Lung Cancer: Focusing on DNA Repair Systems. *Med Oncol* 2017, *34*, 48, doi:10.1007/s12032-017-0905-6.
94. Nitiss, J.L. Targeting DNA Topoisomerase II in Cancer Chemotherapy. *Nat Rev Cancer* 2009, *9*, 338–350, doi:10.1038/nrc2607.
95. Promonet, A.; Padiou, I.; Liu, Y.; Sanz, L.; Biernacka, A.; Schmitz, A.-L.; Skrzypczak, M.; Sarrazin, A.; Mettling, C.; Rowicka, M.; et al. Topoisomerase 1 Prevents Replication Stress at R-Loop-Enriched Transcription Termination Sites. *Nat Commun* 2020, *11*, 3940, doi:10.1038/s41467-020-17858-2.
96. Xu, Y.; Her, C. Inhibition of Topoisomerase (DNA) I (TOP1): DNA Damage Repair and Anticancer Therapy. *Biomol* 2015, *5*, 1652–1670, doi:10.3390/biom5031652.
97. Ström, C.E.; Johansson, F.; Uhlén, M.; Szigartyo, C.A.-K.; Erixon, K.; Helleday, T. Poly (ADP-Ribose) Polymerase (PARP) Is Not Involved in Base Excision Repair but PARP Inhibition Traps a Single-Strand Intermediate. *Nucleic Acids Res* 2011, *39*, 3166–3175, doi:10.1093/nar/gkq1241.

98. Fujinaka, Y.; Matsuoka, K.; Iimori, M.; Tuul, M.; Sakasai, R.; Yoshinaga, K.; Saeki, H.; Morita, M.; Kakeji, Y.; Gillespie, D.A.; et al. ATR–Chk1 Signaling Pathway and Homologous Recombinational Repair Protect Cells from 5-Fluorouracil Cytotoxicity. *Dna Repair* 2012, *11*, 247–258, doi:10.1016/j.dnarep.2011.11.005.
99. Francica, P.; Rottenberg, S. Mechanisms of PARP Inhibitor Resistance in Cancer and Insights into the DNA Damage Response. *Genome Med* 2018, *10*, 101, doi:10.1186/s13073-018-0612-8.
100. Kim, H.; George, E.; Ragland, R.L.; Rafail, S.; Zhang, R.; Krepler, C.; Morgan, M.A.; Herlyn, M.; Brown, E.J.; Simpkins, F. Targeting the ATR/CHK1 Axis with PARP Inhibition Results in Tumor Regression in BRCA-Mutant Ovarian Cancer Models. *Clin Cancer Res* 2017, *23*, 3097–3108, doi:10.1158/1078-0432.ccr-16-2273.
101. Sanjiv, K.; Hagenkort, A.; Calderón-Montaña, J.M.; Koolmeister, T.; Reaper, P.M.; Mortusewicz, O.; Jacques, S.A.; Kuiper, R.V.; Schultz, N.; Scobie, M.; et al. Cancer-Specific Synthetic Lethality between ATR and CHK1 Kinase Activities. *Cell Reports* 2016, *14*, 298–309, doi:10.1016/j.celrep.2015.12.032.
102. Zhu, H.; Swami, U.; Preet, R.; Zhang, J. Harnessing DNA Replication Stress for Novel Cancer Therapy. *Genes-basel* 2020, *11*, 990, doi:10.3390/genes11090990.
103. Wallez, Y.; Dunlop, C.R.; Johnson, T.I.; Koh, S.-B.; Fornari, C.; Yates, J.W.; Fernández, S.B. de Q.; Lau, A.; Richards, F.M.; Jodrell, D.I. The ATR Inhibitor AZD6738 Synergizes with Gemcitabine in Vitro and in Vivo to Induce Pancreatic Ductal Adenocarcinoma Regression. *Mol Cancer Ther* 2018, *17*, molcanther.0010.2018, doi:10.1158/1535-7163.mct-18-0010.
104. Liu, S.; Ge, Y.; Wang, T.; Edwards, H.; Ren, Q.; Jiang, Y.; Quan, C.; Wang, G. Inhibition of ATR Potentiates the Cytotoxic Effect of Gemcitabine on Pancreatic Cancer Cells through Enhancement of DNA Damage and Abrogation of Ribonucleotide Reductase Induction by Gemcitabine. *Oncol Rep* 2017, *37*, 3377–3386, doi:10.3892/or.2017.5580.
105. Liu, Y.; Li, Y.; Wang, X.; Liu, F.; Gao, P.; Quinn, M.M.; Li, F.; Merlino, A.A.; Benes, C.; Liu, Q.; et al. Gemcitabine and Chk1 Inhibitor AZD7762 Synergistically Suppress the Growth of Lkb1-Deficient Lung Adenocarcinoma. *Cancer Res* 2017, *77*, 5068–5076, doi:10.1158/0008-5472.can-17-0567.
106. Aarts, M.; Sharpe, R.; Garcia-Murillas, I.; Gevensleben, H.; Hurd, M.S.; Shumway, S.D.; Toniatti, C.; Ashworth, A.; Turner, N.C. Forced Mitotic Entry of S-Phase Cells as a Therapeutic Strategy Induced by Inhibition of WEE1. *Cancer Discov* 2012, *2*, 524–539, doi:10.1158/2159-8290.cd-11-0320.
107. Hirai, H.; Iwasawa, Y.; Okada, M.; Arai, T.; Nishibata, T.; Kobayashi, M.; Kimura, T.; Kaneko, N.; Ohtani, J.; Yamanaka, K.; et al. Small-Molecule Inhibition of Wee1 Kinase by MK-1775 Selectively Sensitizes P53-Deficient Tumor Cells to DNA-Damaging Agents. *Mol Cancer Ther* 2009, *8*, 2992–3000, doi:10.1158/1535-7163.mct-09-0463.
108. Ku, B.M.; Bae, Y.-H.; Koh, J.; Sun, J.-M.; Lee, S.-H.; Ahn, J.S.; Park, K.; Ahn, M.-J. Mutational Status of TP53 Defines the Efficacy of Wee1 Inhibitor AZD1775 in KRAS-Mutant Non-Small Cell Lung Cancer. *Oncotarget* 2017, *8*, 67526–67537, doi:10.18632/oncotarget.18728.
109. Oza, A.M.; Estevez-Diz, M.; Grischke, E.-M.; Hall, M.; Marmé, F.; Provencher, D.; Uyar, D.; Weberpals, J.I.; Wenham, R.M.; Laing, N.; et al. A Biomarker-Enriched, Randomized Phase II Trial of Adavosertib (AZD1775) Plus Paclitaxel and Carboplatin for Women with Platinum-Sensitive

TP53-Mutant Ovarian Cancer. *Clin Cancer Res* 2020, 26, 4767–4776, doi:10.1158/1078-0432.ccr-20-0219.

110. Do, K.; Wilsker, D.; Ji, J.; Zlott, J.; Freshwater, T.; Kinders, R.J.; Collins, J.; Chen, A.P.; Doroshow, J.H.; Kummar, S. Phase I Study of Single-Agent AZD1775 (MK-1775), a Wee1 Kinase Inhibitor, in Patients With Refractory Solid Tumors. *J Clin Oncol* 2015, 33, 3409–3415, doi:10.1200/jco.2014.60.4009.

111. Leijen, S.; Geel, R.M.J.M. van; Pavlick, A.C.; Tibes, R.; Rosen, L.; Razak, A.R.A.; Lam, R.; Demuth, T.; Rose, S.; Lee, M.A.; et al. Phase I Study Evaluating WEE1 Inhibitor AZD1775 As Monotherapy and in Combination With Gemcitabine, Cisplatin, or Carboplatin in Patients With Advanced Solid Tumors. *J Clin Oncol* 2016, 34, 4371–4380, doi:10.1200/jco.2016.67.5991.

112. Leijen, S.; Geel, R.M.J.M. van; Sonke, G.S.; Jong, D. de; Rosenberg, E.H.; Marchetti, S.; Pluim, D.; Werkhoven, E. van; Rose, S.; Lee, M.A.; et al. Phase II Study of WEE1 Inhibitor AZD1775 Plus Carboplatin in Patients With TP53-Mutated Ovarian Cancer Refractory or Resistant to First-Line Therapy Within 3 Months. *J Clin Oncol* 2016, 34, 4354–4361, doi:10.1200/jco.2016.67.5942.

113. Guertin, A.D.; Martin, M.M.; Roberts, B.; Hurd, M.; Qu, X.; Miselis, N.R.; Liu, Y.; Li, J.; Feldman, I.; Benita, Y.; et al. Unique Functions of CHK1 and WEE1 Underlie Synergistic Anti-Tumor Activity upon Pharmacologic Inhibition. *Cancer Cell Int* 2012, 12, 45–45, doi:10.1186/1475-2867-12-45.

114. Chaudhuri, L.; Vincelette, N.D.; Koh, B.D.; Naylor, R.M.; Flatten, K.S.; Peterson, K.L.; McNally, A.; Gojo, I.; Karp, J.E.; Mesa, R.A.; et al. CHK1 and WEE1 Inhibition Combine Synergistically to Enhance Therapeutic Efficacy in Acute Myeloid Leukemia Ex Vivo. *Haematologica* 2014, 99, 688–696, doi:10.3324/haematol.2013.093187.

115. Davies, K.D.; Cable, P.L.; Garrus, J.E.; Sullivan, F.X.; Carlowitz, I. von; Huerou, Y.L.; Wallace, E.; Woessner, R.D.; Gross, S. Chk1 Inhibition and Wee1 Inhibition Combine Synergistically to Impede Cellular Proliferation. *Cancer Biol Ther* 2011, 12, 788–796, doi:10.4161/cbt.12.9.17673.

116. Carrassa, L.; Chilà, R.; Lupi, M.; Ricci, F.; Celenza, C.; Mazzoletti, M.; Broggin, M.; Damia, G. Combined Inhibition of Chk1 and Wee1: In Vitro Synergistic Effect Translates to Tumor Growth Inhibition in Vivo. *Cell Cycle* 2012, 11, 2507–2517, doi:10.4161/cc.20899.

117. Austin, W.R.; Armijo, A.L.; Campbell, D.O.; Singh, A.S.; Hsieh, T.; Nathanson, D.; Herschman, H.R.; Phelps, M.E.; Witte, O.N.; Czernin, J.; et al. Nucleoside Salvage Pathway Kinases Regulate Hematopoiesis by Linking Nucleotide Metabolism with Replication Stress. *J Exp Med* 2012, 209, 2215–2228, doi:10.1084/jem.20121061.

118. Berthold, M.R.; Cebron, N.; Dill, F.; Fatta, G.D.; Gabriel, T.R.; Georg, F.; Meinl, T.; Ohl, P.; Sieb, C.; Wiswedel, C. Knime The Konstanz Information Miner. *Springer*.

119. Walters, W.P.; Murcko, M.A. Prediction of ‘Drug-Likeness.’ *Adv Drug Deliver Rev* 2002, 54, 255–271, doi:10.1016/s0169-409x(02)00003-0.

120. Baell, J.B.; Holloway, G.A. New Substructure Filters for Removal of Pan Assay Interference Compounds (PAINS) from Screening Libraries and for Their Exclusion in Bioassays. *J Med Chem* 2010, 53, 2719–2740, doi:10.1021/jm901137j.

121. Lipinski, C.A.; Lombardo, F.; Dominy, B.W.; Feeney, P.J. Experimental and Computational Approaches to Estimate Solubility and Permeability in Drug Discovery and Development Settings. *Adv Drug Deliver Rev* 1997, *23*, 3–25, doi:10.1016/s0169-409x(96)00423-1.
122. Shelley, J.C.; Cholleti, A.; Frye, L.L.; Greenwood, J.R.; Timlin, M.R.; Uchimaya, M. Epik: A Software Program for PKa Prediction and Protonation State Generation for Drug-like Molecules. *J Comput Aid Mol Des* 2007, *21*, 681–691, doi:10.1007/s10822-007-9133-z.
123. Friesner, R.A.; Murphy, R.B.; Repasky, M.P.; Frye, L.L.; Greenwood, J.R.; Halgren, T.A.; Sanschagrin, P.C.; Mainz, D.T. Extra Precision Glide: Docking and Scoring Incorporating a Model of Hydrophobic Enclosure for Protein–Ligand Complexes. *J Med Chem* 2006, *49*, 6177–6196, doi:10.1021/jm051256o.
124. Friesner, R.A.; Banks, J.L.; Murphy, R.B.; Halgren, T.A.; Klicic, J.J.; Mainz, D.T.; Repasky, M.P.; Knoll, E.H.; Shelley, M.; Perry, J.K.; et al. Glide: A New Approach for Rapid, Accurate Docking and Scoring. 1. Method and Assessment of Docking Accuracy. *J Med Chem* 2004, *47*, 1739–1749, doi:10.1021/jm0306430.
125. Halgren, T.A.; Murphy, R.B.; Friesner, R.A.; Beard, H.S.; Frye, L.L.; Pollard, W.T.; Banks, J.L. Glide: A New Approach for Rapid, Accurate Docking and Scoring. 2. Enrichment Factors in Database Screening. *J Med Chem* 2004, *47*, 1750–1759, doi:10.1021/jm030644s.
126. Niesen, F.H.; Berglund, H.; Vedadi, M. The Use of Differential Scanning Fluorimetry to Detect Ligand Interactions That Promote Protein Stability. *Nat Protoc* 2007, *2*, 2212–2221, doi:10.1038/nprot.2007.321.
127. Jafari, R.; Almqvist, H.; Axelsson, H.; Ignatushchenko, M.; Lundbäck, T.; Nordlund, P.; Molina, D.M. The Cellular Thermal Shift Assay for Evaluating Drug Target Interactions in Cells. *Nat Protoc* 2014, *9*, 2100–2122, doi:10.1038/nprot.2014.138.
128. Walter, M.; Herr, P. Re-Discovery of Pyrimidine Salvage as Target in Cancer Therapy. *Cells* 2022, *11*, 739, doi:10.3390/cells11040739.
129. Maia, E.H.B.; Assis, L.C.; Oliveira, T.A. de; Silva, A.M. da; Taranto, A.G. Structure-Based Virtual Screening: From Classical to Artificial Intelligence. *Front Chem* 2020, *8*, 343, doi:10.3389/fchem.2020.00343.
130. Cui, W.; Aouidate, A.; Wang, S.; Yu, Q.; Li, Y.; Yuan, S. Discovering Anti-Cancer Drugs via Computational Methods. *Front Pharmacol* 2020, *11*, 733, doi:10.3389/fphar.2020.00733.
131. Leelananda, S.P.; Lindert, S. Computational Methods in Drug Discovery. *Beilstein J Org Chem* 2016, *12*, 2694–2718, doi:10.3762/bjoc.12.267.
132. Macarron, R.; Banks, M.N.; Bojanic, D.; Burns, D.J.; Cirovic, D.A.; Garyantes, T.; Green, D.V.S.; Hertzberg, R.P.; Janzen, W.P.; Paslay, J.W.; et al. Impact of High-Throughput Screening in Biomedical Research. *Nat Rev Drug Discov* 2011, *10*, 188–195, doi:10.1038/nrd3368.
133. Bender, B.J.; Gahbauer, S.; Lutten, A.; Lyu, J.; Webb, C.M.; Stein, R.M.; Fink, E.A.; Balias, T.E.; Carlsson, J.; Irwin, J.J.; et al. A Practical Guide to Large-Scale Docking. *Nat Protoc* 2021, 1–34, doi:10.1038/s41596-021-00597-z.

134. Willems, H.; Cesco, S.D.; Svensson, F. Computational Chemistry on a Budget: Supporting Drug Discovery with Limited Resources. *J Med Chem* 2020, 63, 10158–10169, doi:10.1021/acs.jmedchem.9b02126.
135. Kaldor, S.W.; Kalish, V.J.; Davies, J.F.; Shetty, B.V.; Fritz, J.E.; Appelt, K.; Burgess, J.A.; Campanale, K.M.; Chirgadze, N.Y.; Clawson, D.K.; et al. Viracept (Nelfinavir Mesylate, AG1343): A Potent, Orally Bioavailable Inhibitor of HIV-1 Protease. *J Med Chem* 1997, 40, 3979–3985, doi:10.1021/jm9704098.
136. Cui, J.J.; Tran-Dubé, M.; Shen, H.; Nambu, M.; Kung, P.-P.; Pairish, M.; Jia, L.; Meng, J.; Funk, L.; Botrous, I.; et al. Structure Based Drug Design of Crizotinib (PF-02341066), a Potent and Selective Dual Inhibitor of Mesenchymal–Epithelial Transition Factor (c-MET) Kinase and Anaplastic Lymphoma Kinase (ALK). *J Med Chem* 2011, 54, 6342–6363, doi:10.1021/jm2007613.
137. Zhu, T.; Cao, S.; Su, P.-C.; Patel, R.; Shah, D.; Chokshi, H.B.; Szukala, R.; Johnson, M.E.; Hevener, K.E. Hit Identification and Optimization in Virtual Screening: Practical Recommendations Based on a Critical Literature Analysis. *J Med Chem* 2013, 56, 6560–6572, doi:10.1021/jm301916b.
138. Murray, D.; Wigglesworth, M. High Throughput Screening Methods: Evolution and Refinement. *Chem Biology* 2017, 1–15, doi:10.1039/9781782626770-00001.
139. Scior, T.; Bender, A.; Tresadern, G.; Medina-Franco, J.L.; Martínez-Mayorga, K.; Langer, T.; Cuanalo-Contreras, K.; Agrafiotis, D.K. Recognizing Pitfalls in Virtual Screening: A Critical Review. *J Chem Inf Model* 2012, 52, 867–881, doi:10.1021/ci200528d.
140. Lipinski, C.A. Lead- and Drug-like Compounds: The Rule-of-Five Revolution. *Drug Discov Today Technologies* 2004, 1, 337–341, doi:10.1016/j.ddtec.2004.11.007.
141. Dahlin, J.L.; Walters, M.A. How to Triage PAINS-Full Research. *Assay Drug Dev Techn* 2016, 14, 168–174, doi:10.1089/adt.2015.674.
142. Hopkins, A.L.; Groom, C.R.; Alex, A. Ligand Efficiency: A Useful Metric for Lead Selection. *Drug Discov Today* 2004, 9, 430–431, doi:10.1016/s1359-6446(04)03069-7.
143. Kenny, P.W. The Nature of Ligand Efficiency. *J Cheminformatics* 2019, 11, 8, doi:10.1186/s13321-019-0330-2.
144. Hopkins, A.L.; Keserü, G.M.; Leeson, P.D.; Rees, D.C.; Reynolds, C.H. The Role of Ligand Efficiency Metrics in Drug Discovery. *Nat Rev Drug Discov* 2014, 13, 105–121, doi:10.1038/nrd4163.
145. Itaya, K.; Ui, M. A New Micromethod for the Colorimetric Determination of Inorganic Phosphate. *Clin Chim Acta* 1966, 14, 361–366, doi:10.1016/0009-8981(66)90114-8.
146. Massolo, E.; Pirola, M.; Benaglia, M. Amide Bond Formation Strategies: Latest Advances on a Dateless Transformation. *Eur J Org Chem* 2020, 2020, 4641–4651, doi:10.1002/ejoc.202000080.
147. Lassalas, P.; Gay, B.; Lasfargeas, C.; James, M.J.; Tran, V.; Vijayendran, K.G.; Brunden, K.R.; Kozlowski, M.C.; Thomas, C.J.; Smith, A.B.; et al. Structure Property Relationships of Carboxylic Acid Isosteres. *J Med Chem* 2016, 59, 3183–3203, doi:10.1021/acs.jmedchem.5b01963.
148. Shiryayev, S.A.; Cheltsov, A.V.; Gawlik, K.; Ratnikov, B.I.; Strongin, A.Y. Virtual Ligand Screening of the National Cancer Institute (NCI) Compound Library Leads to the Allosteric Inhibitory

- Scaffolds of the West Nile Virus NS3 Proteinase. *Assay Drug Dev Techn* 2011, 9, 69–78, doi:10.1089/adt.2010.0309.
149. Monga, M.; Sausville, E. Developmental Therapeutics Program at the NCI: Molecular Target and Drug Discovery Process. *Leukemia* 2002, 16, 520–526, doi:10.1038/sj.leu.2402464.
150. Peterson, L.E. Small Molecule Docking of DNA Repair Proteins Associated with Cancer Survival Following PCNA Metagene Adjustment: A Potential Novel Class of Repair Inhibitors. *Molecules* 2019, 24, 645, doi:10.3390/molecules24030645.
151. Elmenier, F.M.; Lasheen, D.S.; Abouzid, K.A.M. Design, Synthesis, and Biological Evaluation of New Thieno[2,3-d] Pyrimidine Derivatives as Targeted Therapy for PI3K with Molecular Modelling Study. *J Enzym Inhib Med Ch* 2021, 37, 315–332, doi:10.1080/14756366.2021.2010729.
152. Elmongy, E.I.; Attallah, N.G.M.; Altwaijry, N.; AlKahtani, M.M.; Henidi, H.A. Design and Synthesis of New Thiophene/Thieno[2,3-d]Pyrimidines along with Their Cytotoxic Biological Evaluation as Tyrosine Kinase Inhibitors in Addition to Their Apoptotic and Autophagic Induction. *Molecules* 2021, 27, 123, doi:10.3390/molecules27010123.
153. Chen, Y.; Yang, L.; Qiao, H.; Cheng, Z.; Xie, J.; Zhou, W.; Huang, X.; Jiang, Y.; Yu, B.; Zhao, W. Discovery of New Thieno[3,2-d]Pyrimidine Derivatives Targeting EGFR L858R/T790M NSCLCs by the Conformation Constrained Strategy. *Eur J Med Chem* 2020, 199, 112388, doi:10.1016/j.ejmech.2020.112388.
154. Boehr, D.D.; Farley, A.R.; Wright, G.D.; Cox, J.R. Analysis of the π - π Stacking Interactions between the Aminoglycoside Antibiotic Kinase APH(3')-IIIa and Its Nucleotide Ligands. *Chem Biol* 2002, 9, 1209–1217, doi:10.1016/s1074-5521(02)00245-4.
155. Mao, L.; Wang, Y.; Liu, Y.; Hu, X. Molecular Determinants for ATP-Binding in Proteins: A Data Mining and Quantum Chemical Analysis. *J Mol Biol* 2004, 336, 787–807, doi:10.1016/j.jmb.2003.12.056.
156. Hubbard, R.E.; Haider, M.K. Hydrogen Bonds in Proteins: Role and Strength. *eLS* 2010, doi:10.1002/9780470015902.a0003011.pub2.
157. Kurczab, R.; Śliwa, P.; Rataj, K.; Kafel, R.; Bojarski, A.J. Salt Bridge in Ligand–Protein Complexes - Systematic Theoretical and Statistical Investigations. *J Chem Inf Model* 2018, 58, 2224–2238, doi:10.1021/acs.jcim.8b00266.
158. Forli, S. Charting a Path to Success in Virtual Screening. *Molecules* 2015, 20, 18732–18758, doi:10.3390/molecules201018732.
159. Tokmakov, A.A.; Kurotani, A.; Takagi, T.; Toyama, M.; Shirouzu, M.; Fukami, Y.; Yokoyama, S. Multiple Post-Translational Modifications Affect Heterologous Protein Synthesis*. *J Biol Chem* 2012, 287, 27106–27116, doi:10.1074/jbc.m112.366351.
160. Audagnotto, M.; Peraro, M.D. Protein Post-Translational Modifications: In Silico Prediction Tools and Molecular Modeling. *Comput Struct Biotechnol J* 2017, 15, 307–319, doi:10.1016/j.csbj.2017.03.004.
161. Cuzzo, J.W.; Soutter, H.H. Overview of Recent Progress in Protein-Expression Technologies for Small-Molecule Screening. *Slas Discov* 2014, 19, 1000–1013, doi:10.1177/1087057114520975.

162. Assenberg, R.; Wan, P.T.; Geisse, S.; Mayr, L.M. Advances in Recombinant Protein Expression for Use in Pharmaceutical Research. *Curr Opin Struc Biol* 2013, 23, 393–402, doi:10.1016/j.sbi.2013.03.008.
163. Dondapati, S.K.; Stech, M.; Zemella, A.; Kubick, S. Cell-Free Protein Synthesis: A Promising Option for Future Drug Development. *Biodrugs* 2020, 34, 327–348, doi:10.1007/s40259-020-00417-y.
164. Bunnage, M.E.; Chekler, E.L.P.; Jones, L.H. Target Validation Using Chemical Probes. *Nat Chem Biol* 2013, 9, 195–199, doi:10.1038/nchembio.1197.
165. Hughes, J.; Rees, S.; Kalindjian, S.; Philpott, K. Principles of Early Drug Discovery. *Brit J Pharmacol* 2011, 162, 1239–1249, doi:10.1111/j.1476-5381.2010.01127.x.
166. Morgan, P.; Graaf, P.H.V.D.; Arrowsmith, J.; Feltner, D.E.; Drummond, K.S.; Wegner, C.D.; Street, S.D.A. Can the Flow of Medicines Be Improved? Fundamental Pharmacokinetic and Pharmacological Principles toward Improving Phase II Survival. *Drug Discov Today* 2012, 17, 419–424, doi:10.1016/j.drudis.2011.12.020.
167. Workman, P.; Collins, I. Probing the Probes: Fitness Factors For Small Molecule Tools. *Chem Biol* 2010, 17, 561–577, doi:10.1016/j.chembiol.2010.05.013.
168. Nowak, R.P.; Jones, L.H. Target Validation Using PROTACs: Applying the Four Pillars Framework. *Slas Discov* 2021, 26, 474–483, doi:10.1177/2472555220979584.
169. Weiss, W.A.; Taylor, S.S.; Shokat, K.M. Recognizing and Exploiting Differences between RNAi and Small-Molecule Inhibitors. *Nat Chem Biol* 2007, 3, 739–744, doi:10.1038/nchembio1207-739.
170. Peng, R.; Lin, G.; Li, J. Potential Pitfalls of CRISPR/Cas9-mediated Genome Editing. *Febs J* 2016, 283, 1218–1231, doi:10.1111/febs.13586.
171. Fu, Y.; Foden, J.A.; Khayter, C.; Maeder, M.L.; Reyon, D.; Joung, J.K.; Sander, J.D. High-Frequency off-Target Mutagenesis Induced by CRISPR-Cas Nucleases in Human Cells. *Nat Biotechnol* 2013, 31, 822–826, doi:10.1038/nbt.2623.
172. Durham, T.B.; Blanco, M.-J. Target Engagement in Lead Generation. *Bioorg Med Chem Lett* 2015, 25, 998–1008, doi:10.1016/j.bmcl.2014.12.076.
173. Weidemann, A.; Johnson, R.S. Biology of HIF-1 α . *Cell Death Differ* 2008, 15, 621–627, doi:10.1038/cdd.2008.12.
174. Zhu, G.; Pan, C.; Bei, J.-X.; Li, B.; Liang, C.; Xu, Y.; Fu, X. Mutant P53 in Cancer Progression and Targeted Therapies. *Frontiers Oncol* 2020, 10, 595187, doi:10.3389/fonc.2020.595187.
175. Kollareddy, M.; Dimitrova, E.; Vallabhaneni, K.C.; Chan, A.; Le, T.; Chauhan, K.M.; Carrero, Z.I.; Ramakrishnan, G.; Watabe, K.; Haupt, Y.; et al. Regulation of Nucleotide Metabolism by Mutant P53 Contributes to Its Gain-of-Function Activities. *Nat Commun* 2015, 6, 7389, doi:10.1038/ncomms8389.
176. Townsend, M.H.; Robison, R.A.; O'Neill, K.L. A Review of HPRT and Its Emerging Role in Cancer. *Med Oncol* 2018, 35, 89, doi:10.1007/s12032-018-1144-1.

177. Huang, C.-Y.; Yagüe-Capilla, M.; González-Pacanowska, D.; Chang, Z.-F. Quantitation of Deoxynucleoside Triphosphates by Click Reactions. *Sci Rep-uk* 2020, *10*, 611, doi:10.1038/s41598-020-57463-3.
178. Bae, E.; Kim, H.E.; Koh, E.; Kim, K.-S. Phosphoglucomutase1 Is Necessary for Sustained Cell Growth under Repetitive Glucose Depletion. *Febs Lett* 2014, *588*, 3074–3080, doi:10.1016/j.febslet.2014.06.034.
179. Jang, C.; Chen, L.; Rabinowitz, J.D. Metabolomics and Isotope Tracing. *Cell* 2018, *173*, 822–837, doi:10.1016/j.cell.2018.03.055.
180. Wang, X.; Liu, R.; Zhu, W.; Chu, H.; Yu, H.; Wei, P.; Wu, X.; Zhu, H.; Gao, H.; Liang, J.; et al. UDP-Glucose Accelerates SNAI1 mRNA Decay and Impairs Lung Cancer Metastasis. *Nature* 2019, *571*, 127–131, doi:10.1038/s41586-019-1340-y.
181. Teoh, S.T.; Ogrodzinski, M.P.; Lunt, S.Y. UDP-Glucose 6-Dehydrogenase Knockout Impairs Migration and Decreases in Vivo Metastatic Ability of Breast Cancer Cells. *Cancer Lett* 2020, *492*, 21–30, doi:10.1016/j.canlet.2020.07.031.
182. Wolfe, A.L.; Zhou, Q.; Toska, E.; Galeas, J.; Ku, A.A.; Koche, R.P.; Bandyopadhyay, S.; Scaltriti, M.; Lebrilla, C.B.; McCormick, F.; et al. UDP-Glucose Pyrophosphorylase 2, a Regulator of Glycogen Synthesis and Glycosylation, Is Critical for Pancreatic Cancer Growth. *Proc National Acad Sci* 2021, *118*, e2103592118, doi:10.1073/pnas.2103592118.
183. Lin, Y.; Cradick, T.J.; Brown, M.T.; Deshmukh, H.; Ranjan, P.; Sarode, N.; Wile, B.M.; Vertino, P.M.; Stewart, F.J.; Bao, G. CRISPR/Cas9 Systems Have off-Target Activity with Insertions or Deletions between Target DNA and Guide RNA Sequences. *Nucleic Acids Res* 2014, *42*, 7473–7485, doi:10.1093/nar/gku402.
184. Cho, S.W.; Kim, S.; Kim, Y.; Kweon, J.; Kim, H.S.; Bae, S.; Kim, J.-S. Analysis of Off-Target Effects of CRISPR/Cas-Derived RNA-Guided Endonucleases and Nickases. *Genome Res* 2014, *24*, 132–141, doi:10.1101/gr.162339.113.
185. Neves, B.J.; Braga, R.C.; Melo-Filho, C.C.; Moreira-Filho, J.T.; Muratov, E.N.; Andrade, C.H. QSAR-Based Virtual Screening: Advances and Applications in Drug Discovery. *Front Pharmacol* 2018, *9*, 1275, doi:10.3389/fphar.2018.01275.
186. Rixe, O.; Fojo, T. Is Cell Death a Critical End Point for Anticancer Therapies or Is Cytostasis Sufficient? *Clin Cancer Res* 2007, *13*, 7280–7287, doi:10.1158/1078-0432.ccr-07-2141.
187. Rafahi, H.; Orłowski, C.; Georgiadis, G.T.; Ververis, K.; El-Osta, A.; Karagiannis, T.C. Clonogenic Assay: Adherent Cells. *J Vis Exp* 2011, doi:10.3791/2573.
188. Prabhu, N.; Dai, L.; Nordlund, P. CETSA in Integrated Proteomics Studies of Cellular Processes. *Curr Opin Chem Biol* 2020, *54*, 54–62, doi:10.1016/j.cbpa.2019.11.004.

9. Appendix – Research contributions

9.1 Publications

1) Literature review:

Walter, M., & Herr, P. (2022). Re-Discovery of Pyrimidine Salvage as Target in Cancer Therapy. *Cells*, 11(4), 739. <https://doi.org/10.3390/cells11040739>

2) Conference paper:

Walter, M., Homan, E., Koolmeister, T., Almlöf, I., Mortusewicz, O., Helleday, T., & Herr, P. (2021). Development of Small Molecule NUDT22 Inhibitors for Uses in Cancer. *Medical Sciences Forum*, 3(1), 1. <https://doi.org/10.3390/iecc2021-09197>

3) Preprint:

Walter, M., Mayr, F., Hanna, B. M. F., Cookson, V., Mortusewicz, O., Helleday, T., & Herr, P. (2022). NUDT22 promotes cancer growth through pyrimidine salvage and the TCA cycle. <https://doi.org/10.21203/rs.3.rs-1491465/v1>

4) In review/under consideration:

Walter M, Mayr F, Hanna BMF, Cookson V, Mortusewicz O, Helleday T, Herr P; NUDT22 promotes cancer growth through pyrimidine salvage.

Under review in Oncogenes.

Franco, J., Piacente F., **Walter, M.**, Fratta, S., Ghanem, M., Benzi, A., Caffa, I., Kurkin, A.V., Altieri, A., Herr, P., Martinez-Bailen, M., Robina, I., Bruzzone, S., Necioni, A. & Del Rio, A.. Structure-based identification and biological characterization of new NAPRT Inhibitors.

Under review in Pharmaceuticals.

9.2 Conferences and presentations

ORAL

- 19th Symposium on Purine and Pyrimidine Metabolism in Men, virtual. 5 minutes flash presentation (June 2021)
- The Medical School Annual Research Day, University of Sheffield. 1 minute flash presentation (June 2021)

POSTER

- 5th DNA Repair/Replication Structures and Cancer Conference, Mexico (April 2022)
- 19th Symposium on Purine and Pyrimidine Metabolism in Men, virtual (June 2021)
- The Medical School Annual Research Day, University of Sheffield, UK (June 2021)
- IECC2021: The first international electronic conference on cancers: Exploiting cancer vulnerability by targeting the DNA damage response, virtual (February 2021)
- North East Postgraduate Conference 2020, virtual, (November 2020)
- SYNTRAIN Conference: Genomic Instability in Cancer, virtual, international (October 2020)

OTHER INVITED TALKS/SEMINARS

- First year presentation, University of Sheffield (June 2020)
- Oncology and Metabolism Departmental Seminar Series, University of Sheffield, virtual (March 2022)
- H2020 MSCA ITN Integrata meetings, University of Genoa, Italy (January 2020), virtual (January 2021), University of Sheffield, UK (May 2022)